

DESIGN STRATEGIES FOR TISSUE ENGINEERING SCAFFOLDS

This work was financially supported by the Spearhead program: 'Advanced Polymeric Microstructures for Tissue Engineering' of the University of Twente, Institute for Biomedical Technology (BMTi)

Committee members

| | | |
|---------------------------------|--------------------|--|
| Prof. dr.-ing. M. Wessling | promotor | University of Twente |
| Dr. D. Stamatialis | assistant promotor | University of Twente |
| Prof. dr. K. Boller | chairman | University of Twente |
| Prof. dr. C.A. van Blitterswijk | | University of Twente |
| Prof. dr. D.W. Grijpma | | University of Twente, University of Groningen |
| Prof. D. Kaplan | | Tufts University, USA |
| Prof. A. Boccaccini | | Imperial College London, UK |
| Prof. dr. R.A Bank | | University Medical Center Groningen |

© 2009 Bernke Papenburg, Enschede, The Netherlands

All rights reserved

Design Strategies for Tissue Engineering Scaffolds

Bernke Papenburg

PhD thesis, University of Twente, The Netherlands

ISBN: 978-94-9012-239-3

Printed by: Gildeprint Drukkerijen, Enschede, The Netherlands

Cover design by Bernke Papenburg

The cover shows a fluorescence microscopy image of pre-myoblast cells organized on a poly(L-lactic acid) scaffold featuring pillars; green indicates the cytoskeleton of the cells whereas the nuclei are labeled blue

DESIGN STRATEGIES FOR TISSUE ENGINEERING SCAFFOLDS

PROEFSCHRIFT

ter verkrijging van
de graad van doctor aan de Universiteit Twente,
op gezag van de rector magnificus,
prof. dr. H. Brinksma
volgens besluit van het College voor Promoties
in het openbaar te verdedigen
op vrijdag 19 juni 2009 om 13.15 uur

door

Berendien Jacoba Papenburg

Geboren op 22 juli 1981
te Dedemsvaart

Dit proefschrift is goedgekeurd door:

Promotor:

Prof. Dr.-Ing. M. Wessling

en Assistent promotor:

Dr. D. Stamatialis

*Voor mijn oma, Berendina Hartkamp,
die dit proefschrift nog zo graag zelf had ingezien*

***“Dancing in all its forms cannot be excluded from the curriculum of all
noble education; dancing with the feet, with ideas, with words, and,
need I add that one must also be able to dance with the pen?”***

Friedrich Nietzsche

Table of Contents

| | |
|---|-----------|
| Chapter 1 General Introduction | 1 |
| 1.1 Tissue engineering | 1 |
| 1.2 Tissue engineering in the clinic | 3 |
| 1.3 Scope and outline of the thesis | 4 |
| 1.3.1 Scope of the project at large | 4 |
| 1.3.2 Scope thesis | 4 |
| 1.4 Outline thesis | 8 |
| References | 10 |
| Chapter 2 Scaffolds for Tissue Engineering | 11 |
| 2.1 Requirements scaffold | 11 |
| 2.2 Materials | 12 |
| 2.2.1 Common biomaterials | 12 |
| 2.2.2 Poly(lactic acid) | 13 |
| 2.2.3 Poly(ϵ -caprolactone) | 14 |
| 2.2.4 Poly(tri-methylene carbonate) | 14 |
| 2.2.5 Poly(ethylene oxide)/poly(butylene terephthalate) | 15 |
| 2.2.6 Poly(dimethyl siloxane) | 15 |
| 2.3 Fabrication methods | 16 |
| 2.3.1 Emulsion freeze-drying | 16 |
| 2.3.2 Foaming | 16 |
| 2.3.3 Particle leaching | 17 |
| 2.3.4 Electrospinning | 17 |
| 2.3.5 Sintering | 18 |
| 2.3.6 Polymer casting and phase separation | 18 |
| 2.4 Scaffold design | 20 |
| References | 21 |

| | |
|---|-----------|
| Chapter 3 One-step Fabrication of Porous Micropatterned Scaffolds | 27 |
| to Control Cell Behavior | |
| 3.1 Introduction | 28 |
| 3.2 Background phase separation micromolding (PSμM) | 30 |
| 3.3 Materials and Methods | 31 |
| 3.3.1 Micropatterned porous scaffold preparation | 31 |
| 3.3.2 Porosity and pore morphology determination | 32 |
| 3.3.3 Nutrient transport | 33 |
| 3.3.4 Cell culturing | 34 |
| 3.3.5 3-D scaffolds proof-of-principle | 36 |
| 3.4 Results and Discussion | 37 |
| 3.4.1 Micropatterned sheet preparation | 37 |
| 3.4.2 Porosity and pore morphology determination | 37 |
| 3.4.3 Nutrient transport | 40 |
| 3.4.4 Cell culturing | 42 |
| 3.4.5 3-D scaffolds proof-of-principle | 47 |
| 3.5 Conclusions | 48 |
| References | 49 |

| | |
|--|-----------|
| Chapter 4 A Facile Method to Fabricate Poly(L-lactide) Nano-fibrous | 51 |
| Morphologies by Phase Inversion | |
| 4.1 Introduction | 52 |
| 4.2 Materials and Methods | 53 |
| 4.2.1 PLLA synthesis and characterization | 53 |
| 4.2.2 Scaffold preparation and characterization | 53 |
| 4.2.3 Cell culturing and analysis | 54 |
| 4.3 Results and Discussion | 56 |
| 4.3.1 PLLA synthesis and characterization | 56 |
| 4.3.2 Scaffold preparation | 56 |
| 4.3.3 Scaffold characterization | 57 |
| 4.3.4 Cell culture and analysis | 62 |
| 4.4 Conclusions | 65 |
| References | 66 |

Chapter 5 Designing Porosity and Topography of

| Poly(1,3-trimethylene carbonate) Scaffolds | | 69 |
|---|---|-----------|
| 5.1 | Introduction | 70 |
| 5.2 | Materials and Methods | 71 |
| 5.2.1 | PTMC synthesis and characterization | 71 |
| 5.2.2 | Scaffold preparation | 72 |
| 5.2.3 | PEO content | 74 |
| 5.2.4 | Porosity and pore morphology | 74 |
| 5.2.5 | Sheet morphology under physiological conditions | 75 |
| 5.2.6 | Cell culturing | 75 |
| 5.2.7 | Cell culture analysis | 75 |
| 5.3 | Results and Discussion | 77 |
| 5.3.1 | PTMC synthesis and characterization | 77 |
| 5.3.2 | PTMC scaffold preparation | 77 |
| 5.3.3 | Porosity and pore morphology | 79 |
| 5.3.4 | Sheet morphology under physiological conditions | 82 |
| 5.3.5 | Cell morphology | 84 |
| 5.3.6 | Cell proliferation | 85 |
| 5.4 | Conclusions | 92 |
| | References | 93 |

Chapter 6 Cell Behavior as Function of Contact Angle and Surface

| Topography | | 95 |
|-------------------|--|------------|
| 6.1 | Introduction | 96 |
| 6.2 | Materials and Methods | 98 |
| 6.2.1 | Topography design | 98 |
| 6.2.2 | Micropatterned scaffold sheet preparation and characterization | 98 |
| 6.2.3 | Cell culturing and analysis | 100 |
| 6.3 | Results and Discussion | 101 |
| 6.3.1 | Micropatterned scaffold sheet preparation | 101 |
| 6.3.2 | Contact angle - wettability | 103 |
| 6.3.3 | Protein adsorption | 106 |
| 6.3.4 | Cell attachment and proliferation | 108 |
| 6.3.5 | Cell morphology | 111 |
| 6.4 | Conclusions | 117 |
| | References | 118 |

Chapter 7 An Arrayed Approach to Screening Cell-Surface Topographic

| | |
|--|------------|
| Interactions | 123 |
| 7.1 Introduction | 124 |
| 7.2 Concept | 125 |
| 7.2.1 Paradigm | 125 |
| 7.2.2 Design | 127 |
| 7.3 Materials and Methods | 128 |
| 7.3.1 Mask design and mold fabrication | 128 |
| 7.3.2 TopoChip fabrication | 128 |
| 7.3.3 TopoChip seeding and culturing | 129 |
| 7.4 Results and Discussion | 130 |
| 7.4.1 TopoChip fabrication | 130 |
| 7.4.2 Uniform seeding | 132 |
| 7.4.3 Cell-material interactions | 134 |
| 7.5 Conclusions | 136 |
| References | 137 |

Chapter 8 Understanding Nutrient Supply through Multi-Layer

| | |
|---|------------|
| Scaffolds | 139 |
| 8.1 Introduction | 140 |
| 8.2 Model | 143 |
| 8.2.1 Concept | 143 |
| 8.3 Materials and Methods | 144 |
| 8.3.1 Scaffold sheets preparation | 144 |
| 8.3.2 Porosity and pore morphology determination | 144 |
| 8.3.3 Cell culturing | 145 |
| 8.4 Results and Discussion | 148 |
| 8.4.1 Scaffold sheets characterization | 148 |
| 8.4.2 Nutrient transport limitations | 149 |
| 8.4.3 Static culture conditions: multi-layer WS scaffolds | 150 |
| 8.4.4 Static culture conditions: multi-layer TS scaffolds | 154 |
| 8.4.5 Model results and validation | 157 |
| 8.4.6 Dynamic culture conditions | 160 |
| 8.5 Conclusions | 165 |
| References | 166 |
| Appendix to Chapter 8 Model description | 169 |

| | |
|---|----------------|
| Chapter 9 Reflections and Outlook | 177 |
| 9.1 Scaffold design at large | 177 |
| 9.2 Scaffold design in this thesis | 178 |
| 9.2.1 General discussion | 178 |
| 9.2.2 General conclusions | 179 |
| 9.3 Future directions | 180 |
| 9.3.1 Materials properties: reinforcements | 180 |
| 9.3.2 Surface characteristics: layer-by-layer architecture | 181 |
| 9.3.3 3D-architecture: nutrient supply <i>in-vivo</i> style | 181 |
| References | 184 |
| Summary | 185 |
| Nederlandse Samenvatting | 188 |
| Acknowledgments - Dankwoord | 192 |
| Cirriculum Vitae - List of Publications | 195 |

A grayscale scanning electron micrograph (SEM) showing a highly porous, interconnected network of fibers and cells, characteristic of a scaffold or biological tissue structure. The image has a complex, mesh-like appearance with many small, dark, circular or oval features scattered throughout a lighter, fibrous background.

Chapter 1 General Introduction

1.1 Tissue engineering

The replacement of organs since long has been the subject of debate, however, the field of engineering tissue *in vitro* to repair damaged tissue *in vivo* originated only about two decades ago [1, 2]. In fact, tissue engineering (TE) originates from reconstructive surgery where direct transplantation of (allogenic) donor tissue is practiced to repair the function of damaged tissue. Many difficulties arise with direct transplantation due to insufficient donor organs, pathogen transmission and rejection of the donor organ [3-5]. As a result, patients can be waiting for a donor organ for years, and when they receive one in time, they need to take immunosuppressive medication for the rest of their lives and risk the need of a replacement organ within days to years after the surgery. An autogenic tissue engineering transplant (using patient's own cells) would address most limitations of direct transplantation and avoid difficulties concerning rejection and pathogen transmission. Additionally, there would be no dependency on donors. Therefore, constructing a tissue engineered replacement *in vitro* is considered an excellent alternative to direct transplantation of donor organs [1, 3-5].

TE is defined as the interdisciplinary field applying the principles and methods of engineering and life sciences to fundamentally understand and develop biological substitutes to restore, maintain or improve tissue functions [1]. In basis, TE attempts to mimic the function of natural tissue. Therefore, to optimize the development of functional biological substitutes, the natural circumstances of the specific tissue have to be fundamentally understood. Biological tissues basically consist of cells, signaling systems and extracellular matrix (ECM) [4]. The cells are the core of the tissue, however, can not function in the absence of signaling systems and/or of the ECM. The signaling system consists of genes that secrete transcriptional products when differentially activated, and urges cues for tissue formation and differentiation [4]. The ECM is a meshwork-like substance within the extracellular space and supports cell attachment and promotes cell proliferation [6, 7].

TE approaches can generally be sub-divided based on these 3 phenomena, either studied single or combined [1, 3]:

- cell-based therapies
- induction of tissue-formation by soluble signaling factors
- and/or biocompatible support by an artificial ECM (scaffold)

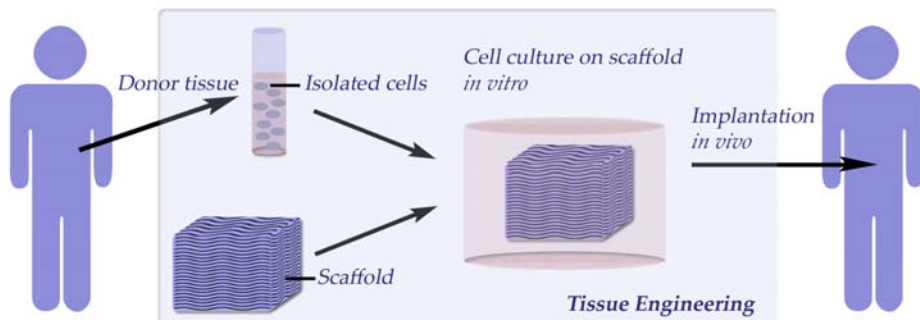


Figure 1 Schematic illustration of the tissue engineering principle.

Figure 1 illustrates the basic principle of the general TE approach based on the introduction of a scaffold. Cells are isolated from either the patient (autogenic) or from a donor (allogenic). After isolation, the cells are cultured *in vitro* and subsequently introduced to a scaffold. Finally, the cell-cultured scaffold is implanted *in vivo* into the patient. Many aspects in this process add to the final suitability and functionality of the tissue engineered construct. Isolation of the cells and *in vitro* culturing requires optimal processing and environmental conditions, e.g. pH, temperature, medium composition. Each type of tissue requires distinct conditions and therefore, demands the understanding of the specific natural biological environment *in vivo* to allow optimization of culturing *in vitro*. Supplementing tissue-inducing soluble factors can be combined within the scaffold-based approach to guide cell behavior by triggering specific reactions through pathway activation [8-10]. Another approach to guide cell behavior lies within the architectural design of the scaffold. The scaffold should allow tissue formation in 3D by good support of cell attachment, proliferation and organization, as well as enabling sufficient nutrient supply to the cells and waste elimination from the cells [6, 11, 12]. Design of well-functioning tissue engineered constructs requires optimization of these aspects for the specific application.

1.2 Tissue engineering in the clinic

A well-known example of tissue engineering is the 'mouse with the human ear' [13]. This study describes seeding of chondrocytes isolated from bovine articular cartilage on a polymer (polyglycolic acid-poly(lactic acid)) scaffold in the form of a human ear, and subsequent transplantation of the construct subcutaneous in a nude mouse. Even though the scaffold had the form of a human ear, actually no human material was involved; this study attempted to demonstrate growth of new cartilage in a specific form to be used in plastic or reconstructive surgery. And they did, new cartilage formed within 12 weeks post-implantation.

With respect to human application, successful clinical trials of tissue engineering constructs have been reported in literature. Nowadays, major areas of tissue-engineered replacements in clinical trials and applications are skin, cardiovascular, bone and cartilage [5, 7, 14-16]. One example is the work performed by Matsumura et al. [17] who reported application of tissue-engineered autografts in cardiovascular surgery on children with various complex heart diseases. They applied a tissue engineering technique where patients own (autogenic) cells were isolated, cultured and subsequently seeded on a biodegradable polymer scaffold of poly(glycolic acid) combined with poly(lactic acid- ϵ -caprolactone). The first operation was performed in May 1999, and over 40 patients were treated the following years. Post-operative analysis revealed no complications related to the tissue engineering autograft.

Another recent example is the design and implantation of a tissue-engineered airway [18]. In this case, the researchers first removed all donor cell and antigens of an allogenic donor trachea (wind-pipe) to prevent an immune reaction of the host towards the donor material. Subsequently, they re-cultured the matrix with autogenic cells and transplanted the cell-seeded scaffold into the patient's main bronchus. Immediately, the tissue engineered trachea became functional and after 4 months, the scaffold still showed normal appearance and good mechanical properties.

1.3 Scope and outline of the thesis

1.3.1 Scope of the project at large

Within the definition of tissue engineering lays the need of an interdisciplinary approach and therewith, the collaboration of experts of all participating disciplines. To facilitate collaboration within the interdisciplinary fields combined in (bio)medical research at large, the University of Twente initiated the Institute of Biomedical Engineering (BMTi). The work presented in this thesis is performed within the spearhead program of the BMTi 'Advanced Polymeric Microstructures for Tissue Engineering'. This project aimed at strengthening the collaboration between the departments of Membrane Science and Technology (MST), Polymer Chemistry & Biomaterials (PBM) and Biophysical Engineering (BPE). With this in mind, several collaborations between these departments followed resulting in a number of papers presenting work of the combined disciplines. Additionally, good collaboration was initiated with the another member of BMTi, the department of Tissue Regeneration (TR), and all experiments involving cell culturing described in this thesis were performed in collaboration with TR.

1.3.2 Scope thesis

This thesis focuses on various aspects involved in scaffold design and the interaction of scaffolds with the cells. The ultimate goal is to design a scaffold that supports functional tissue formation, resembling *in vivo* tissue organization, combined with good nutrient supply to the cells. Our concept to reach this goal is based on 3D multi-layer scaffolds consisting of porous micropatterned sheets. Figure 2 illustrates this concept, where cells grow within micropatterned channels giving a clear direction to the cells inducing cell organization (Figure 2a). Subsequent stacking of these micropatterned porous sheets (Figure 2b) results in a 3D scaffold where the microchannels also provide space allowing perfusion of nutrients throughout the complete scaffold [19]. Additionally, the porosity of the single layers enables diffusion of nutrients and signalling factors between the layers.

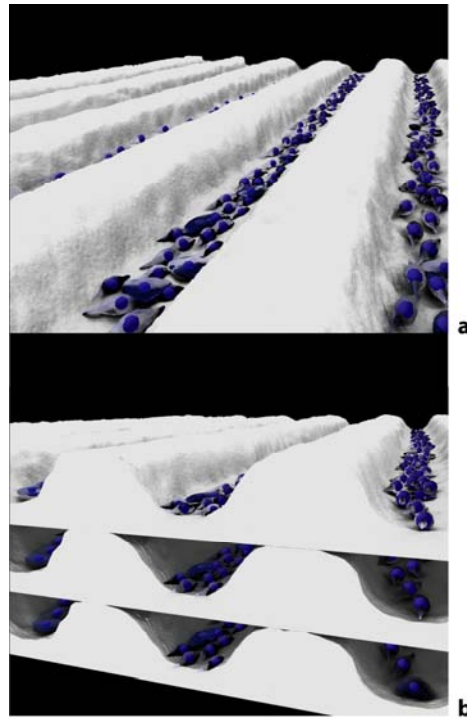


Figure 2 Schematic illustration of the 3D multi-layer scaffold concept.

To produce functional scaffolds based on this concept, many parameters need to be understood and optimized regarding the role of scaffold design in the cell-scaffold interaction at various levels. The work described in this thesis aims at acquiring insight into the role of a number of these aspects and how those affect cell-material interaction. At large, scaffold design aspects can be divided into three main classes: material properties, surface characteristics and 3D architecture. These three main classes are again subdivided into many sub-categories, as schematically represented in Figure 3.

This thesis aims to fill in which topics make up the sub-categories within scaffold design and which parameters are involved when addressing these topics.

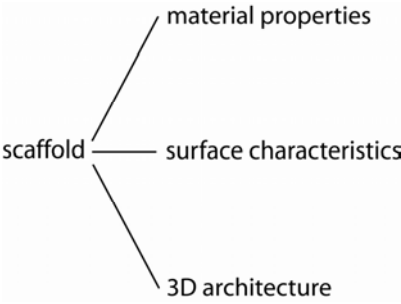


Figure 3 Data tree representing the main scaffold design classes.

Nonetheless, this thesis cannot address all sub-categories within the large scaffold design framework, hence; a selection of topics is evaluated regarding the main design concept of a multi-layer 3D scaffold incorporating porosity as well as topography. Certain topics within this concept at large are studied in more detail, amongst which material processing, scaffold-cell interaction regarding surface topography and nutrient supply through this multi-layer scaffold. Figure 4 schematically illustrates these topics studied in more detail and how these topics mutually interact, in order to obtain the final goal. In fact each topic, originating from the either the engineering, life sciences or the interdisciplinary field in between, has to be studied properly to successfully convert a scaffold from material into part of a TE construct.

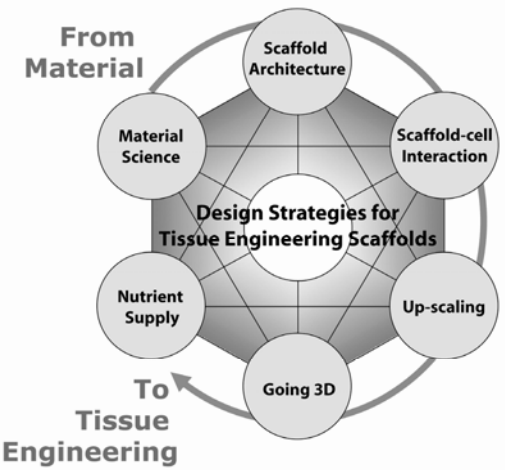


Figure 4 Representation of various topics regarding scaffold design and their mutual relations, addressed in this thesis.

Parameters involved within these addressed topics are e.g.:

- **Material science:** material nature and processing
- **Scaffold architecture:** surface topography design, porosity, size
- **Scaffold-cell interaction:** cell attachment, cell proliferation, cell morphology regarding distinct surface characteristics
- **Up-scaling:** high-throughput screening of variables, top-down design
- **Going 3D:** multi-layer stacking methods, culturing in 3D
- **Nutrient supply:** mass transport through layers, perfusion of the channels, theoretical modelling

Even though this thesis cannot address each topic involved within the large scaffold design framework, **this thesis aims at providing distinct strategies for functional scaffold design as part of the development of tissue engineering constructs.**

1.4 Outline thesis

Whereas this first Chapter presents a general overview of the tissue engineering field, **Chapter 2** gives a more detailed literature overview of various aspects in scaffold design. Topics discussed are the general requirements involved in scaffold design, well-known and frequently used biomaterials, commonly applied scaffold fabrication methods and the importance of surface topography. Additionally, these sections highlight the specific biomaterials and fabrication method adopted in the various chapters of this thesis.

The method used to fabricate the micropatterned porous scaffolds, as illustrated in Figure 2, is Phase Separation Micromolding (PS μ M). **Chapter 3** offers an overall description of our approach and is related to the vast majority of the topics addressed in this thesis, i.e. materials science, scaffold architecture, scaffold-cell interaction, going 3-D as well as nutrient supply. This chapter is dedicated to the application of PS μ M in scaffold fabrication and how to tune the morphology of the scaffolds by variation in processing parameters. Application of different polymers is evaluated, followed by a more detailed study of the most porous poly(L-lactic acid) (PLLA) scaffold sheets with respect to nutrient diffusion through the inner-porosity of the sheets. Additionally, this chapter demonstrates pre-myoblast cells (C2C12) alignment tuned by distinct micropatterns and finally, a proof-of-principle for stacking of the micropatterned sheets into a 3D scaffold.

Chapter 4 and **Chapter 5** more specifically relate to materials science and the corresponding scaffold-cell interaction. **Chapter 4** presents the effect of the molecular weight of PLLA on the porous sheet morphology during phase separation processing. Very high molecular weight PLLA yields a nano-fibrous morphology in contrast to a solid-wall pore morphology generally obtained using lower molecular weight PLLA, described in Chapter 3. The nano-fibrous sheets comprise nano-fibers within similar range to collagen fibers, which is the main component of the ECM. The suitability of these nano-fibrous PLLA scaffold sheets is evaluated regarding cell attachment and morphology.

Chapter 5 deals with the development of micropatterned porous scaffold sheets based on flexible poly(tri-methylene carbonate) (PTMC). Poly(ethylene oxide) PEO addition to the casting solution plays an important role in the phase separation process and the obtained porous morphology, and this role is discussed in detail. C2C12 attachment, proliferation, differentiation and organization on the PTMC porous sheets are systematically studied.

Chapter 6 and **Chapter 7** focus on scaffold-cell interaction and up-scaling. **Chapter 6** presents a detailed study of the role of material properties and surface topography on cell behavior. Protein adsorption to scaffold surfaces determines cell behavior on these surfaces, and it is thought that for instance wettability of a surface plays an important role in this. Applying a micropillar array to a selection of three polymers enables altering the surface wettability of these polymers without variation in the surface chemistry. Evaluation of protein adsorption to these surfaces and correlation to cell attachment, proliferation and cell morphology is described.

Chapter 7 deals with complexity involved in tissue engineering and more specific, scaffold design. Proper functioning of the human body requires a full set of highly complex functions from single cell to complete tissue levels. Translating this complexity into the design of *in vitro* tissue engineering brings about a tremendous number of variations, and grows to virtually innumerable considered that optimal design is fully subject to the specific application. High-throughput screening of a library comprising a multitude of surface topographical variations, presented in this chapter, may give a first indication of the most suitable surface designs for a specific TE application.

The work in **Chapter 8** relates to scaffold architecture, going 3D and nutrient supply, herewith following up on the work described in Chapter 3 by studying the development of 3D multi-layer scaffolds. This chapter comprises the evaluation of nutrient transport throughout the 3D scaffold under both static as well as dynamic conditions and the resulting effect on cell behavior. Besides, a theoretical model is designed and validated to predict optimal use of the multi-layer scaffold by introduction of nutrient perfusion throughout the scaffold.

Chapter 9 reflects back on the results of this thesis and presents an outlook on a number of topics to be explored in the future to improve and optimize the 3D multi-layer scaffold as proposed in this thesis.

References

1. Langer R, Vacanti JP. Tissue Engineering. *Science* 1993;260:920-926.
2. Vacanti CA. History of Tissue Engineering and A Glimpse Into Its Future. *Tissue Engineering* 2006;12(5):1137-1142.
3. Fuchs JR, Nasser BA, Vacanti JP. Tissue engineering: A 21st century solution to surgical reconstruction. *Annual Thorac Surgery* 2001;72:577-591.
4. Lanza RP, Langer RS, Vacanti J. Principles of tissue engineering. 2nd ed. San Diego, CA :: Academic Press, 2000.
5. Saltzman WM. Tissue Engineering: principles for the design of replacement organs and tissues. 1st ed. Oxford: Oxford University Press, 2004.
6. Badylak SF. The extracellular matrix as a biologic scaffold material. *Biomaterials* 2007;28(25):3587-3593.
7. Blitterswijk CA, Thomsen P. Tissue engineering. 1st ed. Amsterdam; Boston: Elsevier/Academic Press, 2008.
8. Baud V, Jacque E. The alternative NF-kappa B activation pathway and cancer : friend or foe? *M S-Med Sci* 2008 Dec;24(12):1083-1088.
9. Chen Y, Alman BA. Wnt Pathway, an Essential Role in Bone Regeneration. *Journal of Cellular Biochemistry* 2009 Feb 15;106(3):353-362.
10. Landmesser U, Wollert KC, Drexler H. Potential novel pharmacological therapies for myocardial remodelling. *Cardiovasc Res* 2009 Feb;81(3):519-527.
11. Hollister SJ. Porous scaffold design for tissue engineering. *Nature Materials* 2005;4:518-524.
12. Takezawa T. A strategy for the development of tissue engineering scaffolds that regulate cell behavior. *Biomaterials* 2003;24(13):2267-2275.
13. Cao YMDPD, Vacanti JPMD, Paige KTMD, Upton JMD, Vacanti CAMD. Transplantation of Chondrocytes Utilizing a Polymer-Cell Construct to Produce Tissue-Engineered Cartilage in the Shape of a Human Ear. *Plastic & Reconstructive Surgery* 1997;100(2):297-302.
14. Fong P, Shin'oka T, Lopez-Soler RI, Breuer C. The use of polymer based scaffolds in tissue-engineered heart valves. *Progress in Pediatric Cardiology* 2006;21(2):193-199.
15. Jawad H, Ali NN, Lyon AR, Chen QZ, Harding SE, Boccaccini AR. Myocardial tissue engineering: a review. *Journal of Tissue Engineering and Regenerative Medicine* 2007;1(5):327-342.
16. Nesic D, Whiteside R, Brittberg M, Wendt D, Martin I, Mainil-Varlet P. Cartilage tissue engineering for degenerative joint disease. *Advanced Drug Delivery Reviews* 2006;58(2):300-322.
17. Matsumura G, Hibino N, Ikada Y, Kurosawa H, Shin'oka T. Successful application of tissue engineered vascular autografts: clinical experience. *Biomaterials* 2003;24(13):2303-2308.
18. Macchiarini P, Jungebluth P, Go T, Asnaghi MA, Rees LE, Cogan TA, et al. Clinical transplantation of a tissue-engineered airway. *The Lancet* 2008;372(9655):2023-2030.
19. Stamatialis DF, Papenburg BJ, Gironés M, Saiful S, Bettahalli SNM, Schmitmeier S, et al. Medical applications of membranes: Drug delivery, artificial organs and tissue engineering. *Journal of Membrane Science* 2008;308(1-2):1-34.

Chapter 2 Scaffolds for Tissue Engineering

2.1 Requirements scaffold

Within tissue engineering (TE), one of the major research themes is scaffold design. A scaffold is a 3-D construct that serves as temporary support for isolated cells to grow into new tissue before transplantation back to the host, as described in Chapter 1. The design of the scaffold determines the functionality of the construct to a high extent. Although the final requirements depend on the specific purpose of the scaffold, several general characteristics and requirements need to be considered for all designs [1-4]. The scaffold should be/have:

- biocompatible; the scaffold should provoke an appropriate biological response in a specific application and prevent any adverse response of the surrounding tissue [5, 6]
- biodegradable; the scaffold materials should degrade in tandem with tissue regeneration and remodeling of the extracellular matrix (ECM) into smaller non-toxic substances without interfering with the function of the surrounding tissue [7]
- promote cell attachment, spreading and proliferation; vital for the regulation of cell growth and differentiation [8]
- suitable mechanical strength; its strength should be comparable to *in vivo* tissue at the site of implantation as evidently, a scaffold requires more flexibility or rigidity depending on the application in e.g. cardiovascular versus bone prostheses [9]
- good transport properties; to ensure sufficient nutrient transport towards the cells and removal of waste products the scaffold should be highly porous with good pore connectivity, however, it should maintain sufficient mechanical strength implying optimization of porosity [1, 10-12]
- easy to connect to the vascularization system of the host; to ensure good nutrient supply throughout the scaffold post-implantation, the scaffold should be connected to the natural nutrient supplying system [1, 10, 13]
- suitable surface characteristics; apart from optimal physiochemical properties, research suggests that the introduction of e.g. surface topography into the scaffold improves tissue organization leading to increased tissue function [14-17]

Parts of this chapter are included within a review paper:

D.F. Stamatialis, Bernke J. Papenburg, M. Gironés, S. Saiful, S.N.M. Bettahalli, S. Schmitmeier, M. Wessling

Journal of Membrane Science, 308 (2008) 1-34

2.2 Materials

2.2.1 Common biomaterials

Due to the variation in mechanical properties required in 'soft' versus 'hard' TE applications, the constructs for these two sub-categories generally use different classes of biomaterials. For soft TE applications, e.g. skeletal muscle or cardiovascular substitutes, generally a wide variety of polymers are applied. On the other hand, hard tissue replacements, e.g. bone substitutes, are generally based on more rigid polymers, ceramics and metals. Frequently used biomaterials originate from a wide range of natural as well as synthetic sources. It is beyond the scope of this chapter to discuss all sources in detail. This section only describes a selection of widely used materials and focuses more on the materials used in this thesis. For in-depth information on other frequently used materials for scaffold fabrication, excellent reviews are available [10, 11, 18-20]. Table 1 lists polymers extensively applied in scaffold fabrication for 'soft' TE applications. Apart from single polymers, scaffolds are also commonly fabricated from co-polymers of two or more polymers (not listed) to improve the overall characteristics; co-polymers generally have an average of the mechanical properties of the incorporated single polymers.

Table 1 Materials frequently applied in soft TE applications.

| Origin | Polymer (family) |
|-----------|--|
| Natural | Collagen <i>component of the extra cellular matrix - ECM</i> |
| | Fibrin |
| | Gelatin |
| | Poly(hydroxybutyrate) |
| | Polysaccharides most common are hyaluronic acid, chitosan, starch and alginates |
| Synthetic | Poly(esters) <i>most common are poly (α-hydroxy acids): poly(lactic acid) (PLA) and poly(glycolic acid) (PGA)</i> |
| | Poly(ϵ -caprolactones) |
| | Poly(propylene fumarates) |
| | Poly(anhydrides) |
| | Poly(orthoesters) |

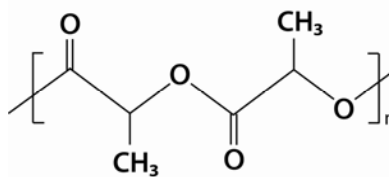
Scaffold fabrication for hard TE applications employs a wider variety of classes of materials; including polymers, ceramics, composites and metals. Table 2 presents materials extensively used in hard TE, besides the polymers already listed in Table 1. Often, polymers alone might not have sufficient mechanical strength, which can be improved by adding reinforcements resulting in composites. Herewith, combining two or more classes of materials improves the mechanical properties, similar to the principle behind co-polymer.

Table 2 Materials frequently applied in hard TE applications.

| Class of material | Type |
|-----------------------------|---|
| Crystalline ceramics | Hydroxyapatite |
| | <i>most common since it is the inorganic component of natural bone</i> |
| | Tricalcium phosphate |
| | Calcium metaphosphate |
| Amorphous glasses | Silica |
| | Bio-glass |
| Composites | Hydroxyapatite / poly(ϵ -caprolactone), chitosan, and/or collagen |
| | Titanium/calcium phosphate, polyvinyl alcohol, and/or boron |
| | Poly(lactic acid)/ tricalcium phosphate, silica, and/or ceramic |
| | |
| Metals | Stainless steel |
| | Titanium |
| | Alumina |

2.2.2 Poly(lactic acid)

In this thesis, we primarily use one of the most common and well-known biomaterials: poly(lactic acid) (PLA). PLA belongs to the polyester family, as is the case for the vast majority of biodegradable polymers. PLA exists in different isomeric forms, namely semi-crystalline D(-) (PDLA), semi-crystalline L(+) (PLLA) and amorphous racemic D,L (PDLLA) [21, 22].

**Figure 1** Molecular structure of PLA.

PLA degrades by bulk hydrolysis and leads to the production of lactic acid. In case of PLLA, degradation results in L(+) lactic acid, a substance that exists in the human body under natural circumstances as well, therefore PLLA is generally preferred over PDLA [21]. The body transports the produced L(+) lactic acid to the liver, converts it into pyruvic acid and upon entering the tricarboxylic acid cycle, secreting it as water and carbon dioxide [10].

Despite the FDA-approval of PLLA and the large number of clinical applications, a number of literature studies report inflammatory responses [23, 24]. During degradation, the produced lactic acid can lower the pH in the environment adjacent to the polymer. This local acidity can adversely affect cellular function [25] and induce inflammatory response [26]. Additionally, highly crystalline parts might stay behind which can cause an inflammatory response of the surrounding tissue. However, it was also noted that in case of relatively small material volume, no adverse biological

responses occur. In addition, other literature reports that PLA does not leave significant amounts of accumulating degradation products behind in the body.

The degradation of PLLA *in vitro* occurs in the order of years, whereas *in vivo* degradation takes approximately 8-10 months; degradation of PDLLA is in the order of months [1, 27]. The degradation rate of PLA scaffolds highly depends on amongst others molecular weight and polydispersity of the polymer, process parameters and scaffold design [1].

PLLA exhibit superior mechanical strength compared to PDLLA due to its semi-crystalline nature (10-40 % crystallinity) and higher T_g of around 65 °C versus around 54 °C for PDLLA [28]. Therefore, mostly PLLA is selected over PDLLA as scaffold material, as is also the case for the vast majority of the work presented in this thesis.

2.2.3 Poly(ϵ -caprolactone)

Another polymer selected of the polyester family is poly(ϵ -caprolactone (PCL), a semi-crystalline rubbery polymer with a very low T_g of around -60 °C [21]. Generally PCL degrades by bulk hydrolysis like PLA, although also enzymatic degradation can occur under certain conditions. Degradation is significantly slower compared to PLA due to limited fluid inflow as result of the close packed macromolecules; *in vivo* degradation time extents to over 2 years [1, 29]. Therewith, PCL is mainly suitable for long-term implants.

2.2.4 Poly(tri-methylene carbonate)

Poly(tri-methylene carbonate) (PTMC) is another rubbery material with high elasticity which can be attractive in certain soft TE applications. Amorphous PTMC exhibits a T_g of around -15 °C. High molecular weight PTMC yields relatively good mechanical properties [30].

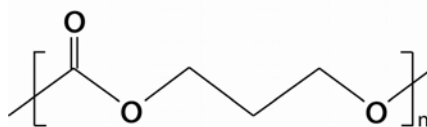


Figure 2 Molecular structure of PTMC.

PTMC hardly degrades in aqueous solutions, whereas it degrades in the order of weeks via enzymatic degradation *in vivo*. Degradation of PTMC does not lead to local decrease of pH in the surrounding tissue of the scaffold, as in the case of e.g. PLA [31, 32]. Chapter 5 is dedicated to scaffold design based on high molecular weight PTMC.

2.2.5 Poly(ethylene oxide)/poly(butylene terephthalate)

This copolymer consists of hydrophilic poly(ethylene oxide) (PEO) and hydrophobic poly(butylene terephthalate) (PBT) segments. Variation in the composition of the PEOT/PBT copolymers allows tailoring of the mechanical, biological and physicochemical properties of the material [33]. Herewith allows PEOT/PBT application in a range of TE constructs, of both soft as well as hard TE origin [34]. PEOT/PBT is well studied as bone filler material, due to the bone-bonding character of the copolymer (especially with a high PEO content) [35-37]. Degradation occurs upon hydrolysis and oxidation and is in the order of months, depending on its composition [33, 35, 36].

2.2.6 Poly(dimethyl siloxane)

Poly(dimethyl siloxane) (PDMS) is extensively used in microfluidics and “lab on a chip” applications as it is easy processable, cheap and transparent offering the opportunity of easy imaging. In the past 10–15 years, there has been an increased interest in the use of microfluidics in TE. The lab on a chip approach allows scientists to control the accuracy of tests, perform high throughput screening of biomaterials regarding cell response or biological reactions in general [38-42]. As these fields more and more expand to biomedical applications, often PDMS is selected within specific studies related to these disciplines [43]. Beneficial is the high gas permeability of PDMS which can be exploited for O₂ supply and CO₂ removal during cell culture. However, thin PDMS sheets have relatively poor mechanical strength and often needs to be coated with e.g. fibronectin to allow good cell attachment.

2.3 Fabrication methods

A great variety of well-known fabrication techniques are used in scaffold design for TE applications. This section briefly describes frequently applied techniques, with in the end special attention to polymer casting and phase separation as these are the main fabrication methods used in this thesis.

2.3.1 Emulsion freeze-drying

In emulsion freeze-drying, homogenization of a polymer–solvent system and water leads to formation of an emulsion [44, 45]. An emulsion exists of two phases, a continuous phase and a dispersed phase within; here, the continuous phase consists of the polymer-rich phase, whereas water is the dispersed phase. The emulsion is cooled down quickly to freeze the solvent and water, resulting in solidification of the polymer directly from the liquid state and the creation of a porous polymer structure. Subsequently, the frozen solvent and water are removed by freeze-drying. Emulsion freeze-drying is attractive for creation of relatively thick scaffolds with large pores. Additionally, incorporation of proteins is enabled during the fabrication of the scaffold. The obtained morphology is mainly non-percolated (solid-wall like pores), which is the major drawback of freeze-drying as this often limits cell in-growth and nutrient transport through the scaffold.

2.3.2 Foaming

In general, foaming uses a soluble inert gas, e.g. CO₂ or N₂, in the supercritical region as blowing agent to create porosity in polymers via pressure quenching [46-48]. Variation of the process conditions enables tuning of the scaffold properties [49]. Instead of using a single polymer, this method is also applicable for composites of polymer and (bio)ceramic to employ in hard TE constructs [50]. Beneficial is the lack of solvent, eliminating the risk of remaining residues, and the low processing temperatures preventing degradation of the polymer during processing. The scaffolds often have a closed surface (skin) and mainly non-percolated pores which can be a serious drawback of the method as these characteristics limit nutrient transport through the scaffold. Nonetheless, it is possible to obtain open porous morphologies in particular cases [51-53]; however, the pore size is often too small for TE applications. Through additional post-processing steps, interconnected pores can be introduced by, for example, plasma treatment or pulsed ultrasound to break the walls of the non-percolated pores [48].

2.3.3 Particle leaching

Particle (or particulate, salt, porogen) leaching combines with various different techniques such as solvent casting [54, 55], compression-molding [56] or foaming [46, 50]. Particle leaching incorporates particles, e.g. salt, sugar or specifically prepared spheres, dissolved in a polymer sample and subsequently washed out after processing the polymer sample into the final form creating (additional) porosity in the scaffold. The biggest advantage of particle leaching is the creation of scaffolds with big pores, well-controlled high interconnected porosity and pore morphology. However, the method is not applicable for all materials such as soluble protein scaffolds and additionally, it may be a time-consuming post-processing method with the risks of remaining residues after processing.

2.3.4 Electrospinning

Electrospinning (ESP) is based upon charging of a polymer solution and subsequent ejection through a capillary tip or needle [57, 58]. The jet coming from the needle draws towards a collector due to an electric field ranging from 10 to 30 kV. Evaporation of the solvent from the jet after leaving the needle results in fiber deposition on the collector. To obtain continuous fibers, the method requires using solutions containing relatively high polymer concentrations of usually around 10-15 wt%. Rotating the collector creates a non-woven mesh with a preferential orientation of the fiber. The diameter of the fibers is within the range of nanometers to microns. Varying the process parameters, e.g. strength of the electric field, distance between needle-collector, polymer concentration, allows tuning of the fiber diameter [36, 59]. Figure 3 presents an example of an electrospun scaffold from PEOT/PBT (reprinted from [36]) with permission from Elsevier). A major advantage of electrospinning is the high flexibility and fiber resolution of the obtained scaffold. Additionally, alignment of the electrospun fibers is enabled to induce cell and tissue alignment [60]. A drawback of electrospinning is the risk of breaking fibers during fabrication, which might lead to inferior quality of the scaffold.

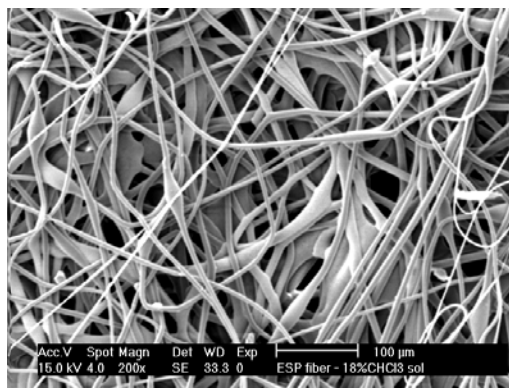


Figure 3 Typical SEM image of a PEOT/PBT 300/55/45 electrospun scaffold (printed from [36] with permission from Elsevier).

2.3.5 Sintering

Sintering refers to heat-treatment of a powder to make the particles adhere to each other. Application of scaffolds fabricated by sintering is mainly in hard TE constructs. Traditionally, sintering uses ceramic powders; however, this method is also applicable for other materials such as metals, glasses and certain polymers as well as composites. In the latter, the heat-treatment pyrolyzes the polymer and the ceramic particles adhere, taking over the porous design of the polymer sheet [20, 61]. The possibility of creating controlled and graded porosity is the main advantage of sintering. Detrimental is the possible risk of low interconnectivity of the pores and the brittleness of the fabricated scaffold in case of using certain materials.

2.3.6 Polymer casting and phase separation

Several fabrication methods based on polymer casting, with or without subsequent phase separation, are frequently applied to produce TE scaffolds. Methods often used for phase separation are e.g. liquid induced phase separation (LIPS, immersion precipitation) [62-64] and thermally induced phase separation (TIPS) [65-68]. Without phase separation, polymer solidification is generally achieved by solvent evaporation [69-72]. These methods allow processing of pure polymers as well as composites of polymer-(bio)ceramic for application in hard TE [73]. In this thesis, generally polymer casting is performed on a micropatterned mold. In this case, due to the solidification of the polymer on the mold, the inverse micropattern is imprinted in the polymer sheet. When combined with LIPS, this technique is called phase separation micro-molding (PSμM) [17, 74-76]. The advantage of PSμM is the combination of micropatterning with porosity both in one fabrication step. Variation of the mold design enables variation in the obtained micropattern.

whereas tuning of the process parameters allows tailoring of the sheet porosity. Figure 4 presents an example of a PLLA sheet fabricated by PS μ M. Chapter 3 describes extensively the application of PS μ M for scaffold fabrication.

The advantage of polymer casting is the possibility to create a wide range of porosities, pore sizes and morphologies. The major drawback of these techniques, however, is the use of organic solvents, which may leave residues after processing and therefore possibly harm the cells. Therefore, effectively washing the scaffolds prior to their contact with cells is essential.

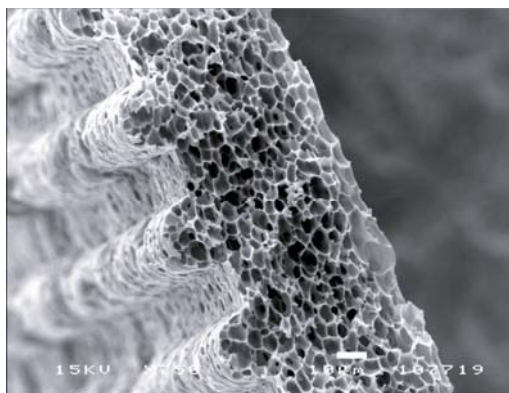


Figure 4 Typical SEM cross-section image of a PLLA sheet prepared by PS μ M. The sheet is prepared of a 5 wt% PLLA-dioxane solution using isopropanol at 4 °C as the non-solvent. The sheet was prepared on a mold featuring 30 μ m wide continuous channels. The bar in the image represents 10 μ m.

2.4 Scaffold design

The design of a scaffold ultimately determines the functionality of the grown tissue. Scaffold design comprehends the material and method used, and additionally the appearance of the construct, i.e. shape, size and surface topography. Applying surface topography in the form of a micropattern can control the behavior of attached cells; tailoring the architectural design of the micropattern can tune the impact on tissue organization [77, 78]. Mimicking the *in vivo* micro-architecture around cells can improve the functionality of the growing tissue [79]. Figure 5 shows an example of cultured C2C12 mouse pre-myoblast cells on a micropatterned PLLA sheet as presented in Figure 4. The arrow indicates the channel direction; clearly the cells align well within the micropatterned channels.

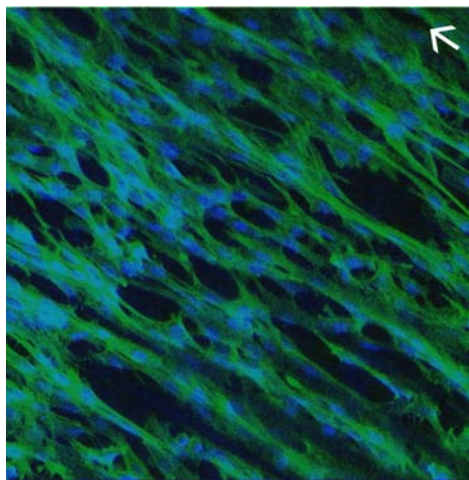


Figure 5 Confocal fluorescence microscopy image of 4 day C2C12 cell cultures on porous PLLA sheets featuring 30 μm wide channels (cell density 25 000 cells/cm²). Magnification 63x, cytoskeleton labeled with Bodipy phalloidin (green) and nucleus labeled with Hoechst (blue). The direction of the channel is indicated by the arrow.

Certain fabrication methods allow fixation of the final scaffold shape and size during processing. Others methods need post-processing steps to obtain the scaffold structure. One way is a multi-layer based design that obtains final 3D shape and size via lamination of stacked 2D layers [80, 81]. First 2D sheets are fabricated using one of the methods described previously. Subsequently, these sheets are stacked together and laminated using heat or chemical adhesion products, e.g. solvent of the material (see Chapter 3, [17]). Benefit of a multi-layer approach is that it allows the introduction of surface topography throughout the 3D-scaffold.

References

1. Hutmacher DW. Scaffolds in tissue engineering bone and cartilage. *Biomaterials* 2000;21(24):2529-2543.
2. Kretlow JD, Mikos AG. From material to tissue: Biomaterial development, scaffold fabrication, and tissue engineering. *AIChE Journal* 2008;54(12):3048-3067.
3. Liu C, Xia Z, Czernuszka JT. Design and Development of Three-Dimensional Scaffolds for Tissue Engineering. *Chemical Engineering Research and Design* 2007;85(7):1051-1064.
4. Moroni L, De Wijn JR, Van Blitterswijk CA. Integrating novel technologies to fabricate smart scaffolds. *Journal of Biomaterials Science-Polymer Edition* 2008;19(5):543-572.
5. Babensee JE, Anderson JM, McIntire LV, Mikos AG. Host response to tissue engineered devices. *Advanced Drug Delivery Reviews* 1998 Aug;33(1-2):111-139.
6. Williams DF. On the mechanisms of biocompatibility. *Biomaterials* 2008;29(20):2941-2953.
7. Hutmacher DW. Scaffold design and fabrication technologies for engineering tissues state of the art and future perspectives. *Journal of Biomaterials Science, Polymer Edition* 2001;12:107-124.
8. Ito Y, Zheng J, Imanishi Y. Enhancement of cell growth on a porous membrane co-immobilized with cell-growth and cell adhesion factors. *Biomaterials* 1997 Feb;18(3):197-202.
9. Mitragotri S, Lahann J. Physical approaches to biomaterial design. *Nat Mater* 2009;8(1):15-23.
10. Agrawal CM, Ray RB. Biodegradable polymeric scaffolds for musculoskeletal tissue engineering. *Journal of Biomedical Materials Research* 2001;55(2):141-150.
11. Karageorgiou V, Kaplan D. Porosity of 3D biomaterial scaffolds and osteogenesis. *Biomaterials* 2005;26:5474-5491.
12. Karande TS, Ong JL, Agrawal CM. Diffusion in musculoskeletal tissue engineering scaffolds: Design issues related to porosity, permeability, architecture, and nutrient mixing. *Annals of Biomedical Engineering* 2004 Dec;32(12):1728-1743.
13. Kannan RY, Salacinski HJ, Sales K, Butler P, Seifalian AM. The roles of tissue engineering and vascularisation in the development of micro-vascular networks: a review. *Biomaterials* 2005;26(14):1857-1875.
14. Dunn GA, Heath JP. A new hypothesis of contact guidance in tissue cells. *Experimental Cell Research* 1976;101(1):1-14.
15. Falconnet D, Csucs G, Michelle Grandin H, Textor M. Surface engineering approaches to micropattern surfaces for cell-based assays. *Biomaterials* 2006;27(16):3044-3063.
16. Flemming RG, Murphy CJ, Abrams GA, Goodman SL, Nealey PF. Effects of synthetic micro- and nano-structured surfaces on cell behavior. *Biomaterials* 1999;20(6):573-588.
17. Papenburg BJ, Vogelaar L, Bolhuis-Versteeg LAM, Lammertink RGH, Stamatialis D, Wessling M. One-step fabrication of porous micropatterned scaffolds to control cell behavior. *Biomaterials* 2007;28(11):1998-2009.
18. Gunatillake PA, Adhikari R. Biodegradable Synthetic Polymers for Tissue Engineering. *European Cells and Materials* 2003;5:1-16.
19. Ramakrishna S, Mayer J, Wintermantel E, Leong KW. Biomedical applications of polymer-composite materials: a review. *Composites Science and Technology* 2001 Jul;61(9):1189-1224.

20. Rezwan K, Chen QZ, Blaker JJ, Boccaccini AR. Biodegradable and bioactive porous polymer/inorganic composite scaffolds for bone tissue engineering. *Biomaterials* 2006;27(18):3413-3431.
21. Engelberg I, Kohn J. Physico-mechanical properties of degradable polymers used in medical applications: A comparative study. *Biomaterials* 1991;12(3):292-304.
22. Gupta AP, Kumar V. New emerging trends in synthetic biodegradable polymers - Polylactide: A critique. *European Polymer Journal* 2007;43(10):4053-4074.
23. Athanasiou KA, Niederauer GG, Agrawal CM. Sterilization, toxicity, biocompatibility and clinical applications of polylactic acid/ polyglycolic acid copolymers. *Biomaterials* 1996;17(2):93-102.
24. Vert M, Christel P, Chabot F, Leray J. *Macromolecular Biomaterials*. 1st ed. New York: CRC / Press Inc., 1984.
25. Sachlos E, Czernuszka JT. Making Tissue Engineering Scaffolds Work. Review: The application of solid freeform fabrication technology to the production of tissue engineering scaffolds *European Cells & Materials Journal* 2003;5:29-40.
26. Karp JM, Shoichet MS, Davies JE. Bone formation on two-dimensional poly(DL-lactide-co-glycolide) (PLGA) films and three-dimensional PLGA tissue engineering scaffolds *in vitro*. *Journal of Biomedical Materials Research Part A* 2003;64A(2):388-396.
27. Laaksovirta S. Biodegradable, Self-Reinforced, Self-Expandable Lactic and Glycolic Acid (SR-PLGA80/20) Copolymer Spiral Prostatic Stent: Analysis of mechanical and biological properties and clinical results. Tampere: Tampere University; 2003.
28. Joziassse CAP, Veenstra H, Grijpma DW, Pennings AJ. On the chain stiffness of poly(lactide)s. *Macromolecular Chemistry and Physics* 1996 Jul;197(7):2219-2229.
29. Coombes AGA, Rizzi SC, Williamson M, Barralet JE, Downes S, Wallace WA. Precipitation casting of polycaprolactone for applications in tissue engineering and drug delivery. *Biomaterials* 2004;25(2):315-325.
30. Pego AP, Poot AA, Grijpma DW, Feijen J. Physical properties of high molecular weight 1,3-trimethylene carbonate and D,L-lactide copolymers. *J Mater Sci-Mater Med* 2003 Sep;14(9):767-773.
31. Zhang Z, Kuijter R, Bulstra SK, Grijpma DW, Feijen J. The *in vivo* and *in vitro* degradation behavior of poly(trimethylene carbonate). *Biomaterials* 2006;27(9):1741-1748.
32. Zhu KJ, Hendren RW, Jensen K, Pitt CG. Synthesis, properties, and biodegradation of poly(1,3-trimethylene carbonate). *Macromolecules* 1991;24(8):1736-1740.
33. Deschamps AA, Claase MB, Sleijster WJ, de Bruijn JD, Grijpma DW, Feijen J. Design of segmented poly(ether ester) materials and structures for the tissue engineering of bone. *Journal of Controlled Release* 2002;78(1-3):175-186.
34. Claase MB. Cell-seeded scaffolds based on poly(ethylene oxide) and poly(butylene terephthalate) block copolymers for bone tissue engineering. Enschede: University of Twente; 2004.
35. Moroni L, de Wijn JR, van Blitterswijk CA. 3D fiber-deposited scaffolds for tissue engineering: Influence of pores geometry and architecture on dynamic mechanical properties. *Biomaterials* 2006;27(7):974-985.
36. Moroni L, Licht R, de Boer J, de Wijn JR, van Blitterswijk CA. Fiber diameter and texture of electrospun PEOT/PBT scaffolds influence human mesenchymal stem cell proliferation and morphology, and the release of incorporated compounds. *Biomaterials* 2006;27(28):4911-4922.
37. Papadaki M, Mahmood T, Gupta P, Claase MB, Grijpma DW, Riesle J, et al. The different behaviors of skeletal muscle cells and chondrocytes on PEGT/PBT block copolymers are related to the

surface properties of the substrate. *Journal of Biomedical Materials Research Part A* 2001;54(1):47-58.

38. Anderson DG, Putnam D, Lavik EB, Mahmood TA, Langer R. Biomaterial microarrays: rapid, microscale screening of polymer-cell interaction. *Biomaterials* 2005 Aug;26(23):4892-4897.

39. Andersson H, Berg Avd. Microfabrication and microfluidics for tissue engineering: state of the art and future opportunities. *Lab on a Chip* 2004;4:98-103.

40. Andersson H, van den Berg A. Microfluidic devices for cellomics: a review. *Sensors and Actuators B-Chemical* 2003 Jul 15;92(3):315-325.

41. Andersson H, van den Berg A. Microtechnologies and nanotechnologies for single-cell analysis. *Current Opinion in Biotechnology* 2004 Feb;15(1):44-49.

42. El-Ali J, Sorger PK, Jensen KF. Cells on chips. *Nature* 2006 Jul 27;442(7101):403-411.

43. Mata A, Fleischman A, Roy S. Characterization of Polydimethylsiloxane (PDMS) Properties for Biomedical Micro/Nanosystems. *Biomedical Microdevices* 2005;7(4):281-293.

44. Ho M-H, Kuo P-Y, Hsieh H-J, Hsien T-Y, Hou L-T, Lai J-Y, et al. Preparation of porous scaffolds by using freeze-extraction and freeze-gelation methods. *Biomaterials* 2004;25(1):129-138.

45. Whang K, Thomas CH, Healy KE, Nuber G. A novel method to fabricate bioabsorbable scaffolds. *Polymer* 1995;36(4):837-842.

46. Harris LD, Kim B-S, Mooney DJ. Open pore biodegradable matrices formed with gas foaming. *Journal of Biomedical Materials Research* 1998;42(3):396-402.

47. Singh L, Kumar V, Ratner BD. Generation of porous microcellular 85/15 poly (dl-lactide-co-glycolide) foams for biomedical applications. *Biomaterials* 2004;25(13):2611-2617.

48. Wang X, Li W, Kumar V. A method for solvent-free fabrication of porous polymer using solid-state foaming and ultrasound for tissue engineering applications. *Biomaterials* 2006;27(9):1924-1929.

49. Lips PAM, Velthoen IW, Dijkstra PJ, Wessling M, Feijen J. Gas foaming of segmented poly(ester amide) films. *Polymer* 2005 Oct 24;46(22):9396-9403.

50. Kim S-S, Sun Park M, Jeon O, Yong Choi C, Kim B-S. Poly(lactide-co-glycolide)/hydroxyapatite composite scaffolds for bone tissue engineering. *Biomaterials* 2006;27(8):1399-1409.

51. Krause B, Diekmann K, van der Vegt NFA, Wessling M. Open nanoporous morphologies from polymeric blends by carbon dioxide foaming. *Macromolecules* 2002 Feb 26;35(5):1738-1745.

52. Krause B, Koops GH, van der Vegt NFA, Wessling M, Wubbenhorst M, van Turnhout J. Ultralow-k dielectrics made by supercritical foaming of thin polymer films. *Advanced Materials* 2002 Aug 5;14(15):1041-+.

53. Krause B, Sijbesma HJP, Munuklu P, van der Vegt NFA, Wessling M. Bicontinuous nanoporous polymers by carbon dioxide foaming. *Macromolecules* 2001 Dec 4;34(25):8792-8801.

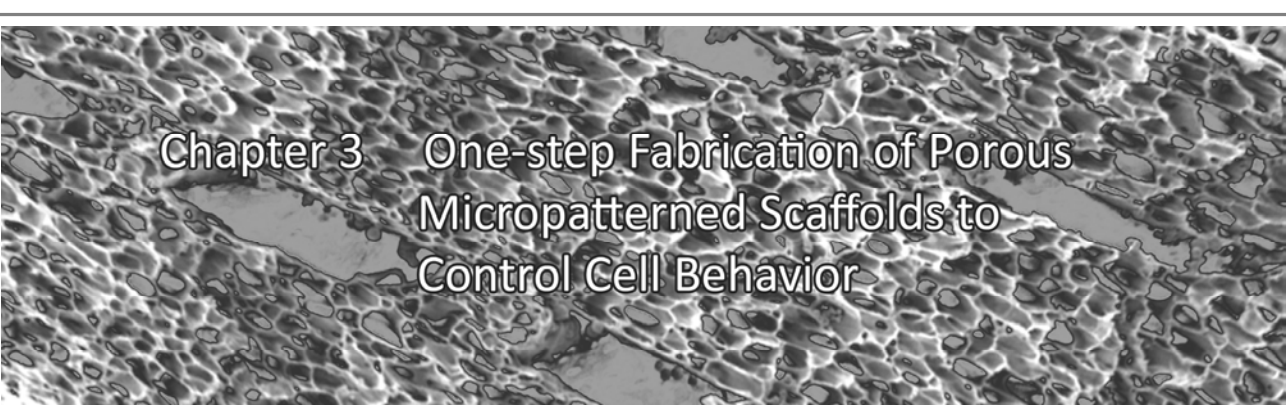
54. Ma PX, Choi J-W. Biodegradable Polymer Scaffolds with Well-Defined Interconnected Spherical Pore Network. *Tissue Engineering* 2001;7(1):23-33.

55. RoyChowdhury P, Kumar V. Fabrication and evaluation of porous 2,3-dialdehyde cellulose membrane as a potential biodegradable tissue-engineering scaffold. *Journal of Biomedical Materials Research Part A* 2006;76A(2):300-309.

56. Katoh K, Tanabe T, Yamauchi K. Novel approach to fabricate keratin sponge scaffolds with controlled pore size and porosity. *Biomaterials* 2004;25(18):4255-4262.

57. Bhattarai SR, Bhattarai N, Viswanathamurthi P, Yi HK, Hwang PH, Kim HY. Hydrophilic nanofibrous structure of polylactide; fabrication and cell affinity. *Journal of Biomedical Materials Research Part A* 2006;78A(2):247-257.
58. Riboldi SA, Sampaolesi M, Neuenschwander P, Cossu G, Mantero S. Electrospun degradable polyesterurethane membranes: potential scaffolds for skeletal muscle tissue engineering. *Biomaterials* 2005;26(22):4606-4615.
59. Boudriot U, Dersch R, Greiner A, Wendorff JH. Electrospinning Approaches Toward Scaffold Engineering - A Brief Overview. *Artificial Organs* 2006;30(10):785-792.
60. Buttafoco L, Engbers-Buijtenhuijs P, Poot AA, Dijkstra PJ, Vermes I, Feijen J. Physical characterization of vascular grafts cultured in a bioreactor. *Biomaterials* 2006 Apr;27(11):2380-2389.
61. Deisinger U, Stenzel F, Ziegler G. Development of hydroxyapatite ceramics with tailored pore structure. *Bioceramics* 2004;254-2(16):977-980.
62. Kim SY, Kanamori T, Noumi Y, Wang O-C, Shinbo T. Preparation of porous poly(d,l-lactide) and poly(d,l-lactide-co-glycolide) membranes by a phase inversion process and investigation of their morphological changes as cell culture scaffolds. *Journal of Applied Polymer Science* 2004;92:2082-2092.
63. Liu H-C, Lee IC, Wang J-H, Yang S-H, Young T-H. Preparation of PLLA membranes with different morphologies for culture of MG-63 Cells. *Biomaterials* 2004;25(18):4047-4056.
64. Zoppi RA, Contant S, Duek EAR, Marques FR, Wada MLF, Nunes SP. Porous poly(L-lactide) films obtained by immersion precipitation process: morphology, phase separation and culture of VERO cells. *Polymer* 1999 Jun;40(12):3275-3289.
65. Guan J, Fujimoto KL, Sacks MS, Wagner WR. Preparation and characterization of highly porous, biodegradable polyurethane scaffolds for soft tissue applications. *Biomaterials* 2005;26(18):3961-3971.
66. Hua FJ, Kim GE, Lee JD, Son YK, Lee DS. Macroporous poly(L-lactide) scaffold 1. Preparation of a macroporous scaffold by liquid-liquid phase separation of a PLLA-dioxane-water system. *Journal of Biomedical Materials Research* 2002;63(2):161-167.
67. Li S, Carrubba VL, Piccarolo S, Sannino D, Brucato V. Preparation and properties of poly(L-lactic acid) scaffolds by thermally induced phase separation from a ternary polymer-solvent system. *Polymer International* 2004;53(12):2079-2085.
68. Nam YS, Park TG. Porous biodegradable polymeric scaffolds prepared by thermally induced phase separation. *Journal of Biomedical Materials Research* 1999;47(1):8-17.
69. Htay AS, Teoh SH, Hutmacher DW. Development of perforated microthin poly(epsilon-caprolactone) films as matrices for membrane tissue engineering. *Journal of Biomaterials Science-Polymer Edition* 2004;15(5):683-700.
70. Park YJ, Nam KH, Ha SJ, Pai CM, Chung CP, Lee SJ. Porous poly(L-lactide) membranes for guided tissue regeneration and controlled drug delivery: Membrane fabrication and characterization. *Journal of Controlled Release* 1997 Jan 18;43(2-3):151-160.
71. Tanaka M, Takebayashi M, Miyama M, Nishida J, Shimomura M. Design of novel biointerfaces (II). Fabrication of self-organized porous polymer film with highly uniform pores. *Bio-Medical Materials And Engineering* 2004;14(4):439-446.
72. Vaquette C, Fawzi-Grancher S, Lavalley P, Frochot C, Viriot ML, Muller S, et al. In vitro biocompatibility of different polyester membranes. *Bio-Medical Materials And Engineering* 2006;16(4):S131-S136.

73. Causa F, Netti PA, Ambrosio L, Ciapetti G, Baldini N, Pagani S, et al. Poly- ϵ -caprolactone/hydroxyapatite composites for bone regeneration: In vitro characterization and human osteoblast response. *Journal of Biomedical Materials Research Part A* 2006;76A(1):151-162.
74. Jong Jd, Ankone B, Lammertink RGH, Wessling M. New replication technique for the fabrication of thin polymeric microfluidic devices with tunable porosity. *Lab on a chip* 2005;5(11):1240-1247.
75. Rijn CJMV, Vogelaar L, Nijdam W, Barsema JN, Wessling M, inventors. Method of making a product with a micro or nano-sized structure and product, 2002.
76. Vogelaar L, Barsema JN, Rijn CJMv, Nijdam W, Wessling M. Phase separation micromolding - PSM. *Advanced Materials* 2003;15(16):1385-1389.
77. Singhvi R, Stephanopoulos G, Wang DIC. Effects of substratum morphology on cell physiology. *Biotechnology and Bioengineering* 1994;43(8):764-771.
78. Vernon RB, Gooden MD, Lara SL, Wight TN. Microgrooved fibrillar collagen membranes as scaffolds for cell support and alignment. *Biomaterials* 2005;26(16):3131-3140.
79. Tsang VL, Bhatia SN. Three-dimensional tissue fabrication. *Advanced Drug Delivery Reviews* 2004;56(11):1635-1647.
80. Borenstein JT, Terai H, King KR, Weinberg EJ, Kaazempur-Mofrad MR, Vacanti JP. Microfabrication technology for vascularized tissue engineering. *Biomedical Microdevices* 2002 Jul;4(3):167-175.
81. Vozzi G, Flaim C, Ahluwalia A, Bhatia S. Fabrication of PLGA scaffolds using soft lithography and microsyringe deposition. *Biomaterials* 2003;24:2533-2540.

A scanning electron micrograph (SEM) showing a highly porous, interconnected network of fibers or ridges, forming a scaffold structure. The pores are irregular in shape and size, creating a complex, sponge-like appearance. The text is overlaid on the top left of this image.

Chapter 3 One-step Fabrication of Porous Micropatterned Scaffolds to Control Cell Behavior

Abstract

This paper reports a one-step method to fabricate highly porous micropatterned 2-D scaffold sheets. The scaffold sheets have high glucose diffusion, indicating that the porosity and pore morphology of the scaffolds are viable with respect to nutrient transport, and a micropattern for cell alignment. HUVEC culturing proved that the scaffold sheets are suitable for cell culturing. More extensive culturing experiments with mouse myoblasts, C2C12, and mouse osteoblasts, MC3T3, showed that tissue organization can be controlled; the micropattern design affects the extent of cell alignment and tissue formation. Cells are favourably placed in the micropattern and even at higher confluence levels, when the cells start to overgrow the ridges of the micropattern, these cells align themselves in the direction of the micropattern. Preliminary multi-layer stacking experiments indicate that the 2-D scaffold sheets are very promising as basis for building 3-D scaffolds.

This chapter has been published:

Bernke J. Papenburg, L. Vogelaar, L.A.M. Bolhuis-Versteeg, R.G.H. Lammertink, D. Stamatialis, M. Wessling

Biomaterials, 28 (2007) 1998-2009

3.1 Introduction

Tissue engineering originates from reconstructive surgery using donor tissue to repair damaged tissue. Direct transplantation of tissue is still the most common method to restore tissue functions. However, direct transplantation of a whole organ or large areas such as skin is often not feasible. Frequently, autogenic transplants are not available and problems of rejection, pathogen transmission and lack of sufficient donor organs are inevitable for allogenic transplants. Therefore, the possibility to provide an autogenic transplant by constructing a tissue engineered replacement *in vitro* can be an excellent alternative. Consequently, the last years great efforts have been focused on tissue engineering [1-4].

One of the major themes in tissue engineering is scaffold fabrication. A scaffold is an artificial extra cellular matrix (ECM) which serves as temporary support where isolated cells are introduced to form tissue. The scaffold should be biocompatible, biodegradable, promote cell attachment and should be mechanical stable [5-8]. High porosity and pore connectivity is essential to ensure sufficient nutrient diffusion through the scaffold, i.e., transport of oxygen and nutrients towards the cells and allow metabolic products to be removed [9]. Furthermore, porosity appears to have a positive effect on cell attachment as well [10]. Moreover, early studies suggest micropatterned scaffolds improve tissue formation. Cell attachment and cell orientation are promoted due to guidance of the cells by a patterned micro-architecture, leading to better implants since *in vitro* tissue which closely mimics *in vivo* tissue organization will maintain its functionality better. An optimum design of the micropatterned scaffold appears to be crucial for tissue engineering [11-14].

Current fabrication methods do not combine the production of porous scaffolds with pore-sizes in the micrometer-scale and the enclosure of micropatterning. Several researchers design scaffolds which are only porous using various methods e.g., foaming [15, 16], particulate-leaching [17, 18], immersion precipitation [19, 20] and freeze drying [21, 22]. These methods prepare porous scaffolds in geometries like sheets and cubes. Others design only micropatterned scaffolds using various techniques [14, 23-25], such as soft lithography. In soft lithography, micro-contact printing is commonly used. In this case, an elastomeric 'stamp' (e.g. Poly(dimethyl)-siloxane (PDMS)) is produced to stamp an ink micropattern on the scaffold surface. Subsequently, a coating is often applied on the parts of the surface without ink. Soft lithography requires rigid surfaces for precise patterning which limits the materials that can be used for patterning. Furthermore, all these additional post-processing steps result in a chemically coated surface which might be unstable on the long-term since the serum in the cell culture medium can affect the coating [23, 26].

Only recently research has been performed to create porosity into an already prepared dense micropatterned scaffold. This method involved the combination of soft-lithography and melt molding to fabricate the dense micropatterned sheets and post processing particulate leaching of

micro/nanospheres to create pores [27]. Although the diffusion of nutrients through these scaffolds was increased compared to dense scaffolds, the pores appeared to be isolated voids without good interconnectivity.

It is evident that there is need for a easy fabrication method which combines micro-patterning directly with the fabrication of highly porous scaffolds, resulting in highly improved scaffolds [27]. Additionally, the exact regulation of the pore size of the micropatterned scaffolds is highly significant, too. If the pores have an average size of tens of micrometers or more, the cells will conform to this pore morphology instead of the applied micropattern, leading to decreased cell organization [27]. However, if the pores are too small, nutrient diffusion will be limited. Therefore, an optimal pore-size should be addressed, which depends on various parameters, e.g. the type of cell, and has to be determined experimentally.

In this work, we fabricate scaffolds having both high porosity with controllable micrometer-scale pores and incorporated micropatterns of excellent quality. Our method is called Phase Separation Micromolding (PS μ M). In one step highly porous micropatterned sheets can be obtained due to immersion precipitation of a polymer on a micropatterned mold [28, 29]. A great advantage of PS μ M is the broad range of pore size, porosity and interconnectivity that can be obtained by fine-tuning the phase separation process parameters. The pore morphology can be tuned such that adequate nutrient diffusion to the cells can be achieved without disturbing the tissue organization induced by the micropattern. Additionally, PS μ M enables processing of a large range of materials. The only requirement for a material to be suitable for PS μ M is the existence of a solvent and a non-solvent which is miscible with the solvent [28, 29]. Therefore, directly implantable materials can be used as well.

In this study we use PS μ M to prepare in one step micropatterned porous 2-D scaffold sheets using various polymers. The porosity and pore size is tuned for adequate nutrient diffusion and the scaffold sheets control cell organization through micropatterning. A proof-of-principle is presented of multi-layer stacking 2-D scaffold sheets into a 3-D scaffold for tissue engineering.

3.2 Background phase separation micromolding (PS μ M)

PS μ M is a microfabrication method based on immersion precipitation on a micropatterned mold (see Figure 1) [28, 29]. Prior to preparation of the micropatterned polymer sheets, a master mold with a micro-architecture has to be fabricated from a silicon wafer using technologies derived from microelectronics and photolithography [28, 29]. PS μ M comprises of three parts: (I) casting a polymer solution onto the mold, (II) immersing the mold with the polymer solution into the non-solvent bath. Phase separation is initiated due to solvent and non-solvent liquid exchange leading to a situation where the polymer solution contains sufficient non-solvent to precipitate. Solidification of the micropatterned polymer sheet takes place on the mold, where the inverse replication of the micropattern is imprinted in the polymer sheet. (III) the solidified micropatterned polymer sheet is released from the mold.

Many parameters influence the porosity and pore morphology of polymer sheets obtained by immersion precipitation [30, 31], e.g. the choice of polymer, solvent and non-solvent, polymer solution concentration, the temperature of the polymer solution and/or the coagulation bath. Concerning tissue engineering, often the average scaffold porosity is evaluated. This can often be misleading; some sheets might have relatively high porosity yet might not be suitable for nutrient diffusion mainly due to two key features: non-percolating cellular structure and skin formation. Sheets with a cellular structure contain isolated closed pores, implying low interconnectivity, and sheets containing a skin show a thin dense outer layer limiting the diffusion.

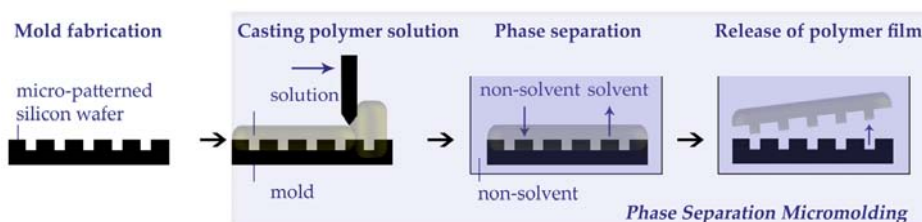


Figure 1 Schematic illustration of the Phase Separation Micromolding process.

3.3 Materials and Methods

3.3.1 Micropatterned porous scaffold preparation

Micropatterned sheets were fabricated using various recipes of PS μ M. The molecular weight (M_w) of the polymer can have a significant effect on the mechanical properties of the prepared sheets. Sheets prepared by polymers of high M_w usually have better mechanical stability. Therefore, in this study we selected known biocompatible and biodegradable polymers of relatively high M_w . The polymers used were: poly(L-lactic acid) (PLLA, $M_w = 1.6 \times 10^5$ g/mol, kindly provided by Dr. D. Grijpma, University of Twente, The Netherlands), poly(D,L-lactic acid) (PDLLA, Polysciences, $M_w = 3.3 - 6 \times 10^5$ g/mol) and poly(ϵ -caprolactone) (PCL, Solvay, CAPA 680, $M_w = \sim 8 \times 10^4$ g/mol). Dioxane and chloroform (both Merck, analytical quality) were used as solvent whereas several alcohols with increasing number of carbons: methanol, ethanol, isopropanol, isobutanol (Merck, analytical quality) and isopentanol (Acros, extra pure) were used as non-solvents. The polymer concentrations of the PLLA and PDLLA polymer solutions were 5, 7.5, and 10 wt%, whereas the PCL polymer solutions were 12.5 and 15 wt%. Generally, the micropatterned sheets were prepared at room temperature ($T = 23 \pm 2$ °C); however, in some cases the temperature of the non-solvent bath was decreased to 4 °C (see details later). The sheets were first casted on the mold and directly placed in the non-solvent bath. After releasing from the mold, they were left in the non-solvent for one day to ensure complete removal of the solvent. Subsequently, the sheets were washed thoroughly with Milli-Q water and dried in a controlled atmosphere ($T = 20$ -23 °C).

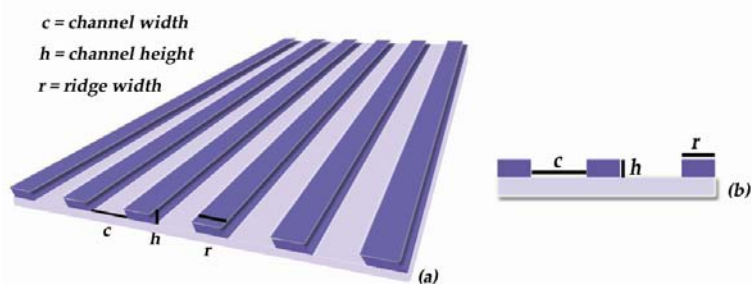


Figure 2 Schematic illustration of the mold design with (a) top view and (b) side view.

The micropatterned molds are fabricated by silicon micromachining. First, a micro-architecture is designed and a mask is prepared of this design. Then, the mask is used for specific application of photo-resist on a flat silicon wafer, which is subsequently etched to create the micropatterned mold. More detail on fabrication of the molds can be found in [29].

Various micropatterned molds were designed to determine the effect of the patterning on cell growth and alignment. Figure 2 illustrates the mold whereas Table 1 presents their specifications (c: channel width, h: channel height, r: ridge width). Mold I has no channels/pattern, mold II and III have channels of various dimensions and for mold IV, the ridges are periodically broken up to enable cells in adjacent channels to be in contact.

Table 1 Specification of the micropatterned molds and the polymer sheet replicas.

| Mold type | Mold design (μm) | | | Polymer sheet replication (μm) | | | Remarks |
|-----------|-------------------------------|----|----|---|-----|-----|---|
| | c | h | r | c | h | r | |
| I | -- | -- | -- | --- | --- | --- | non-patterned, as reference |
| II | 25 | 30 | 25 | 20 | 15 | 25 | |
| III | 300 | 70 | 50 | 250 | 45 | 40 | |
| IV | 20 | 15 | 10 | 16 | 7 | 9 | ridges are broken up periodical every 95 μm for 10 μm |

3.3.2 Porosity and pore morphology determination

The inner- and surface porosity and pore morphology of the sheets was determined via image analysis using Scanning Electron Microscopy (SEM, JEOL T220 and JEOL 5600LV). Besides image analysis, the porosity of the micropatterned sheets was estimated using the equations:

$$\text{porosity (\%)} = \frac{\text{bulk volume (m}^3\text{)} - \text{skeletal volume (m}^3\text{)}}{\text{bulk volume (m}^3\text{)}} \times 100 \quad (1)$$

Where:

$$\text{bulk volume (m}^3\text{)} = \text{width (m)} \times \text{length (m)} \times \text{thickness (m)} \quad (2)$$

$$\text{skeletal volume (m}^3\text{)} = \frac{\text{weight (g)}}{\text{density (g/m}^3\text{)}} \quad (3)$$

The density of the polymers was determined by a pycnometer (Micromeritics Accupyc 1330).

3.3.3 Nutrient transport

Evaluation of the micropatterned sheets as scaffold for tissue engineering was also performed via glucose diffusion experiments. Glucose is one of the nutrients for cells and is therefore a representative indicator for nutrient transport through the sheets. Figure 3 shows a schematic representation of the glucose diffusion device. A 10-fold of the glucose concentration in blood was used in all experiments; 10 g/L (57 mmol/l, SigmaUltra, D-(+)-glucose, 99.5% GC).

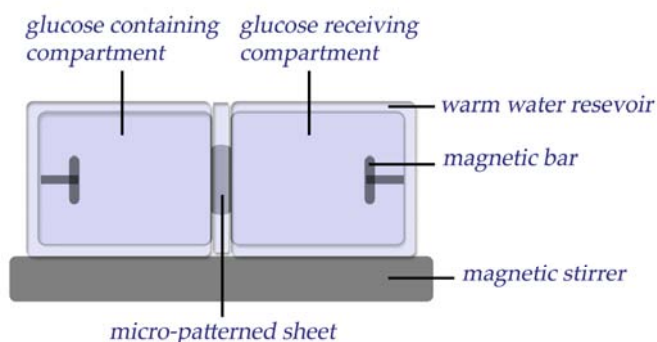


Figure 3 Schematic representation of the glucose diffusion device.

One compartment (donor) contained the glucose solution, whereas the other compartment (acceptor) contained pure water. The sheet was placed in the middle of the two compartments. Before starting the experiment, the sheet was pre-wetted for several hours with an ethanol to water gradient to ensure full wetting. Both compartments were double walled and kept at 37 °C with circulating water. At various time intervals, samples of 0.5 ml were taken from both compartments. The glucose concentration was determined using an enzymatic assay (PGO Enzymes, Sigma) [32]. The glucose in the sample reacted with the enzyme, resulting in an orange coloured solution. The sample was subsequently analyzed by a UV spectrophotometer (Varian Cary 300 scan) at $\lambda = 450$ nm.

Due to the concentration difference, glucose passes through the sheet from the donor to the acceptor compartment. The amount of glucose that passes through the sheet vs. time is an indication for the porosity and interconnectivity of the sheet. The permeability is a measure for the diffusion in time and can be calculated through the flux using the equation:

$$flux \ (g \ m^{-2} \ s^{-1}) = \frac{[C_{acceptor} \ (g \ m^{-3}) \times V_{acceptor} \ (m^3) / S \ (m^2)]}{time \ (s)} \quad (4)$$

where $C_{acceptor}$, the glucose concentration in the acceptor, $V_{acceptor}$, the volume of the acceptor compartment and S , the surface area of the micropatterned sheet is. The glucose permeability can be calculated:

$$permeability \ (m^2 \ s^{-1}) = \frac{flux \ (g \ m^{-2} \ s^{-1})}{\Delta C \ (g \ m^{-3})} \times l \ (m) \quad (5)$$

where ΔC is the concentration difference between the donor and the acceptor and l is the average thickness of the micropatterned sheet. From the permeability, the diffusion coefficient can be determined:

$$diffusion \ coefficient \ (m^2 \ s^{-1}) = \frac{permeability \ (m^2 \ s^{-1})}{K} \quad (6)$$

with K being the partitioning coefficient. Because the glucose molecule is small in comparison to the pore size, K can be assumed to be equal to one.

3.3.4 Cell culturing

Cell culturing experiments were performed using various cell types. HUVEC (human umbilical vein endothelial cells) and HMEC (human microvascular endothelial cells) were used in preliminary experiments to determine the effectiveness of the sheets as scaffold material. C2C12 (mouse myoblasts) and MC3T3 (mouse osteoblasts) cells were used to study the influence of the micropattern on cell alignment and tissue formation.

Culturing: The micropatterned scaffold sheets were placed in 24-well-plates (Corning Inc., Costar 3526), an o-ring (Viton, type 51414, 14x1) of exactly the inner diameter of the well was placed on top of each sheet to keep the scaffolds down to the bottom of the well. Then, the scaffold sheets were

sterilized with ethanol and isopropanol and subsequently washed and pre-wetted with phosphate buffer saline solution (PBS). Cells were trypsinized from a culture flask and diluted with medium to the desired concentration. The cells were added on top of the micropatterned sheets at a cell density of 40,000 (HUVEC and HMEC) or 25,000 cells/cm² (C2C12 and MC3T3). The medium used for HUVEC/HMEC was 1:1 RPMI 1640/M 199 supplemented with 1 % Pen/Strep, 1 % glutamax and 20 % human serum. For C2C12, the medium was DMEM supplemented with 1 % Pen/Strep and 10 % FBS. Medium used for MC3T3 was α -MEM supplemented with 1 % Pen/Strep, 1 % L-glutamine, 1 % Sodium Pyruvate and 10 % FBS. Every 2-3 days, the medium was renewed. The cell-cultured sheets were kept in an incubator at 37 °C and 5 % CO₂ for several days (varied between 2 and 10 days).

Fixation and staining: The cells were fixated for at least 30 min using a 4 %-formaldehyde solution. After fixation, the C2C12/MC3T3 cultured scaffold sheets were stained by methylene blue for light-microscopy. After adding methylene blue for approx. 5 min, the sheets were washed 3 times with PBS before analysis. For confocal fluorescence microscopy, the scaffold sheets were washed with PBS directly after fixation. Subsequently, the cells were permeabilized by a 0.1 % triton-X100 solution for 1 min, washed with PBS and incubated with a 0.05 % Bodipy-phalloidin solution (Molecular probes) for 10 min to label the cell cytoskeleton. After washing with PBS, the scaffold sheets were ready for analysis.

Analysis: The HUVEC/HMEC cultured scaffold sheets were analyzed by light microscopy (Zeiss Axiovert 40 mat & AxioCam MRC 5 camera) during the cell culture without harming the cells.

The C2C12/MC3T3 cell-cultured sheets were analyzed by light microscopy and complementary with confocal fluorescence microscopy (Zeiss LSM 510). To determine the extent of alignment, a grid was projected on the confocal fluorescence microscopy images [33, 34]. One axis (Y) of the grid ran parallel to the channels, where the other axis (X) ran perpendicular to the channels. The extent of alignment was calculated determining the amount of cells crossing the grid lines:

$$alignment (\%) = \frac{X - Y}{X + Y} \times 100 \quad (7)$$

For a 3-D scaffold, nutrient transport through the scaffold should be enabled by the inner-porosity. In addition to the glucose diffusion experiments, a culturing experiment was performed to simulate nutrient diffusion through the scaffold sheet. Scaffold sheets of exactly the size of the inner diameter of a well (24-well plate) were prepared. Subsequently C2C12 cells were seeded on the micropattern (see method described previously). After approximately 3 hours attaching of the cells, half of the cell-cultured sheets were turned up side down in the wells. The o-ring was placed tightly on top of each sheet to ensure that no leakage of nutrients via the sides would take place. In this case, nutrient supply to the cells can only be achieved by nutrient transport through the inner-porosity of the sheets. After 2 and 4 days, the turned sheets were compared to the reference sheets where the cells were in direct contact to the medium and oxygen (fixation, staining and analysis described previously).

3.3.5 3-D scaffolds proof-of-principle

The 2-D micropatterned sheets can be built into a 3-D scaffold by multi-layer stacking immediately after casting. Then, residues of the solvent are still present in the sheets enabling the layers to bond. Stacking was achieved through two different methods; by either clamping several films between glass-plates or rolling up one or more sheets around a tube. Through the combination of pressure applied and softened material, the layers bond. After clamping or rolling up, the sheets were left in the non-solvent bath for one day. Subsequently, the sheets were washed thoroughly with water (Milli-Q) and dried in a controlled atmosphere after which, in case of clamping, the glass-plates were removed. Both methods achieve firm contact of the sheets.

3.4 Results and Discussion

3.4.1 Micropatterned sheet preparation

In order to determine the effect of the micro-architecture on cell behavior, various molds were fabricated from silicon wafers. Table 1 presents the dimensions (length, width, dept) of the designed micro-architectures of the master molds. The molds featuring the different micropattern designs are indicated in the rest of the text as type I – IV (see details Table 1). Using PS μ M, polymer replicas were prepared. Table 1 presents the dimensions of these replicas as well. Since low polymer concentrations were used, the shrinkage during the phase separation process was significant. In fact, the micropattern dimensions of the polymer sheet surface were up to 20% smaller compared to the master mold design where the channel dept shrunk up to 50%. The shrinkage was taken into account when designing the master mold, therefore, it was well controlled and the replicated features were of very good quality. Besides, the shrinkage helps easy release of the sheet from the mold.

3.4.2 Porosity and pore morphology determination

Figure 4 shows typical SEM pictures of the wide variety of prepared morphologies, varying from very dense to very porous depending on the recipe. For three different polymers the effect of various parameters, i.e. solvent, polymer concentration and non-solvent, was determined.

Table 2 represents the results of the porosity of the various structures determined by Equations 1-3. As mentioned in the remarks of Table 2, in some cases cellular structure and/or skin formation was observed. Both characteristics are disadvantageous since they will lead to decreased nutrient transport trough the sheet.

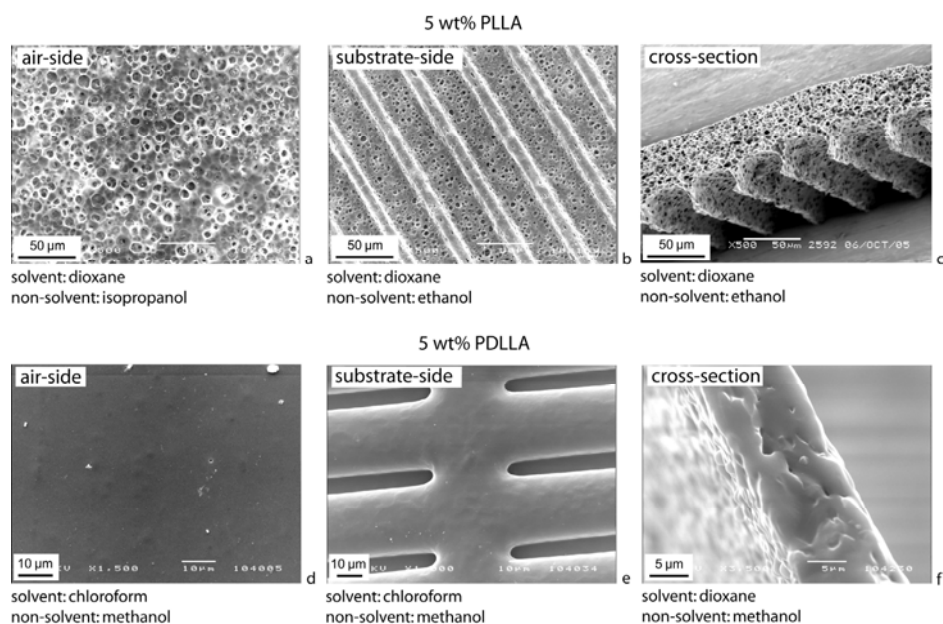


Figure 4 Typical SEM pictures of films obtained by PS μ M indicating broad porosity that can be obtained; (a-c) non-solvent at 4 °C, (d-f) non-solvent bath at 23 °C.

PLLA: In the case of PLLA, the solvent has a significant effect on the porous structure. Dioxane appears most suitable as solvent since higher porosities and generally higher pore size is obtained in comparison to chloroform (Table 2). Since dioxane is less volatile compared to chloroform, the evaporation rates are decreased. Therefore, the solidification is delayed and the film has less skin formation and higher overall porosity. When increasing the PLLA concentration from 5 to 7.5 and 10wt% in dioxane, the sheet becomes less porous (Table 2). Finally, the effect of the different alcohols as non-solvents seems to be marginal in terms of porosity. However, the quality of the structure was better for ethanol and isopropanol.

More experiments were performed to optimize the structure of these sheets. In these experiments, the temperature of the non-solvent bath was decreased to 4 °C. This had an extensive impact on the skin formation of the sheets leading to significantly higher surface porosity and probably pore-interconnectivity. Figure 4a-c presents very porous structures obtained for PLLA-dioxane sheets using these two non-solvents at 4 °C.

Table 2 Porosity determination various films prepared by PS μ M.

| Polymer | Solvent | Wt% | Non-solvent | Porosity (%) | Average porosity (%) | Pore size range (μ m) | Remarks |
|---------|------------|------|------------------------|--------------|----------------------|----------------------------|-------------------------|
| PLLA | chloroform | 5 | ethanol isopropanol | 55.2 67.9 | 61.6 | 2 - 4 | cellular & skin |
| PLLA | dioxane | 5 | methanol | 82.1 | 81.3 | 5 - 6 | good quality structures |
| | | | ethanol | 78.9 | | 5 - 8 | |
| | | | isopropanol | 83.9 | | 5 - 9 | |
| | | | isobutanol | 79.9 | | 5 - 9 | |
| | | | isopentanol | 81.7 | | 2 - 10 | |
| PLLA | dioxane | 7.5 | ethanol | 75.9 | 75.7 | 1 - 3 | good quality structures |
| | | | isopropanol | 75.5 | | 2 - 5 | |
| PLLA | dioxane | 10 | ethanol | 61.9 | 70.3 | 3 - 4 | good quality structures |
| | | | isopropanol | 78.6 | | 2 - 4 | |
| PDLLA | chloroform | 5 | methanol | no | no | --- | dense |
| | | | ethanol | 63.7 | 64.0 | 0.2-1.5 | cellular & skin |
| | | | isopropanol | 64.2 | | 0.5-1.5 | |
| PDLLA | dioxane | 5 | methanol | no | no | --- | dense |
| | | | ethanol | 28.3 | 28.2 | 0.2 - 2 | collapsed pores |
| | | | isopropanol | 28.0 | | 0.2 - 1 | |
| PCL | chloroform | 12.5 | ethanol | 47.1 | 51.7 | 3-13 | cellular & skin |
| | | | isopropanol | 56.3 | | 5-13 | |

PDLLA: In the case of PDLLA, the solvent and non-solvent have a significant effect on the sheet structure. With either chloroform or dioxane as solvent and methanol as non-solvent, the structure is non porous (Table 2 and Figure 4d-f). For dioxane, porosity of only 28 % can be achieved when ethanol and isopropanol are used as non-solvents, which is probably due to pore collapse during solidification (Table 2). For chloroform, however, a porosity of ~64 % can be achieved using these alcohols as non-solvent, although a dense skin was formed.

PCL: PCL sheets could not be prepared at polymer concentrations lower than 10 wt%. Due to the high polymer content, less polymer lean phase is formed resulting in rather moderate porosity of 51.7% (Table 2).

Considering the purpose of the sheets as scaffolds, and the accompanying requirements, sheets prepared from 5 wt% PLLA in dioxane solutions with the non-solvent bath at 4°C show the most promising features, i.e., high porosity and probably pore-interconnectivity. Estimation of the porosity by calculation does not always give the best insight into the real porosity and most importantly pore-interconnectivity, which are highly important with respect to nutrient diffusion limitations. Therefore, these 5 wt% PLLA-dioxane scaffolds were examined in more detail with regard to nutrient transport.

3.4.3 Nutrient transport

Figure 5 shows typical results of glucose diffusion in time through a 5 wt% PLLA-dioxane sheet. Figure 5a shows the transport over a period of 96 hours, whereas Figure 5b focuses on the first 24 hours. In both graphs, the results of two different sheets are displayed. One is porous and interconnected, where high diffusion is reached (sheet prepared by isopropanol as the non-solvent at 4 °C). The second is denser or has lower pore-interconnectivity limiting the nutrient transport (sheet prepared by ethanol as the non-solvent at 23 °C).

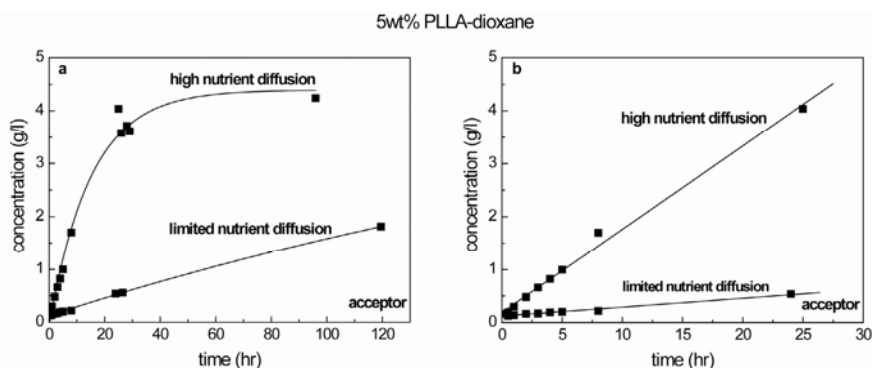


Figure 5 Typical graphs of glucose diffusion towards the acceptor as function of time; high nutrient diffusion: 29 μm thick sheet prepared with isopropanol as the non-solvent at 4 °C, limited nutrient diffusion: 52 μm thick sheet prepared with ethanol as the non-solvent at 23 °C. (a) 96 hours, (b) zoom at the first 24 hours.

The glucose transport was rather linear at low time period (up to 24 hours). Subsequently, the glucose concentration difference between donor and acceptor decreases and the concentration reaches a plateau. Table 3 presents the glucose diffusion coefficients for various sheets prepared using a 5 wt% PLLA-dioxane solution, determined by Equations 4-6. Parameters that were altered are the non-solvent (ethanol or isopropanol), initial casting thickness (100 and 200 μm) and the temperature of the non-solvent bath (room temperature, i.e. $\sim 23^\circ\text{C}$, or $\sim 4^\circ\text{C}$). Due to the low polymer concentration in the polymer solution, the sheets shrink extensively during solidification. Therefore, the final (real) sheet thickness is mentioned as well (Table 3). Although porosity is a good estimation of nutrient diffusion through a sheet, it does not comprehend the existence of a dense skin layer and/or pore-interconnectivity. These phenomena have a major impact on the diffusion of glucose through the sheet.

Table 3 Glucose diffusion through of sheets prepared by a 5 wt% PLLA in dioxane solution (using a glucose solution of 10 mg/ml).

| Non-solvent | $d_{\text{initial}}/d_{\text{real}}$ (μm) | $T_{\text{non-solvent}}$ ($^\circ\text{C}$) | Porosity (%) | Diffusion Coefficient ($10^{-11} \text{ m}^2/\text{s}$) ^a |
|-------------|---|--|-----------------|---|
| ethanol | 200 / 52 | 23 | 84.3 ± 2.1 | 1.5 ± 0.5 |
| | 100 / 27 | 23 | 82.6 ± 0.7 | 3.3 ± 0.1 |
| | 100 / 21 | 4 | 75.2 ± 1.6 | 10.4 ± 4.5 |
| isopropanol | 200 / 57 | 23 | 86.0 ± 0.8 | 2.6 ± 0.2 |
| | 100 / 36 | 23 | 86.0 ± 1.2 | 6.4 ± 1.7 |
| | 100 / 29 | 4 | 83.0 ± 2.6 | 8.6 ± 1.5 |

^a Free diffusion of glucose in water (or saline) at 37°C is $9 \cdot 10^{-10} \text{ m}^2/\text{s}$ [35].

For both ethanol and isopropanol as non-solvents, it seems that the initial casting thickness has an effect on the sheet structure. When the initial casting thickness becomes half (200 to 100 μm), the glucose diffusion coefficient is doubled (in the calculations, the real thickness of the sheet is used and the diffusion coefficient should generally not change with thickness). Therefore, this increase in the diffusion coefficient indicates that the structure and/or interconnectivity of the sheet are influenced by the initial casting thickness. For the thicker films (casting thickness 200 μm), even though the calculated porosity does not differ from the thinner ones (casting thickness 100 μm), the pore-interconnectivity is probably lower resulting into lower glucose diffusion.

When subsequently the temperature of the non-solvent bath is decreased from room temperature ($\sim 23^\circ\text{C}$) to $\sim 4^\circ\text{C}$, the final thickness is decreased more probably due to decreasing pore size. However, decreasing the non-solvent bath temperature also causes a significant increase of surface porosity (removal of skin). This effect might counterbalance the overall porosity change. Therefore, with a decrease of the non-solvent bath temperature from room temperature to $\sim 4^\circ\text{C}$, the diffusion

of glucose increases significantly (for ethanol more severely compared to isopropanol). For the non-solvent bath at room temperature, isopropanol results in higher diffusion compared to ethanol. For the non-solvent bath at $\sim 4^\circ\text{C}$, ethanol leads to higher diffusion coefficients compared to isopropanol. For the most optimal sheets, i.e., prepared from 5 wt% PLLA-dioxane solution and the non-solvent at 4°C , the glucose diffusion coefficient is $8\cdot 10\cdot 10^{-11}\text{ m}^2/\text{s}$ and rather close to the self diffusion of glucose in water or saline solution which is $9\cdot 10^{-10}\text{ m}^2/\text{s}$ [35]. This result is very promising, since the high glucose diffusion through the scaffold sheets implies that the porosity and pore-interconnectivity are most likely adequate for sufficient nutrient supply to the cells.

3.4.4 Cell culturing

Sheets prepared from a 5 wt% PLLA-dioxane solution using ethanol or isopropanol as the non-solvent, at both room temperature and $\sim 4^\circ\text{C}$, showed the most optimal results considering pore-morphology and -interconnectivity and were used in cell culturing. It is often argued that the phase separation process can lead to sheet formation where residues of the toxic solvents (as dioxane in our case) and/or non-solvent remain. In order to evaluate the sheets as scaffold material, preliminary culturing experiments were performed using HUVEC's and HMEC's. These results (not shown here) showed high affinity of the cells to the material (good cell growth was observed) indicating no solvent or non-solvent remained and these sheets are suitable as scaffold material. Moreover, the non-solvents (i.e., ethanol and isopropanol) are sterilizing agents, which is an additional advantage. More extensive experiments on the influence of patterning on cell alignment were performed using C2C12 and MC3T3 cells. The cell-cultured sheets were analyzed by light-microscopy and subsequently with confocal fluorescence microscopy to observe the quality of the tissue formation by cytoskeleton staining (Figure 6).

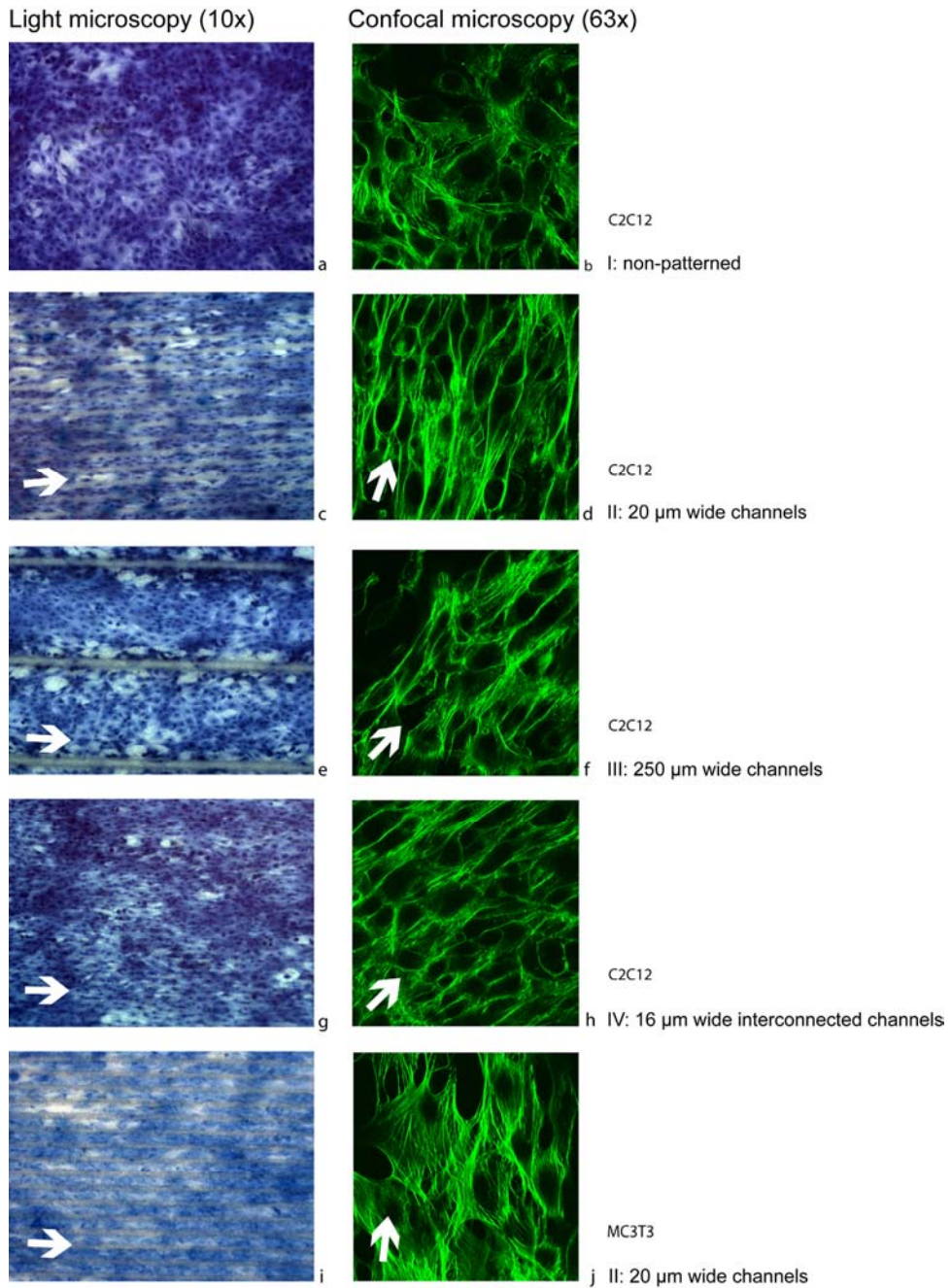


Figure 6 Typical pictures of culturing cells on PLLA sheets featuring different patterns, after 4 days, seeding density of 25,000 cells/cm². The arrows indicate channel direction. (a, c, e, g, i) light microscopy (magnification 10x, methylene blue used for staining), (b, d, f, h, j) confocal fluorescence microscopy (magnification 63x).

Cell culturing on micropatterned scaffold sheets induces alignment of both the C2C12 as well as the MC3T3 cells, and the level of orientation is influenced by the micropattern design. Figure 7 presents the extent of alignment of C2C12 cells for the various micropatterned sheets in comparison to non-patterned sheets, calculated by equation 7.

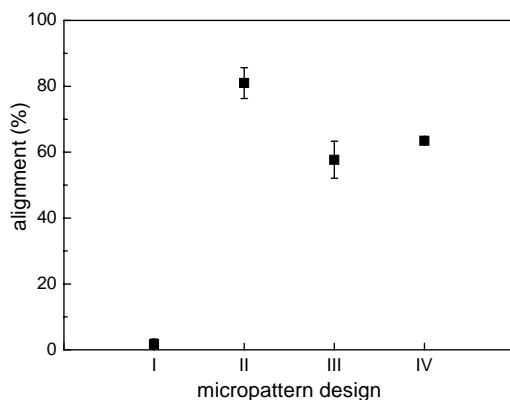


Figure 7 Cell alignment on sheets featuring various micropattern designs.

As expected, the non-patterned reference samples (type I) showed a random orientation of the cells (Figure 6a, b). Sheets featuring 20 µm wide channels (type II) showed high orientation of 81 ± 5 % (Figure 6c, d). When the channels are wide (250 µm, Figure 6e, f) the orientation of the cells was lower (58 ± 6 %). The cells aligned in the direction of the channels, although within the wide channels, the individual cells showed a slightly higher variation in orientation compared to the 20 µm wide channels (see confocal fluorescence microscopy, Figure 6f). Figure 6g, h show cells grown on sheets featuring interconnected 16 µm wide channels (type IV) with good cell alignment as well; 64 ± 1 %. In this case, due to connections between the channels, the cells in adjacent channels are in contact leading to lower alignment compared to continuous channels of approximately the same width (i.e., 20 µm, type II). Confocal fluorescence microscopy images show that the cells grow through these connections.

It is important to note that for samples containing lower cell numbers, the cells are favourably placed in the channels. Only at higher confluence (i.e., more days of culturing), the cells start to overgrow the ridges of the micropattern. Nevertheless, the overgrowing cells are still well aligned in the direction of the micropattern channels. Figure 8 shows confocal fluorescence microscopy pictures at various depths of tissue grown in the micropatterns of a scaffold type II (20 µm channels). Figure 8a shows cells grown on the bottom of the channels, where Figure 8b shows cells halfway the depth of the channels. Figure 8c shows cells grown directly on top of the micropattern. Figure 8d and e show cells in the overgrowing layers. In all cases, the cell alignment is clear. The various micropattern

designs induce cell alignment; consequently, the formation of the *in-vitro* tissue is stimulated to mimic *in-vivo* tissue organization. This alignment is known to be advantageous for the tissue quality [10, 11].

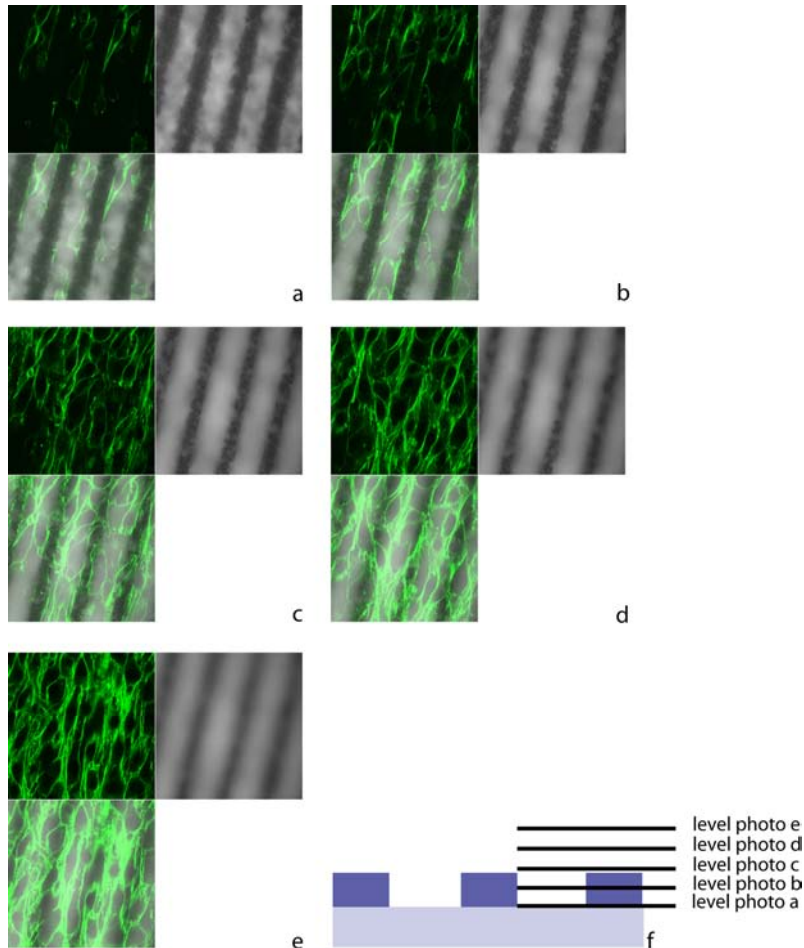


Figure 8 C2C12 cells at various depths of the micropattern (20 μm wide channels, after 4 days, seeding density of 25,000 cells/ cm^2); (a-e) upper left picture is taken with confocal fluorescence microscopy, upper right picture is taken with light microscopy on exactly the same place of the sample, lower left is the super-positioned picture of the confocal fluorescence microscopy and light microscopy picture.

To determine directly if the nutrient transport through the inner-porosity of the sheets is sufficient for cells to proliferate, sheets were turned up side down. In this case, the nutrients have to diffuse through the scaffold sheet to reach the cells. These turned sheets were compared to a reference where the cells were in direct contact to the medium and oxygen. Figure 9 present results after 2 and 4 days of culturing for the turned micropatterned sheets (type III), Figure 9a, c respectively, and the references, Figure 9b, d respectively. These images support the concept that the interconnected porous scaffold sheets enable sufficient nutrient transport through one scaffold sheet for cell proliferation; the number of cells on both the turned and reference scaffold sheets are comparable.

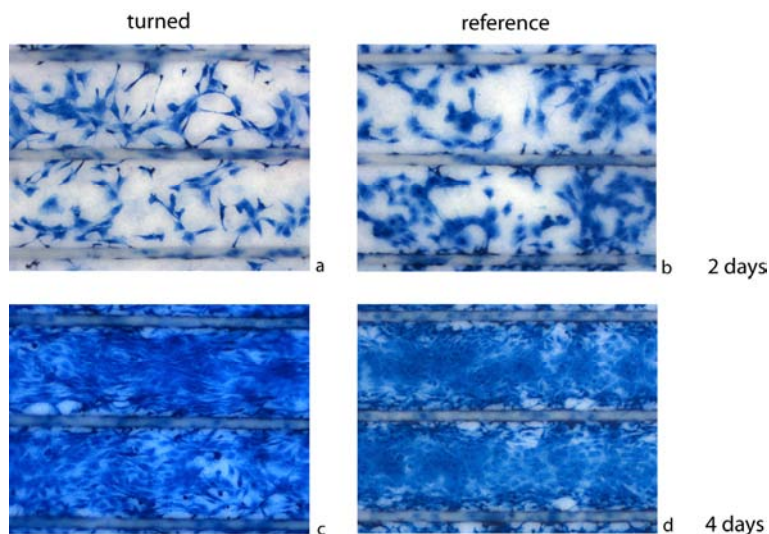


Figure 9 Light microscopy images of C2C12 cells on micro-patterned scaffold sheets containing 250 μm wide channels after 2 (a, b) and 4 (c, d) days of culturing (seeding density 25.000 cells/cm²); (a, c) scaffold sheets turned up side down in the well to determine nutrient transport through the sheet towards the cells; (b, d) reference where cells are in direct contact to the nutrients.

Our results show that PS μ M is an excellent method to prepare highly porous micropatterned scaffold sheets with sufficient nutrient diffusivity for cell proliferation, high cell alignment and good tissue formation, even for multiple cell layers.

3.4.5 3-D scaffolds proof-of-principle

The micropatterned sheets can build 3-D scaffolds by multi-layer stacking of the 2-D sheets. Figure 10a and b present stacked layers through clamping and rolling up, respectively. In contrast to clamping, in the rolling up process no extensive pressure is applied on the polymer sheets and possible damage to the inner-structure of the sheets can be avoided. By tuning the size of the channels and the sheet thickness, the scaffold architecture can be designed. Although only a few layers have been stacked up till now, the outcome seems promising for stacking more layers into an optimized 3-D scaffold.

In this concept, the channels of the 3-D scaffold can be used for two purposes; either growing cells aligned in the direction of the channels as presented in 2-D and/or for extra nutrient supply to the cells by perfusion. The inner-porosity should ensure nutrient transport of the nutrient supplying layers to the cell growing layers. Interference of possible nutrient limitations on the quality of cell proliferation has not been studied yet. Therefore, nutrient limitations occurring in 3-D scaffolds containing a higher number of sheets, and how nutrient supplying layers can assist, will be subject of further research. Then, the maximum nutrient diffusivity path length[36] can be taken into account in the 3-D scaffold design.

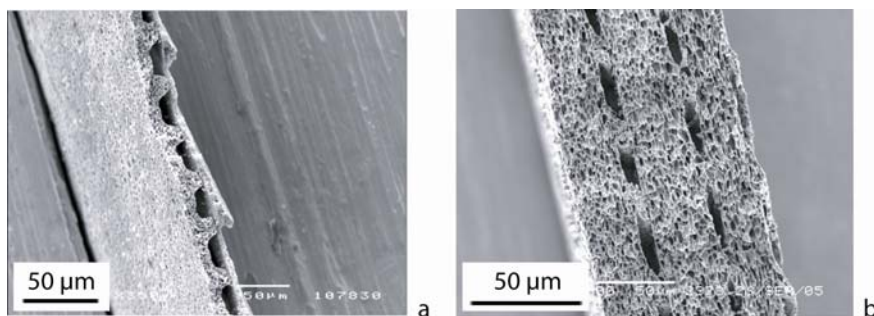


Figure 10 Stacking scaffold sheets as proof-of-principle of 3-D scaffolds using (a) clamping two films, (b) rolling up one film.

3.5 Conclusions

Phase separation micromolding is an easy method to design micropatterned porous 2-D scaffold sheets in one step. Through fine-tuning of various parameters, highly interconnected porous scaffold sheets can be prepared with high nutrient diffusivity. Cell culturing of various cell types demonstrates that the micropatterned sheets are suitable as scaffold and good cell attachment and tissue formation can be obtained. Cell alignment is induced by the micropattern, where the level of orientation can be influenced by adjusting micropattern feature and dimensions. Cells are favourably placed in the channels and even at higher confluence levels where cells start to overgrow the ridges of the micropattern, these cells align themselves in the direction of the channels. The micropatterned sheets are very promising as basis for building a 3-D scaffold with respect to porosity, interconnectivity and control of tissue orientation.

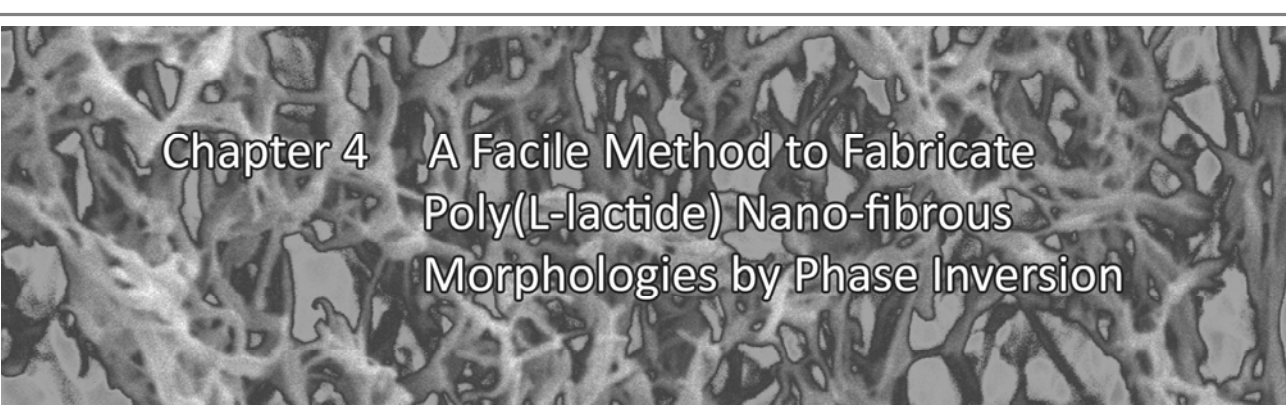
Acknowledgment

The authors would like to thank: D. Grijpma and A. Poot (Polymer Chemistry and Biomaterials Group, University of Twente, The Netherlands) for supplying the polymers and for fruitful discussions; I. van den Brink, J. Boer, and C. van Blitterswijk (Department of Tissue Regeneration, University of Twente, The Netherlands) for technical assistance and guidance concerning the cell culturing experiments; H.-J. Van Manen for technical assistance concerning confocal fluorescence microscopy. This project is supported by the Spearhead program: 'Advanced Polymeric Microstructures for Tissue Engineering' of the University of Twente (BMTi, Institute for Biomedical Technology).

References

1. Levenberg S, Langer R, Gerald PS. Advances in Tissue Engineering. Current Topics in Developmental Biology 2004;Volume 61:113-134.
2. Takezawa T. A strategy for the development of tissue engineering scaffolds that regulate cell behavior. Biomaterials 2003;24(13):2267-2275.
3. Fuchs JR, Nasser BA, Vacanti JP. Tissue engineering: A 21st century solution to surgical reconstruction. Annual Thorac Surgery 2001;72:577-591.
4. Langer R, Vacanti JP. Tissue Engineering. Science 1993;260:920-926.
5. Ma PX. Scaffolds for tissue fabrication. Materials Today 2004;7(5):30-40.
6. Yeong W-Y, Chua C-K, Leong K-F, Chandrasekaran M. Rapid prototyping in tissue engineering: challenges and potential. Trends in Biotechnology 2004;22(12):643-652.
7. Agrawal CM, Ray RB. Biodegradable polymeric scaffolds for musculoskeletal tissue engineering. Journal of Biomedical Materials Research 2001;55(2):141-150.
8. Hutmacher DW. Scaffolds in tissue engineering bone and cartilage. Biomaterials 2000;21(24):2529-2543.
9. Yang S, Leong K-F, Du Z, Chua C-K. The Design of Scaffolds for Use in Tissue Engineering. Part I. Traditional Factors. Tissue Engineering 2001;7(6):679-689.
10. Hollister SJ. Porous scaffold design for tissue engineering. Nature Materials 2005;4:518-524.
11. Andersson H, Berg Avd. Microfabrication and microfluidics for tissue engineering: state of the art and future opportunities. Lab on a Chip 2004;4:98-103.
12. Snyder JD, Desai TA. Fabrication of Multiple Microscale Features on Polymer Surfaces for Applications in Tissue Engineering. Biomedical Microdevices 2001;3(4):293-300.
13. Desai TA. Micro- and nanoscale structures for tissue engineering constructs. Medical Engineering & Physics 2000;22(9):595-606.
14. Flemming RG, Murphy CJ, Abrams GA, Goodman SL, Nealey PF. Effects of synthetic micro- and nano-structured surfaces on cell behavior. Biomaterials 1999;20(6):573-588.
15. Kim TK, Yoon JJ, Lee DS, Park TG. Gas foamed open porous biodegradable polymeric microspheres. Biomaterials 2006;27(2):152-159.
16. Wang X, Li W, Kumar V. A method for solvent-free fabrication of porous polymer using solid-state foaming and ultrasound for tissue engineering applications. Biomaterials 2006;27(9):1924-1929.
17. Katoh K, Tanabe T, Yamauchi K. Novel approach to fabricate keratin sponge scaffolds with controlled pore size and porosity. Biomaterials 2004;25(18):4255-4262.
18. Ma PX, Choi J-W. Biodegradable Polymer Scaffolds with Well-Defined Interconnected Spherical Pore Network. Tissue Engineering 2001;7(1):23-33.
19. Kim SY, Kanamori T, Noumi Y, Wang O-C, Shinbo T. Preparation of porous poly(D,L-lactide) and poly(D,L-lactide-co-glycolide) membranes by a phase inversion process and investigation of their morphological changes as cell culture scaffolds. Journal of Applied Polymer Science 2004;92:2082-2092.
20. Zoppi RA, Contant S, Duek EAR, Marques FR, Wada MLF, Nunes SP. Porous poly(L-lactide) films obtained by immersion precipitation process: morphology, phase separation and culture of VERO cells. Polymer 1999 Jun;40(12):3275-3289.

21. Ho M-H, Kuo P-Y, Hsieh H-J, Hsien T-Y, Hou L-T, Lai J-Y, et al. Preparation of porous scaffolds by using freeze-extraction and freeze-gelation methods. *Biomaterials* 2004;25(1):129-138.
22. O'Brien FJ, Harley BA, Yannas IV, Gibson L. Influence of freezing rate on pore structure in freeze-dried collagen-GAG scaffolds. *Biomaterials* 2004;25(6):1077-1086.
23. Falconnet D, Csucs G, Michelle Grandin H, Textor M. Surface engineering approaches to micropattern surfaces for cell-based assays. *Biomaterials* 2006;27(16):3044-3063.
24. Gadegaard N, Martinez E, Riehle MO, Seunarine K, Wilkinson CDW. Applications of nano-patterning to tissue engineering. *Microelectronic Engineering* 2006 Apr-Sep;83(4-9):1577-1581.
25. Vozzi G, Flaim C, Ahluwalia A, Bhatia S. Fabrication of PLGA scaffolds using soft lithography and microsyringe deposition. *Biomaterials* 2003;24:2533-2540.
26. Lussi JW, Falconnet D, Hubbell JA, Textor M, Csucs G. Pattern stability under cell culture conditions--A comparative study of patterning methods based on PLL-g-PEG background passivation. *Biomaterials* 2006;27(12):2534-2541.
27. Sarkar S, Lee GY, Wong JY, Desai TA. Development and characterization of a porous micro-patterned scaffold for vascular tissue engineering applications. *Biomaterials* 2006;27(27):4775-4782.
28. Vogelaar L, Lammertink RGH, Barsema JN, Nijdam W, Bolhuis-Versteeg LAM, Rijn CJMv, et al. Phase Separation Micromolding: A New Generic Approach for Microstructuring Various Materials. *Small* 2005;1(6):645-655.
29. Vogelaar L, Barsema JN, Rijn CJMv, Nijdam W, Wessling M. Phase separation micromolding - PS μ M. *Advanced Materials* 2003;15(16):1385-1389.
30. Stropnik C, Musil V, Brumen M. Polymeric membrane formation by wet-phase separation; turbidity and shrinkage phenomena as evidence for the elementary processes. *Polymer* 2000;41(26):9227-9237.
31. Witte Pvd, Dijkstra PJ, van den Berg JWA, Feijen J. Phase separation processes in polymer solutions in relation to membrane formation. *Journal of Membrane Science* 1996;117(1-2):1-31.
32. Alexandre E, Schmitt B, Boudjema K, Merrill EW, Lutz PJ. Hydrogel networks of poly(ethylene oxide) star-molecules supported by expanded polytetrafluoroethylene membranes: characterization, biocompatibility evaluation and glucose diffusion characteristics. *Macromolecular Bioscience* 2004;4:639-648.
33. Sarkar S, Dadhania M, Rourke P, Desai TA, Wong JY. Vascular tissue engineering: microtextured scaffold templates to control organization of vascular smooth muscle cells and extracellular matrix. *Acta Biomaterialia* 2005;1:93-100.
34. Motlagh D, Hartman TJ, Desai TA, Russell B. Microfabricated grooves recapitulate neonatal myocyte connexin43 and N-cadherin expression and localization. *Journal of Biomedical Materials Research Part A* 2003;67A(1):148-157.
35. Saltzman WM. *Tissue Engineering: principles for the design of replacement organs and tissues*. 1st ed. Oxford: Oxford University Press, 2004.
36. Dunn JCY, Chan W-Y, Cristini V, Kim JS, Lowengrub J, Singh S, et al. Analysis of Cell Growth in Three-Dimensional Scaffolds. *Tissue Engineering* 2006;12(4):705-716.

A scanning electron micrograph (SEM) showing a highly porous, interconnected network of nano-fibers. The fibers are thin and randomly oriented, creating a complex, web-like structure with many small voids and larger interconnected chambers. The overall appearance is that of a natural extracellular matrix or a synthetic scaffold designed for tissue engineering.

Chapter 4 A Facile Method to Fabricate Poly(L-lactide) Nano-fibrous Morphologies by Phase Inversion

Abstract

For certain tissue engineering applications, scaffolds with a nano-fibrous morphology are favourable as the tissue's natural environment, consisting of the extracellular matrix secreted by the cells, as well contains nano-fibers like collagen fibers with diameters ranging from 50-400 nm.

Porous poly(L-lactide) (PLLA) scaffolds obtained by phase inversion methods generally have a solid-wall pore morphology. In contrast, this work presents a facile method to fabricate highly porous and highly interconnected nano-fibrous scaffold sheets by phase inversion using PLLA with a Mw of 5.7×10^5 g/mol. The scaffold sheets consist of nano-fibers within the range of 50-500 nm. When applying phase separation micromolding (PS μ M) as fabrication method an additional topography can be introduced into these sheets, besides the porous nano-fibrous morphology. Culturing C2C12 pre-myoblasts on these nano-fibrous sheets reveals very good cell adhesion and spreading. Excellent alignment of the cells was induced by the introduction of 30 μ m wide microchannels in these sheets. These results warrant further evaluation of these sheets as tissue engineering scaffolds.

4.1 Introduction

In tissue engineering (TE), many methods are applied to design and manufacture porous scaffolds as carriers for cell growth. Several commonly used fabrication methods base on phase separation including liquid-induced (LIPS, immersion precipitation) or thermally-induced phase separation (TIPS) [1, 2]. The obtained morphology as well as the corresponding feature sizes may vary widely depending on the processing conditions; from dense to highly porous, with pores from sub-micron scale to tens of microns and non-percolated to highly interconnected. There are also many literature reports on scaffold preparation using the well-known biopolymer poly(L-lactic acid) (PLLA) via LIPS [3-6] or TIPS [7-9]. In most of these studies, the resulting porous sheets comprise generally of non-percolated pore morphology distinguished by rather rounded pores.

In certain tissue engineering applications, fibrous morphologies are favoured over solid-wall pore morphologies as the nano-fibers resemble the natural environment that surrounds the cells [10-14]. E.g., collagen fibers, which make up the main component of the extracellular matrix secreted by cells, have fiber diameters ranging from 50-400 nm [11]. To prepare sheets with a nano-fibrous morphology, electrospinning is the most commonly fabrication method. Variation of the electrospinning process conditions enables e.g. tuning fiber dimensions generally within a range of around 100 nm to 100 μ m or more [15-18]. Recently, some literature reports appeared on the formation of nano-fibrous porous sheets by LIPS [19, 20]. However, the reported protocols require thermal quenching steps and are relatively time-consuming and elaborate processes.

In this work, we present a facile method to fabricate highly porous nano-fibrous sheets via LIPS using very high molecular weight PLLA. The dimensions of the nano-fibers range between 50-500 nm. These nano-fibrous sheets are prepared by phase separation micromolding (PS μ M) [3] where casting the polymer solution on a micropatterned mold enables replication of the inverse micropattern into a polymer sheet during solidification. Micropatterning of the scaffold surface is known to assist cell organization and to promote functionality of the cells or tissue [21]. The effect of polymer concentration, initial casting thickness as well as micropattern replication onto the final nano-fibrous morphologies is extensively studied. Finally, cell adhesion, spreading and alignment of C2C12 pre-myoblasts on these sheets is evaluated.

4.2 Materials and Methods

4.2.1 PLLA synthesis and characterization

Very high molecular weight poly(L-lactide) (PLLA) was prepared on a 100 g scale by ring opening polymerization of L-lactide (Purac Biochem) under vacuum in a heat-sealed glass ampoule. The polymerization was conducted at 130 ± 1 °C for 3 days using stannous octoate (2×10^{-4} mol per mol L-lactide) as catalyst. The polymer was purified by dissolution in chloroform, precipitated into an excess of ethanol and subsequently dried *in vacuo* at room temperature.

The number average (M_n) and weight average (M_w) molecular weights, molecular weight distribution (M_w/M_n) and intrinsic viscosity ($[\eta]$, in chloroform) of the polymer were determined by gel permeation chromatography (GPC) using chloroform as eluent at 30 °C. The GPC setup (Viscotec) consisted of a GPCmax VE-2001 GPC solvent/sample module, a series of ViscoGEL I columns, and a TDA 302 triple detector array comprising a light scattering detector, a differential refractive index detector and a four-capillary differential viscometer.

The peak melting temperature (T_m) and the glass transition temperature (T_g) of the polymer were determined by differential scanning calorimetry (Pyris 1 DSC, Perkin Elmer) at a heating rate of 10 °C per min. Indium and gallium were used as standards for temperature calibration. The peak melting temperature was determined from the first heating scan (up to 225 °C). The glass transition temperature was determined after quenching to -80 °C in a second scan. The glass transition temperature was taken as the midpoint of the heat capacity change.

4.2.2 Scaffold preparation and characterization

Precipitated very high molecular weight PLLA was dissolved in 1,4-dioxane at concentrations of 0.5 – 2 wt% and ethanol was used as nonsolvent at 2-4 °C (both Merck, analytical quality). The sheets were cast at initial casting thicknesses between 150 and 1000 µm and immediately after casting they were submerged into the nonsolvent to induce phase separation. After a couple of minutes, the sheets released from the molds. The sheets were left in the nonsolvent for 18-24 hours and subsequently washed thoroughly in Milli-Q water for 4-8 hours to ensure removal of the residual solvent and nonsolvent and were finally dried in a controlled atmosphere ($T = 19-21$ °C).

For the cell culturing experiments, circular samples of 15 mm were cut from the sheets, and immersed in a 70% ethanol solution for 20-30 min, followed by evaporation of the ethanol in the air. The samples were placed in 24-well plates (tissue culture treated surface, Nunc) and an o-ring (Viton type 51414, 14x1, Eriks) of the exact inner diameter of the well was placed on top to prevent floating of the samples. The samples were sprayed with 70% isopropanol solution and placed in a laminar

flow cabinet to allow isopropanol evaporation. The sheets were finally washed and stored for at least 24 hours in PBS at 37 °C in a humid atmosphere with 5% CO₂ to ensure complete wetting.

Sheets with and without a pattern were prepared. The nonpatterned sheets, indicated with 'np' were cast on flat molds where the patterned sheets were cast on molds featuring 30 µm wide channels and are indicated with '30 µm'. Besides, the 'air side' of the sheets indicates the top side of the scaffold during casting, where the 'substrate side' indicates the side in contact with the mold during casting, i.e. the possibly patterned side.

Scanning electron microscopy (SEM, JEOL 5600LV) was applied for the primary characterization of the sheet morphology. For this, the samples were sputter-coated with a nm-thick gold layer prior to imaging. The sheet thickness was determined from these images and was used to calculate the overall porosity by volume, weight and density (a method described in [3]).

4.2.3 Cell culturing and analysis

Morphology of pre-myoblasts, C2C12, on the PLLA scaffolds was visualized by fluorescence microscopy and SEM to evaluate cell behavior.

Culturing: C2C12 cells were cultured in proliferation medium containing Dulbecco's Modified Eagle's Medium (D-MEM, Gibco) supplemented with 10% fetal bovine serum (FBS, Cambrex), 100 U/ml penicillin (Gibco) and 100 µg/ml streptomycin (Gibco) at 37 °C in a humid atmosphere with 5% CO₂. In the expansion phase, the cells were plated at 2000-3000 cells/cm² and upon reaching 70-80% confluency detached by trypsinization (0.05% trypsin containing 1 mM EDTA) and subsequently sub-cultured or seeded on the PLLA sheets at a seeding density of 5000 cells/cm². The medium was refreshed every other day. Cell numbers were determined by manual counting with a haemocytometer. To prevent confluence and therefore to enable the visualization of single cells, the culturing period was only 3 days. Culturing experiments were performed in duplicate for every type of scaffold sheet including the air- as well as the substrate side of the sheets.

Fixation and staining for fluorescence microscopy: At day 3, the medium was aspirated from the wells, the sheets were washed with PBS, fixated by incubation with 4%-paraformaldehyde (Merck) in PBS for 30-60 min. and again washed with PBS. To stain the cells, PBS was aspirated and the cells were permeabilized by a 0.1% Triton-X100 solution for 2-3 min and washed twice with PBS. Subsequently, the cells were incubated for 10-15 min with the staining solution containing 2.5 vol% AlexaFluor 488 phalloidin and 0.1 vol% Hoechst (both Invitrogen) in PBS to stain the cytoskeleton (F-actin) and nucleus, respectively. Finally, the sheets were washed and stored in PBS and placed at 4 °C upon imaging (within 1 week) by fluorescence microscopy (BD Pathway 435, BD Biosciences).

SEM imaging: SEM imaging was performed on the same samples after fluorescence microscopy. PBS was aspirated and the sheets were washed twice with water to ensure full removal of all salts. Subsequently, the sheets were dehydrated using a water to ethanol gradient (ratio's water:ethanol 100:0, 50:50, 25:75, 10:90, 5:95, and 0:100) and finally dried in air at room temperature. Finally, the samples were kept under vacuum at 30 °C to ensure complete drying and the nm-thick gold coating was applied.

4.3 Results and Discussion

4.3.1 PLLA synthesis and characterization

High molecular weight PLLA was synthesized with M_w of 5.72×10^5 g/mol, M_n of 4.33×10^5 g/mol and a molecular weight distribution (M_w/M_n) of 1.32. The intrinsic viscosity ($[\eta]$), using chloroform, was 6.69 dl/g. The semi crystalline polymer has a glass transition temperature of 60 °C, a melting temperature of 179.4 °C and a heat of fusion of 40 J/g.

4.3.2 Scaffold preparation

During phase separation demixing results in two phases, a polymer rich phase and a solvent rich (or polymer lean) phase. One phase forms the continuous phase and the second phase forms the dispersed phase. At very low polymer concentrations, the solvent rich phase forms the continuous phase with a dispersed polymer rich phase. As the concentration increases reaching the critical polymer concentration, the polymer rich phase becomes the continuous phase instead resulting in a polymer matrix with pores evolving from the dispersed solvent rich phase.

Initially in this study, low polymer concentrations were used for sheet formation. With polymer solutions of 0.5 and 0.75 wt% PLLA in dioxane, no sheet formation occurs for initial casting thicknesses up to 500 μm . Presumably, these concentrations are below the critical polymer concentration necessary to obtain a continuous polymer matrix. However, a 1 wt% polymer solution cast with an initial thickness of 400 μm results the formation of a very thin sheet. Therefore, 1 wt% is considered as a concentration equal to or above the critical polymer concentration for this system. For a 1.25 wt% polymer solution, sheet formation occurs at initial casting thicknesses of 150 μm or more, although the mechanical strength of the sheets is only acceptable for an initial casting thickness of 350 μm or more. Polymer concentrations of 1.5 and 2 wt% cast at 150 μm or thicker result in the formation of good quality, well manageable sheets. Nonetheless, the viscosity of the 2 wt% solution is high and casting is not practical and therefore, 2 wt% was the upper limit used in this study. Based on the above results, PLLA-dioxane solutions of 1, 1.5 and 2 wt% were selected to further explore sheet formation from casts with initial thicknesses of 500 μm and 1000 μm .

4.3.3 Scaffold characterization

In previous work, high molecular weight PLLA ($M_w = 1.6 \times 10^5$ g/mol, $M_n = 8.4 \times 10^4$ g/mol) was used to fabricate micropatterned sheets with a solid-wall like pore morphology by PS μ M [3]. There, the critical polymer concentration was determined at 5 wt% for all casting thicknesses [3]. Application of PLLA with very high molecular weight allows using solutions with lower polymer concentrations for achieving sheet formation. Interestingly, under similar processing conditions, the very high molecular weight PLLA ($M_w = 5.72 \times 10^5$ g/mol) used in this work leads to nano-fibrous morphologies. The SEM images presented in Figure 1, Figure 2 and Figure 3 show the morphology of the sheets cast of 1, 1.5 and 2 wt% solutions of very high Mw PLLA in dioxane, respectively. Clearly, the sheets prepared using such low concentration polymer solutions are highly porous and interconnected consisting of fibers with a very small diameter in the range of 50-500 nm. In general, the majority of the fibers at the inner part of the sheets have a diameter of 50-200 nm and at the surfaces of 100-300 nm. A clear indication of high pore-connectivity is the high flux of fluids through these scaffolds during the various handling steps involved in washing and/or incubation with various liquids.

The molecular weight of the polymer clearly influences the obtained morphology and can be related to fundamental aspects of phase separation. At the critical overlap concentration of a polymer in solution, the molecular chains start to overlap with each other resulting in the formation of intermolecular entanglements. At a given polymer concentration (expressed as wt% or vol%) above the critical overlap concentration, the molecular weight between these entanglements is constant. The number of entanglements per polymer chain is therefore higher for polymer chains of higher molecular weight. Furthermore, their relaxation times are longer as well. This leads to increased strength of the transient network.

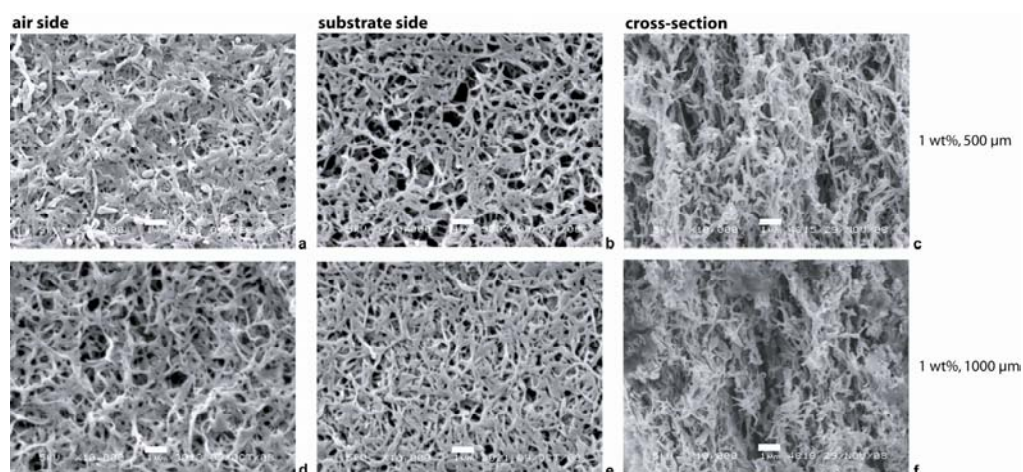
During the phase separation process, mixing of the solvent with a nonsolvent will reduce the solvent quality and allow the poly(L-lactide) rich phase to crystallize and solidify [22]. Increased network strength will enable the formation of a continuous nucleated polymer phase at lower concentrations (i.e. critical polymer concentration). As a result, characteristic sizes will be smaller, which can lead to the formation of nano-sized fiber structures.

Besides the polymer concentration, also the initial casting thickness influences the final sheet morphology and therefore, both variables were optimized and discussed in more detail.

Table 1 Porosity of PLLA sheets; np refers to the nonpatterned mold and 30 μm refers to the mold featuring 30 μm wide continuous channels.

| Polymer concentration | Initial casting thickness | Mold pattern | Final thickness (average, μm) | Porosity (%) | Pattern replication |
|-----------------------|---------------------------|------------------|---|--------------|---------------------|
| 1 wt% | 500 μm | np | 13 | 68 ± 3 | no |
| | | 30 μm | 13 | 64 ± 3 | |
| | 1000 μm | np | 14 | 45 ± 5 | no |
| | | 30 μm | 14 | 50 ± 1 | |
| 1.5 wt% | 500 μm | np | 15 | 65 ± 3 | no |
| | | 30 μm | 13 | 61 ± 1 | |
| | 1000 μm | np | 21 | 52 ± 5 | superficial |
| | | 30 μm | 27 ^a | 60 ± 1 | |
| 2 wt% | 500 μm | np | 26 | 75 ± 2 | superficial |
| | | 30 μm | 26 | 71 ± 1 | |
| | 1000 μm | np | 35 | 63 ± 1 | yes |
| | | 30 μm | 80 | 81 ± 1 | |

^a Locally macrovoid formation was observed for these sheets; thickness presented of the part of the sheet excluding the macrovoids (see Figure 4d)

**Figure 1** Typical SEM images of sheets cast from a 1 wt% PLLA solution at initial casting thickness of (a-c) 500 μm and (d-f) 1000 μm . Scale bar in images represents 1 μm .

PLLA concentration 1 wt%: In general, increasing the initial casting thickness from 500 to 1000 μm leads to an increased final sheet thickness. In contrast, for the sheets cast of the 1 wt% solution (Figure 1) the final thickness is almost similar independent of the casting thickness, as presented in Table 1. It seems that the pores of the sheets cast at 1000 μm are compressed leading to a reduced porosity in comparison to the sheets cast at 500 μm . For these sheets with relative weak morphology, the imprint of the micropattern is not preserved either (Figure 1b, e).

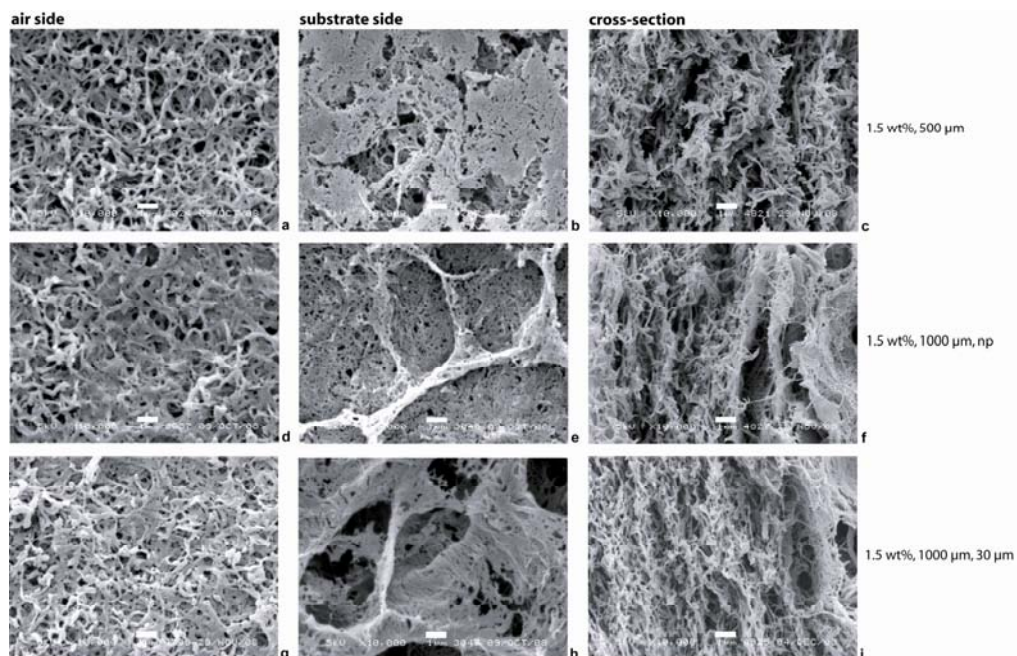


Figure 2 Typical SEM images of sheets cast from a 1.5 wt% PLLA solution at initial casting thickness of (a-c) 500 μm and (d-i) 1000 μm on both nonpatterned (np) molds as on molds featuring 30 μm wide continuous channels (30 μm). Scale bar in images represents 1 μm .

PLLA concentration 1.5 wt%: A transition occurs for the sheets cast of the 1.5 wt%, as shown in Figure 2. The sheets cast at 1000 μm are thicker and have a slightly reduced porosity compared to the sheets cast at 500 μm . Besides, the fiber morphology present at the substrate surface appears to be denser in comparison to the fiber morphology of sheets cast from the 1 wt% solution. The sheets cast on the patterned molds reveal an imprint of the channel pattern at the substrate side, but only on the surface with almost no channel depth, as visualized in Figure 4a and c. Interestingly, the sheets cast at 1000 μm on the micropatterned mold show local macrovoid formation as a result of fast inflow of the nonsolvent at the substrate side. It can be envisaged that the channel pattern on the mold creates space for the nonsolvent to enter the polymer sheet at a higher rate as compared the nonpatterned molds where all nonsolvent inflow is from the top and sides of the sheets.

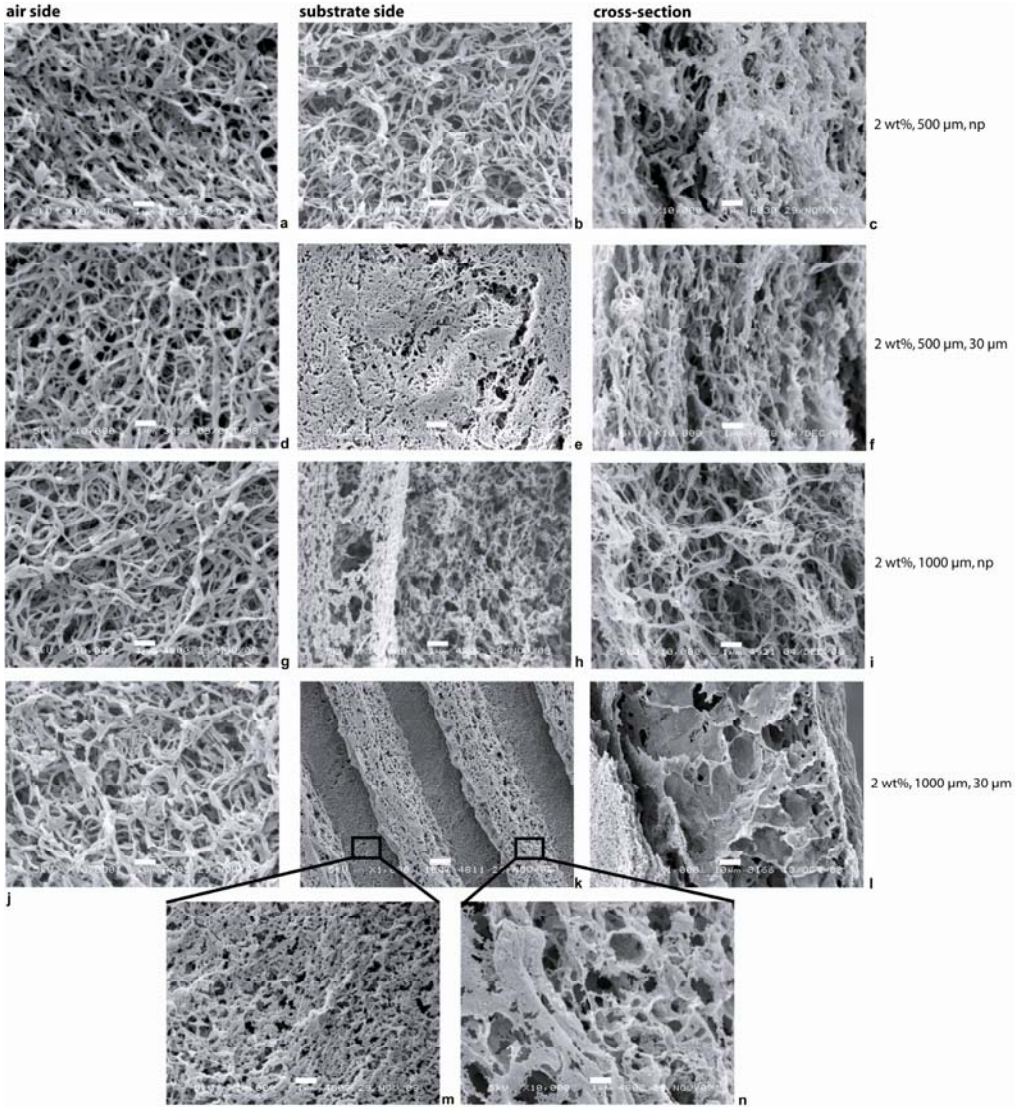


Figure 3 Typical SEM images of sheets cast from a 2 wt% PLLA solution at initial casting thickness of (a-f) 500 μm and (g-n) 1000 μm on both nonpatterned (np) molds as on molds featuring 30 μm wide continuous channels (30 μm). Images m and n present close-ups of the divergent morphologies of the channel bottom and channel ridge parts observed in image k. Scale bar in images represents 1 μm ; with the exceptions of images k and l, where the scale bar represents 10 μm .

PLLA concentration 2 wt%: The sheets cast of the 2 wt% solution have a higher thickness and porosity compared to those cast of the 1 and 1.5 wt% solutions, see Figure 3 and Table 1. In fact, in these sheets the fiber thicknesses are rather similar to those of the sheets produced of the 1 and 1.5 wt% solutions, but the packing of the fibers appears to be less dense yielding sheets with a higher porosity. Only for the sheets cast at 1000 μm , microchannels clearly imprint into the polymer sheets indicating that these sheets have sufficient mechanical strength to maintain the micropattern during solidification of the polymer matrix, see Figure 4g and h.

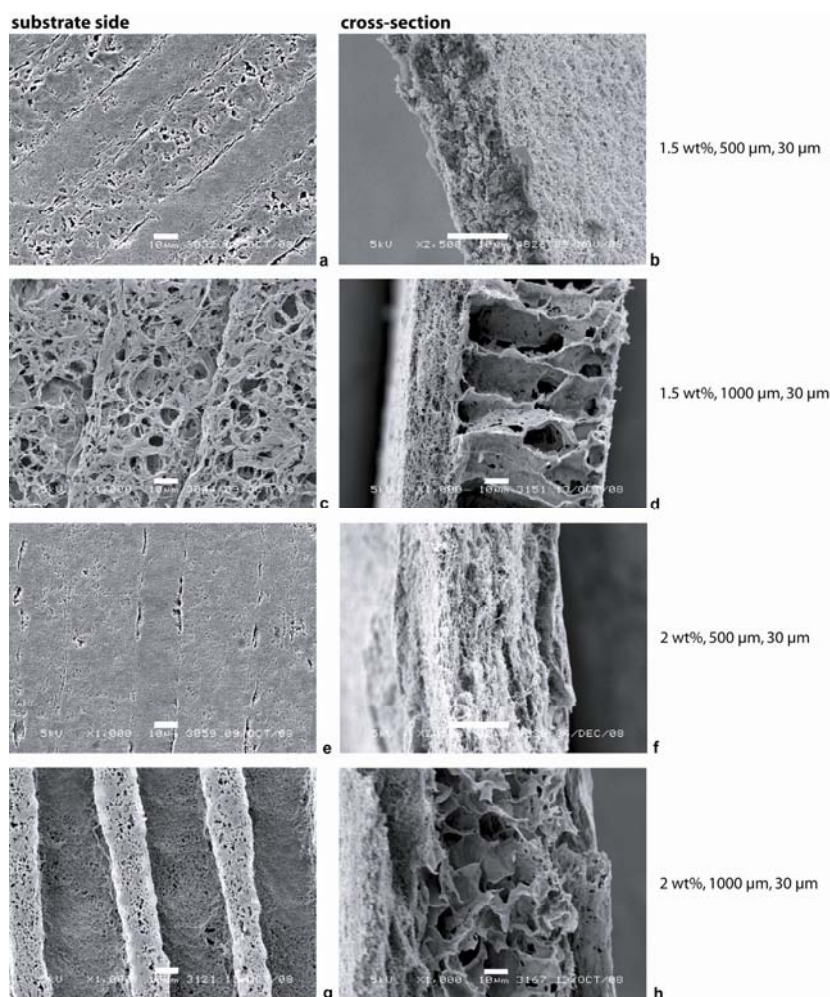


Figure 4 Typical SEM images of various sheets cast on the mold featuring continuous 30 μm wide channels cast from the (a-d) 1.5 wt% and (e-h) 2 wt% polymer solutions with initial casting thickness of (a-b, e-f) 500 μm or (c-d, g-h) 1000 μm . Bar in images represents 10 μm .

Besides, the imprint of the microchannels also causes a change in the morphology of these sheets (see Figure 3l and Figure 4h). These sheets are not highly fibrous, but have more solid wall-like pores. Nevertheless, these sheets still have a very high porosity of 81 % and their surfaces comprise the nano-fibrous morphology, especially on the air side. The morphological transition noticed when using solutions with a higher polymer concentration necessary to preserve the micropattern could already be observed by the macrovoid formation of the sheets cast from 1.5 wt% solutions on the patterned mold.

4.3.4 Cell culture and analysis

Figure 5 displays typical fluorescent microscopy images of stained cytoskeletons and nuclei of cultured pre-myoblasts, C2C12, on the PLLA sheets and Figure 6 presents typical SEM images. The data reveal that the cells adhered well and were able to grow on all sheets. Also the cells spread and showed filopodia. Additionally, for the micropatterned sheets (2 wt% solution cast at 1000 μm) the cells align perfectly in the direction of the channels (see Figure 5j). For the sheets cast at 500 μm , the cells also appear to align to a certain extent along the channels, even though the pattern is not prominent imprinted into the sheets (Figure 5h). Topographical patterning with these dimensions is known to induce good alignment of C2C12 cells [3]. These results confirm that these cells adhere and spread very well on the PLLA surfaces with a nano-fiber morphology and that excellent cell alignment can be reached using patterned sheets.

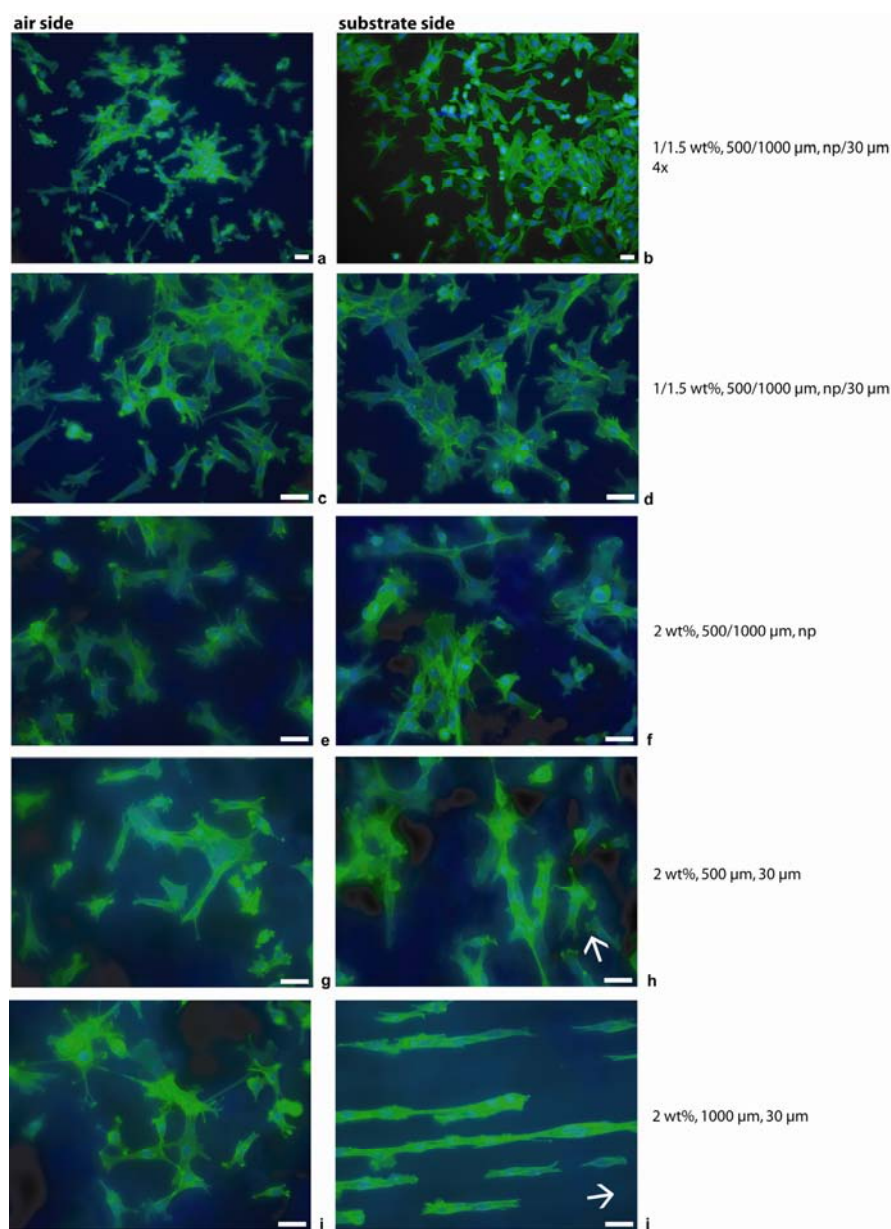


Figure 5 Typical fluorescence microscope images illustrating typical C2C12 growth on sheets cast from (a-d) 1 or 1.5 wt% solutions, independent of initial casting thickness or mold type, (e-f) 2 wt% solutions on the nonpatterned mold, independent of initial casting thickness, (g-h) 2 wt% solutions at 500 μm on the 30 μm wide channel mold, and (i-j) 2 wt% solutions at 1000 μm on the 30 μm channel mold; (a-b) magnification 4x, (c-j) magnification 10x. Seeding density 5000 cells/cm², cells stained for cytoskeleton (green, AlexaFluor 488 phalloidin) and nuclei (blue, Hoechst) at day 3, bar in images represents 25 μm, arrow indicates channel direction.

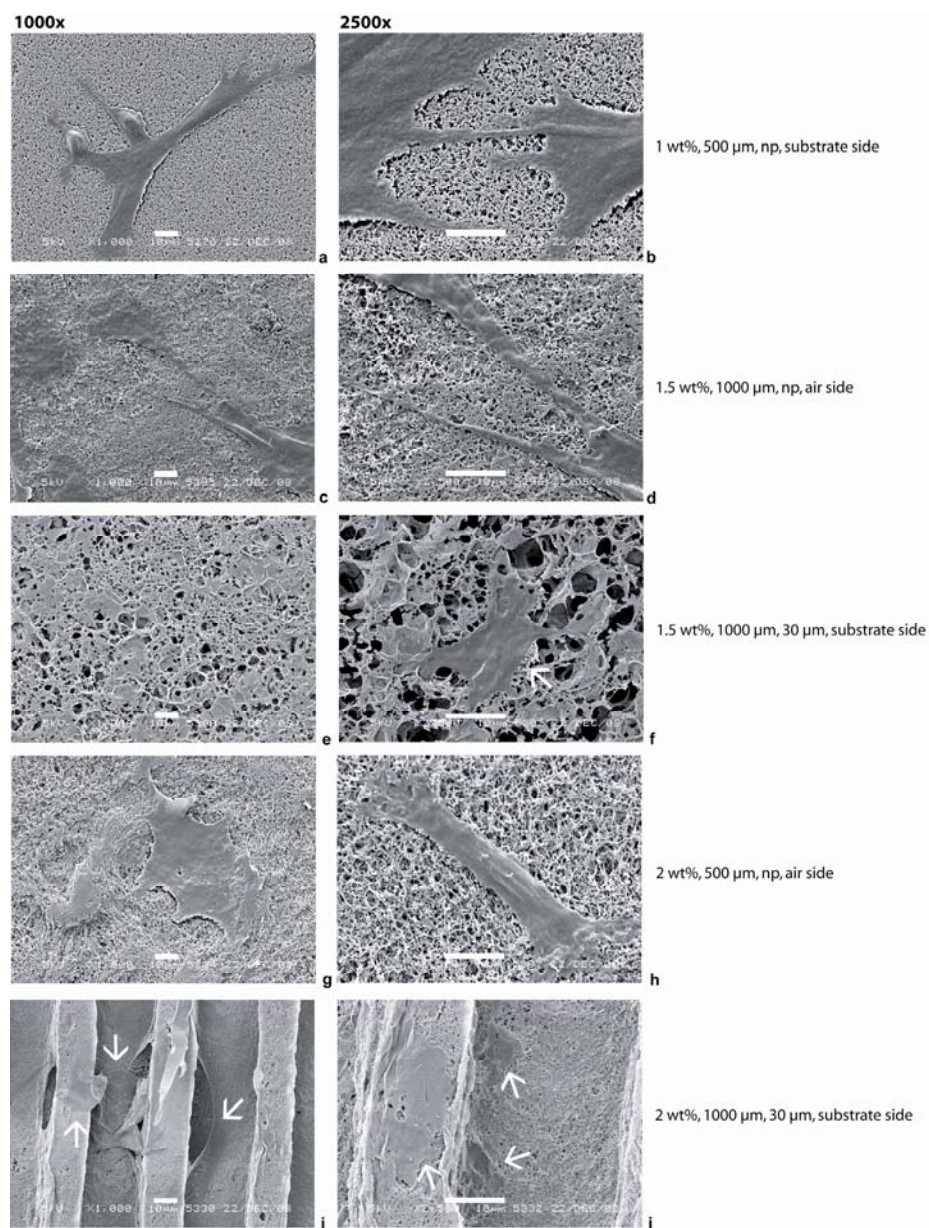


Figure 6

Typical SEM images illustrating typical C2C12 growth on sheets cast from (a-b) 1 wt% solutions at 500 μm on the nonpatterned mold, substrate side, (c-d) 1.5 wt% solutions at 1000 μm on the nonpatterned mold, air side, (e-f) 1.5 wt% solutions at 1000 μm on the 30 μm wide channel mold, substrate side, (g-h) 2 wt% solutions at 500 μm on the nonpatterned mold, air side and, (i-j) 2 wt% solutions at 1000 μm on the 30 μm wide channel mold, substrate side. (a, c, e, g, i) magnification 1000x, (b, d, f, h, j) magnification 2500x, bar in images represents 10 μm , (f, i, j) Arrows indicate cells.

4.4 Conclusions

This work presents the preparation of highly porous PLLA scaffold sheets with nano-fibrous morphology. The sheets were produced by phase inversion using polymer solutions based on very high molecular weight PLLA (Mw of 5.72×10^5 g/mol) with very low concentrations. As the molecular weight of the PLLA increases, the critical polymer concentration for sheet formation decreases; therewith allowing the formation and preservation of a highly interconnected porous nano-fibrous morphology with nano-fiber dimensions within the range of 50-500 nm. This morphology contrasts the more solid-wall pore of sheets morphology obtained with PLLA of lower molecular weight (Mw of 1.6×10^5 g/mol [3]). Besides, PS μ M enables micropatterning of these nano-fibrous sheets at optimized polymer concentrations. Culturing of C2C12 cells on these nano-fibrous sheets reveals good cell adhesion, spreading and morphology; and in case of imprinted microchannels, excellent alignment of the cells along the channels.

The work presented in this paper shows that PS μ M is a facile method to produce micropatterned nano-fibrous sheets with morphologies comparable to those obtained by more elaborate methods such as electrospinning. These micropatterned nano-fibrous sheets will be further evaluated for tissue engineering applications.

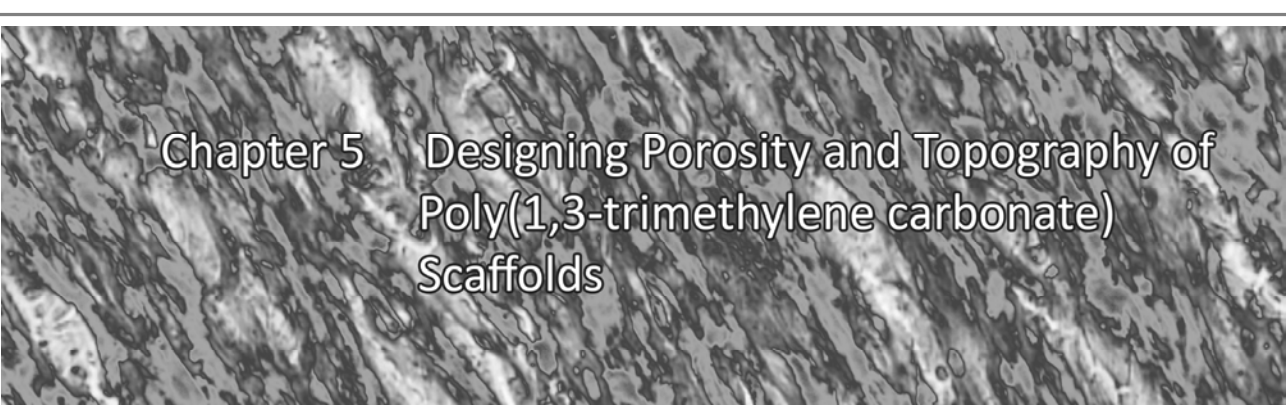
Acknowledgment

The authors would like to thank Dr. J. de Boer and Prof. Dr. C.A. van Blitterswijk (Department of Tissue Regeneration, University of Twente, The Netherlands) for facilitating the cell culture experiments. This project is financially supported by the Spearhead program: 'Advanced Polymeric Microstructures for Tissue Engineering' of the University of Twente (BMTi, Institute for Biomedical Technology).

References

1. Ma PX. Scaffolds for tissue fabrication. *Materials Today* 2004;7(5):30-40.
2. Yang S, Leong K-F, Du Z, Chua C-K. The Design of Scaffolds for Use in Tissue Engineering. Part I. Traditional Factors. *Tissue Engineering* 2001;7(6):679-689.
3. Papenburg BJ, Vogelaar L, Bolhuis-Versteeg LAM, Lammertink RGH, Stamatialis D, Wessling M. One-step fabrication of porous micropatterned scaffolds to control cell behavior. *Biomaterials* 2007;28(11):1998-2009.
4. Sawalha H, Schroën K, Boom R. Polylactide films formed by immersion precipitation: Effects of additives, nonsolvent, and temperature. *Journal of Applied Polymer Science* 2007;104(2):959-971.
5. Tu C, Cai Q, Yang J, Wan Y, Bei J, Wang S. The fabrication and characterization of poly(lactic acid) scaffolds for tissue engineering by improved solid-liquid phase separation. *Polymers for Advanced Technologies* 2003;14(8):565-573.
6. Zoppi RA, Contant S, Duek EAR, Marques FR, Wada MLF, Nunes SP. Porous poly(L-lactide) films obtained by immersion precipitation process: morphology, phase separation and culture of VERO cells. *Polymer* 1999 Jun;40(12):3275-3289.
7. Hua FJ, Kim GE, Lee JD, Son YK, Lee DS. Macroporous poly(L-lactide) scaffold 1. Preparation of a macroporous scaffold by liquid-liquid phase separation of a PLLA-dioxane-water system. *Journal of Biomedical Materials Research* 2002;63(2):161-167.
8. Li S, Carrubba VL, Piccarolo S, Sannino D, Brucato V. Preparation and properties of poly(L-lactic acid) scaffolds by thermally induced phase separation from a ternary polymer-solvent system. *Polymer International* 2004;53(12):2079-2085.
9. Nam YS, Park TG. Porous biodegradable polymeric scaffolds prepared by thermally induced phase separation. *Journal of Biomedical Materials Research* 1999;47(1):8-17.
10. Boudriot U, Dersch R, Greiner A, Wendorff JH. Electrospinning Approaches Toward Scaffold Engineering - A Brief Overview. *Artificial Organs* 2006;30(10):785-792.
11. Chen R, Hunt JA. Biomimetic materials processing for tissue-engineering processes. *Journal of Materials Chemistry* 2007;17(38):3974-3979.
12. Ma Z, Ramakrishna S. Nanostructured Extracellular Matrix. *Encyclopedia of Nanoscience and Nanotechnology* 2004;7:641-655.
13. Moroni L, De Wijn JR, Van Blitterswijk CA. Integrating novel technologies to fabricate smart scaffolds. *Journal of Biomaterials Science-Polymer Edition* 2008;19(5):543-572.
14. Stevens MM, George JH. Exploring and engineering the cell surface interface. *Science* 2005 Nov 18;310(5751):1135-1138.
15. Bhattarai SR, Bhattarai N, Viswanathamurthi P, Yi HK, Hwang PH, Kim HY. Hydrophilic nanofibrous structure of polylactide; fabrication and cell affinity. *Journal of Biomedical Materials Research Part A* 2006;78A(2):247-257.
16. Inai R, Kotaki M, Ramakrishna S. Structure and properties of electrospun PLLA single nanofibres. *Nanotechnology* 2005;16(2):208.
17. Moroni L, Licht R, de Boer J, de Wijn JR, van Blitterswijk CA. Fiber diameter and texture of electrospun PEOT/PBT scaffolds influence human mesenchymal stem cell proliferation and morphology, and the release of incorporated compounds. *Biomaterials* 2006;27(28):4911-4922.
18. Riboldi SA, Sampaioles M, Neuenschwander P, Cossu G, Mantero S. Electrospun degradable polyesterurethane membranes: potential scaffolds for skeletal muscle tissue engineering. *Biomaterials* 2005;26(22):4606-4615.

19. Woo KM, Jun J-H, Chen VJ, Seo J, Baek J-H, Ryoo H-M, et al. Nano-fibrous scaffolding promotes osteoblast differentiation and biomineralization. *Biomaterials* 2007;28(2):335-343.
20. Yang F, Murugan R, Ramakrishna S, Wang X, Ma YX, Wang S. Fabrication of nano-structured porous PLLA scaffold intended for nerve tissue engineering. *Biomaterials* 2004;25(10):1891-1900.
21. Park H, Cannizzaro C, Vunjak-Novakovic G, Langer R, Vacanti CA, Farokhzad OC. Nanofabrication and Microfabrication of Functional Materials for Tissue Engineering. *Tissue Engineering* 2007;13(8):1867-1877.
22. Witte Pvd, Dijkstra PJ, van den Berg JWA, Feijen J. Phase separation processes in polymer solutions in relation to membrane formation. *Journal of Membrane Science* 1996;117(1-2):1-31.



Chapter 5 Designing Porosity and Topography of Poly(1,3-trimethylene carbonate) Scaffolds

Abstract

Using Phase Separation Micromolding (PS μ M), we developed porous micropatterned sheets from amorphous poly(1,3-trimethylene carbonate) (PTMC). The use of these PTMC sheets can be advantageous in tissue engineering applications requiring highly flexible constructs. Addition of poly(ethylene oxide) (PEO) in various amounts to PTMC casting solutions provides PTMC sheets with a tailored porosity and pores sizes in the range of 2-20 μ m. The pore-forming effect of PEO during the phase separation process is evaluated and glucose transport measurements show that the pores are highly interconnected. Additionally, tailoring the micropattern design yields PTMC sheets with various surface topographies. Cell culturing experiments with pre-myoblasts C2C12 reveal that cell attachment and proliferation on these sheets is relatively high and that the micropattern topography induces clearly defined cell organization.

This chapter has been accepted for publication:

Bernke J. Papenburg, S. Schüller-Ravoo, L.A.M. Bolhuis-Versteeg, L. Hartsuiker,
D.W. Grijpma, J. Feijen, M. Wessling, D. Stamatialis

Acta Biomaterialia, 2009

5.1 Introduction

In tissue engineering, the choice of scaffold material plays an important role in the functionality of the designed scaffold in various applications. Characteristics of the material should correspond to the required properties at the site of implantation, e.g. suitable flexibility, mechanical strength and degradation in pace with tissue growth [1, 2]. Amongst the synthetic biodegradable biomaterials, poly(lactic acid) (PLA) and poly(glycolic acid) (PGA) and their co-polymers are studied intensively [3, 4]. However, the stiffness and degradation profiles of these materials can be unfavourable especially when considering certain soft tissue engineering applications. Poly(1,3-trimethylene carbonate) (PTMC) is a good alternative material in these cases due to its elasticity combined with slow degradation in aqueous solutions and rapid degradation *in vivo* via enzymatic degradation without leading to the formation of acidic products as in the case of e.g. PLA [5, 6]. Besides, selecting high molecular weight PTMC's yields relatively good mechanical properties [7]. Alternatively, one can synthesize co-polymers of PTMC with other polymers, e.g. PLA and poly(ϵ -caprolactone) (PCL), to obtain a co-polymer that has improved flexibility and degradation properties compared to e.g. PLA and increased Young modulus compared to PTMC [8-11]. *In vivo* studies using PTMC-based scaffolds reveal suitability of these materials for application in e.g. protein delivery systems [12] and prevention of post-operative adhesions [13].

Besides the choice of material, scaffold design is highly important for the functionality of the engineered tissue [2, 14]. One of the most important requirements is ensuring good nutrient supply to the cells which can be achieved via scaffold inner-porosity. Another important issue is the cell organization, which can be influenced by varying the scaffold topography. In this way, organization of the cells can be tuned thereby improving the functionality of the grown tissue [15, 16].

In previous work, we showed that Phase Separation Micromolding (PS μ M) enables fabrication of porous micropatterned sheets that can be stacked into 3D-scaffolds [17]. Various polymers like poly(L-lactic acid) (PLLA), poly(D,L-lactic acid) (PDLLA) and poly(ϵ -caprolactone) (PCL) were processed and the most suitable PLLA fabricated sheets were selected to analyze the functionality of the micropatterned porous sheets as scaffold sheets. In this work, we use PS μ M to fabricate porous micropatterned PTMC scaffold sheets. Porosity is introduced and tuned by applying PTMC casting solutions with various amounts of poly(ethylene oxide) (PEO). The pore-forming effect of PEO during the phase separation process of the PTMC sheets is studied and various micropatterned PTMC sheets are manufactured by casting on properly designed molds. Micropattern replication, pattern and morphology stability of these PTMC sheets are studied systematically. We successfully fabricated micropatterned porous PTMC sheets that support very well cell attachment, proliferation and morphology.

5.2 Materials and Methods

5.2.1 PTMC synthesis and characterization

The PTMC synthesis is slightly modified with respect previously reported protocols [7, 11]. Briefly, in an argon atmosphere trimethylene carbonate (TMC) (1,3-dioxan-2-one) monomer (Boehringer Ingelheim, polymer grade) was charged into a freshly silanized dried glass ampoule (silanized by silicone solution SERVA in isopropanol, SERVA Electrophoresis GmbH, Heidelberg, Germany) and 1.8×10^{-4} mol of catalyst stannous octoate (stannous 2-ethylhexanoate, SnOct_2 , Sigma) per mol of monomer was added. The ampoule was purged three times with dry argon, heat-sealed under vacuum and conditioned in a pre-heated oil bath. To assure homogeneous mixing of monomer and catalyst the ampoule was shaken vigorously for the first reaction hour. The polymerization was carried out at 130 °C for 3 days. For purification, the obtained polymer was dissolved in chloroform (2 wt/vol% solution, Merck, analytical quality), filtered and precipitated into a 5-fold volume of ethanol (Merck, analytical quality). Subsequently, the precipitated polymer was collected and dried prior to use.

Monomer conversion of the synthesized polymer was characterized by nuclear magnetic resonance (NMR) spectroscopy. ^1H -NMR (Varian Unity 300 MHz) spectra were recorded using solutions of the polymer in deuterated chloroform (CDCl_3 , Merck).

The molecular weight, molecular weight distribution and intrinsic viscosity of PTMC were determined by gel permeation chromatography (GPC) using chloroform (p.a., filtered through a Whatman Schleicher & Schuell RC58 membrane filter, 0.2 μm , prior to use) as eluent. The GPC setup consisted of a GPCmax VE-2001 GPC solvent/sample module, a series of ViscoGEL I columns, and a TDA 302 triple detector array comprising a light scattering detector (RALS and LALS), a differential refractive index detector and a four-capillary differential viscometer. A polystyrene standard ($M_n = 6.4 \times 10^4$ g/mol) with narrow molecular weight distribution was used for calibration.

Thermal properties of the pure polymers and their blends were evaluated by differential scanning calorimetry (DSC) using a Perkin Elmer Pyris1 (USA). Samples of 5-10 mg were heated from -100 °C to 100 °C at a heating rate of 10 °C/min. The glass transition temperature (T_g) was obtained from the midpoint of the heat capacity change and the melting range and peak temperature (T_m) were determined from the melting endotherm. Cyclohexane, indium and lead were used as standards for temperature calibration.

5.2.2 Scaffold preparation

PS μ M, which was used as fabrication method, has been described in detail in our previous work [17, 18].

PTMC: In this study, the synthesized high Mw PTMC was dissolved in chloroform (Merck, analytical quality) in a concentration of 3 wt%. In order to prepare porous PTMC sheets, poly(ethylene oxide) (PEO, Aldrich, Mw = 6×10^6 g/mol) was used as additive to the 3 wt% PTMC-CHCl₃ solution, as PEO is water-soluble and therefore can be leached after the phase separation process. Concentrations varying from 0.1 – 1.0 wt% with respect to the total final casting solution were used. Table 1 lists an overview of the various casting solution compositions and the notations that will be used from this point on.

Table 1 Composition of PTMC casting solutions.

| Notation | Polymer content (g) | | | Chloroform content (g) |
|-------------------|---------------------|------|-------|------------------------|
| | PTMC | PEO | Total | |
| Dense / 0 wt% PEO | 3 | 0 | 3.0 | 97.0 |
| 0.1 wt% PEO | 3 | 0.1 | 3.1 | 96.9 |
| 0.3 wt% PEO | 3 | 0.3 | 3.3 | 96.7 |
| 0.5 wt% PEO | 3 | 0.5 | 3.5 | 96.5 |
| 0.75 wt% PEO | 3 | 0.75 | 3.75 | 96.25 |
| 1.0 wt% PEO | 3 | 1.0 | 4.0 | 96.0 |

The polymer solutions were cast on flat or micropatterned molds to obtain nonpatterned or micropatterned sheets, respectively. Two micropattern designs were applied and are illustrated in Figure 1. Table 2 lists their dimension specifications.

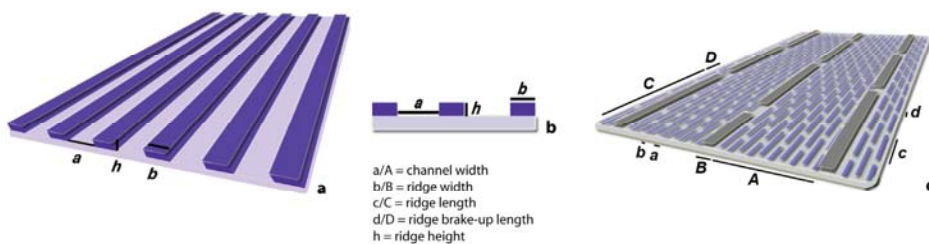


Figure 1 Schematic illustration of the mold designs, (a) top view channel pattern, (b) side view, (c) double pattern with larger and smaller channels that are both periodically broken-up (referred to as double brick pattern).

Table 2 Specifications of micropattern dimensions for both molds and corresponding PTMC sheets cast from various solutions. A represents the channel width, B the ridge width, C the ridge length till interconnection, D the ridge interconnection length, and H the ridge height; as also illustrated in Figure 1. For the double brick pattern, uppercase letters refer to the larger pattern where the lowercase letters refer to the smaller pattern.

| Pattern feature | | Mold (μm) | dense (μm) | 0.5 wt% PEO (μm) | 1 wt% PEO (μm) |
|--------------------------|-------|------------------------|-------------------------|-------------------------------|-----------------------------|
| double brick | A - a | 300 – 20 | 160 – 7 | 220 – 11 | 170 – 10 |
| | B - b | 50 – 10 | 21 – 8 | 27 – 7 | 28 – 7 |
| | C - c | 500 – 100 | 210 – 35 | 320 – 60 | 285 – 55 |
| | D - d | 150 – 10 | 120 – 21 | 140 – 8 | 100 – 8 |
| | H - h | 100 – 15 | ~35 – ~8 | 40 – 10 | 40 – 10 |
| 25 μm channel | a | 25 | 10 | 25 | ~15 |
| | b | 25 | 15 | 15 | ~20 |
| | h | 30 | 9 | 10 | ~10 |

As nonsolvent a mixture of ethanol (Merck, analytical quality) and Milli-Q water in a ratio of 8:1 at room temperature (ranging from 18-21 °C) was used. All sheets were cast with an initial casting thickness of 500 μm . After casting, the sheets were left in the nonsolvent for 1 day to leach the PEO. Subsequently, the sheets were washed in Milli-Q water for 1-3 days and dried in a temperature-controlled atmosphere ($T = 18\text{-}21\text{ }^{\circ}\text{C}$). Sheets used in cell culturing experiments were conditioned in culture medium at 4 °C (C2C12 proliferation medium, for composition see cell culturing section) up to 5 hours before washing with Milli-Q water and drying. To preserve the porous morphology, the nonsolvent and washing bath were kept at 4 °C and after drying the sheets were stored at -20 °C.

PLLA: Porous and dense PLLA sheets were used as reference in the cell culturing experiments. Porous PLLA sheets were prepared from 5 wt% PLLA ($M_w = 1.6 \times 10^5\text{ g/mol}$, $M_n = 8.4 \times 10^4\text{ g/mol}$) in 1,4-dioxane using ethanol at 3-4 °C as nonsolvent. Dense PLLA sheets were prepared from 10 wt% PLLA in chloroform (all Merck, analytical quality), left for evaporation for 30-60 seconds and placed in a nonsolvent bath of ethanol at room temperature. Both dense and porous PLLA sheets were left in the nonsolvent bath for 1 day to ensure full removal of the solvent and subsequently washed for 5-8 hours in Milli-Q water which was refreshed 2-3 times and subsequently dried under controlled atmosphere ($T = 18\text{-}21\text{ }^{\circ}\text{C}$).

5.2.3 PEO content

To determine the amount of PEO remaining in the PTMC sheets after phase separation, washing and drying, ^1H -NMR spectra were recorded for sheets cast from 0.5 wt% PEO casting solutions. Besides, a similar sheet was cast and after phase separation, left for washing for only 3 hours. Another 0.5 wt% PEO sheet was also cast but instead of solvent/nonsolvent exchange, the sheet was left in a controlled atmosphere over night for complete chloroform evaporation. One part of this sheet was stored until measured, another part was washed in Milli-Q water for 3 hours and the last part was washed in Milli-Q water for 3 days before drying. For these 3 sheets, also ^1H -NMR spectra were recorded, as well as for pure PTMC and PEO controls.

5.2.4 Porosity and pore morphology

To study sheet morphology, porosity and pore size range, image analysis using scanning electron microscopy (SEM, JEOL 5600LV) was performed where the samples were gold-coated (~15 nm-thick layer). Porosity was calculated from weight, volume (thickness is determined from the SEM images) and density, as described in our previous work [17] and the pore size range was based on the SEM images. As indication of pore interconnectivity and nutrient transport through the sheets, diffusion of glucose through the sheets was measured using the set-up described in detail elsewhere [17]. Basically, sheets are placed between a donor and an acceptor compartment and the transport of glucose from the donor to the acceptor side was measured over a surface area of 0.50 cm^2 . From the change of the concentrations in time, the glucose diffusion coefficient was calculated. For these experiments, a 10-fold of the blood glucose concentration was used: 10 g/L (57 mmol/L, SigmaUltra, D(+)-glucose, 99.5% GC) in Milli-Q water. Samples of 0.15 ml were taken at various time points from both the donor and acceptor compartment; time points were 0 min, 30 min, 1 hr, 2 hr, 3 hr, 4 hr, 5 hr, 8 hr and 24 hr. For the porous sheets additional time points were taken at 5 min, 10 min and 15 min. The glucose concentrations in the donor and acceptor compartments were determined for triplicate sheets by an enzymatic assay according to the manufacturer's protocol (PGO enzymes, Sigma). Through an enzymatic reaction with glucose, the solutions coloured orange and were analyzed by UV spectrophotometry (Varian Cary 300 scan) at $\lambda=450\text{ nm}$.

5.2.5 Sheet morphology under physiological conditions

Change of morphology in time of PTMC sheets cast of 0.5 and 1 wt% PEO solutions was studied under physiological conditions, simulated by placing the sheets either in PBS or in culture medium (C2C12 proliferation medium, see next paragraph) at 37 °C in a humid atmosphere with 5% CO₂. Triplicate samples with a diameter of 15 mm were taken at various time points: 0hr (control), 4hr, 8hr, 1d, 2d, 4d, 1wk, 2wk, 3wk, 4wk. Sheet morphology was determined by SEM imaging. Besides, some PTMC sheets were crosslinked by γ -irradiation (50 kGy, performed at Isotron Nederland B.V., Ede, The Netherlands) while kept under vacuum in 24 well-plates (Nunc).

5.2.6 Cell culturing

Cell culturing experiments were performed using mouse pre-myoblasts C2C12, to study cell attachment, proliferation and morphology on the PTMC sheets. In some cases PLLA sheets were used as reference material. For all cell culturing experiments, sheets were placed in 24 well-plates (Nunc) and performed in biological triplicate unless stated otherwise. To prevent floating of the sheets in the wells, o-rings (Viton, type 51414, 14x1mm, Eriks, The Netherlands) were placed on top of the sheets with the exact size of the inner diameter of the well.

C2C12 cells were cultured in proliferation medium containing Dulbecco's Modified Eagle's Medium (D-MEM, Gibco) supplemented with 10 % fetal bovine serum (FBS, Cambrex), 100 U/ml penicillin (Gibco) and 100 μ g/ml streptomycin (Gibco). Cells were grown at 37 °C in a humid atmosphere with 5 % CO₂. Medium was refreshed every two-three days. For proliferation, the cells were plated at 2000-3000 cells/cm² until they reached ~80 % confluence, then they were detached by trypsinization (0.05 % trypsin containing 1mM EDTA) and further sub-cultured or used for seeding on the polymer sheets with a density of 15.000 cells/cm² (unless stated otherwise). Cell numbers were determined by manual counting using a haemocytometer.

5.2.7 Cell culture analysis

Fixation and staining for light microscopy: After the medium was aspirated from the wells, the cell cultured sheets were incubated in 4 %-paraformaldehyde (Merck) in PBS for 30-60 minutes to fixate the cells. Subsequently, the sheets were washed with PBS and a few drops of a methylene blue (1 % in borax) solution were added for 3-5 minutes to stain the cells. Then, the sheets were thoroughly washed with demineralised water to ensure full removal of all excess Methylene blue. The sheets were stored in PBS at 4 °C till time of measurement (within 1 week). Images were taken using light microscopy (Zeiss Axiovert 40 mat and AxioCam MRC 5 camera).

Attachment: Attachment of the cells onto the sheets was determined 4 hours post-seeding by aspirating the seeding suspension and manually counting the number of cells in this suspension. Cell attachment was calculated by the total number of cells seeded minus the number of cells counted in the seeding suspension after 4 hours of attachment.

Proliferation - Trypan blue exclusion: Proliferation of cells after 4 and 8 days was determined via trypan blue exclusion using manual counting. Cells were detached from the sheets by trypsinization, the cell suspension was aspirated and trypan blue (0.4 % solution, Sigma) was added in a 1:1 ratio before counting. Statistical significance was calculated using the student's t-test at $p < 0.05$.

Proliferation - DNA assay: A DNA assay was performed to determine the total concentration of DNA per sample to determine cell proliferation on the various sheets. After washing the sheets with PBS, the cells were lysed (cell culture lysis reagent part #E153A, Promega) and DNA concentrations were measured using a cell proliferation assay according to the manufacturer's protocol (CyQuant Cell Proliferation Assay Kit, Invitrogen/Molecular Probes). Statistical significance was calculated using the student's t-test at $p < 0.05$.

qRT-PCR method: To analyze gene expression, the quantitative reverse transcriptase polymerase chain reaction (qRT-PCR) method was used to determine myogenic differentiation of the C2C12 cells using early and late marker MyoD and Myogenin (primer assay for mouse MyoD1 and MyoG, SABiosciences, Frederick, MD, USA); expression was corrected for murine glyceraldehyde 3-phosphate dehydrogenase (Mus GAPDH, forward: 5'-AACGACCCCTTCATTGAC-3' and reverse: 5'-TCCACGACATACTCAGCAC-3'). To obtain enough RNA, the surface area of the sheets was increased. Therefore, the sheets were placed in 12 well-plates (Nunc) and o-rings of size 19.5x1mm were placed to prevent floating. C2C12 cells were seeded with a seeding density of 15.000 cells/cm² and cultured in triplicate for 4 and 8 days. Medium was refreshed every 2 days. At day 4 and 8, cells on the respective sheets were detached by trypsinization and pellets were prepared. RNA was isolated from the pellets using a Qiagen RNeasy kit (Qiagen, Chatsworth, CA, USA) following the manufacture's protocol. RNA concentration and quality was determined by the Nanodrop method and quality was also confirmed by running the RNA on a 1 wt/vol% agarose gel by electrophoresis. 1 µg of RNA was synthesized into cDNA using Superscript II (Invotrogen, Calsbad, CA, USA) according to the manufacture's protocol. 1µl cDNA was used with 0.5 µM primer in SYBR green I master mix (Invitrogen) and gene expression was determined by real-time qPCR (Bio-Rad iCycler) (40 cycles, melting 15 sec at 95 °C , annealing 30 sec at 55 °C and extension 30 sec at 72 °C). Expression of the MyoD and Myogenin genes was calculated relative to the GAPDH housekeeping gene levels by the $2^{-\Delta\Delta C_T}$ method [19] and statistical significance was calculated using the student's t-test at $p < 0.05$.

5.3 Results and Discussion

5.3.1 PTMC synthesis and characterization

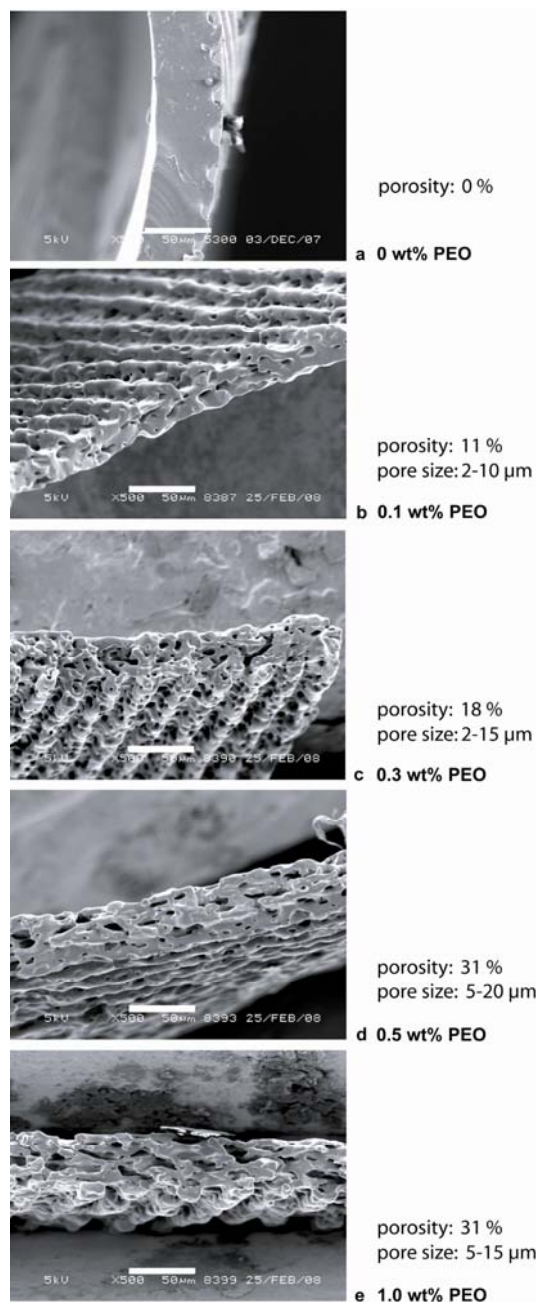
The synthesized PTMC has an average number molecular weight (M_n) of 2.66×10^5 g/mol and shows a polydispersity index (PDI) of 1.39 and an intrinsic viscosity of 3.75 dl/g. More details on the thermal and mechanical properties of PTMC have been reported earlier by Pêgo et al. [7]. DSC data of the sheets prepared with PEO confirm the presence of two separate phases; one corresponding to PTMC ($T_g = -17^\circ\text{C}$) and one corresponding to PEO ($T_g = -56^\circ\text{C}$) in agreement with the DSC results of the pure components ($T_g = -16$ and -51°C , respectively).

5.3.2 PTMC scaffold preparation

Shrinkage and micropattern replication: The polymer sheets shrink extensively during the fabrication process; the sheets cast without PEO shrink up to 200-300% whereas the sheets with PEO shrink up to 130-180%. Although shrinkage influences the final dimensions of the micropattern imprinted into the sheets, the replication of the features of both molds applied is good. The micropattern replication into various sheets can also be observed in SEM images presented in Figure 2, which will be described in more detail in the next paragraph.

There is some variation within the quality and size of the imprinted micropattern, Table 2 lists the original feature dimensions and the final dimensions of the imprinted features of sheets prepared with 0 wt%, 0.5 wt% and 1 wt% PEO for both the 25 μm channel and double brick pattern. The sheets experiencing most shrinkage, i.e. those without PEO, show also the highest deviation of the feature dimensions as could be expected. Apart from the influence in feature dimensions, the sheets prepared with 0.5 and 1 wt% PEO display large surface pores that affect the micropattern to a certain extent. This effect is especially apparent for the 1 wt% PEO sheets including the double brick pattern. In any case, the shrinkage can be taken into account when designing the molds to obtain sheets with the desired final dimensions.

It is finally important to note that handling these thin PTMC sheets ($<30\ \mu\text{m}$) was often difficult due to their flexibility and stickiness. Conditioning of the sheets in culture medium improved handling by decreasing the 'stickiness' of the sheets.

**Figure 2**

Typical SEM cross-section images of 25 μm channel featuring sheets cast from 3 wt% PTMC- CHCl_3 with various amounts of PEO as additive. Amount of PEO with respect to the total weight of the polymer solution (a) 0 wt%, (b) 0.1 wt%, (c) 0.3 wt%, (d) 0.5 wt%, (e) 1.0 wt%. Magnification of all images 500x and the bar in images represents 50 μm .

5.3.3 Porosity and pore morphology

Porosity with additive concentration: Dense sheets were obtained by using a 3 wt% polymer solution of PTMC in chloroform. To introduce porosity, PEO was used as additive at various concentrations (Table 1). Figure 2 shows the SEM images of sheets prepared with increasing concentration of PEO in the casting solution; for each sheet type the porosity and pore size range are presented as well. Both porosity and pore size increase as the PEO concentration in the casting solution increases to 0.5 wt%. Above this value, both porosity and pore size are rather constant (within the measured range). Sheets cast from solutions with 0.1 wt% and 0.3 wt% PEO obtain porosities of 11 % and 18 % combined with a pore size range of 2-10 μm and 2-15 μm respectively (Figure 2b and c). Whereas sheets cast from the 0.5 (Figure 2d) and 1 wt% PEO casting solution (Figure 2e) yield porosities up to 31 % with a pore size range of 5-20 μm . Figure 2a presents the sheets prepared without addition of PEO.

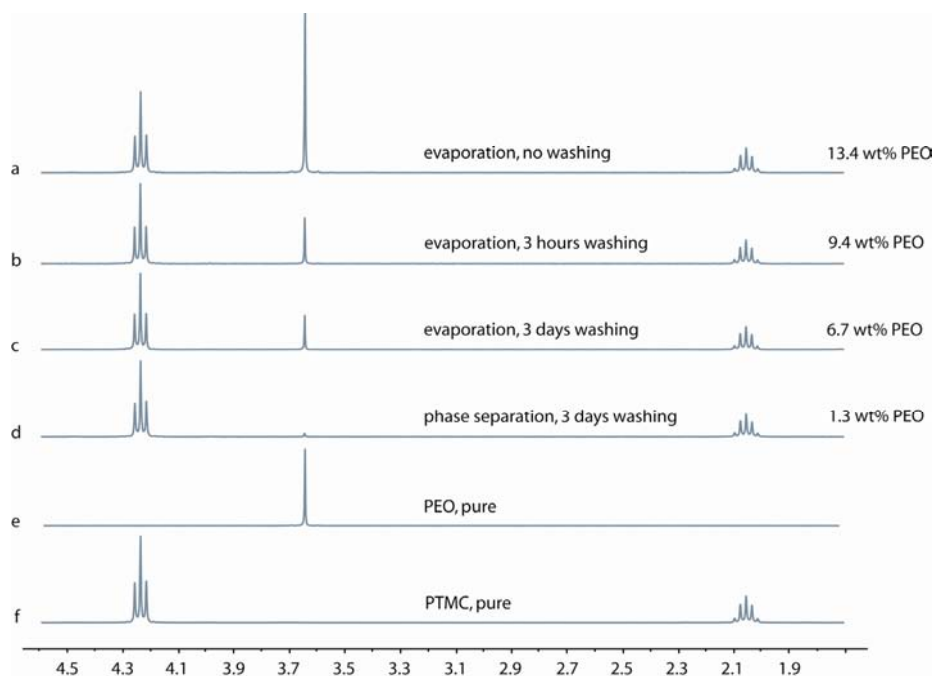


Figure 3 ^1H -NMR spectra of sheets cast from a 0.5 wt% PEO solution after various processing conditions, (a-c) evaporation with subsequently (a) no washing, (b) washing for 3 hours and (c) washing for 3 days, (d) phase separation in non-solvent followed by 3 days of washing, (e) pure PEO and (f) pure PTMC as reference. Peaks represent: $-\text{CH}_2\text{-O}-$ group of PTMC (4.24 ppm), PEO (3.64 ppm), $-\text{CH}_2\text{-}$ group of PTMC (2.05 ppm). The chemical shifts of PTMC (4.24 ppm, 4H and 2.05 ppm, 2H) and PEO (3.64 ppm, 4H) are reported against CDCl_3 (7.26 ppm) reference.

Role PEO in pore formation process: To fully understand the role of PEO in the pore formation and to analyze the influence of the different processing steps, the amount of PEO remaining in the sheets after solidification and washing was determined by ^1H -NMR analysis. Additionally, PTMC sheets cast from 0.5 wt% PEO casting solution processed in different ways were analyzed by SEM. A number of sheets were phase separated; others were left for the solvent to evaporate after casting to preserve the PEO during solidification. Furthermore, various washing times were applied.

Figure 3 e and f show the reference ^1H -NMR spectra recorded for pure PEO and pure PTMC, respectively. Figure 3a-c show the spectra recorded for the solvent-evaporated sheets that were not washed, washed for 3 hours and 3 days, respectively. All these spectra show a clear peak of PEO at 3.65 ppm which decreases significantly when washing is applied. The PEO content in these polymer sheets, calculated from the area under the PEO peak, is 13.4 wt% when no washing is applied which is in close agreement with the theoretically expected amount of 14.3 wt% PEO. After 3 hours washing the PEO content is still 9.4 wt% and after 3 days 6.7 wt%. These results clearly indicate that PEO is entrapped in the solidified sheet, and by washing only up to half of the PEO content can be leached. Figure 3d shows the ^1H -NMR spectrum recorded for the phase separated sheets washed for 3 days, where only a small PEO peak corresponding to 1.3 wt% PEO is observed. When the phase separated sheets were washed for just 3 hours, still the PEO content was only 2.0 wt%. It seems that during phase separation and solvent/nonsolvent exchange, leaching of PEO is promoted and only a small amount of PEO is left in the sheets, perhaps as a nm-thick surface layer. Pêgo et al. suggest that small amounts of PEO staying at the pore wall might actually have a stabilizing effect and assist porosity preservation whereas preparation of porous PTMC by NaCl leaching leads to pore collapse during the washing and/or drying process [20]. Figure 4a-b present SEM images of the solvent evaporated PTMC sheets without washing, whereas Figure 4c-d and e-f present such sheets with washing for 3 hours and 3 days, respectively. These images show that pore formation in the solvent evaporated sheets is poor and pore morphology is not comparable to the interconnected pores observed for the phase separated sheets as presented in Figure 2.

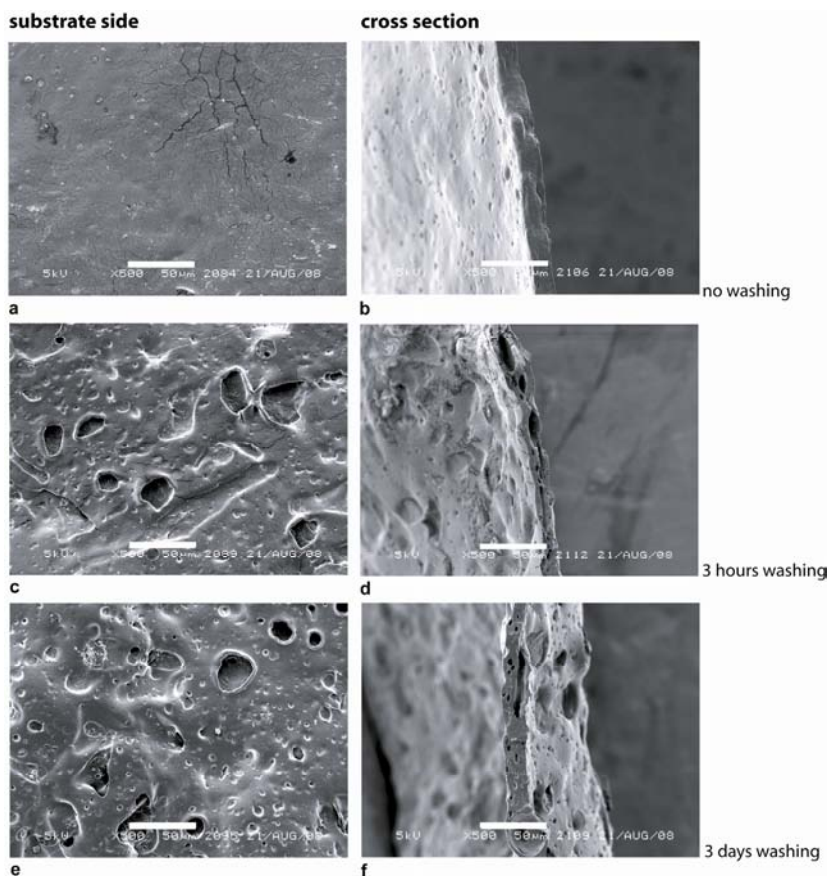


Figure 4 SEM images of the solvent evaporated sheets cast from a 0.5 wt% PEO solution of which the $^1\text{H-NMR}$ spectra are represented in Figure 3. Magnification of all images 500x, bar in images represents 50 μm .

These results clearly indicate that PEO does not act only as pore former or leaching agent, as it happens e.g. with salts such as NaCl, but influences the phase separation process itself, too. The role of high molecular weight PEO in the PTMC-chloroform system seems to resemble that of the high molecular weight additive poly(vinyl pyrrolidone) (PVP) for the preparation of porous membranes of amorphous poly(ether sulfone) (PES) [21]. There, it is suggested that during the first moments (fraction of seconds) after immersing, diffusion of solvent and nonsolvent is dominant and inter-diffusion of the two polymers (main polymer and additive) can be neglected. Therefore, the thermodynamic system can be considered (semi-) ternary with the two polymers regarded as one constituent. On a longer time-scale, inter-diffusion of the polymers becomes more important leading to diffusion into two phases and the system goes from (semi-) ternary to quaternary. By this change in system, demixing conditions are changed and instantaneous demixing can occur leading to the formation of a highly interconnected porous morphology. This phenomenon is in contrast to a more

cellular morphology combined with skin formation at the surface in case of delayed demixing that might occur in the specific ternary system. Furthermore, with increasing polymer concentration in the polymer rich phases, simultaneously the viscosity within these phases rises to the point of vitrification, which is generally considered to finalize the morphology. In most cases, vitrification occurs before the final equilibrium is reached, and therefore still some additive polymer will be present in the main polymer rich phase and can be entrapped permanently.

Our results seem to be in agreement with this theory, the phase separation process does not only facilitate leaching of PEO, but the PEO has an additional role as pore former during phase separation creating highly interconnected pores as discussed in the next section.

Pore interconnectivity: To determine the interconnectivity of the pores, glucose diffusion through the sheets was measured. For dense sheets, prepared without PEO, there is no glucose transport over 24 hours. For porous sheets prepared with 0.5 and 1 wt% PEO, where the pores are 5-20 μm , the glucose transport is equal to the free diffusion coefficient of glucose in water ($9 \times 10^{-10} \text{ m}^2/\text{s}$) [22]. In fact, convective flow of the glucose solution through the sheets was observed while preparing the set-up, showing that these porous sheets have highly interconnected pores despite the relatively moderate porosity of 31 %. The high glucose diffusion is really remarkable when compared to the glucose diffusion of PLLA sheets comprising porosities up to 86 % reported previously [17]. In these systems, the highest diffusion coefficient measured was still one order of magnitude lower compared to the PTMC sheets. This result once more highlights the high pore interconnectivity of the PTMC sheets and supports that PEO induces a change in the thermodynamic system during the phase separation process.

5.3.4 Sheet morphology under physiological conditions

Physiological conditions: The degradation properties of high molecular weight PTMC vary strongly depending on the environment. In PBS, PTMC degrades very slowly with minor decrease of the molecular weight and mass loss over a period of 6 months. On the contrary, degradation *in vivo* is fast by enzymatic surface erosion [5, 6].

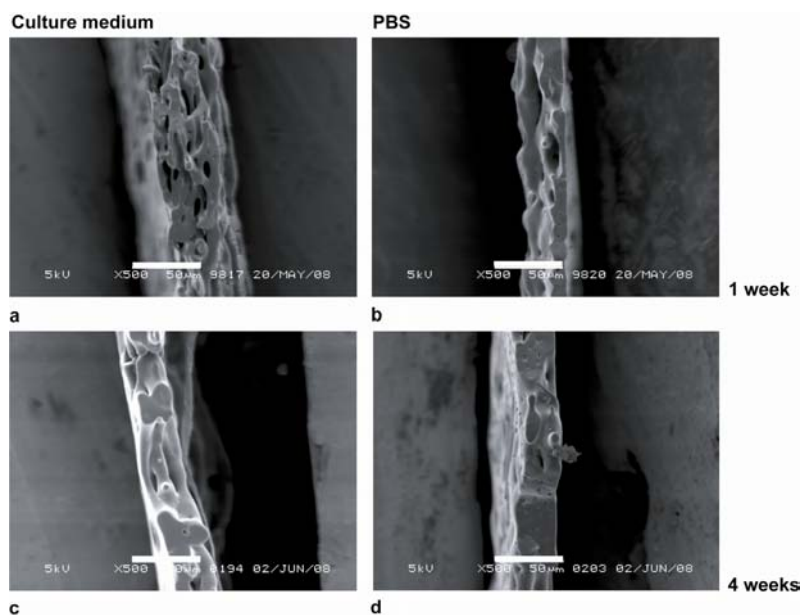


Figure 5 Typical cross-sectional SEM images of sheets cast from a 0.5 wt% PEO solution featuring the 25 μm channel pattern in (a, c) medium or (b, d) PBS at 37 $^{\circ}\text{C}$ for 1 (a, b) and 4 (c, d) weeks. Magnification of all images 500x, bar in images represents 50 μm .

To study the morphology of the processed micropatterned porous PTMC sheets under physiological conditions, the sheets were placed in medium and PBS at 37 $^{\circ}\text{C}$ and at various time-points samples were taken and analyzed. Figure 5 depicts SEM images of 0.5 wt% PEO sheets after 1 and 4 weeks in medium and PBS. When placed in medium, within 1 week the walls thicken and the porosity decreases (Figure 5a), which is even more pronounced for sheets in PBS (Figure 5b). After 4 weeks, sheets placed in both medium and PBS have no pores (Figure 5c-d). Similar phenomena are observed for PTMC sheets with 1 wt% PEO (data not shown). Since PTMC only has about 1.3 % water uptake after 30 days [20], it seems unlikely that swelling causes the change of morphology. It may be envisaged that creep as result of the low T_g in combination with the low Young modulus of the PTMC induces loss of porosity in time.

The porous PTMC sheets also lose their porosity with γ -irradiation, probably due to the high dose of 50 kGy used in these experiments. Therefore, all sheets were stored at -20 $^{\circ}\text{C}$ after preparation as these conditions the porous morphology of the sheets is preserved without the need of any post-processing. It is finally important to note that the stickiness of the thin PTMC sheets is reduced significantly after submerging in medium probably due to adsorption of proteins or other compounds present in the medium on the surface of PTMC sheets.

5.3.5 Cell morphology

Light microscopy images of γ -irradiated PTMC sheets featuring 25 μm wide channels prepared from 0 wt% PEO (Figure 6a) and 0.5 wt% PEO (Figure 6b and c) casting solutions respectively, show good alignment of the C2C12 cells to the pattern. For comparison, Figure 6d-e present the results for PLLA patterned sheets. In both cases (PTMC and PLLA) cell alignment is $75 \pm 2\%$ which is in close agreement with earlier results for PLLA: $81 \pm 5\%$ for 25 μm channel pattern [17]. Despite similar alignment, for the PTMC sheets the cell morphology appears different to PLLA. The cells spread more on the PLLA surface, and are highly organized and stretched on the PTMC surfaces. Additionally, the PTMC patterned sheets seem to facilitate fusion of multiple cells (examples indicated with an arrow in Figure 6c); a first sign of myogenic differentiation, which is the formation of skeletal muscular tissue by myoblast cells fusing into multi-nucleated myotubes [23]. C2C12 cells are known to differentiate into muscular tissue under serum deprived conditions, but might also differentiate under activation by other environmental queues e.g. the surface the cells grow on [24, 25]. To have a more detailed look into this phenomenon, cell proliferation on these sheets was examined in relation to entering the myogenic lineage, as the cells exit the cell cycle and proliferation will be inhibited [26, 27].

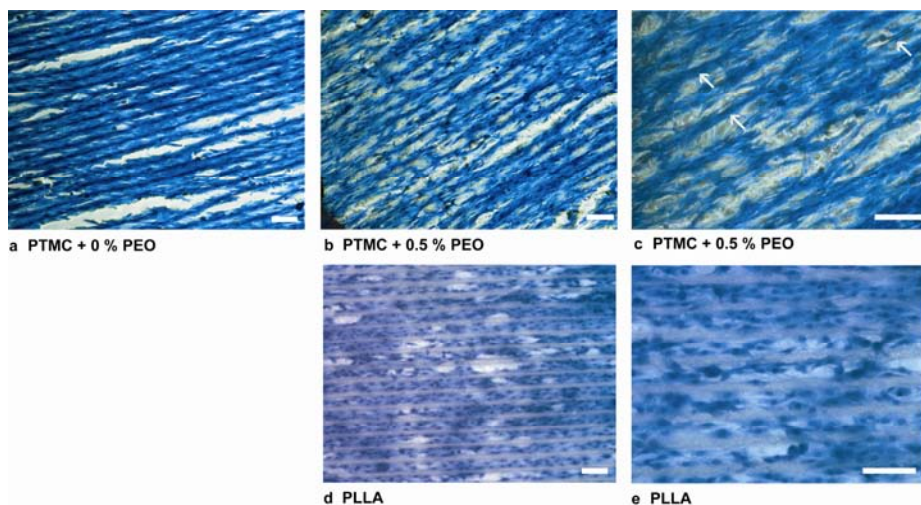


Figure 6 Light microscopy images of C2C12 cells aligning on PTMC sheets (a-c) and PLLA (d-e) featuring 25 μm channels. PTMC sheets were cast from (a) 0 wt% PEO, magnification 10x and (b) 0.5 wt% PEO solutions, magnification 10x (c) close-up of image b, magnification 20x, all sheets were γ -irradiated. As reference porous PLLA sheets also featuring the 25 μm channels are presented as well (d) magnification 10x and (e) a close up of image d, magnification 20x. Seeding density of 15.000 cells/ cm^2 , 4 days of culturing, bars represent 100 μm , arrows indicate specific cell morphology on PTMC sheets.

5.3.6 Cell proliferation

First, the influence of various parameters of the PTMC sheet fabrication process on proliferation of the C2C12 cells was studied; a DNA assay was performed on different cell-cultured sheets. Porous sheets prepared with 0.5 and 1 wt% PEO both nonpatterned and micropatterned, featuring 25 μm wide channels, were studied. Additionally γ -irradiated sheets were taken along in this study to determine the effect of porosity without changing the fabrication conditions of the sheets, including non-porous PTMC sheets without PEO.

Figure 7 presents the DNA concentrations at day 4 for the standard sheets (Figure 7a) and irradiated sheets (Figure 7b) with respect to the corresponding values for TCPS. The results of the standard sheets indicate a decrease in cell proliferation with increasing PEO content in the polymer solution; both patterned as well as nonpatterned sheets cast from the 1 wt% PEO show a significant decrease in cell proliferation compared to TCPS as do the patterned sheets of the 0.5 wt% PEO solution. For the γ -irradiated sheets, with low porosity, only the patterned sheets cast from the 1 wt% PEO solution show a significant decrease compared to the TCPS, all other sheets exhibit similar DNA concentrations (Figure 7b). Comparison of the standard to the non-irradiated sheets indicates only a significant decrease for the patterned sheets cast from the 1 wt% PEO solution.

Combined, the results suggest that the high porosity of the standard sheets seems to affect cell proliferation whereas neither the residue PEO in the sheets as the irradiation process seems to have any effect.

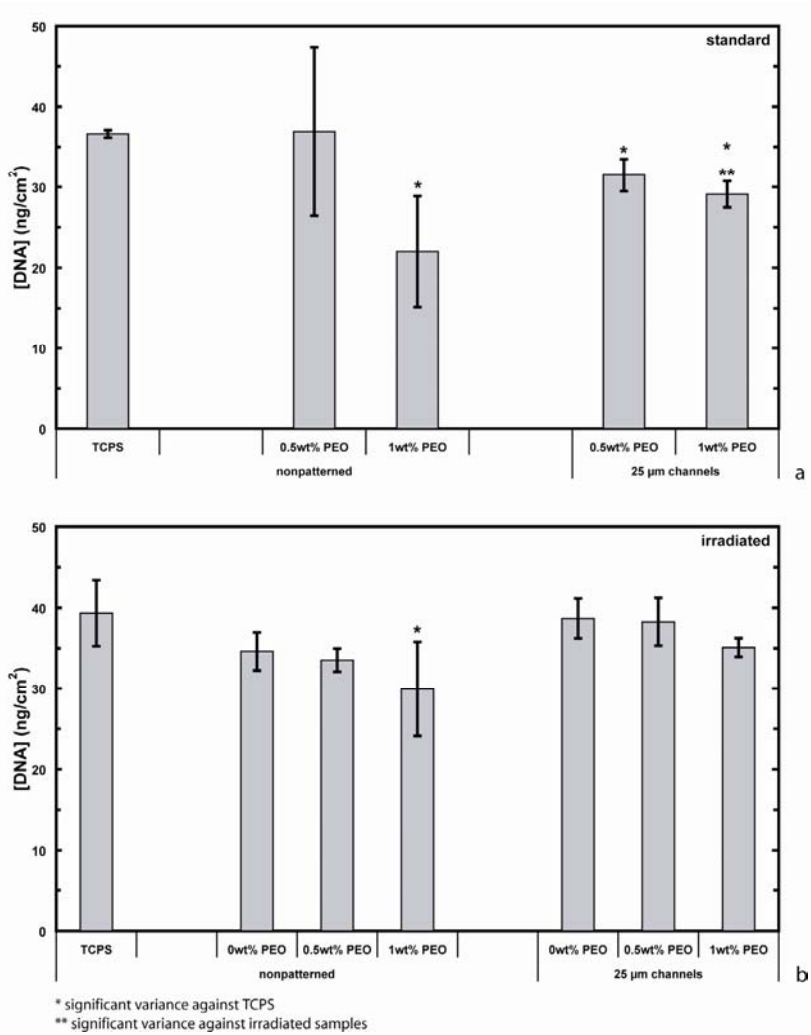


Figure 7 DNA assay for dense (0 wt% PEO) and porous (0.5 and 1 wt% PEO) PTMC sheets with and without pattern for both (a) standard sheets used shortly after casting, washing and drying as (b) sheets that were subsequently γ -irradiated. Seeding density 15.000 cells/cm², culturing for 4 days, significance was calculated by a two-tailed t-test with $P < 0.05$, error-bars indicate standard deviation.

To study the effect of porosity in these PTMC sheets in more detail, additionally cell attachment and proliferation (by trypan blue exclusion and count) up to 8 days was determined for sheets of 0.75 wt% vs. 0 wt% PEO using besides TCPS also dense and porous PLLA sheets as reference material. Figure 8a shows that cell attachment to both dense and porous PTMC sheets is comparable to TCPS and PLLA controls; over 85-95 % of the total number of seeded cells were attached within 4 hours after seeding. Figure 8b indicates no significant variation in cell proliferation on PTMC and PLLA sheets compared to TCPS at day 4, but at day 8 proliferation seems decreased on the porous PTMC

sheets when compared to both the TCPS control and the porous PLLA. This observation is in line with the suggested decrease in proliferation on the 1 wt% PEO sheets at day 4 as presented in Figure 7a. All other sheets are comparable at day 8. When the percentage of dead cells was analyzed, it appeared that the number of dead cells was comparable for all sheets; between 2-5 % at day 4 and 3-7 % at day 8.

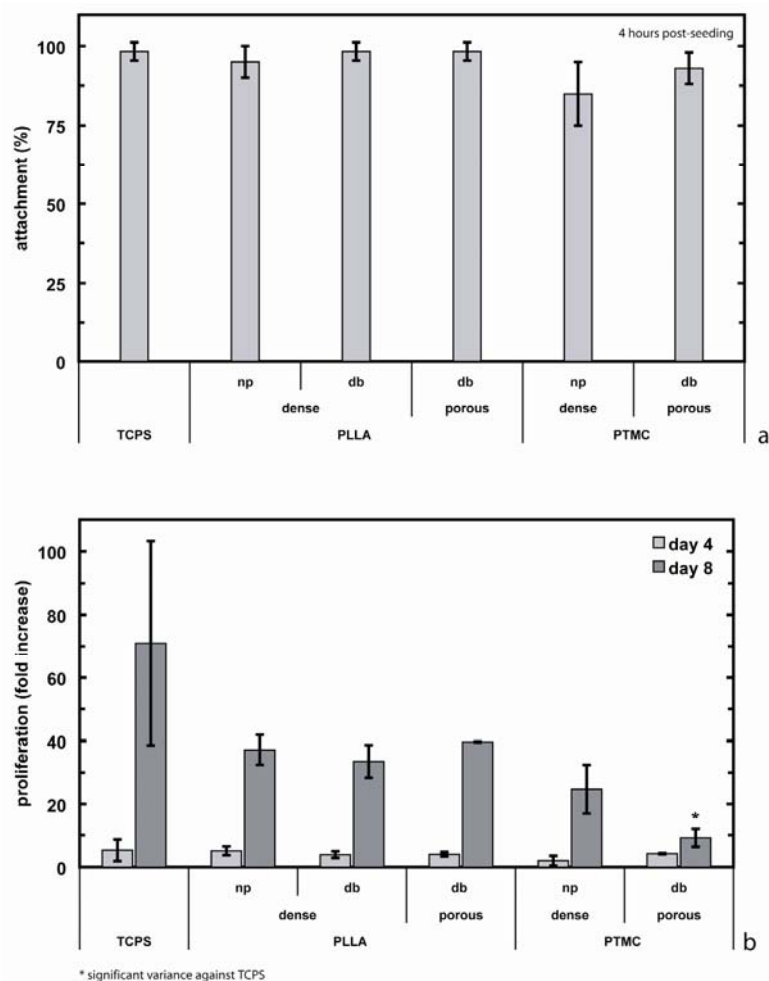


Figure 8 C2C12 cell behavior with respect to PTMC and PLLA sheets including TCPS as reference, (a) attachment after 4 hours of initial seeding, (b) cell proliferation at day 4 and 8 by trypan blue exclusion. For the porous PTMC sheets a 0.75 wt% PEO solution is used. np = nonpatterned, db = double brick pattern, seeding density of 15.000 cells/cm², significance was calculated by a two-tailed t-test with P<0.05, error-bars indicate standard deviation.

These results suggest that neither the type of scaffold material nor the processing conditions, but yet another variable causes the decrease in cell proliferation. The first hypothesis, as also suggested by the cell morphology presented in Figure 6, is that the cells exit from the cell cycle and start differentiating into the myogenic lineage. Another explanation could be the influence of the porosity and/or surface pores, as suggested by the DNA assay data. Perhaps the cells migrate within the scaffold's big surface pores when reaching higher confluency levels, i.e. for longer culturing time. During trypsinization, these cells may be entrapped within the scaffold resulting in lower cell numbers available for counting. In addition, cells grown into the inner-porosity might experience decreased levels of nutrients leading to reduced proliferation rates when the cells on the surface form a monolayer.

To test the first hypothesis of differentiation into the myogenic lineage, expression of two markers upregulated during myogenic differentiation was analyzed. Early and late myogenesis markers, MyoD and Myogenin respectively, were measured at day 4 and 8 for both dense and porous PTMC where PLLA sheets and TCPS again were used as reference. To test the second hypothesis of cell entrapment into the pores, the scaffolds have been fixed and stained by Methylene blue after trypsinization to visualize entrapped cells. Due to the porosity of the scaffolds, and the observed high flux through the porous scaffolds, we assume that the fixative and staining will easily diffuse through the inner-pores of the scaffold and therefore, stain any remaining cells.

Gene expression for myogenic differentiation: Figure 9 presents the fold induction for MyoD and Myogenin (MyoG) of the various scaffold sheets versus the TCPS control. At day 4, the nonpatterned PTMC sheets, both porous and dense, and the patterned dense sheets show down-regulated expression of MyoD (fold induction of 0.3-0.4) and MyoG (fold induction of 0.1-0.2), as do the PLLA nonpatterned dense sheets for MyoG (fold induction of 0.3). The other sheets do not show significant up- or down-regulation at day 4. In general, both myogenesis markers are expressed to a higher extent at day 8 compared to day 4; however, at day 8 the values for the scaffold sheets are more similar to TCPS. At day 8, only the dense nonpatterned PTMC sheets still show significant down-regulation in MyoG expression (fold induction of 0.7). On the other hand, both the porous and dense micropatterned PLLA sheets show an increase in MyoD expression (fold induction of 3.1-3.4) and the porous sheets also for MyoG (fold induction of 2.2) compared to TCPS.

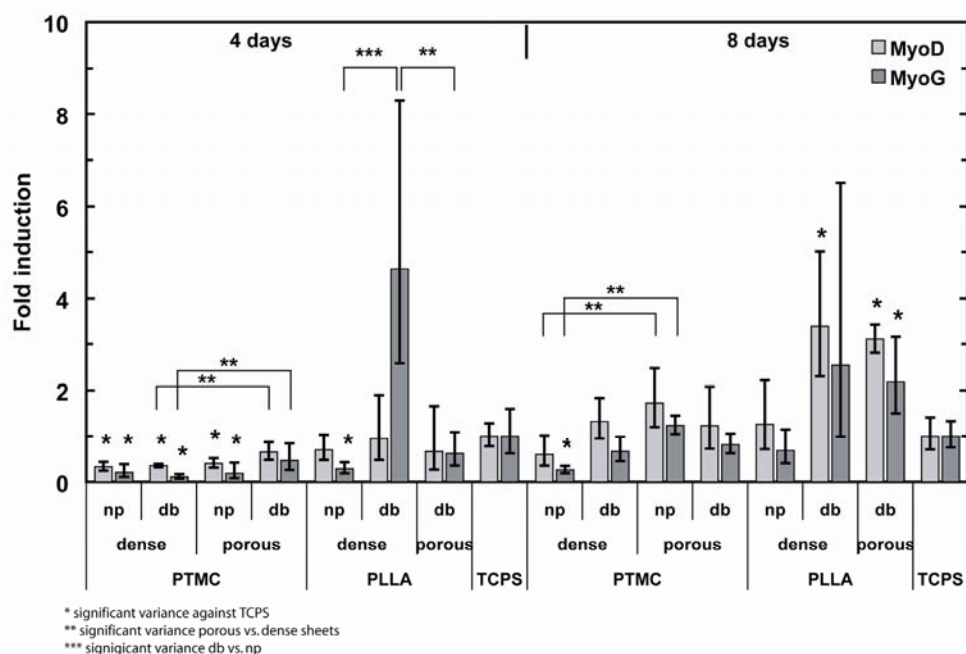


Figure 9 qRT-PCR data on myogenesis for early and late marker MyoD and Myogenin (MyoG), respectively. Fold induction in gene expression with respect to the TCPS control and normalized over GAPDH as determined by the $2^{-\Delta\Delta C_T}$ method. np = nonpatterned, db = double brick pattern, seeding density of 15,000 cells/cm², significance was calculated by a two-tailed t-test with $P < 0.05$, error-bars indicate standard deviation.

From this data, it is clear that the apparent decrease in proliferation rate of the cells on the porous PTMC sheets is not due to the activation of the myogenesis pathway. When comparing the porous PTMC sheets with the corresponding dense sheets, significant increased MyoD and MyoG expression is observed for the patterned sheets at day 4 and nonpatterned sheets at day 8. However, all PTMC sheets except for the porous patterned, inhibit MyoD and MyoG expression at day 4 compared to TCPS implying delayed myogenic differentiation. On day 8, these sheets express similar gene expression levels as the TCPS control except for the dense nonpatterned sheets for which still reduced levels of MyoG are expressed. This phenomenon might suggest that the PTMC material suppresses myogenic differentiation; especially when considering the porous and dense patterned PLLA sheets at day 8 where MyoD expression is significantly up-regulated, as well as MyoG expression for the porous patterned PLLA sheets suggesting that the double brick pattern applied might activate myogenic differentiation. Although, when patterned sheets are compared to the corresponding nonpatterned sheets, only for the dense PLLA sheets at day 4 yield a significant increase in gene expression. The counter effects of the micropatterning and porosity might have reversed the inhibitory effect of PTMC on gene expression of the porous patterned PTMC sheets at day 4, levelling the MyoD and MyoG expression causing only these porous patterned sheets of all

PTMC sheets to express similar MyoD and MyoG levels as compared to TCPS at day 4. However, this effect is not seen for all patterned and/or porous PTMC sheets and therefore, more detailed gene expression analysis is necessary to draw any firm conclusions on the exact effect of PTMC, porosity and the double brick pattern on stimulating or suppressing the myogenic pathway in C2C12 cells.

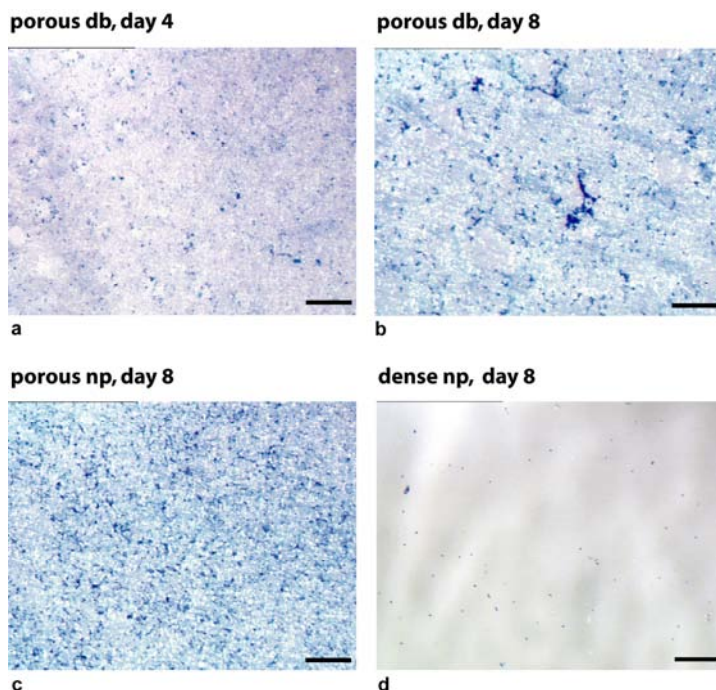


Figure 10 Light microscope images of PTMC sheets after trypsinization, fixation and staining to visualize remaining cells; (a) porous sheet incorporating the double brick pattern, day 4, (b) dense nonpatterned sheet, day 8, (c-d) porous sheets, day 8, without (c) and with (d) the double brick pattern. Magnification 5x, bar represents 200 μm .

Cell entrapment: Figure 10 presents light microscopy images of a dense nonpatterned sheet after 8 days (Figure 10d) and nonpatterned and patterned porous sheets after 4 and 8 days (Figure 10a-c) after trypsinization. A clear contrast between the dense and porous sheets can be observed; cells remain within the porous PTMC sheets whereas no cells remain on the dense sheets after trypsinization, a phenomenon which is more pronounced at day 8 than on day 4. Whether these remaining cells can completely make up for the variation between the dense nonpatterned sheet and the porous patterned sheet can not be concluded from these images. There might be an additional effect of the pores present in the surface inducing reduced surface area where the cells can attach to affecting cell growth when cell number rises. Or creep of the PTMC at the surface might affect cell growth, although no drastic morphological changes were observed for sheets incubated in medium for a period similar to the culture period (Figure 5a); additionally, no increased number of dead cells was seen with the trypan blue exclusion assay as discussed before.

5.4 Conclusions

Porous micropatterned sheets of flexible and amorphous PTMC were prepared using PS μ M. An important finding of this work is the role of PEO as additive in the pore formation process. PEO seems to induce a highly interconnected porous morphology into otherwise dense sheets by changing the thermodynamic conditions during the phase separation process. As a result, the obtained PTMC sheets revealed high glucose diffusivity.

Due to the low Young modulus of PTMC, the sheets shrink significantly during fabrication and the porous morphology changes in time under culturing conditions. Perhaps co-polymers of PTMC with PLA, which combine flexibility and good degradation properties of PTMC with improved mechanical properties of PLA may be used in future studies to avoid shrinkage of the sheets. Despite their rather low Young modulus, the patterned PTMC sheets were replicated well.

The exact effect of PTMC, porosity and micropatterning on the activation of myogenic differentiation in C2C12 cells is not completely clear, although there are indications that PTMC might suppress differentiation at first and porosity and micropatterning might facilitate myogenesis.

The cells attach, align and proliferate well on the surface of PTMC sheets with relatively small pores. Cells partially migrate into the inner-pores of the PTMC scaffolds with relatively large pores.

Acknowledgment


The authors would like to thank Dr. J. de Boer and Prof. Dr. C.A. van Blitterswijk (Department of Tissue Regeneration, University of Twente, The Netherlands) for facilitating the cell culture experiments.

This project is financially supported by the Spearhead program: 'Advanced Polymeric Microstructures for Tissue Engineering' of the University of Twente (BMTi, Institute for Biomedical Technology).

References

1. Murugan R, Ramakrishna S. Design Strategies of Tissue Engineering Scaffolds with Controlled Fiber Orientation. *Tissue Engineering* 2007;13(8):1845-1866.
2. Ma PX. Scaffolds for tissue fabrication. *Materials Today* 2004;7(5):30-40.
3. Gunatillake PA, Adhikari R. Biodegradable Synthetic Polymers for Tissue Engineering. *European Cells and Materials* 2003;5:1-16.
4. Agrawal CM, Ray RB. Biodegradable polymeric scaffolds for musculoskeletal tissue engineering. *Journal of Biomedical Materials Research* 2001;55(2):141-150.
5. Zhang Z, Kuijter R, Bulstra SK, Grijpma DW, Feijen J. The in vivo and in vitro degradation behavior of poly(trimethylene carbonate). *Biomaterials* 2006;27(9):1741-1748.
6. Zhu KJ, Hendren RW, Jensen K, Pitt CG. Synthesis, properties, and biodegradation of poly(1,3-trimethylene carbonate). *Macromolecules* 1991;24(8):1736-1740.
7. Pêgo AP, Grijpma DW, Feijen J. Enhanced mechanical properties of 1,3-trimethylene carbonate polymers and networks. *Polymer* 2003;44(21):6495-6504.
8. Edlund U, Albertsson AC. Degradable Polymer Microspheres for Controlled Drug Delivery, 2001.
9. Engelberg I, Kohn J. Physico-mechanical properties of degradable polymers used in medical applications: A comparative study. *Biomaterials* 1991;12(3):292-304.
10. Jia Y, Shen X, Gu X, Dong J, Mu C, Zhang Y. Synthesis and characterization of tercopolymers derived from ϵ -caprolactone, trimethylene carbonate, and lactide. *Polymers for Advanced Technologies* 2008;19(2):159-166.
11. Zhang Z, Grijpma DW, Feijen J. Triblock Copolymers Based on 1,3-Trimethylene Carbonate and Lactide as Biodegradable Thermoplastic Elastomers. *Macromolecular Chemistry and Physics* 2004;205(7):867-875.
12. Chapanian R, Tse MY, Pang SC, Amsden BG. The role of oxidation and enzymatic hydrolysis on the in vivo degradation of trimethylene carbonate based photocrosslinkable elastomers. *Biomaterials* 2009;30(3):295-306.
13. Qin Y, Yuan M, Li L, Guo S, Yuan M, Li W, et al. Use of polylactic acid/polytrimethylene carbonate blends membrane to prevent postoperative adhesions. *Journal of Biomedical Materials Research Part B-Applied Biomaterials* 2006;79B(2):312-319.
14. Yang S, Leong K-F, Du Z, Chua C-K. The Design of Scaffolds for Use in Tissue Engineering. Part I. Traditional Factors. *Tissue Engineering* 2001;7(6):679-689.
15. Lim JY, Donahue HJ. Cell Sensing and Response to Micro- and Nanostructured Surfaces Produced by Chemical and Topographic Patterning. *Tissue Engineering* 2007;13(8):1879-1891.
16. Khademhosseini A, Langer R, Borenstein J, Vacanti JP. Tissue Engineering Special Feature: Microscale technologies for tissue engineering and biology. *PNAS* 2006 February 21, 2006;103(8):2480-2487.
17. Papenburg BJ, Vogelaar L, Bolhuis-Versteeg LAM, Lammertink RGH, Stamatialis D, Wessling M. One-step fabrication of porous micropatterned scaffolds to control cell behavior. *Biomaterials* 2007;28(11):1998-2009.
18. Vogelaar L, Barsema JN, Rijn CJMv, Nijdam W, Wessling M. Phase separation micromolding - PS μ M. *Advanced Materials* 2003;15(16):1385-1389.

19. Livak KJ, Schmittgen TD. Analysis of Relative Gene Expression Data Using Real-Time Quantitative PCR and the 2- $[\Delta][\Delta]CT$ Method. *Methods* 2001;25(4):402-408.
20. Pego AP, Poot AA, Grijpma DW, Feijen J. Copolymers of trimethylene carbonate and epsilon-caprolactone for porous nerve guides: Synthesis and properties. *J Biomater Sci-Polym Ed* 2001;12(1):35-53.
21. Wienk IM, Boom RM, Beerlage MAM, Bulte AMW, Smolders CA, Strathmann H. Recent advances in the formation of phase inversion membranes made from amorphous or semi-crystalline polymers. *Journal of Membrane Science* 1996;113(2):361-371.
22. Saltzman WM. *Tissue Engineering: principles for the design of replacement organs and tissues*. 1st ed. Oxford: Oxford University Press, 2004.
23. Tannu NS, Rao VK, Chaudhary RM, Giorgianni F, Saeed AE, Gao Y, et al. Comparative Proteomes of the Proliferating C2C12 Myoblasts and Fully Differentiated Myotubes Reveal the Complexity of the Skeletal Muscle Differentiation Program. *Molecular & Cellular Proteomics* 2004 November 1, 2004;3(11):1065-1082.
24. Grossi A, Yadav K, Lawson MA. Mechanical stimulation increases proliferation, differentiation and protein expression in culture: Stimulation effects are substrate dependent. *Journal of Biomechanics* 2007;40(15):3354-3362.
25. Lan MA, Gersbach CA, Michael KE, Keselowsky BG, García AJ. Myoblast proliferation and differentiation on fibronectin-coated self assembled monolayers presenting different surface chemistries. *Biomaterials* 2005;26(22):4523-4531.
26. Boonthekul T, Hill EE, Kong HJ, Mooney DJ. Regulating myoblast phenotype through controlled gel stiffness and degradation. *Tissue Engineering* 2007 Jul;13(7):1431-1442.
27. Yoshida N, Yoshida S, Koishi K, Masuda K, Nabeshima Y. Cell heterogeneity upon myogenic differentiation: down-regulation of MyoD and Myf-5 generates 'reserve cells'. *Journal of Cell Science* 1998 March 1, 1998;111(6):769-779.



Chapter 6 Cell Behavior as Function of Contact Angle and Surface Topography

Abstract

Tuning of surface topography is a tool to vary the wettability of various materials without changing the surface chemistry. This work evaluates the effect of both surface topography and wettability on one another as well as on protein adsorption, cell attachment, proliferation and morphology and reveals insights in the complexity of cell-material interactions. Here, we used three materials, i.e. poly(dimethyl siloxane) (PDMS), poly(L-lactic acid) (PLLA) and a co-polymer of poly(ethylene oxide) and poly(butylene terephthalate) (PEOT/PBT). These materials are used extensively in biomedical applications and tissue engineering and have by nature distinct hydrophobicity. Patterning of the materials with a micropattern array of pillars with variable pillar spacing and pillar height induces changes in hydrophobicity of their surfaces.

C2C12 cells culturing on these surfaces indicates that increased hydrophobicity improves initial cell attachment, which is more pronounced for surfaces already with higher material hydrophobicity, whereas more hydrophilic surfaces support proliferation to a higher extent. With respect to cell morphology, the effect of surface topography appears dominant over the effect of wettability of the surface. Nonetheless, the transition where cells change from growing on top of the pillars to the underlying surface appears to be determined by the wettability of the surface.

6.1 Introduction

Surface characteristics of a tissue engineering scaffolds are of great importance. Besides scaffold material properties as e.g. mechanical strength, flexibility, 3D design and biodegradability, the extent that cells adhere and spread, proliferate and differentiate on the surface determines the final suitability of the scaffold [1, 2]. Protein adsorption to the material plays a key role as cells attach to the material via proteins adsorbed to the surface [3, 4]. *In vivo*, cells attach via proteins in the extra cellular matrix (ECM); whereas *in vitro*, the proteins provided by the serum-enriched medium take over this role. In fact, within seconds after exposure to blood or serum, proteins adsorb to the material [3]. Blood/serum houses many different proteins; nonetheless, cell attachment depends on specific proteins for anchorage and extracellular communications [4]. Therefore, the composition of the protein layer adsorbed onto the material plays a crucial role in the final behavior of the cells towards the scaffold. E.g. vitronectin and/or fibronectin are of vital importance for initial adhesion and spreading of osteoblastic cells (and various other cell types) on many materials [5, 6]. Although the initial composition of the adsorbed protein layer is highly important, the ability of cells to alter and/or capability of cells to adapt to their environment should not be neglected. Cells can e.g. secrete proteins such as fibronectin or regulate its integrin expression to adapt to the available ligands. In addition, the protein layer is a dynamic system of which the composition varies in time by competitive protein adsorption due to displacement of faster diffusing proteins that adhered first by other proteins with higher surface-affinity (Vroman effect) [7].

Distinct characteristics such as surface composition, charge and wettability are reported to influence protein adsorption therewith influencing cell attachment and proliferation on these surfaces [8-15]. Besides, also physical characteristics such as surface topography at nano- (roughness) and micro-scale are known to influence cell attachment and proliferation [16-25].

Studies evaluating the effect of certain parameters on protein adsorption and/or cell behavior often mix two or more parameters due to processing or material selection, causing difficulty to distinguish the dominant factors. When e.g. applying topography to a certain material with methods as etching or oxidation, additionally the roughness of the material and surface energy alters as well. Comparison of various materials amongst one another is usually difficult as surface composition and physicochemical properties, such as hydrophobicity, cannot often be discriminated. Therewith, these studies are open for ambiguous interpretations and report inconsistent roles of e.g. material wettability or surface roughness and topography on specific protein adsorption and cell attachment separately and on each other.

In this paper, we study the effect of wettability as well as surface topography on protein adsorption, cell attachment, proliferation and morphology separately as well as combined. Applying solvent casting on a micropatterned mold allows altering the surface topography of three well-known

biocompatible materials without changing the surface composition or charge. As control, nonpatterned (smooth) surfaces are prepared in similar manner. The materials we selected are: poly(dimethyl siloxane) (PDMS), an highly hydrophobic material often used in microfluidics and lab-on-a-chip applications [26-32]; poly(L-lactic acid) (PLLA), moderately hydrophobic and FDA-approved biomaterial commonly applied in tissue engineering [2, 33, 34]; and PEOT/PBT, a block co-polymer consisting of hydrophilic poly(ethylene oxide) (PEO) and hydrophobic poly(butylene terephthalate) (PBT) segments, FDA-approved and used in bone tissue engineering applications [13, 14, 35, 36].

The micropattern topography is composed of a micropattern pillar array that alters in pillar height and/or repetition frequency allowing tuning of the overall wettability of the substrate. This way, equal contact angles can be acquired for the materials with originally distinct contact angles. Herewith, this study can bring importance to defining cell-material interactions for tissue engineering surfaces.

6.2 Materials and Methods

6.2.1 Topography design

Various silicon molds were fabricated by standard clean-room lithography and etching techniques [37]. The applied topography includes pillars of $5 \times 5 \mu\text{m}^2$ with variable pillar spacing and height. Pillar spacing varies between 2–26 μm , where pillar height varies between 4.5 and 14 μm . Figure 1 illustrates the topography design as imprinted in the polymer sheet, which is the inverse topography etched into the silicon molds. To facilitate release of the hydrophobic polymer sheets, the molds were coated with a nm-thick layer of hydrophobic perfluoro-octyl-trichloro-silane (FOTS). Nonpatterned molds were also used to obtain sheets without pattern as controls.

6.2.2 Micropatterned scaffold sheet preparation and characterization

Casting: To obtain a liquid PDMS solution (Silicone RTV 615 A/B, General Electric), base tetra(trimethylsiloxy)silane (compound A) and curing agent tetramethyl-tetravinyl-cyclotetra-siloxane (compound B) were mixed in a ratio of A:B = 10:1 and placed in a vacuum desiccator to remove all air from the solution. The liquid PDMS solution was cast at an initial thickness of 400 μm and the mold with PDMS film was placed in an oven at 80 °C overnight to crosslink the PDMS.

High molecular weight PLLA (Mw of 5.72×10^5 g/mol, Mn of 4.33×10^5 g/mol, kindly provided by Prof. D. Grijpma, Department of Polymer Chemistry and Biomaterials, University of Twente, The Netherlands) was dissolved in chloroform (Merck, analytical quality, polymer concentration of 2 wt%). The PLLA-CHCl₃ solution was cast at an initial casting thickness of 1500 μm and the solvent was evaporated at room temperature in the air.

Block co-polymer PEOT/PBT with chemical composition 300/55/45 was used; where 300 represents the molecular weight of the starting PEO segments before polymerization, while 55 and 45 represent the percentage of PEO and PBT blocks, respectively. The PEOT/PBT copolymer was dissolved at a polymer concentration of 10 wt% in chloroform and subsequently cast at an initial casting thickness of 1000 μm . The solvent was evaporated in the air at room temperature.

Sterilization: In case of the protein adsorption and cell culturing experiments, 15 mm circular samples were cut from the sheets and immersed in 70% ethanol for 20-30 min. Subsequently, the ethanol was allowed to evaporate in the air and the samples were placed in 24-well plates (tissue culture treated surface, Nunc). To prevent floating of the samples, o-rings (Viton type 51414, 14x1, Eriks, The Netherlands) of the exact inner diameter of the well were placed on top. 70% isopropanol solution was sprayed on the samples, which was allowed to evaporate in a laminar flow cabinet. Finally, the sheets were washed and stored in PBS at 37 °C in humid atmosphere with 5% CO₂ for at least 24 hours to ensure complete wetting.

Contact angle: The water contact angle (CA) of all patterned and nonpatterned sheets was determined by the sessile drop method using an optical contact angle goniometer (contact angle system OCA, Dataphysics instruments GmbH, Germany). All measurements were performed by applying 2 µl drops of Milli-Q water at a rate of 0.5 µl/s at room temperature. A 0.5 ml syringe was used with a needle coated with hydrophobic FOTS to facilitate drop release from the needle. Contact angles were determined manually from images taken 3 seconds after deposition of the droplet, as an average of at least 5 measurements per sample.

Protein adsorption assay: The total amount of proteins adsorbed to the various sheets from full culture medium was determined using a BCA (bicinchoninic acid) kit for colorimetric detection for biological triplicates. The culture medium applied was C2C12 proliferation medium, see cell culturing section. After wetting in PBS for at least 24 hours, the PBS was aspirated from the sheets and 1 ml/well of culture medium was added. The sheets were incubated in the medium for 4 hours at 37 °C in humid atmosphere with 5 % CO₂. Then, medium was aspirated; the sheets were washed in PBS and were placed in new well-plates to eliminate adsorbed proteins to the TCPS. The sheets were incubated for 60-90 min with a 0.1 % triton-X100 solution to lyse the proteins. Total protein adsorbed to the sheets was determined using the BCA protein assay (BCA protein assay kit, Pierce, Rockford, IL) according to the manufacturer's protocol. The obtained values were normalized over the surface area of the nonpatterned samples. For the patterned surfaces, the increased surface area due to the pillars was corrected by normalizing the protein adsorption using the Wenzel's area correction factor [38]. This correction factor is calculated by the dividing the real surface area by the nonpatterned surface area. Statistical significance was calculated using the two-tailed t-test at $p < 0.05$.

6.2.3 Cell culturing and analysis

Pre-myoblasts, C2C12, were cultured on the various sheets to study to what extent cell behavior is influenced by substrate material, surface pattern and contact angle.

Culturing: C2C12 cells were cultured in proliferation medium containing Dulbecco's Modified Eagle's Medium (D-MEM, Gibco) supplemented with 10% fetal bovine serum (FBS, Cambrex), 100 U/ml penicillin (Gibco) and 100 µg/ml streptomycin (Gibco) at 37 °C in a humid atmosphere with 5 % CO₂. The cells were plated at 2000-3000 cells/cm² during expansion phase and upon reaching 70-80% confluency, they were detached by trypsin (0.05% trypsin containing 1mM EDTA). Subsequently the cells were sub-cultured or seeded at a seeding density of 5000 cells/cm² and cultured on the various sheets for 1-4 days with every other day refreshing the medium. A haemocytometer was used for cell number determination by manual counting.

Proliferation assay: The total concentration of DNA was determined per sheet as measure for cell proliferation, performed in biological triplicates. First, the medium was aspirated and the sheets were washed with PBS. Next, the cells were lysed (cell culture lysis reagent part #E153A, Promega) and the DNA concentration was determined by a cell proliferation assay according to the manufacturer's protocol (CyQuant Cell Proliferation Assay Kit, Invitrogen/Molecular Probes). Statistical significance was calculated using the two-tailed t-test at $p < 0.05$.

Fixation and staining for fluorescence microscopy: After aspirating the medium from the wells, the sheets (biological duplicates) were washed with PBS and the cells were fixated by incubation with 4 %-paraformaldehyde (Merck) in PBS for 30-60 min. and washed with PBS. The cells were permeabilized by a 0.1 % Triton-X100 solution for 2-3 min and washed with PBS in excess volume to enable staining of the cells. The cell-cultured sheets were incubated for 10-15 min with the staining solution containing 2.5 vol% AlexaFluor 488 phalloidin and 0.1 vol% Hoechst in PBS to stain the cytoskeleton (F-actin) and nucleus, respectively. After washing the sheets once again with PBS, they were stored in PBS at 4 °C until imaging (within 1 week) by fluorescence microscopy (BD Pathway 435, BD Biosciences).

SEM sample preparation: Scanning electron microscopy (SEM, JEOL 5600LV) was performed on the same samples after fluorescence microscopy. For this, PBS was aspirated and the sheets were washed twice with Milli-Q water to eliminate all residual salts. Then, the sheets were dehydrated in water-ethanol solutions following a gradient (ratio water:ethanol of 100:0, 50:50, 25:75, 10:90, 5:95, and 0:100) and dried in the air at room temperature. The samples were placed at 30 °C under vacuum to ensure complete drying and finally, sputter-coated with a nm-thick gold layer prior to imaging.

6.3 Results and Discussion

6.3.1 Micropatterned scaffold sheet preparation

Solvent casting allows fabrication of patterned as well as nonpatterned sheets for a large variety of materials. The method only requires the existence of a suitable solvent, or the polymer should exist in a liquid state by its own as is the case with un-crosslinked PDMS. Variation in the design of the silicon molds yields different inverse pattern imprints into the polymer sheets. The limitations of the pattern depend on the resolution of the mold fabrication methods, which is in the submicron range. Besides, the mechanical strength of the polymer should be sufficient to preserve the pattern without any additional support; mainly determined by the aspect ratio of the pattern features.

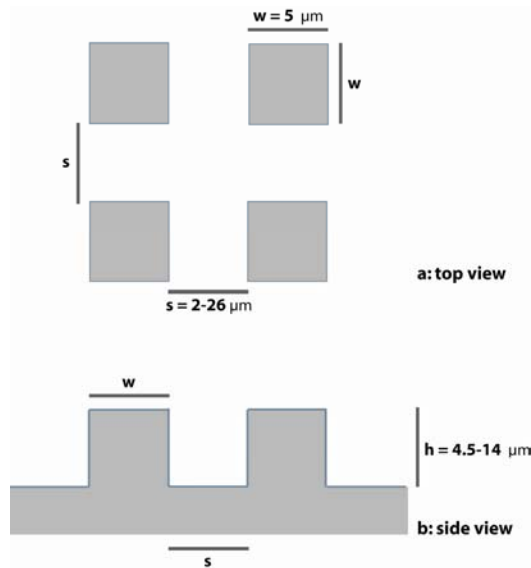


Figure 1 Schematic illustration of the designed pillar arrangement, (a) top view and (b) cross-sectional view. 'w' represents the pillar width, fixed at $5 \times 5 \mu\text{m}^2$, 's' represents pillar spacing, varied between 2–26 μm in combination with a pillar height, varied between 4.5 and 14 μm .

The applied topography features were square pillars of $5 \times 5 \mu\text{m}^2$ of variable spacing and height. Pillar spacing varies between 2–26 μm , whereas pillar height varies between 4.5–14 μm , as illustrated in Figure 1. After solidification of the polymer by evaporation of the solvent or crosslinking, the release of the polymer sheet occurs without problems. For a pillar height between 4.5 and 10 μm , the micropattern replication is good for all polymers and all pillar spacing applied, except for the 10 μm high pillars in PDMS. For pillar height of 14 μm , only for the PLLA sheets the pillar morphology is replicated well; for PDMS and PEOT/PBT, both with lower young's modulus, the pillars do not have

sufficient strength or do not replicate at all. For pillar height of $15.5\text{ }\mu\text{m}$, the replication was not successful for all applied materials and therefore excluded from the study. Figure 2 presents typical SEM images displaying the accuracy of the pillar replication for PEOT/PBT sheets with a pillar height of $10\text{ }\mu\text{m}$.

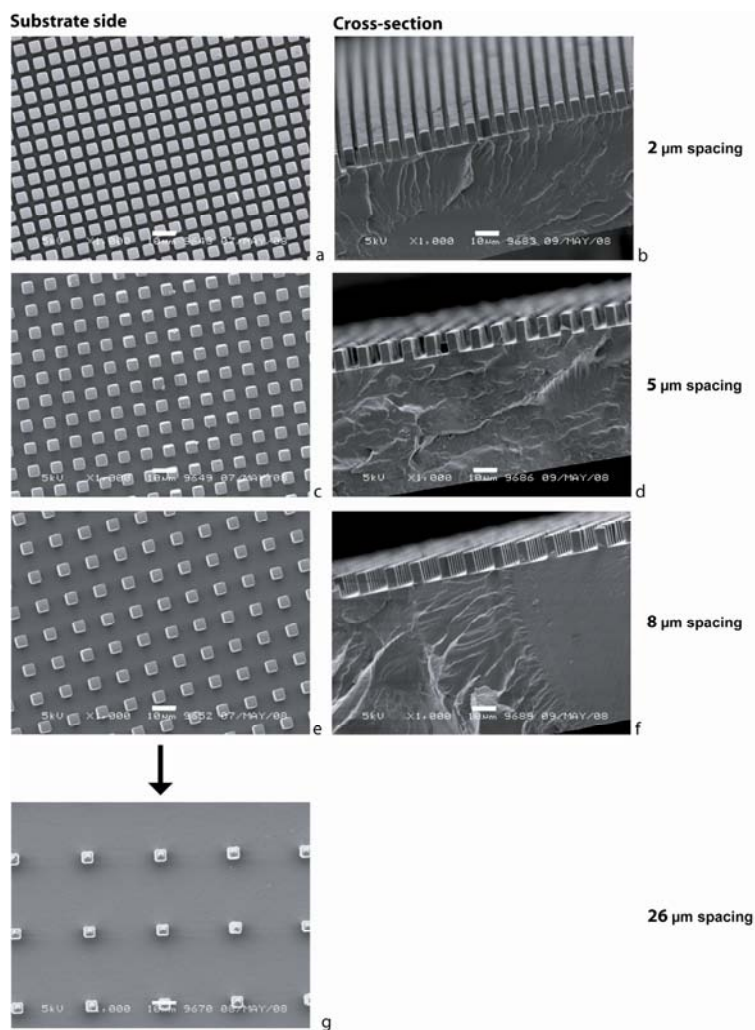


Figure 2 Typical SEM images of micropatterned PEOT/PBT sheets featuring $5 \times 5\text{ }\mu\text{m}^2$ pillars of $10\text{ }\mu\text{m}$ height with varying pillar spacing, (a-b) $2\text{ }\mu\text{m}$, the minimum pillar spacing included in this study, (c-d) $5\text{ }\mu\text{m}$, (e-f) $8\text{ }\mu\text{m}$ and (g) $26\text{ }\mu\text{m}$, the maximum pillar spacing included in this study; (a, c, e, g) substrate side, (b, d, f) cross section. Magnification of all images $1000\times$, bar in images represents $10\text{ }\mu\text{m}$.

During the solidification of the polymer, shrinkage occurs in all directions facilitating sheet release. The continuous layer of the sheet experiences most shrinkage although the pillars also shrink slightly in both height and width. The final obtained pillar dimensions for one dimension set for the various polymers and the initial pillar dimensions on this mold are listed in Table 1.

Table 1 Replication quality of the pillar dimension for various polymers; specified for the case of a mold design with pillar spacing of 8 μm and pillar height of 4.5 μm .

| Substrate | Pillar dimensions (μm) | | |
|-----------|-------------------------------------|---------------|---------------|
| | width (w) | spacing (s) | height (h) |
| Mold | 5.0 | 8.0 | 4.5 |
| PDMS | 4.2-5.0 \pm 0.4 ^a | 7.9 \pm 0.4 | 4.2 \pm 0.8 |
| PLLA | 5.0 \pm 0.4 | 7.9 \pm 0.4 | 4.2 \pm 0.4 |
| PEOT/PBT | 4.4 \pm 0.6 | 7.8 \pm 0.6 | 3.9 \pm 0.6 |

^a The pillar width varies with height; with the larger value at the bottom of the pillar

6.3.2 Contact angle - wettability

Measurements: First, one standard method to measure the contact angles (CA's) was determined to enable good comparison between the measurements as e.g. droplet size [39] and time after deposition highly influences the final measured value. For example, with a droplet of 1 μl deposited on a glass-slide, the observed CA is $56 \pm 4^\circ$ whereas for a droplet of 2 μl the CA is $49 \pm 1^\circ$ and for a droplet of 4 μl it is $41 \pm 1^\circ$. Additionally, the time between deposition and measurement highly influences the result due to possible absorption of water by the material (swelling), evaporation of the water as well as the state of the droplet in case of patterned surfaces (Cassie-Baxter or Wenzel state) [40] as will be discussed in more detail later in this section. Here, in all measurements a water drop volume of 2 μl deposited at 0.5 $\mu\text{l/s}$ and CA determination 3 seconds after deposition was applied. For some samples besides water, the CA was also determined using full culture medium. These experiments (data not shown) revealed that the medium and water CA's are comparable.

Table 2 lists the measured water CA's on nonpatterned sheets of the various polymers and tissue culture polystyrene (TCPS, used as reference in the cell culture experiments) as well as CA's reported in literature for these substrates for comparison.

Table 2 Experimental and reported water contact angles for nonpatterned substrates.

| Substrate | Experimental CA ($^\circ$) | Reported CA ($^\circ$) |
|-----------|------------------------------|-----------------------------------|
| PDMS | 117 \pm 2 | 100-104 [10, 41], \sim 110 [42] |
| PLLA | 73 \pm 3 | 74 [43], 80 [25] |
| PEOT/PBT | 72 \pm 2 | 66 [44] |
| TCPS | 63 \pm 6 | 36-68 [41] |

Effect of topography: When applying the pattern-array, the wettability changes with pillar spacing as well as pillar height. Figure 3 displays the influence of both pillar spacing and –height on the CA for the various materials. In fact, the CA decreases as the pillar spacing increases and generally increases as the pillar height increases. For sheets with a pillar height of 4.5 μm (Figure 3a), the CA on PDMS varies from around 145 to 123° vs. 117° nonpatterned, on PLLA from 118 to 76° vs. 74° nonpatterned and on PEOT/PBT from 101 to 76° vs. 72° nonpatterned. For sheets with a pillar height of 10 μm (Figure 3b), the CA on PDMS even increases up to 151°, for PLLA 133° and for PEOT/PBT up to 117°. All three materials reveal a similar trend with respect to variation in pillar spacing. The CA's decrease with increasing pillar spacing and reach a plateau from a spacing of 11 on when combined with a pillar height of 4.5 μm (Figure 3a); whereas the plateau region is displaced to larger spacing with increased pillar height of 10 μm (Figure 3b). Based on these results, similar CA can be obtained for different materials tailoring the topography. E.g. patterned PLLA sheets with pillar spacing of 5 μm and PEOT/PBT sheets with pillar spacing of 2 μm , both with pillar height of 10 μm , have CA's similar to nonpatterned PDMS.

It is worth to note here that the state in which the droplet exists during the measurement is very important, too. When depositing a droplet on the patterned surface, air may be trapped below the droplet between the pillars so the droplet rests on top of the pillars. In this state, the Cassie-Baxter state [40], the observed CA rises in comparison to the non-patterned surface. The Cassie-Baxter state is thermodynamically not stable and very fast, generally in seconds to minutes, the droplet replaces the air and wets the complete surface [40]. For this transition to the so-called "Wenzel state", the effect of the roughness depends on the initial CA of the material. For material with CA >90°, the Wenzel CA is expected to increase compared to the CA for the nonpatterned surface. However, for material with CA <90°, the Wenzel CA is expected to decrease in comparison to the CA of the nonpatterned surface. Interestingly, for all patterned materials in this study (including PLLA and PEOT-PBT with CA of ~75°), the CA is higher than for the nonpatterned materials. Despite this phenomenon, for which further investigation is required as it might be related to various aspects [45], the patterned surfaces evaluated for protein adsorption and cellular response were pre-wetted for at least 24 hours with PBS; hence, we anticipate that in all cases full wetting (Wenzel state) has been achieved.

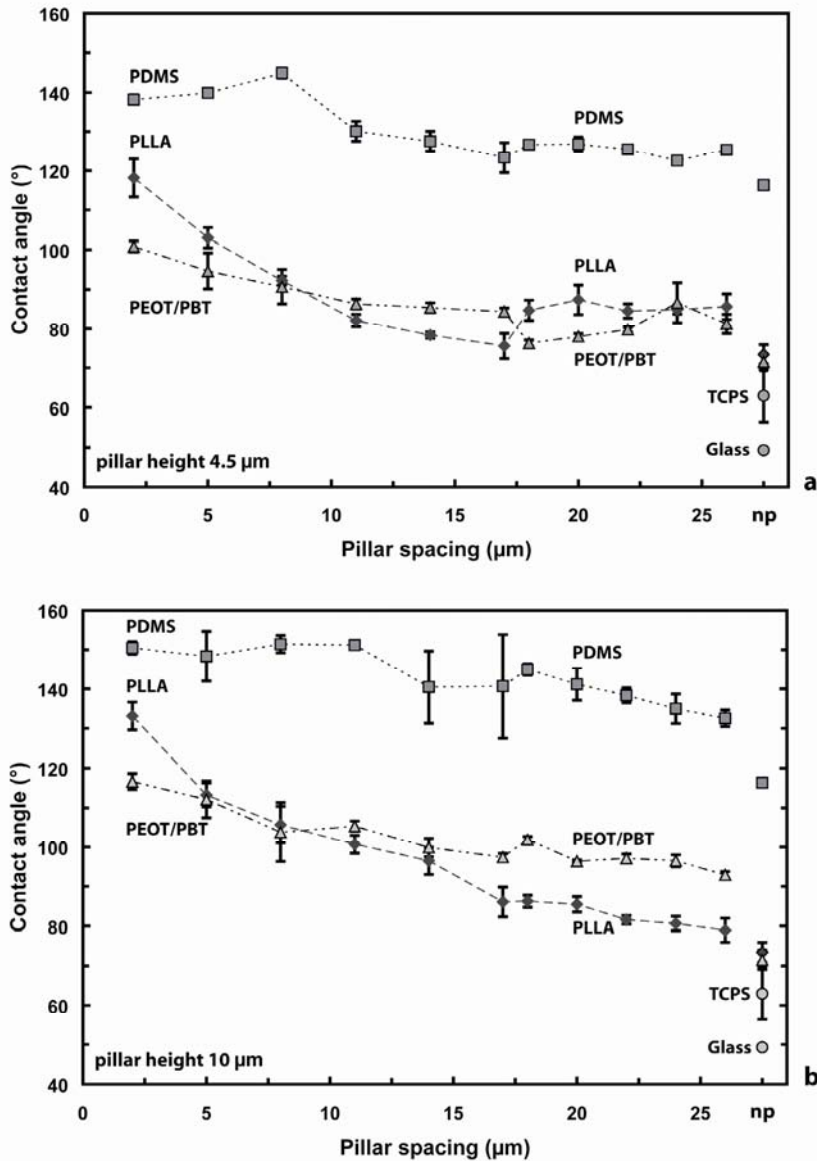


Figure 3 Water contact angles for PDMS, PLLA and PEOT/PBT as function of spacing between the pillars; (a) pillar height of 4.5 μm and (b) pillar height of 10 μm . 'np' stands for nonpatterned, i.e. dense sheet without pillars; error-bars indicate standard deviation.

6.3.3 Protein adsorption

Usually, hydrophobic surfaces appear to have higher overall protein adsorption compared to hydrophilic surfaces; presumably as a result of induced number of adsorption-promoting interactions on the hydrophobic surfaces. These conclusions are based upon the definition that surfaces with water CA's of 65° and higher are considered hydrophobic and CA's below 65° hydrophilic [46]. Nevertheless, the way the proteins adsorb to hydrophobic in comparison to hydrophilic surfaces may cause a reduction in the cell-adhesive function of the surface due to structural changes of the proteins. Unfolding of the protein protects the hydrophobic part of the protein from the aqueous medium and generally induces stronger bonding to hydrophobic surfaces [3, 4, 46]. However, reports in literature on the effect of wettability on protein adsorption vary and some studies show no difference in protein adsorption at all between hydrophobic and hydrophilic surfaces [4]. Besides, proteins adsorption occurs selectively, and therefore, surfaces with varying surface characteristics may express variations in protein adsorption depending on the protein studied [47]. To evaluate the effect of micropatterning on general protein adsorption in correlation with the wettability of the surface, total protein adsorbed to the surfaces after 4 hours incubation in full medium was determined (Figure 4). This data indicates no direct correlation between total protein adsorption and wettability of the surfaces. The nonpatterned PEOT/PBT surface has significantly higher total protein adsorption compared to the other materials. The nonpatterned PDMS, PLLA and TCPS have similar total protein adsorption. The patterned sheets with increased hydrophobicity, featuring pillars with spacing of 2 μm and height of 4.5 μm , reveal no consistent effect on protein adsorption regarding the absolute data (see cross-hatched bars in Figure 4). In this case, the total protein adsorption on hydrophobic PDMS is more than doubled, whereas the value on PLLA remains rather similar and for more hydrophilic PEOT/PBT it decreases significantly compared to the nonpatterned surfaces. However, when the protein adsorption is normalized for the surface enhancement by the pillars [38], the total protein adsorption on all patterned surfaces seem to decrease compared to the nonpatterned surfaces, although only significantly for PEOT/PBT.

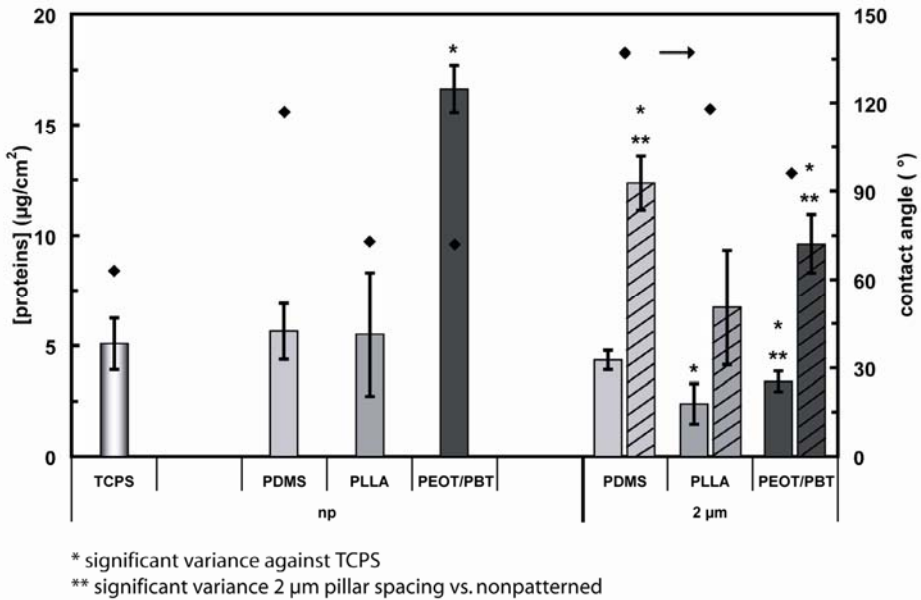


Figure 4 Protein adsorption after 4 hours from full medium on sheets of PDMS, PLLA and PEOT/PBT for nonpatterned (np) and patterned sheets with pillar spacing of 2 µm and pillar height of 4.5 µm, including TCPS as control. On secondary y-axis the corresponding water contact angles of these sheets are presented. Even coloured bars represent protein concentration corrected with Wenzel's area correction factor, where cross-hatched bars represent protein concentrations without this surface enhancement correction. Significance was calculated by a two-tailed t-test with $P < 0.05$, error-bars indicate standard deviation.

This result contrasts the general idea that increasing hydrophobicity leads to enhanced protein adsorption. Nevertheless, it should be noted that there is no consensus in literature on the exact effect of wettability on protein adsorption and part of the observed variations might be due to inconsistent data representation, such as with and without surface enhancement correction [3, 4]. Our data suggests that results should be interpreted carefully and one should be aware how topography affects the surface area and the contact angle.

The reason for the high total protein adsorption of the PEOT/PBT surfaces is not clear, but two hypotheses might explain the phenomenon, either apart or combined. The first hypothesis is related to the swelling behavior of this copolymer leading to high water up-take by the PEOT segments. The absolute values of total protein are normalized over the surface area of the wet sample; increase in surface area by swelling has therefore been taken into account. However, perhaps due to swelling there might be additional protein adsorption within the polymer sheet which cannot be estimated. This phenomenon might explain the generally high total protein values for both nonpatterned and patterned PEOT/PBT sheets. The micropatterned sheets have higher CA's and will swell less due to

the physical restrictions induced by the pillars, which might explain the lower protein adsorption in the matrix in comparison to the nonpatterned PEOT/PBT surfaces. The second hypothesis is related to the composition of the co-polymer: containing hydrophilic (PEO) and hydrophobic (PBT) domains. Protein adsorption on the PEOT/PBT surfaces might be affected by this bi-phase nature. There is well known specific affinity of the proteins towards certain surfaces [47]. When a polymer surface only exposes one phase, this surface will be preferred by only a selection of the proteins present in the serum. However, a surface exposing two phases, such as PEOT/PBT here, with distinct surface characteristics might attract two or more different groups of proteins expressing affinity to either of the phases. Experience with the design and development of dialysis membranes suggest that a delicate balance between hydrophilic and hydrophobic nano-domains can have a significant impact on protein adsorption [48]. Increased protein adsorption on co-polymers with stereocomplexity reported in literature [49] supports this hypothesis.

6.3.4 Cell attachment and proliferation

The total protein adsorption varies for the various surfaces studied here but, as mentioned previously, it is the adsorption of specific proteins that regulate cell attachment on the surfaces. Additionally, protein unfolding might inactivate cell-attachment functions of these specific proteins [3, 4]. A DNA assay on C2C12 cells cultured on the PDMS, PLLA or PEOT/PBT surfaces after 6 hours, 1, 2 and 4 days reveals the cell attachment and cell proliferation in each case (Figure 5). Figure 5a shows DNA concentrations on surfaces with pillar spacing of 2 to 5 μm with a pillar height of 4.5 μm after 6 hours, 1 and 2 days; Figure 5b compares the DNA concentrations on surfaces with pillar spacing varying between 2-14 μm having a pillar height of 4.5 and 10 μm at day 4 (in this latter set of data, PDMS is excluded for the 10 μm pillar height as the pattern did not replicate well).

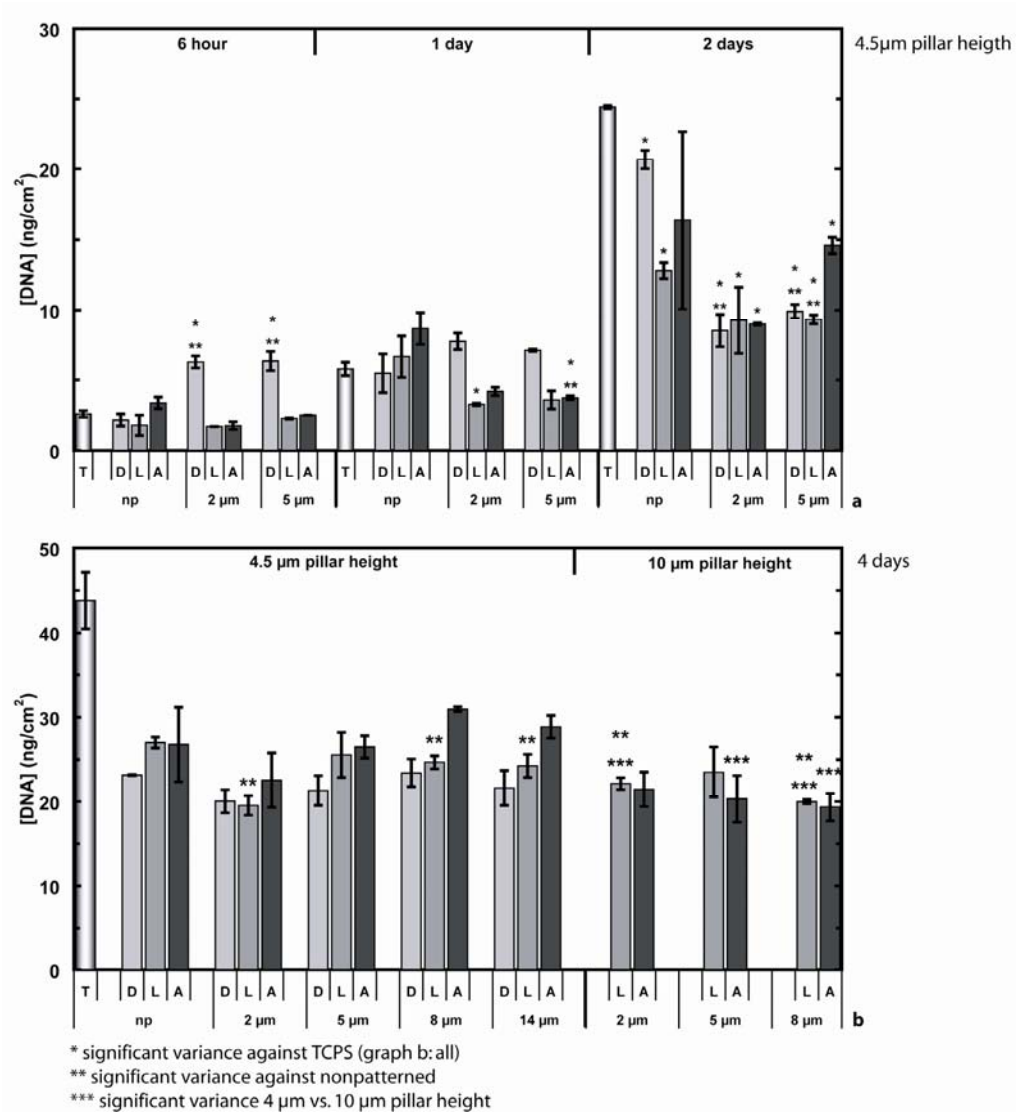


Figure 5

DNA for C2C12 cells cultured on sheets of PDMS (D), PLLA (L) and PEOT/PBT (A) as function of spacing between the pillars (2, 5, and 8 μm), nonpatterned (np) and TCPS (T) are included as controls; (a) pillar height of 4.5 μm after 6, 24 and 48 hours of culture and (b) at day 4 for pillar height of 4.5 and 10 μm. Seeding density 5 000 cells/cm², significance was calculated by a two-tailed t-test with P<0.05, error-bars indicate standard deviation.

These results reveal a number of interesting trends.

- After 6 hours all sheets have rather similar DNA concentration except for the patterned PDMS sheets, which have significantly higher values (Figure 5a). On the contrary, after 48 hours the DNA concentration on the patterned PDMS is significantly lower compared to both TCPS and nonpatterned PDMS. Presumably, proteins responsible for cell attachment adsorb initially to the hydrophobic PDMS surfaces, however, give rather limited support to cell proliferation; maybe due to increased differentiation and/or extracellular matrix synthesis [4].
- The most hydrophilic surface, i.e. TCPS, shows the highest increase in DNA concentration in time. At day 2 (Figure 5a) and day 4 (Figure 5b) all other materials, nonpatterned and patterned, have significantly lower DNA concentrations compared to TCPS. Apparently, TCPS supports proliferation better in comparison to PDMS, PLLA and PEOT/PBT surfaces.
- From day 2 on, patterned PLLA generally has lower DNA concentrations compared to the nonpatterned, except for 2 μm spacing at day 2 (Figure 5a) and 5 μm spacing at day 4 for both pillar heights (Figure 5b). For the PLLA sheets with pillar height of 10 μm , this phenomenon is even more pronounced. The PLLA sheets with both 2 and 8 μm spacing have even significantly lower DNA concentrations when increasing the pillar height from 4.5 to 10 μm .
- For the PEOT/PBT, no clear trend is visible as the DNA concentrations remain rather constant between the nonpatterned and patterned sheets; only at day 1 the sheets with pillar spacing of 5 μm have significantly lower DNA concentrations compared to the nonpatterned sheet (Figure 5a). Additionally, at day 4 a significant decrease in DNA concentration is observed for the PEOT/PBT sheets with 10 versus 4.5 μm pillar height for pillar spacing of 5 and 8 μm (Figure 5b).

These trends reveal that patterning of the surface influences cell attachment as well as proliferation, even though not consistently amongst the materials. Based on these observations, some general trends can be concluded:

- patterning improves initial cell attachment on more hydrophobic materials (PDMS) but reduces proliferation
- more hydrophilic surfaces support proliferation better (TCPS, and to a lesser extent PEOT/PBT)
- attachment to nonpatterned surfaces is not affected by the wettability of the materials

When relating results of the DNA assay (Figure 5) to the total protein adsorption (Figure 4), a weak correlation can be appreciated. After 6 hours, the cells reveal improved attachment to PEOT/PBT for the nonpatterned sheets whereas for the patterned surfaces, the cells attach best to PDMS (Figure 5a). This data is in line with the total protein amount adsorbed to the surfaces, which is also highest for PEOT/PBT amongst the nonpatterned surfaces and for PDMS amongst the patterned surfaces. However, when comparing the protein adsorption values with the DNA assay data for the patterned and nonpatterned surfaces combined, the correlation between amount of protein and DNA concentration does not hold.

Our results suggest that there is no direct correlation between total protein adsorption and cell attachment and proliferation. Effects that might play an important role in this effect are (I) the variation in the specific protein ratio of the adsorbed protein layer and (II) variation in the cell-interaction activity expressed by these proteins due to the level of unfolding. Besides in some cases, the surface topography may be a dominating factor in the cell-material interaction. To get a better understanding of the latter, cell morphology on these surfaces was evaluated as well.

6.3.5 Cell morphology

Figure 6, Figure 7, and Figure 8 present typical fluorescent microscopy and SEM images of C2C12 cells cultured on nonpatterned and patterned PDMS, PLLA and PEOT/PBT surfaces at day 3, respectively. Pillar spacing of 2, 5 and 14 μm are combined with a pillar height of 4.5 and 10 μm ; including the PDMS surfaces with 10 μm high pillars, even though the replication is not accurate due to (partial) pillar merging at the top of the pillars (see Figure 6 j-k). When evaluating the images, distinct changes in cell morphology are visible for the various topographies.

- The cells grown on the nonpatterned PLLA and PEOT/PBT surfaces (images f and l of Figure 7, and Figure 8) spread equally well compared to those on TCPS (data not shown). However, the cells on nonpatterned PDMS (Figure 6 f and l) have a more rounded morphology and grow more in clusters compared to the other materials and TCPS.
- For pillar spacing of 2 μm , spacing well below the cell width, the cells grow on top of the pillars and anchor to the pillars (images a, d, g and j of Figure 6, Figure 7, and Figure 8). The cells spread well; the cells bridge to adjacent pillars to attach while the filopodia of the cells elongate and protrude between the pillars inducing overall a more extended morphology compared to the cells grown on the nonpatterned sheets. This trend is generally more pronounced for a pillar height of 10 versus 4.5 μm . Especially the cells grown on the PEOT/PBT sheets with 2 μm spacing show a distinct pattern of highly stretched filopodia (Figure 8). The cells grown on the sheets with pillar spacing of 5 μm show a transition from growing on top of the pillars to growing on the underlying surface (images b, e, h and k of Figure 6, Figure 7, and Figure 8). On both PLLA (Figure 7) and PEOT/PBT

(Figure 8), the cells tend to grow preferably on the underlying surface for the 4.5 μm high pillars, whereas the cells appear to bridge over the gap to anchor to adjacent pillars with pillars of 10 μm height. When growing on the underlying surface, the cells have a distinct elongated appearance to fit in the limited space between the pillars while directing their filopodia towards other cells along the pillar walls. In contrast, when the cells bridge over to anchor to adjacent pillars, they spread more although their filopodia are elongated and protrude between the pillars towards other cells. These trends are most pronounced on the PEOT/PBT surfaces. On the hydrophobic PDMS (Figure 6), the cells prefer to remain on top of the pillars for both pillar heights. The cells even tend to pull the pillars together to reduce the spacing at certain points, as illustrated in Figure 9a, and will be discussed in more detail later in this section.

- The cells on sheets with pillar spacing of 14 μm grow on the underlying surface between the pillars and preserve a similar morphology to the cells on the respective nonpatterned sheets, independent of the surface material (images c and i of Figure 6, Figure 7, and Figure 8).

Based on the evaluation of the cell morphology on the various surfaces, it appears that the topography itself is dominant concerning cells spreading on the surfaces. Regardless of the material or wettability, the cells grow on top of the pillars for small pillar spacing (2 μm) and on the underlying surface for larger pillar spacing (14 μm). Therefore, the most interesting comparisons with respect to material characteristics arise from the variation at the surfaces featuring 5 μm pillar spacing, which support the trends observed for the DNA concentrations in time (Figure 5). The pulling behavior observed on the PDMS surfaces indicates strong cell attachment to the material. Patterning of highly hydrophobic PDMS initially assists cell attachment by increasing the surface roughness/introducing anchorage points and shows the highest total protein adsorption in comparison to other patterned materials (Figure 4). However, only for PDMS the cells do not tend to grow on the underlying surface of the sheets with 5 μm pillar spacing and pillar height of 4.5 μm , but grow on top of the pillars. This trend suggests that the cells prefer to minimize the contact with PDMS and might explain the limited proliferation on PDMS in comparison to the other materials. On the other hand, cells grown on the PEOT/PBT sheets with 5 μm pillar spacing show the strongest effect of the pillar height; with 4.5 μm height the cells clearly tend to grow on the underlying surface whereas with 10 μm height the cells remain on the top of the pillars. This effect occurs also for PLLA, but not as pronounced, and might account for higher variation in DNA concentration between pillar height on the PEOT/PBT surfaces compared to PLLA at day 4 (Figure 5b) for spacing 5 and 8 μm .

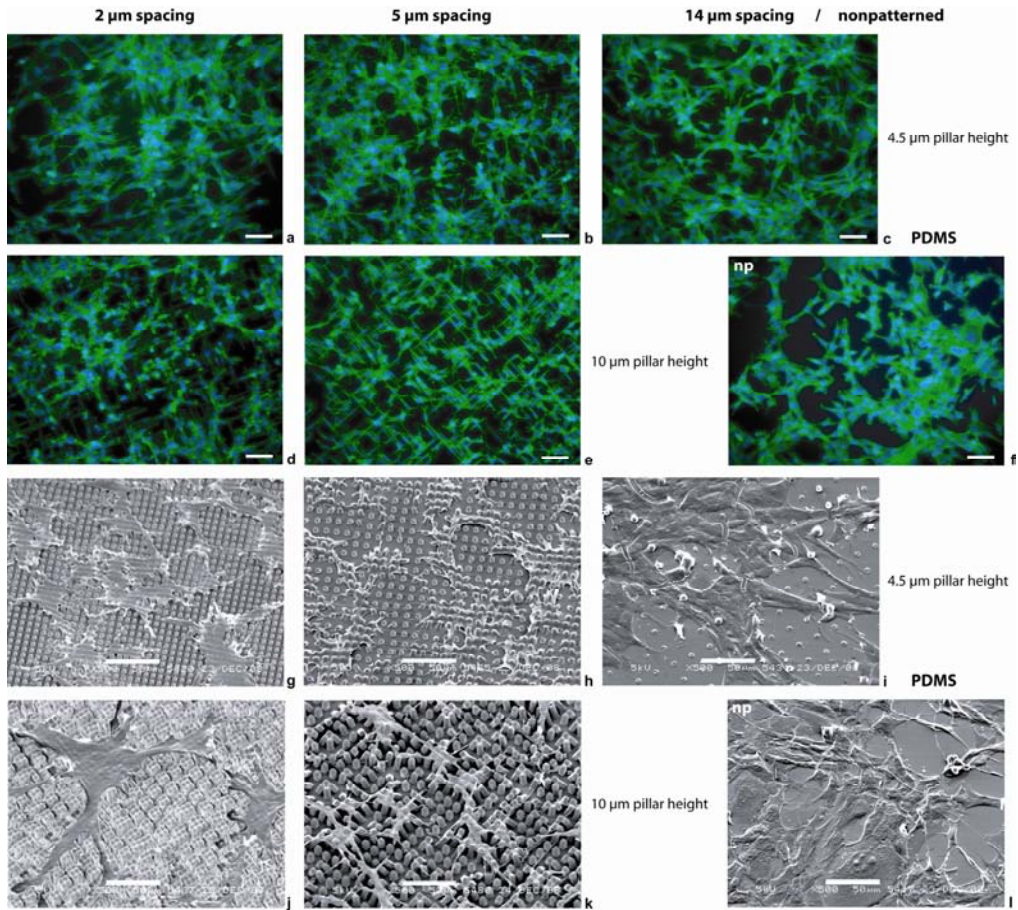
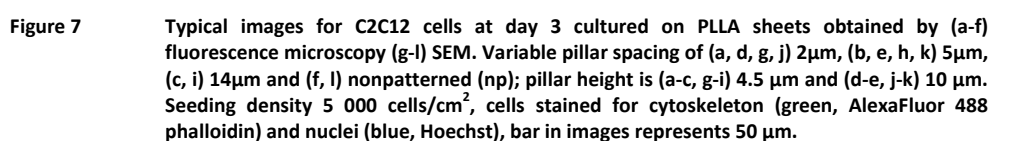


Figure 6 Typical images for C2C12 cells at day 3 cultured on PDMS sheets obtained by (a-f) fluorescence microscopy (g-l) SEM. Variable pillar spacing of (a, d, g, j) 2 μm , (b, e, h, k) 5 μm , (c, i) 14 μm and (f, l) nonpatterned (np); pillar height is (a-c, g-i) 4.5 μm and (d-e, j-k) 10 μm . Seeding density 5 000 cells/ cm^2 , cells stained for cytoskeleton (green, AlexaFluor 488 phalloidin) and nuclei (blue, Hoechst), bar in images represents 50 μm .



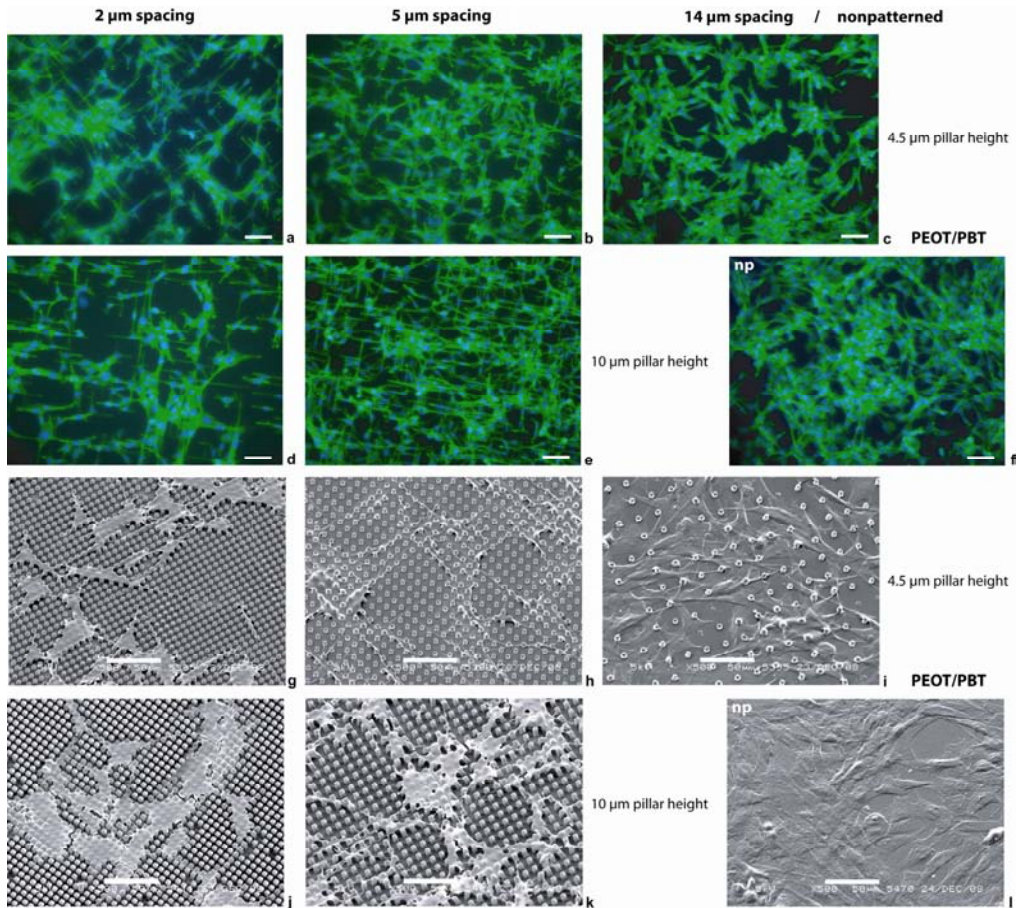


Figure 8 Typical images for C2C12 cells at day 3 cultured on PEOT/PBT sheets obtained by (a-f) fluorescence microscopy (g-l) SEM. Variable pillar spacing of (a, d, g, j) 2 μm , (b, e, h, k) 5 μm , (c, i) 14 μm and (f, l) nonpatterned (np); pillar height is (a-c, g-i) 4.5 μm and (d-e, j-k) 10 μm . Seeding density 5 000 cells/ cm^2 , cells stained for cytoskeleton (green, AlexaFluor 488 phalloidin) and nuclei (blue, Hoechst), bar in images represents 50 μm .

Regarding the pulling phenomenon, Figure 9a and b illustrate the effect of the pulling forces applied by the cells on the flexible PDMS. In fact, stretch-marks appear on the sides of the pillars as well as the underlying surface. Similar stretch-marks appeared in the nonpatterned PDMS surface and to a lesser extent to the PEOT/PBT surfaces with 10 μm high pillars. These results with PDMS are consistent with earlier studies for cardiac myocytes [50]. There, average forces of 140 nN for these cells in the relaxed state and 400 nN in the contracted state were estimated. Clearly, the ease at which the cells can deform the surface is inversely related with the material stiffness. In our case, PDMS has the lowest stiffness (Young's modulus up to 2 MPa [10]), PEOT/PBT has moderate stiffness (Young's modulus \sim 30-70 MPa [51]) and PLLA and TCPS have high stiffness (Young's modulus \sim 2 GPa

[52] and 2-4 GPa [53, 54] respectively). The high stiffness also explains why there is no pulling behavior on the rigid PLLA. Additionally, literature reports that the material stiffness potentially can also affect cell response, attachment and proliferation [10, 55], although the exact effect is not clear and seems to depend on the type of cell and stiffness range of the substrate material [10].

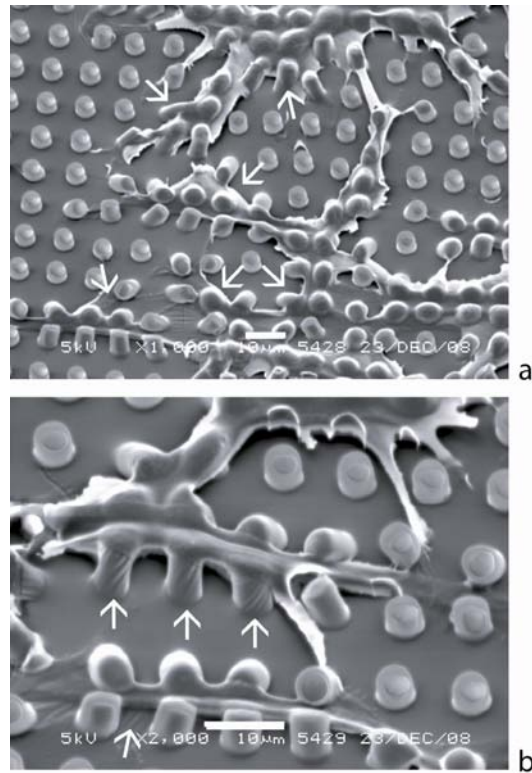


Figure 9

Typical SEM images illustrating the pulling behavior of the C2C12 cells on the PDMS surface for sheets with 5 µm pillar spacing and pillar height of 4.5 µm; (a) arrows indicate pulling together of pillars by the cells, (b) arrows indicate stretch-marks into the PDMS surface due to the pulling force. Seeding density 5 000 cells/cm², pictures imaged at day 3, bar in images represents 10 µm.

6.4 Conclusions

The surface topography of PDMS, PLLA and PEOT/PBT surfaces was altered to vary the wettability of these surfaces without changing the surface chemistry. Small pillar spacing leads to an increase in contact angles. With higher pillar spacing the effect diminishes and reaches a plateau which is nonetheless still higher compared to nonpatterned surfaces.

No clear trend is found between material wettability and total protein adsorption. Presumably, the specific protein ratio in the adsorbed protein layer and/or the cell-interaction activity expressed by these proteins play an important role in the interaction of the surfaces with cells.

Generally, surface topography combined with high hydrophobicity improves initial C2C12 cell attachment, however, more hydrophilic and nonpatterned surfaces seem to support higher cell proliferation and spreading.

With respect to cell morphology, surface topography seems dominant over the wettability; although at a transition between cells growing on top of the pillars to cells growing on the underlying surface, based on pillar spacing, the wettability appears decisive.

Acknowledgment

The authors would like to thank Dr. J. de Boer and Prof. Dr. C.A. van Blitterswijk (Department of Tissue Regeneration, University of Twente, The Netherlands) for facilitating the cell culture experiments.

This project is financially supported by the Spearhead program: 'Advanced Polymeric Microstructures for Tissue Engineering' of the University of Twente (BMTi, Institute for Biomedical Technology).

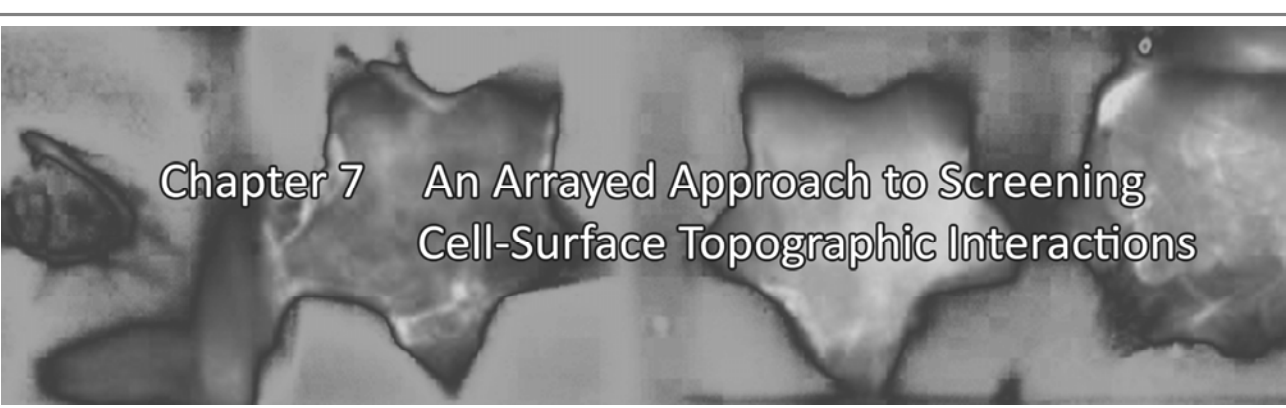
References

1. Chen GP, Ushida T, Tateishi T. Scaffold design for tissue engineering. *Macromol Biosci* 2002 Mar;2(2):67-77.
2. Martina M, Hutmacher DW. Biodegradable polymers applied in tissue engineering research: a review. *Polymer International* 2007;56(2):145-157.
3. Roach P, Eglin D, Rohde K, Perry C. Modern biomaterials: a review—bulk properties and implications of surface modifications. *Journal of Materials Science: Materials in Medicine* 2007;18(7):1263-1277.
4. Wilson CJ, Clegg RE, Leavesley DI, Pearcy MJ. Mediation of Biomaterial-Cell Interactions by Adsorbed Proteins: A Review. *Tissue Engineering* 2005;11(1-2):1-18.
5. Klee D, Hocker H. Polymers for biomedical applications: Improvement of the interface compatibility. *Biomedical Applications: Polymer Blends*. Berlin: Springer-Verlag Berlin, 1999. p. 1-57.
6. Steele JG, McFarland C, Dalton BA, Johnson G, Evans MDM, Howlett CR, et al. Attachment of Human Bone-Cells to Tissue-Culture Polystyrene and to Unmodified Polystyrene - the Effect of Surface-Chemistry Upon Initial Cell Attachment. *J Biomater Sci-Polym Ed* 1993;5(3):245-257.
7. Vroman L, Adams AL. Identification of rapid changes at plasma-solid interfaces. *Journal of Biomedical Materials Research Part A* 1969;3(1):43-67.
8. Allen LT, Tosetto M, Miller IS, O'Connor DP, Penney SC, Lynch I, et al. Surface-induced changes in protein adsorption and implications for cellular phenotypic responses to surface interaction. *Biomaterials* 2006;27(16):3096-3108.
9. Boxshall K, Wu M-H, Cui Z, Cui Z, Watts JF, Baker MA. Simple surface treatments to modify protein adsorption and cell attachment properties within a poly(dimethylsiloxane) micro-bioreactor. *Surface and Interface Science* 2006;38(4):198-201.
10. Brown XQ, Ookawa K, Wong JY. Evaluation of polydimethylsiloxane scaffolds with physiologically-relevant elastic moduli: interplay of substrate mechanics and surface chemistry effects on vascular smooth muscle cell response. *Biomaterials* 2005;26(16):3123-3129.
11. Lee JN, Jiang X, Ryan D, Whitesides GM. Compatibility of Mammalian Cells on Surfaces of Poly(dimethylsiloxane). *Langmuir* 2004;20(26):11684-11691.
12. Lim JY, Shaughnessy MC, Zhou Z, Noh H, Vogler EA, Donahue HJ. Surface energy effects on osteoblast spatial growth and mineralization. *Biomaterials* 2008;29(12):1776-1784.
13. Olde Riekerink MB, Claase MB, Engbers GHM, Grijpma DW, Feijen J. Gas plasma etching of PEO/PBT segmented block copolymer films. *Journal of Biomedical Materials Research Part A* 2003;65A(4):417-428.
14. Papadaki M, Mahmood T, Gupta P, Claase MB, Grijpma DW, Riesle J, et al. The different behaviors of skeletal muscle cells and chondrocytes on PEGT/PBT block copolymers are related to the surface properties of the substrate. *Journal of Biomedical Materials Research Part A* 2001;54(1):47-58.
15. Wei JH, Yoshinari M, Takemoto S, Hattori M, Kawada E, Liu BL, et al. Adhesion of mouse fibroblasts on hexamethydisiloxane surfaces with wide range of wettability. *J Biomed Mater Res Part B* 2007 Apr;81B(1):66-75.
16. Charest JL, Garcia AJ, King WP. Myoblast alignment and differentiation on cell culture substrates with microscale topography and model chemistries. *Biomaterials* 2007;28(13):2202-2210.

17. Hyun J, Chen J, Setton LA, Chilkoti A. Patterning cells in highly deformable microstructures: Effect of plastic deformation of substrate on cellular phenotype and gene expression. *Biomaterials* 2006;27(8):1444-1451.
18. Kidambi S, Udpa N, Schroeder SA, Findlan R, Lee I, Chan C. Cell Adhesion on Polyelectrolyte Multilayer Coated Polydimethylsiloxane Surfaces with Varying Topographies. *Tissue Engineering* 2007;13(8):2105-2117.
19. Kunzler TP, Drobek T, Schuler M, Spencer ND. Systematic study of osteoblast and fibroblast response to roughness by means of surface-morphology gradients. *Biomaterials* 2007;28(13):2175-2181.
20. Lim JY, Donahue HJ. Cell Sensing and Response to Micro- and Nanostructured Surfaces Produced by Chemical and Topographic Patterning. *Tissue Engineering* 2007;13(8):1879-1891.
21. Mata A, Boehm C, Fleischman AJ, Muschler GF, Roy S. Connective tissue progenitor cell growth characteristics on textured substrates. *International Journal of Nanomedicine* 2007;2(3):1-18.
22. Mills CA, Fernandez JG, Martinez E, Funes M, Engel E, Errachid A, et al. Directional alignment of MG63 cells on polymer surfaces containing point microstructures. *Small* 2007 May;3(5):871-879.
23. Mitragotri S, Lahann J. Physical approaches to biomaterial design. *Nat Mater* 2009;8(1):15-23.
24. Sun T, Tan H, Han D, Fu Q, Jiang L. No Platelet Can Adhere - Largely Improved Blood Compatibility on Nanostructured Superhydrophobic Surfaces. *Small* 2005;1(10):959-963.
25. Wang Y-Q, Cai J-Y. Enhanced cell affinity of poly(L-lactic acid) modified by base hydrolysis: Wettability and surface roughness at nanometer scale. *Current Applied Physics* 2007;7(Supplement 1):e108-e111.
26. Chiu DT, Jeon NL, Huang S, Kane RS, Wargo CJ, Choi IS, et al. Patterned deposition of cells and proteins onto surfaces by using three-dimensional microfluidic systems. *PNAS* 2000 March 14, 2000;97(6):2408-2413.
27. Dusseiller MR, Niederberger B, Stadler B, Falconnet D, Textor M, Voros J. A novel crossed microfluidic device for the precise positioning of proteins and vesicles. *Lab On A Chip* 2005;5(12):1387-1392.
28. El-Ali J, Sorger PK, Jensen KF. Cells on chips. *Nature* 2006 Jul 27;442(7101):403-411.
29. Gomez-Sjoberg R, Leyrat AA, Pirone DM, Chen CS, Quake SR. Versatile, Fully Automated, Microfluidic Cell Culture System. *Analytical Chemistry* 2007;79(22):8557-8563.
30. Kim L, Toh Y-C, Voldman J, Yu H. A practical guide to microfluidic perfusion culture of adherent mammalian cells. *Lab on a chip* 2007;7(6):681-694.
31. Korin N, Bransky A, Dinnar U, Levenberg S. A parametric study of human fibroblasts culture in a microchannel bioreactor. *Lab on a chip* 2007;7(5):611-617.
32. Tanaka Y, Morishima K, Shimizu T, Kikuchi A, Yamato M, Okano T, et al. An actuated pump on-chip powered by cultured cardiomyocytes. *Lab on a Chip* 2006 Mar;6(3):362-368.
33. Chan G, Mooney DJ. New materials for tissue engineering: towards greater control over the biological response. *Trends in Biotechnology* 2008;26(7):382-392.
34. Kretlow JD, Mikos AG. From material to tissue: Biomaterial development, scaffold fabrication, and tissue engineering. *AIChE Journal* 2008;54(12):3048-3067.
35. Moroni L, de Wijn JR, van Blitterswijk CA. 3D fiber-deposited scaffolds for tissue engineering: Influence of pores geometry and architecture on dynamic mechanical properties. *Biomaterials* 2006;27(7):974-985.

36. Moroni L, Licht R, de Boer J, de Wijn JR, van Blitterswijk CA. Fiber diameter and texture of electrospun PEOT/PBT scaffolds influence human mesenchymal stem cell proliferation and morphology, and the release of incorporated compounds. *Biomaterials* 2006;27(28):4911-4922.
37. Betancourt T, Brannon-Peppas L. Micro- and nanofabrication methods in nanotechnological medical and pharmaceutical devices. *International Journal of Nanomedicine* 2006;1(4):483-495.
38. Wenzel RN. Resistance of Solid Surfaces To Wetting by Water. *Industrial & Engineering Chemistry* 1936;28(8):988-994.
39. Letellier P, Mayaffre A, Turmine M. Drop size effect on contact angle explained by nonextensive thermodynamics. Young's equation revisited. *Journal of Colloid and Interface Science* 2007;314(2):604-614.
40. Bico J, Marzolin C, Quéré D. Pearl drops. *Europhysics letters* 1999;47(2):220.
41. Saltzman WM. *Tissue Engineering: principles for the design of replacement organs and tissues*. 1st ed. Oxford: Oxford University Press, 2004.
42. Sugiura S, Edaheiro J-i, Sumaru K, Kanamori T. Surface modification of polydimethylsiloxane with photo-grafted poly(ethylene glycol) for micropatterned protein adsorption and cell adhesion. *Colloids and Surfaces B: Biointerfaces* 2008;63(2):301-305.
43. Nisbet DR, Pattanawong S, Nunan J, Shen W, Horne MK, Finkelstein DI, et al. The effect of surface hydrophilicity on the behavior of embryonic cortical neurons. *Journal of Colloid and Interface Science* 2006 Jul 15;299(2):647-655.
44. Claase MB, de Riekerink MB, de Bruijn JD, Grijpma DW, Engbers GHM, Feijen J. Enhanced bone marrow stromal cell adhesion and growth on segmented poly(ether ester)s based on poly(ethylene oxide) and poly(butylene terephthalate). *Biomacromolecules* 2003 Jan-Feb;4(1):57-63.
45. Dorrer C, Ruhe J. Some thoughts on superhydrophobic wetting. *Soft Matter* 2009;5(1):51-61.
46. Vogler EA. Structure and reactivity of water at biomaterial surfaces. *Advances in Colloid and Interface Science* 1998;74(1-3):69-117.
47. Okano T, Nishiyama S, Shinohara I, Akaike T, Sakurai Y. Interaction between Plasma Protein and Microphase Separated Structure of Copolymers. *Polymer Journal* 1978;10(2):223-228.
48. Krause B, Storr M, Ertl T, Buck R, Hildwein H, Deppisch R, et al. Polymeric membranes for medical applications. *Chemie Ingenieur Technik* 2003 Nov;75(11):1725-1732.
49. Nagahama K, Nishimura Y, Ohya Y, Ouchi T. Impacts of stereoregularity and stereocomplex formation on physicochemical, protein adsorption and cell adhesion behaviors of star-shaped 8-arms poly(ethylene glycol)-poly(lactide) block copolymer films. *Polymer* 2007;48(9):2649-2658.
50. Kajzar A, Cesa CM, Kirchgessner N, Hoffmann B, Merkel R. Toward physiological conditions for cell analyses: Forces of heart muscle cells suspended between elastic micropillars. *Biophysical Journal* 2008 Mar 1;94(5):1854-1866.
51. Claase MB. Cell-seeded scaffolds based on poly(ethylene oxide) and poly(butylene terephthalate) block copolymers for bone tissue engineering. Enschede: University of Twente; 2004.
52. Gay S, Arostegui S, Lemaître J. Preparation and characterization of dense nanohydroxyapatite/PLLA composites. *Materials Science and Engineering: C* 2009;29(1):172-177.
53. Kim HI, Takai M, Ishihara K. Bioabsorbable Material-Containing Phosphorylcholine Group-Rich Surfaces for Temporary Scaffolding of the Vessel Wall. *Tissue Engineering* 2009.
54. Lubarsky GV, Davidson MR, Bradley RH. Elastic modulus, oxidation depth and adhesion force of surface modified polystyrene studied by AFM and XPS. *Surface Science* 2004;558(1-3):135-144.

55. Wang H-B, Dembo M, Wang Y-L. Substrate flexibility regulates growth and apoptosis of normal but not transformed cells. *American Journal of Physiology - Cell Physiology* 2000 November 1, 2000;279(5):C1345-1350.



Chapter 7 An Arrayed Approach to Screening Cell-Surface Topographic Interactions

Abstract

High-throughput screening within the field of material science (materiomics) is largely unexplored even though research areas like biomaterials and tissue engineering science would clearly benefit from rapid screening of material surface libraries. Considering the fact that studies involving only a limited number of variations already present distinct effects on cell behavior, one can only imagine the potential outcome of expanding such studies to high-throughput screening.

In this work, we present a new approach within the materiomics concept: a 2x2 cm² chip comprising a library of 40.000 arrayed surface topographies (designated TopoChip) to perform high-throughput screening of cellular responses to different biomaterial surface properties. Nearly 8500 unique surface topographies are enclosed within this proof-of-concept TopoChip design, a number that can dramatically expand by variation in e.g. surface biomaterial. TopoChips were fabricated of biopolymers as poly(lactic acid) (PLA), and were either or not coated with a nanometer-thick titanium or biomimetic calcium phosphate layer. The response of, amongst others, human mesenchymal stem cells to these topographical libraries was evaluated by seeding the cells onto the TopoChips and culturing them for a desired amount of time according to the assay requirements. Seeding and culturing of the cells on the TopoChip is performed using a specially designed device resulting in uniform distribution of the cells along the TopoChip and supporting successful sustained culture of the cells. Distinct cell behavior towards various surface topographies could be distinguished when imaging the cells cultured onto the TopoChip. High-content cellular imaging and computational image analysis were used to aid the image acquisition and analysis for immunofluorescence based assays.

A revised manuscript based on this chapter is in preparation to be submitted, authors are:
Bernke J. Papenburg*, Hemant Unadkat* (* Both authors contributed equally to this manuscript)
R. Truckenmueller, M. Wessling, D. Stamatialis, C.A. van Blitterswijk, J. de Boer

7.1 Introduction

Biomaterials are applied for numerous clinical applications, ranging from stents, orthopedic implants, and sutures to contact lenses. In all these cases the response of the human body to these materials depends on the interface between the materials and cells. In some cases the interaction between cells and materials is not optimal as is the case with certain orthopedic implants which have an average lifetime of 10 to 15 years, due to an increasingly high failure rate. Often, rather than bonding directly with the bone, implants are encapsulated by fibrous tissue upon implantation. Hence, a lot of effort is dedicated to modifying the surfaces of the implants. This can either be done chemically e.g. using calcium phosphate coatings [1] of the implants or by physically modifying the surface of the implant through varying the surface roughness e.g. by sand blasting [2]. Both technologies significantly improved the performance of orthopedic implants, signifying the potential of surface modification for optimising medical devices. One of the drawbacks of these techniques is that they offer only limited control of surface characteristics. However, with the advent of new developments in micro- and nanotechnologies it is possible to create surfaces with precisely designed feature sizes and shapes up to nanometer resolution. Some of the pioneering manuscripts in the field did not only show proof-of-principle for micro- and nanopatterning of biomaterial surfaces but also disclosed an unprecedented control of material surface on the behaviour of cells growing on them. For instance, Chen and co-workers used micro-scale patterning techniques to fabricate planar adhesive islands of defined size and shape. They demonstrated that the shape of the cell dictates whether an individual cell will grow or die [3]. Using a similar approach, the decision of a mesenchymal stem cell to either become a fat cell or bone cell depended on the shape the cell was forced into and correlated with the activation of the RhoA signalling pathway [4]. Micro- and nanotechnology can also be used to control surface topography, a parameter which is known to influence the behaviour of cells growing on it. Micrometer-range patterning is e.g. used to align cells on biomaterial surfaces [5, 6], whereas Dalby et al. reported that randomly placed nanotopographies were able to induce osteogenic differentiation of mesenchymal stem [7]. Unfortunately, nature does not prescribe the optimal surface topography for a given biomedical application and the number of possible surface patterns that can be created is virtually unlimited, considering that cells are in the order of tens of micrometers whereas patterns can be created at nanometer resolution. The underlying mechanisms defining the interplay of a cell with its substrate are only partially understood. Additionally, the specific application of the biomedical device is highly important, as e.g. an orthopedic implant requires a different biological response than a cardiovascular stent. Hence, determining the distinct surface to elicit an appropriate bio-active response is still a challenge. Due to this complex interplay between cells and surfaces, rational approaches may omit unperceived paradigms [8]. Hence, in the recent years there has been a shift from the rational design of biomaterials to combinatorial

screening approaches used typically in the pharmaceutical industry for drug discovery [9], which we refer to as materiomics. In a landmark study Anderson et al. identified a host of unexpected material effects that offered new levels of control over human embryonic stem cell behavior while evaluating an array of nearly 600 different co-polymer compositions [10]. Quintessential aspects of high-throughput biomaterial screening are the preparation of libraries of surfaces and miniaturization of the biological assays to read out the response of cells. When combined with advances in high-content imaging and computational image analysis, this approach will pave a way for finding the right biomimetic surface properties.

7.2 Concept

7.2.1 Paradigm

Figure 1a illustrates the general materiomics paradigm and highlights the application of high-content imaging with libraries expressing variations in surface properties to overcome the usual limitations in number of cell-material interactions. Our approach within the materiomics concept combines high content bio-imaging with libraries comprising gradients in surface topography to screen and identify the surface characteristics expressing bio-activity regarding a specific biomedical application. The distinct biological response requested determines the bio-assay of interest to be applied, similar to pharmaceutical high-throughput screening of compound libraries.

Our library, the so-called TopoChip, in its current formulation comprises a library featuring nearly 8500 unique surface topography combinations. By alteration of the TopoChip material composition, or cell type evaluated, the number of variations dramatically expands exponentially. In addition, modifying the surface topographies comprised within the TopoChip library allows the number of unique patterns to expand to tens of thousands. Examples of modifications could be variation in feature dimension resolution or randomising the allocation of the features. The TopoChip design presented in this work is a proof-of-principle, illustrating the potential outcome of a combinatorial approach of high-throughput screening with surface topography libraries.

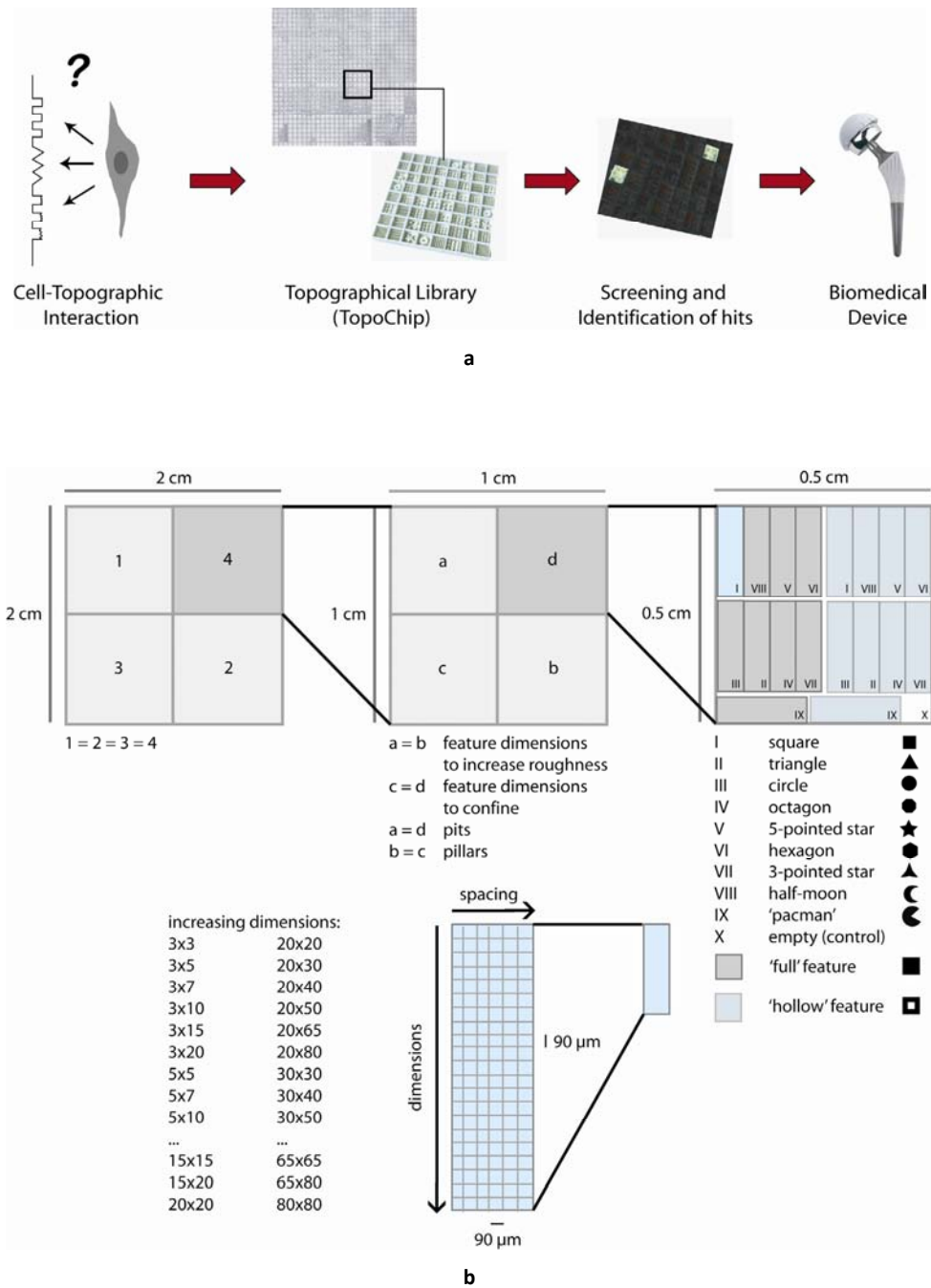


Figure 1 Schematic illustration of (a) the paradigm of high-throughput screening of biomaterial surface properties and (b) the TopoChip design.

7.2.2 Design

The basis of the TopoChip is a $2 \times 2 \text{ cm}^2$ chip incorporating an array of small fields (TopoUnits) comprising an extensive systematically organized variety of micropattern features with a resolution of $3 \text{ }\mu\text{m}$ or more, Figure 1b illustrates the TopoChip design. Possible edge or corner effects are excluded by precise positioning of four repetitions of each unique parameter-set within the TopoChip. The TopoUnit dimensions are $90 \times 90 \text{ }\mu\text{m}^2$ with $10 \text{ }\mu\text{m}$ ridge width, leading to a total number of 40.000 TopoUnits per chip. Cells will be retained to one single TopoUnit by separating the TopoUnits with high-aspect ratio ridges. The TopoChip surface in its current form includes the following features: squares, triangles, circles, octagons, 5-pointed stars, hexagons, 3-pointed stars, half moons and circles excluding one corner ('pacmans'), (some features are illustrated in Figure 1b). The design presented here is rational; in addition, we are currently also in the process of enhancing randomness in the feature shapes.

Here, the variation in feature dimensions comprises feature shape (X- and Y-axis) as well as the spacing between the features. The feature dimensions are grouped into two ranges (Figure 1b):
 feature sizes $3\text{--}20\text{ }\mu\text{m}$, spacing $3\text{--}20\text{ }\mu\text{m}$: within the size of a cell, to increase surface roughness
 feature sizes $20\text{--}80 \text{ }\mu\text{m}$, spacing $5\text{--}30 \text{ }\mu\text{m}$: larger than a cell, to confine the cells within a restricted space with defined form

The feature dimensions scale-up independently in both the X- as Y-direction, resulting in features having discriminating ratios in their X- and Y-dimensions. In addition, each spacing distance is systematically applied to each X-Y-combination.

Protruding features ('pillars') as well as indentations ('pits') are drawn within one design by inverting the pattern. Furthermore, next to the 'full' features, of each feature type also a 'hollow' version is produced; i.e. the feature incorporated a second similar feature inside of 50% of the original to create a hollow space within the feature (illustrated in Figure 1b). Each TopoUnit includes features of only one parameter-set (feature type, X-Y-combination, spacing, full or hollow feature and pillar or pit) of the in total 8422 unique variations; each repeated four times. Additionally, certain TopoUnits feature TopoChip coordinates to indicate their location on the TopoChip; the remaining TopoUnits are empty for now (over 6000 in total distributed over the full TopoChip), used as control.

7.3 Materials and Methods

7.3.1 Mask design and mold fabrication

The fabrication of the micropatterned mold occurred through conventional photolithography technologies applying a projection mask to etch the micropattern into a flat silicon wafer. The micropattern design was drawn using the commercially available software CleWin layout editor version 4.0 (WieWeb Software, Hengelo, The Netherlands).

7.3.2 TopoChip fabrication

The TopoChips can be prepared by two distinct methods: solvent casting and hot embossing. For TopoChip fabrication by hot-embossing, the silicon molds were first functionalized with hydrophobic perfluoro-octyl-trichloro-silane (FOTS, ABCR), deposited in gas phase overnight in a vacuum desiccator, to facilitate the release of the TopoChip from the mold.

The main processing procedures in each case are:

Solvent casting: Poly(L-lactic acid) (PLLA, Mw of 5.72×10^5 g/mol, kindly provided by Prof. D. Grijpma, Department of Polymer Chemistry and Biomaterials, University of Twente, The Netherlands) was dissolved in chloroform (Merck, analytical quality) to obtain a 10 wt% solution. The solution was cast on the TopoChip mold at an initial casting thickness of 500 μm and subsequently, the solvent was evaporated for several hours. The resulting dense polymer sheet contained the inverse replication of the micropattern present on the TopoChip mold.

For some of the solvent cast TopoChips a support layer of poly(dimethyl siloxane) (PDMS, Silicone RTV 615 A/B, General Electric) was applied for easier handling of the PLLA TopoChip. Base tetra(trimethyl-siloxy)silane (compound A) and curing agent tetramethyl-tetravinyl-cyclotetra-siloxane (compound B) were mixed in a ratio of A:B = 10:1 and placed in a vacuum desiccator to remove all air from the solution. Immediately after casting the PLLA layer, the liquid PDMS solution was gently applied at the airside of the PLLA layer and cured at 40 °C over night to crosslink the PDMS leading to solidification.

Prior to releasing the polymer sheets of the TopoChip mold, the sheets were wetted in Milli-Q water for at least 1 hour to facilitate release. Subsequently, the sheets were thoroughly washed in Milli-Q water for 1 day and dried in a controlled atmosphere ($T=19\text{-}20$ °C).

Hot embossing: A commercially available sheet of Poly(DL-lactic acid) (PDLLA, 250 μm thickness, Folienwerk Wolfen GmbH, Germany) was loaded into a hot embossing set-up (Obducat Hot embossing/Nano Imprint tool, Obducat AB, Sweden) together with the TopoChip mold to imprint the PDLLA sheet. First, the sheet and TopoChip mold were heated up to 80 °C, then 3 MPa pressure was applied for 10 min before the temperature was reduced to 38 °C with subsequent release of the

pressure. Prior to the release of the imprinted PDLLA sheet of the TopoChip mold, the sheet was allowed to cool down to room temperature.

Coating: Titanium was sputter coated onto the hot-embossed PDLLA TopoChip to yield a 200 nm-thick titanium layer. Titanium sputtering was performed at 100W for 32 min under an evacuation and working pressure of 3.3×10^{-7} and 6.6×10^{-3} mbar respectively.

7.3.3 TopoChip seeding and culturing

Culturing: An immortalised human mesenchymal stem (iHMSC) cell line was cultured in medium consisting of minimal essential medium (α -MEM, Gibco) supplemented with 10 % fetal bovine serum (FBS, Lonza), 2 mM L-glutamin (Gibco), 0.2 mM ascorbic acid (Sigma), 100 U/ml penicillin and 100 g/ml streptomycin (Gibco) at 37 °C in a humidified 5 % CO₂ environment. The cells were passaged with 0.05 % trypsin containing 1 mM EDTA before reaching confluence. Pre-myoblasts C2C12 cells were cultured under the same conditions in medium containing Dulbecco's Modified Eagle's Medium (DMEM, Gibco) supplemented with 10% FBS, 100 U/ml penicillin and 100 g/ml streptomycin.

A total of 1.8×10^6 cells were seeded onto the TopoChip (4.5×10^5 cells/cm²) placed in a custom made TopoChip carrier of poly(methyl metacrylate) (PMMA). Subsequently, the system was sealed with a cover containing microfluidic channels to supply the cells on the TopoChip with medium to further culture the cells from 6 hours up to 4 days. Prior to staining, the cells were washed with PBS and fixed with 4 wt% paraformaldehyde for 15 min at room temperature. Subsequently, the cells were washed again with PBS and permeabilized with 0.01 % Triton-X 100 solution for 4 min.

Staining for fluorescence microscopy: The samples were again rinsed with PBS and stained with 2.5 vol% Alexa 568 Phalloidin (Molecular Probes) and 1 μ g/ml DAPI (Sigma-Aldrich/Fluka) for 20 minutes in a dark humidified chamber. After staining, the cells were washed once more with PBS and imaged by fluorescence microscopy (BD Pathway 435, BD Biosciences).

Staining for quantification: The cells were stained with 1 μ g/ml DAPI for 10 min for nucleus staining. Fluorescent and bright field microscopy images of the same areas were acquired of triplicate samples using the BD Pathway 435 High Content Bio-imager using a macro with autofocus algorithm. For both fluorescent and bright field images a single image of the total scanned area was montaged. The two montage images were analyzed using CellProfiler [11]. The bright field image was used to identify the TopoUnits using the grinding module whereas the background subtracted fluorescent image was used to count the number of cells which were related to individual TopoUnits to obtain the number of cells per TopoUnit.

7.4 Results and Discussion

7.4.1 TopoChip fabrication

The first step in the fabrication of the TopoChip is the fabrication of a negative replica in a silicon wafer by photolithography and etching. Figure 2a-b presents SEM images of the mold, which indicate good quality and high resolution fabrication of the mold. This mold is subsequently used to imprint the patterns onto biomaterials by hot-embossing or solvent casting. Figure 2c, e, g and h show SEM and photo images of poly(lactic acid) (PLA) TopoChips; these images confirm faithful replication of the features from the mold into the polymers.

To increase the number of unique surface properties, besides surface topography variations we altered the surface composition. Several approaches are applicable, for example variation in the material used for fabrication of the TopoChip or coating the TopoChip with a layer of a second material. Regarding variation in the TopoChip material, results confirm good replication of the TopoChip into various polymers such as PLA and block co-polymers of poly(ethylene oxide) and poly(butylene terephthalate) (PEOT/PBT) by hot embossing as well as solvent casting. With respect to the latter approach, successful coating of PDLLA TopoChip included biomimetic calcium phosphate (data not shown) and titanium. Figure 2d, f and i present images of a PDLLA TopoChip coated with a 200 nm-thick titanium layer that can be distinguished visually even from photos (Figure 2d versus the uncoated PDLLA TopoChip in Figure 2c). The SEM images reveal no adverse effects of the coating on the resolution of the TopoChip features (see close-up images in Figure 2h-i). Coating the TopoChip has the advantage, in contrast to variation of the TopoChip material, of avoiding unintentional variations amongst the TopoChips and minimizing process parameters. In addition, biomaterials originating from a wide range of classes can be coated onto the PLA such as (co)polymers, ceramics and metals.

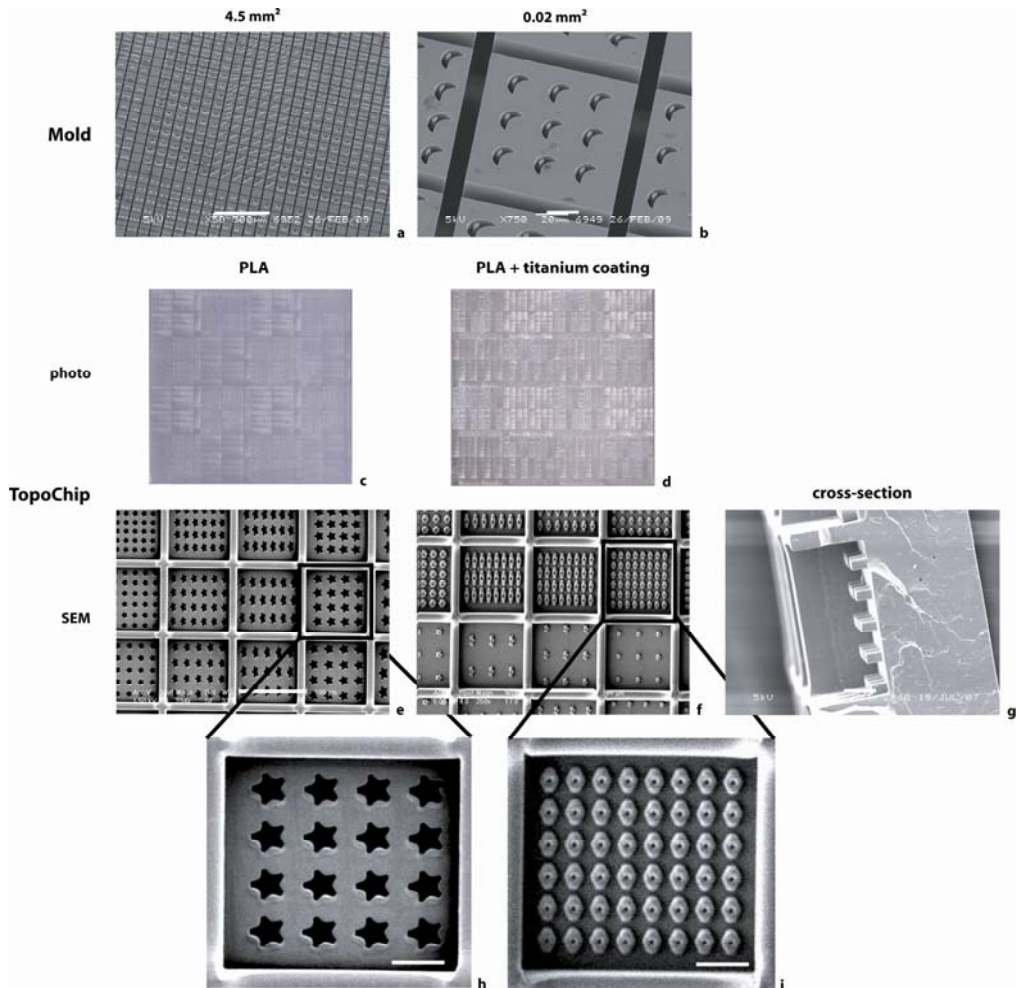


Figure 2 Typical SEM and photo images of the mold and TopoChip; (a, b) mold with an area of (a) 4.5 mm² and (b) 0.02 mm² showing hollow half moon features (one TopoUnit is 0.008 mm², including walls 0.01 mm²); (c-i) TopoChip of (c, e, h) PDLLA prepared by hot embossing and (d, f, i) PDLLA prepared by hot embossing coated with titanium with (h, i) zoom of one single TopoUnit of image e (stars, pits) and f (hollow hexagons, pillars), respectively; (g) presents a cross-section of a PLLA TopoChip prepared by solvent casting with pillar features surrounded by high-aspect ratio walls to separate the TopoUnits. Scale bar in SEM images represents (a) 500 μ m, (e, f) 100 μ m and (b, g, h, i) 20 μ m.

7.4.2 Uniform seeding

High-throughput screening of the TopoChip requires successful and uniform cell distribution along the TopoChip. To reach that goal, first a TopoChip carrier was designed for seeding as well as culturing under controlled settings; Figure 3a illustrates the set-up (more details on seeding and culturing optimization will be presented in a future publication). The TopoChip is subsequently placed in a specially fitting pit in this TopoChip carrier where the cells are seeded onto the TopoChip. Subsequently, sealing of the TopoChip within the carrier occurs through placing a cover on top of the TopoChip leaving a little space between the TopoChip and cover as medium reservoir. The cover has microfluidic channels for controlled medium flow to supply the cells with nutrients during culturing. To evaluate the cell distribution within the TopoUnit after seeding using this TopoChip carrier, immortalized human mesenchymal stem cells (iMSC) were imaged 6 hours after seeding. These results, presented in Figure 3b, reveal good distribution of cells amongst the TopoUnits. Each TopoUnit seems to contain a number of cells, whereas the close-up image (right) indicates that the number of cells is relatively similar per TopoUnit. In fact, quantification of the cell distribution is in good agreement with these observations, see Figure 3c. Over 50 % of the TopoUnits contain 5-12 cells; clearly, the distribution of the cells over the TopoUnits is generally uniform. In addition, subsequent culturing experiments revealed that the TopoChip carrier is also successful in case of sustained culture; various types of cells, such as the iMSC's but also mouse embryonic stem cells (MES), mouse pre-myoblast cells (C2C12) and transgenic Chinese Hamster Ovary (CHO) cells were kept in culture for a period of over 4 days without any deficiencies regarding nutrient supply.

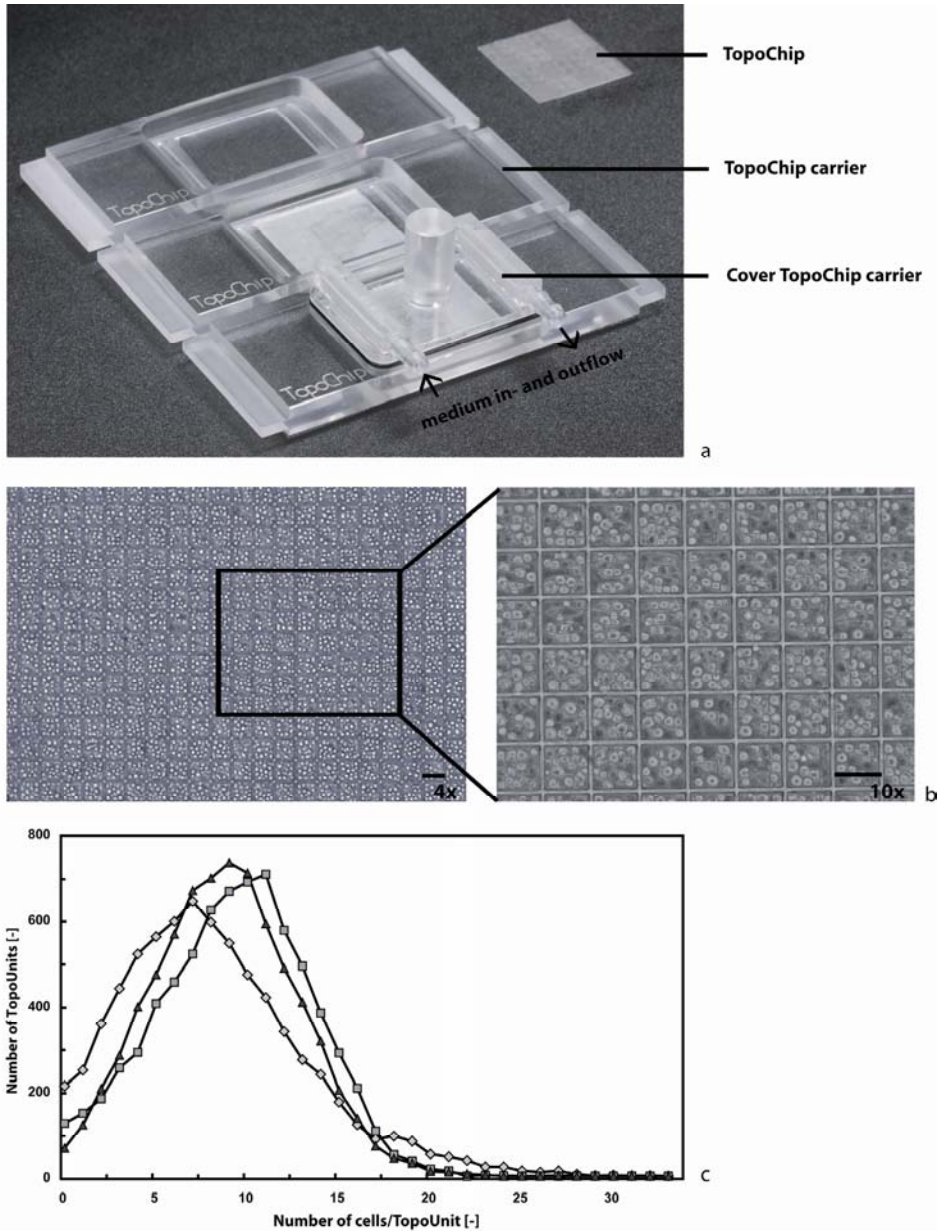
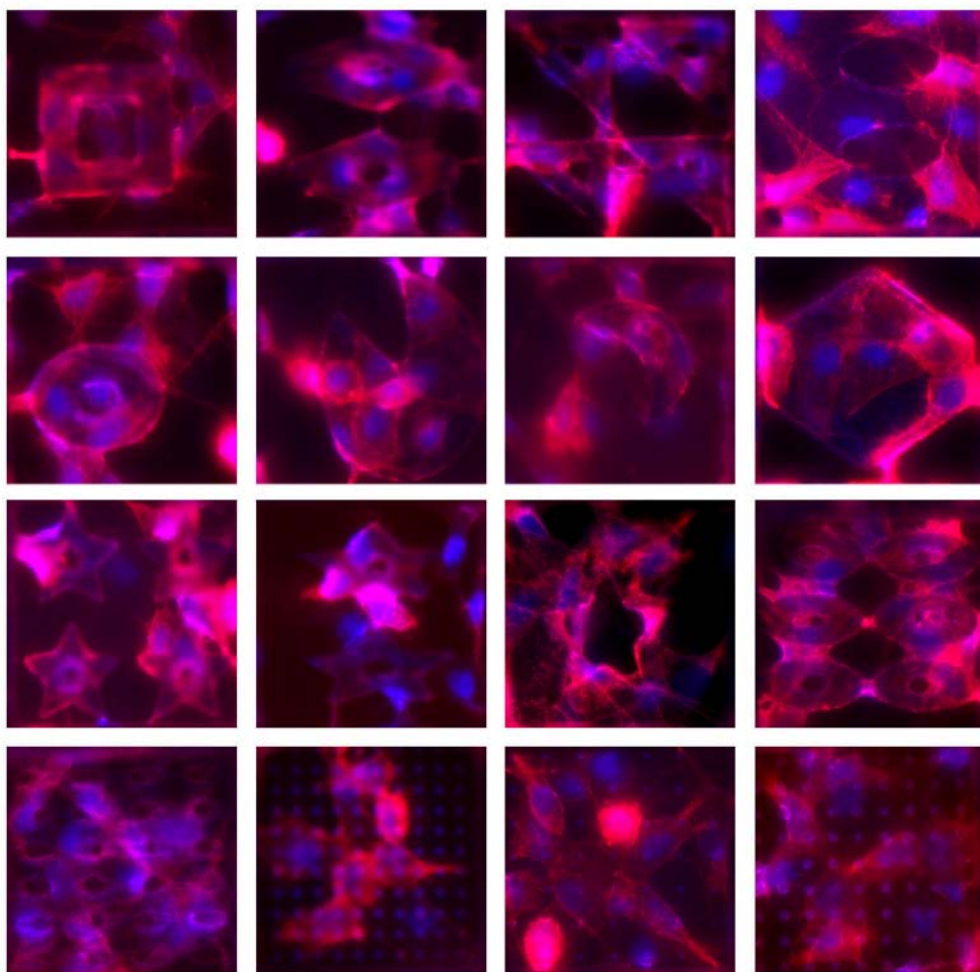


Figure 3 iMSC cell seeding on the TopoChip; (a) TopoChip carrier to place the TopoChip in during seeding and subsequent culturing, (b) light microscopy images showing an even distribution of the number of cells per TopoUnit, the scale bar represents 100 μm , (c) graph representing the number TopoUnits containing a specific number of cells within that TopoUnit (count over 7200 TopoUnits in triplicates, each series represents the count of one of the three individual TopoChip).

7.4.3 Cell-material interactions

Prior to automated high-content imaging, fluorescent labeled C2C12 cells cultured TopoChips were manually screened to observe cell-topography interactions. These observations reveal distinct variations in cell behavior regarding the various features and feature dimensions, as illustrated in Figure 4. The cells clearly respond differently to the features with dimension in the range of 3-20 μm , to increase surface roughness, compared to the features with dimensions of 20-80 μm , to confine the cells. Regarding the smaller features within the surface roughness range (images bottom row Figure 4), the cells spread on top of the features. With respect to the larger features within the confining range (top 3 rows in Figure 4), the cells respond differently to pits and pillars as well as to the shape of the feature. Here, e.g. with the star shape features as pits (3rd row, 3rd image), the cells tend to grow on the surrounding surface leaving the feature empty. In contrast, with the star shape features as pillars (3rd row, 1st and 2nd image), the cells tend to grow on top of the features filling up the star shape. Similar behavior is observed for the other types of features. The image visualizing this effect in the clearest way is the 'pacman' feature (2nd row, 2nd image); all cells spread on top of the feature filling the surface and leaving the 'missing' corner empty. These results clearly indicate that the cells clearly interact differently regarding the various topographies. Which cell behavior is most appropriate depends on the final application and the requested biological response; this is where the high-content screening approach comes in to identify the surface characteristics gaining the appropriate biological response regarding the specific application.

**Figure 4**

Typical fluorescent microscopy images of C2C12 cells labelled by Alexa Fluor phalloidin 568 (pink, cytoskeleton) and dapi (blue, nucleus) cultured on the TopoChip for 6 hours to illustrate cell-topography interactions; each image represents one TopoUnit containing distinct features with discriminating dimensions. Images first three rows present features in the confining dimension range of 20-80 μm , whereas the fourth row present features in the roughness dimension range of 3-20 μm .

7.5 Conclusions

The TopoChip approach as proposed in this paper, placed within the materiomics concept, provides a high-throughput screening platform for surface properties of biomaterials. The TopoChip comprises a library of nearly 8500 unique variations, repeated four times on each TopoChip for internal control. Through tuning of the surface composition, the number of variations can dramatically expand. Seeding and culturing under a controlled environment using the specifically designed TopoChip carrier, supports uniform cell distribution amongst the TopoUnits.

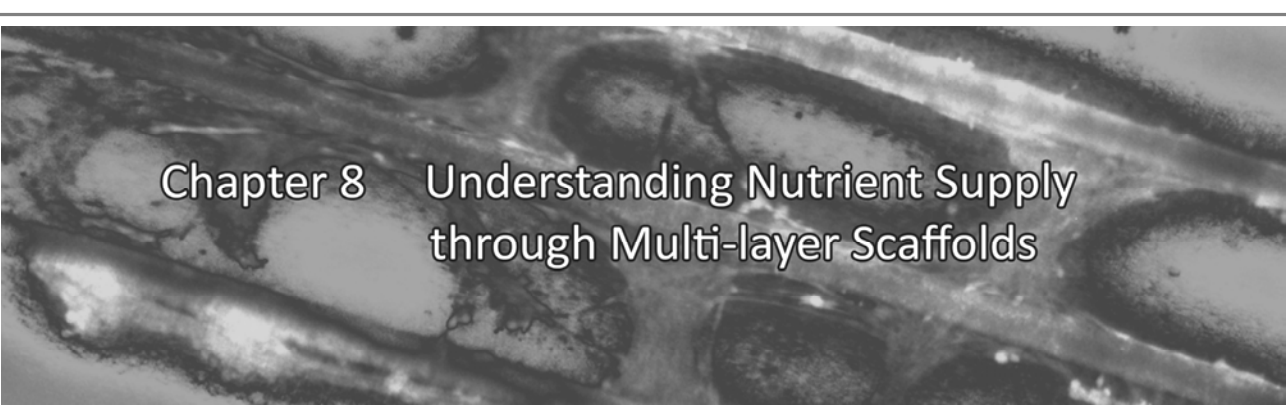
The TopoChip allows fast screening for specific cell behaviour of distinct cell types towards thousands of surface topographies and various surface compositions. Identification of surface characteristics gaining a desired biological response regarding a specific application is feasible using this high-throughput biological screening platform. Close-up images already reveal distinct cell behavior towards various surface topographies present on the TopoChip. The materiomics concept is not only limited to screening of cell behaviour, but also may be applied in discriminating research fields where surface topography affects the suitability of a product, such as protein adsorption and surface bio-fouling [12]. In the near future, as a proof-of-principle, we will screen for surface topographies that promote osteogenic differentiation of human mesenchymal stem cells.

Acknowledgments

B.J. Papenburg, R. Truckenmueller and D. Stamatialis acknowledge the Spearhead program: ‘Advanced Polymeric Microstructures for Tissue Engineering’ of the University of Twente (BMTi, Institute for Biomedical Technology) for financial support. H. Unadkat acknowledges Marie Curie Early Stage Training Join(ed)T program and J. de Boer acknowledges the Smart Mix Program of the Netherlands Ministry of Economic Affairs and the Netherlands Ministry of Education, Culture and Science for financial support.

References

1. Habibovic P, Barrere F, van Blitterswijk CA, de Groot K, Layrolle P. Biomimetic hydroxyapatite coating on metal implants. *Journal of the American Ceramic Society* 2002 Mar;85(3):517-522.
2. Buser D, Schenk RK, Steinemann S, Fiorellini JP, Fox CH, Stich H. Influence of surface characteristics on bone integration of titanium implants. A histomorphometric study in miniature pigs. *Journal of Biomedical Materials Research Part A* 1991;25(7):889-902.
3. Chen CS, Mrksich M, Huang S, Whitesides GM, Ingber DE. Geometric Control of Cell Life and Death. *Science* 1997 May 30, 1997;276(5317):1425-1428.
4. McBeath R, Pirone DM, Nelson CM, Bhadriraju K, Chen CS. Cell shape, cytoskeletal tension, and RhoA regulate stem cell lineage commitment. *Developmental Cell* 2004 Apr;6(4):483-495.
5. Moroni L, Lee LP. Micropatterned hot-embossed polymeric surfaces influence cell proliferation and alignment. *Journal of Biomedical Materials Research Part A* 2009 Mar 1;88A(3):644-653.
6. Papenburg BJ, Vogelaar L, Bolhuis-Versteeg LAM, Lammertink RGH, Stamatialis D, Wessling M. One-step fabrication of porous micropatterned scaffolds to control cell behavior. *Biomaterials* 2007;28(11):1998-2009.
7. Dalby MJ, Gadegaard N, Tare R, Andar A, Riehle MO, Herzyk P, et al. The control of human mesenchymal cell differentiation using nanoscale symmetry and disorder. *Nature Materials* 2007;6(12):997-1003.
8. Chung BG, Kang L, Khademhosseini A. Micro- and nanoscale technologies for tissue engineering and drug discovery applications. *Expert Opinion on Drug Discovery* 2007;2:1653-1668.
9. Holmes PF, Bohrer M, Kohn J. Exploration of polymethacrylate structure-property correlations: Advances towards combinatorial and high-throughput methods for biomaterials discovery. *Progress in Polymer Science* 2008;33(8):787-796.
10. Anderson DG, Levenberg S, Langer R. Nanoliter-scale synthesis of arrayed biomaterials and application to human embryonic stem cells. *Nat Biotech* 2004;22(7):863-866.
11. Carpenter AE, Jones TR, Lamprecht MR, Clarke C, Kang IH, Friman O, et al. CellProfiler: image analysis software for identifying and quantifying cell phenotypes. *Genome Biology* 2006;7(10):R100.
12. Universiteit Twente, Papenburg B, Unadkat H, Wessling M, Stamatialis D, Blitterswijk Cv, et al., inventors. High throughput screening method, 2007.



Chapter 8 Understanding Nutrient Supply through Multi-layer Scaffolds

Abstract

Construction of 3D scaffolds is presented by stacking multi-layered porous Poly(L-lactic acid) (PLLA) sheets featuring microchannels. The cells distribute well within the scaffold as seeding and attaching of the cells occurs on individual layers that are subsequently stacked. The microchannels of the sheets, fabricated by phase separation micromolding (PS μ M), allow nutrient perfusion throughout the 3D scaffold whereas the inner-porosity of the sheets guarantees diffusion between the layers. Additionally, the microchannels facilitate cell organization by alignment. Under static conditions, cell proliferation is inhibited due to nutrient limitations although the cells stay viable. Nonetheless, diffusion between the layers takes place and cells on various layers affect each other. Under dynamic conditions, convective flow leads to perfusion throughout the scaffold accompanied by improved nutrient availability to the cells on the various layers, drastically increasing cell proliferation on all layers compared to static culturing. A theoretical model is designed to predict the effect of various parameters on nutrient transport under static and dynamic conditions; the calculated predictions correspond well to the experimental data.

A revised manuscript based on this chapter has been submitted, authors are:

Bernke J. Papenburg, J. Liu, G.A. Higuera, I.J. de Vries, A.M.C. Barradas,

J. de Boer, C.A. van Blitterswijk, M. Wessling, D. Stamatialis

8.1 Introduction

Nutrient limitation to cells is a major hurdle to overcome in building 3D tissue constructs. Within most *in vivo* tissue, a complex network of blood vessels and capillaries eventuate in a maximum nutrient diffusion distance of about 200 μm to supply the nutrients; within *in vitro* build constructs, the distance to the main nutrient source mostly exceeds this 200 μm [1-3]. This increased distance leads to reduced nutrient supply to tissue further from a direct nutrient source, resulting in nutrient gradients with accompanying variation in cell behaviour including inhomogeneous cell and extra cellular matrix (ECM) distribution throughout the constructs [1, 4]. For example, examination of the oxygen limitations effects within 3D scaffolds showed a large influence on cell distribution and viability with respect to the diffusion distance to the nutrient source [5]. In another study, analysis of cell growth within multi-layer stacked 3D scaffolds displayed that the majority of the cells located within the 200 μm wide peripheral region of the scaffolds [1].

Many studies focus on understanding the effect of nutrient limitations on cell behaviour and, in response, improving the nutrient supply within the 3D tissue constructs. Various developed bioreactor systems introduce convective flow of the medium to perfuse *in vitro* grown 3D tissue constructs, e.g. spinner flasks, rotary vessels or perfusion flow systems [6, 7]. Besides improvements in nutrient transport, the use of these bioreactor systems can also directly or indirectly lead to new challenges to be addressed. Firstly, realization of uniform seeding; non-optimal initial parameters (flow conditions, but also e.g. seeding density, - method and scaffold design) can attribute to non-uniform initial cell density or even aggregate formation throughout the scaffolds, initiating a gradient within the construct from the beginning [8, 9]. Secondly, avoiding the building-up of a nutrient supply gradient; the cells on the exterior of the scaffold are provided most with nutrients, and therewith the scaffold has increased cell number at the exterior inducing reduced nutrient transport to the interior. Additionally, increased cell number might result in scaffold pore blockage by the cells themselves or products they secrete, intensifying a nutrient supply gradient throughout the scaffold [3, 4, 10]. A third challenge is optimizing the mechanical stability of the scaffold and simultaneously enabling optimum nutrient flow throughout the full construct. Often scaffolds are designed to have relatively large pore sizes to favour nutrient transport, which again may lead to reduced mechanical stability of the scaffold [11] and/or lower surface area for the cells to attach. Recently, a 'double porosity' of the scaffold was suggested to overcome this design contradiction; mimicking both the microarchitecture of tissues (with pores in the range of hundreds of microns) as well as the microenvironment surrounding the cells (with pores in the range of $\sim 10 \mu\text{m}$) [12, 13]. Finally, inducing cell organization within the scaffolds is generally not taken into account within 3D-scaffold design although it is well known that for certain tissues, e.g. muscle or cardiovascular, mimicking *in vivo* organization on cell level is advantageous or even a prerequisite for proper functionality of the tissue [14, 15].

In this work, we design 3D scaffolds by stacking multi-layered porous micropatterned sheets featuring microchannels, as illustrated in Figure 1a. This concept actually includes the design of both microarchitecture and microenvironment. The channels, in the range of hundreds of microns, allow perfusion of the nutrients throughout the scaffold as well as provide space for the cells to grow and topography for cell organization. Additionally, the inner-porosity of the sheets is in the range of $\sim 10\ \mu\text{m}$, facilitating transport of nutrients and communication between the layers.

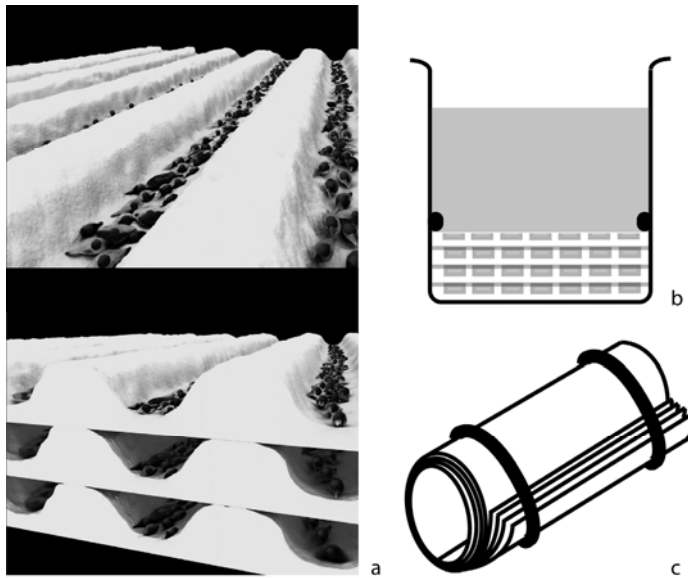


Figure 1 Illustrations of multi-layer stacking; (a) cells cultured on micropatterned sheets which are subsequently multi-layer stacked where the microchannels provide space for cells to grow. Methods to stack are (b) in wells with the channels up (only under static conditions) (c) rolling-up, keeping the sheets in place with o-rings with the channels facing out (all dynamic experiments and part of the static experiments). Part (a) of this figure was adapted from [30].

This multi-layer concept addresses the challenges mentioned earlier. Firstly, cells can distribute evenly throughout the scaffold given that seeding and attaching of the cells occurs on the individual layers before stacking. Secondly, the micropattern channels facilitate nutrient perfusion throughout the entire scaffold preventing nutrient gradients to occur without the need of scaffolds with large pores which often have low mechanical strength. As a result of good nutrient distribution within the scaffold, cells spread more evenly throughout the scaffold. Even when higher confluency is reached over longer periods of time, additional sheet layers without cells could ensure perfusion throughout the complete construct where the inner-porosity of the sheets provides diffusion between the layers. Finally, the channels facilitate cell organization by aligning the cells following the pattern [16].

The porous micropatterned sheets are fabricated by Phase Separation Micromolding (PS μ M) [16]. PS μ M enables the introduction of micropatterning and porosity into the sheets in one step through inducing phase separation of a polymer solution on a micropatterned mold. By selecting the right solvent-nonsolvent system with the specific polymer, the porosity of the resulting sheet can be tuned. Through variation of the micropatterned mold on which the solidification of the polymer occurs, the inverse imprinted micropattern into the sheet can easily be adjusted to the requirements of the specific construct.

This work first explores various aspects of nutrient diffusion through multiple micropatterned porous sheets under static conditions. On the basis of these results, a model is designed and validated to enable prediction of various parameters on nutrient transport in static and dynamic conditions. Based on model predictions, culturing experiments under dynamic conditions are performed using a spinner flask. The analysis of the cells throughout the scaffold can easily be performed as the layers can be un-stacked after culture to determine gradients per layer, therewith allowing a better insight in local nutrient supply variation and clues for optimization.

8.2 Model

8.2.1 Concept

A model to predict nutrient gradients throughout the multi-layer scaffolds was designed for both static and dynamic culturing of the multi-layer scaffolds using COMSOL multiphysics 3.3 modeling software (COMSOL, 2007). Oxygen and glucose were selected as modeling nutrients.

The geometry of the scaffold is composed of multi-layer stacked micropatterned sheets where cells are grown in the microchannels and not in the inner porosity of the sheets. Figure 2 illustrates the geometry of the multi-layer scaffolds and topography dimensions where the model is based on. The model description and details are presented in the Appendix.

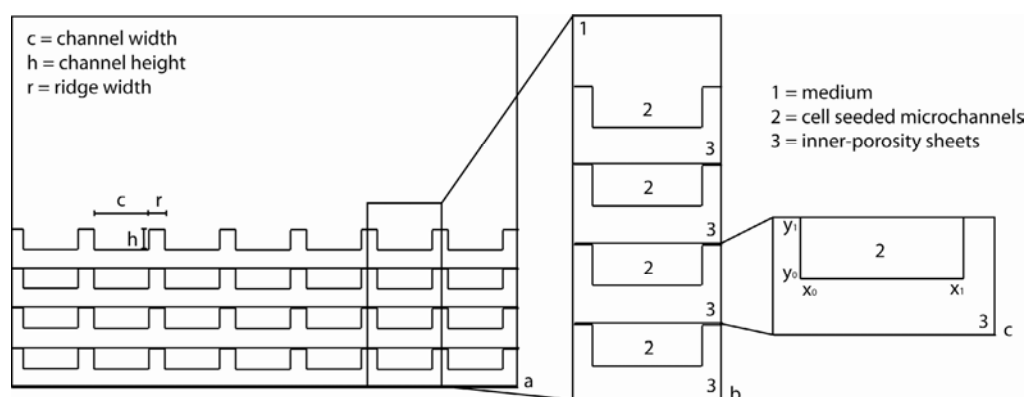


Figure 2 Schematic illustration of the geometry of multi-layer stacked sheets; (a) 4 layers stacked in a well, (b) stack of 4 layers, used as basis for model geometry description for static culturing, number of sheets can be adjusted (c) one symmetry element as described in the model for the dynamic culturing condition. Values for channel width, height and ridge width used in this model are $250\ \mu\text{m}$, $45\ \mu\text{m}$ and $40\ \mu\text{m}$ respectively and for the total height of one symmetry element $90\ \mu\text{m}$, i.e. one sheet layer. 1-3 indicate the various domains that are distinguished in the model.

8.3 Materials and Methods

8.3.1 Scaffold sheets preparation

Micropatterned sheets were cast from poly(L-lactic acid) (PLLA, $M_w = 1.6 \times 10^5$ g/mol), a well-known biocompatible and biodegradable polymer. Sheets with and without porosity were manufactured. Porous PLLA sheets were cast from a 5 wt% solution of PLLA in 1,4-dioxane using ethanol as nonsolvent at 3–4 °C. Dense PLLA sheets were prepared from a 10 wt% solution of PLLA in chloroform with ethanol at room temperature as nonsolvent. For the dense sheets, before immersing the polymer film into the nonsolvent bath, an additional solvent evaporation step of 30–60 seconds was performed. Initial casting thicknesses applied were 225 μm for patterned and 150 μm for nonpatterned sheets. To ensure complete removal of the solvent and at a later stage of the nonsolvent, the sheets were kept in nonsolvent for 1 day and subsequently washed for 5–8 hours in Milli-Q water which was refreshed 2–3 times. Finally, the sheets were dried in a controlled atmosphere ($T = 18\text{--}21$ °C). All solvents and nonsolvent were purchased from Merck (analytical quality).

Depending on the application, samples of various sizes were cut from the sheets (for sizes, see cell culturing section). For sterilization, the samples were immersed in a 70 % ethanol solution for 20–30 min, then the ethanol was allowed to evaporate and the samples were placed in well-plates. Subsequently, the samples were sprayed with 70 % isopropanol, left for evaporation within a laminar flow cabinet and finally washed with PBS. To ensure complete wetting of the sheets, the samples were left in PBS for at least 4–8 hours in an incubator (37 °C, humid atmosphere with 5 % CO_2).

8.3.2 Porosity and pore morphology determination

The morphology and porosity of the obtained PLLA sheets were characterized by scanning electron microscopy (SEM, JEOL 5600LV). Figure 3 presents typical SEM images of these highly porous PLLA sheets featuring 250 μm wide channels applied in this work. Additionally, glucose diffusion through the sheets was measured as model nutrient to validate pore interconnectivity, following the procedure described previously [16]. In brief, diffusion of glucose from a donor to an acceptor compartment through the sheet was analyzed and based on the measured concentrations the diffusion coefficient was calculated. In this study, besides glucose diffusion through the sheets alone, also glucose transport through the sheets including a cell layer was measured to evaluate how the attached cell layer affects the transport of nutrients. For these experiments, A4-4 cell proliferation medium (see cell culturing section) containing 4.8 ± 0.1 mmol/l glucose was introduced to the donor compartment; a similar volume of PBS was added to the acceptor compartment. In the control measurement, a glucose (SigmaUltra, D-(+)-glucose, 99.5% GC) in Milli-Q water solution was used for

the donor compartment containing the same glucose concentration as the medium and Milli-Q water was added to the acceptor compartment. Samples of 0.15 ml were taken after 0 min, 30 min, 1hr, 2hr, 3hr, 4hr, 5hr, 8hr and 24hr from both the donor and acceptor compartment. The glucose concentration was determined using an enzymatic assay according to the manufacturer's protocol (PGO enzymes, Sigma). The glucose follows an enzymatic reaction colouring the solution orange which can be analyzed by UV spectrophotometry (Varian Cary 300 scan) at $\lambda=450$ nm. All measurements were performed in triplicates.

8.3.3 Cell culturing

Cell culturing experiments were performed using mouse pre-myoblasts, C2C12, and A4-4 cells. The A4-4 cells are chinese hamster ovary cells transfected with an construct combining an hypoxia responsive promoter to a luciferase gene (HRE-Luc) to enable hypoxia-report. The A4-4 cells is an established cell line kindly provided by Dr. Kiyoshi Nose (Showa University, Tokyo, Japan).

Culturing: C2C12 cells were cultured in proliferation medium containing Dulbecco's Modified Eagle's Medium (D-MEM, Gibco) supplemented with 10 % fetal bovine serum (FBS, Cambrex), 100 U/ml penicillin (Gibco) and 100 $\mu\text{g}/\text{ml}$ streptomycin (Gibco). A4-4 cells were cultured in alpha Minimum Essential Medium (α -MEM, Gibco) supplemented with 10% FBS, 2 mM l-glutamine, 100 U/ml penicillin and 100 $\mu\text{g}/\text{ml}$ streptomycin. Cells were grown at 37 °C in a humid atmosphere with 5 % CO_2 . For expansion, the cells were plated at 2000-3000 cells/ cm^2 until they reached 70-80 % confluence, after which they were detached by trypsinization (0.05 % trypsin containing 1mM EDTA) and further sub-cultured or seeded on the polymer sheets with a density of 7500-17.500 cells/ cm^2 . Medium was refreshed every two-three days during expansion. Cell number was determined by manual counting using a haemocytometer.

Seeding of the cells was performed on single sheets, subsequently the cells were allowed to attach for 4-6 hours before the layers were stacked into multi-layer scaffolds. Seeding densities applied were 15.000 cells/ cm^2 for both C2C12 and A4-4 cells. Assembling the multi-layer scaffolds was performed in two ways: stacking in wells and by rolling up around a tube, as described in more detail later.

Cell-cultured sheets for glucose transport: A4-4 cells were seeded on single sheets (24 well-plates, tissue culture treated surface, Nunc) at a density of 17.500 cells/ cm^2 and after 1 or 2 days fixated with a 4 wt% paraformaldehyde in PBS solution for 30-60 min before placed in the glucose-diffusion set-up.

Well-stacked (WS) scaffolds: 4 sheet layers were stacked within wells (24 well-plates, tissue culture treated surface, Nunc), and o-rings (Viton type 51414, 14x1, Eriks, The Netherlands) of exactly the inner diameter of the well were placed on top of the stacked sheets to prevent floating, as illustrated in Figure 1b, and in one case also between the layers to create space between the sheets. 2 ml of medium was added per well, which was refreshed every 2 days. In the rest of this paper, these multi-layer scaffolds stacked in wells will be abbreviated to “WS scaffolds”.

Tube-stacked (TS) scaffolds: 1-4 layers of 1.8x1.8 cm² were placed in 25 well replica-plates (Greiner Bio-One, the Netherlands) during seeding and attachment of the cells and subsequently stacked together and rolled around tubing to create a multi-layer scaffold. Two O-rings (Viton type 51414, 5x1 Eriks, The Netherlands) were placed around the sheets to keep them together and prevent unfolding of the layers, as illustrated in Figure 1c. From this point on, these multi-layer tube scaffolds will be abbreviated to “TS scaffolds”. Two types of tubing were used to roll the sheets around, dense polyethylene (PE) tubing and a multi-fiber of Polyethersulfone (PES) [17] both with an outer diameter of 4 mm. In contrast to the dense PE tubing, the PES multi-fiber is porous and allows diffusion of medium from the inside of the TS scaffold. In most cases, the PE tubing/PES multi-fiber was removed immediately after rolling up and fixation by the o-rings to allow direct diffusion of medium from the inside of the TS scaffold. The TS scaffolds, with or without the inner PE tubing/PES multi-fiber, were placed in wells (6 well-plate, non-tissue culture treated surface, Nunc) with 7.5 ml medium or in a spinner flask with 100 ml of medium. For dynamic culturing, the TS scaffold was first kept static in the spinner flask for approx. 24 hrs before stirring was initiated. In all cases, the micropatterned side of the sheet with attached cells faced outwards for all layers; i.e. on the outer layer the cells are in direct contact with the medium whereas on the inside of the TS scaffold cells do not direct contact the medium and receive medium by diffusion through the inner-porosity of the sheets.

Spinner flask: From the cap of the spinner flask, 4 needles (0.7 mm diameter) descended into the flask where the TS scaffolds were attached vertically and immersed fully in the medium. The medium volume added to the spinner flasks was 100 ml, which was refreshed after 4 days, and reached up to the onset of the side arms. The caps on the side arms were slightly opened during culturing to ensure sufficient oxygenation of the medium. On the bottom of the flask a magnetic bar in the form of a cross was placed and for culturing under dynamic conditions, the flasks were placed on a stirring control unit (VARIOMAG Biomodul 40B) to ensure continuous medium flow throughout the whole flask. Stirring speeds applied for culturing under dynamic conditions were 15 and 30 rpm (rotations/min).

Fixation and staining for light microscopy: Medium was aspirated from the wells, the WS scaffolds were un-stacked and the layers were placed in wells separately (biological triplicates). The sheets were incubated with 4 %-paraformaldehyde (Merck) in PBS for 30-60 min to fixate the cells and washed with PBS. Subsequently, the sheets were incubated with a few drops of a 1%-methylene blue in borax solution for 3-5 min to stain the cells. Finally, the sheets were thoroughly washed with demineralised water to ensure full removal of all excess methylene blue and dried in an controlled atmosphere ($T=18-21\text{ }^{\circ}\text{C}$). Images of the sheets were taken by light microscopy (Zeiss Axiovert 40 mat and Axiocam MRc 5 camera).

Proliferation - DNA assay: The total concentration of DNA per layer was determined by a DNA assay as indication of cell proliferation on the different layers within the multi-layer scaffolds. First, the medium was aspirated and the multi-layer scaffolds were un-stacked and each layer was placed in wells separately (biological triplicates). The sheet layers were washed with PBS and subsequently the cells were lysed (cell culture lysis reagent part #E153A, Promega). The DNA concentration per layer was measured using a cell proliferation assay according to the manufacturer's protocol (CyQuant Cell Proliferation Assay Kit, Invitrogen/Molecular Probes). Statistical significance was calculated using the double-tailed t-test at $p<0.05$.

Viability staining: To determine cell viability on the various layers, a LIVE/DEAD staining assay was performed. After un-stacking the multi-layer scaffolds and placing the individual sheets in wells, the sheets were incubated for 10 min with an $6\text{ }\mu\text{M}$ ethidium homodimer/ $1\mu\text{M}$ calcein in PBS solution (LIVE/DEAD viability/cytotoxicity Kit, Invitrogen/Molecular Probes). Images were taken by fluorescent microscopy (Nikon Eclipse E600 and Qimaging Retiga 1300 camera) using a Nikon Texas Red/FITC filter set.

Luciferase activity: Luciferase activity of the A4-4 cells was determined from the lysate obtained with the DNA assay. $20\text{ }\mu\text{l}$ of the obtained cell lysate was added to $100\text{ }\mu\text{l}$ of luciferin substrate (Luciferase activity kit, Promega) and luminescence was detected by a Bio-orbit Luminometer (Aboatox1253) at a wavelength of 560 nm . The luciferase activity was normalized over DNA amount and statistical significance was calculated using the double-tailed t-test at $p<0.05$.

Glucose and lactate concentrations medium: The glucose and lactate levels were analysed by loading $11\text{ }\mu\text{l}$ medium onto glucose or lactate slides (Vitros), respectively, using a DT60 II Chemistry System (Vitros) according to the manufacturer's protocol. Statistical significance was calculated using the double-tailed t-test at $p<0.05$.

8.4 Results and Discussion

8.4.1 Scaffold sheets characterization

The porous PLLA sheets have porosity of $75 \pm 2\%$ and pore sizes in the range of 2-10 μm . The glucose diffusion coefficient through these sheets is in the order of $10^{-10} \text{ m}^2/\text{s}$ [16]. Figure 3 presents SEM images of the porous PLLA sheets featuring the two topography designs applied where both patterns as well as the inner-porosity can be appreciated. Figure 3a and b show the substrate side and cross-section, respectively, of a sheet featuring 250 μm wide continuous channels with a ridge height of 45 μm . Figure 3c and d show the substrate side and cross-section, respectively, of a sheet with an interconnected channel pattern. The larger channels are about 250 μm wide and are interconnected by periodically breaking-up of the ridges; in the channel length direction every 500 μm the ridges are broken-up for 150 μm . The smaller pattern features 20 μm wide channels where every 100 μm the ridges are broken-up for 10 μm . The ridge height of the larger channels is 50 μm and of the smaller channels 10 μm . This second topography will be referred to as “double brick” pattern.

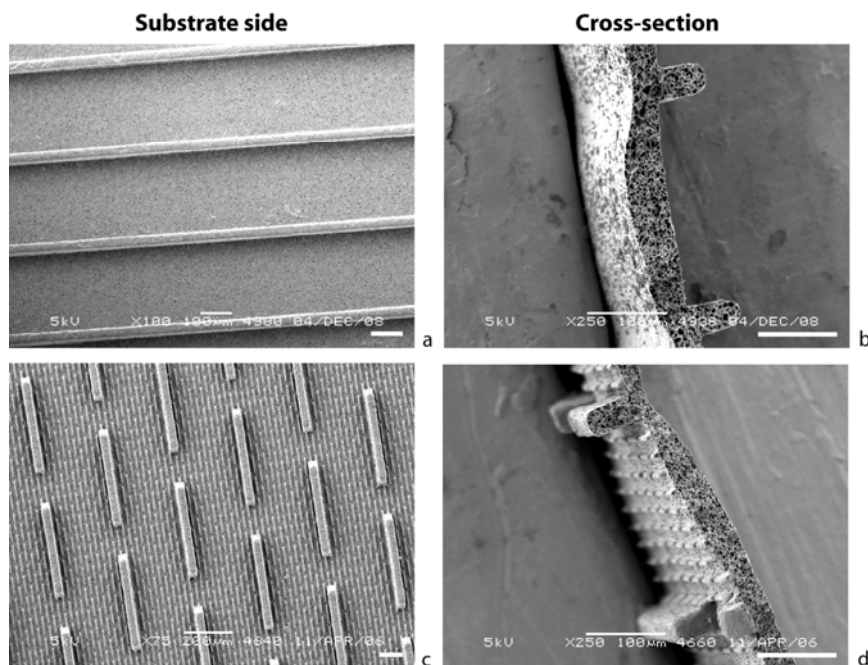


Figure 3 Typical SEM images of porous PLLA sheets featuring (a-b) 250 μm channels and (c-d) double brick pattern fabricated by PSM. Bar at the bottom right corner in the images represents 100 μm .

8.4.2 Nutrient transport limitations

The diffusivity of glucose through porous PLLA sheets was already determined [16], but in a 3D scaffold the cell layer attached to the surface plays an important role in the glucose transport as well. Figure 4 visualises that spreading cells on the surface of a porous sheet cover and block the pores. In this image cell number is still rather low but one can imagine that at higher confluency pore blocking may be much more severe. In fact, the effect of the cell layer on nutrient diffusion was determined on sheets cultured for 24 or 48 hours with A4-4 cells. These fixed cell-cultured sheets were placed in the glucose diffusion set-up and the transport of glucose through these sheets was measured. The results were compared to control sheets only wetted in PBS and reference sheets placed for the same time period in medium without cells. Interestingly, no glucose transport was detected through the cell-cultured sheets over 24 hours, similar to dense sheets, whereas low glucose transport through the reference sheets was measured. These results imply that already the compounds in the medium, e.g. proteins, cause significant decrease in nutrient diffusion and that the cell layer even blocks the glucose transport. This is an important result indicating that sheet porosity might not be sufficient for effective nutrient delivery to the cells in a multi-layer scaffold. Nonetheless, as presented later, the inner sheet porosity does play an important role in cell communication between the layers. Besides, the channels can dramatically improve nutrient supply to the cells.

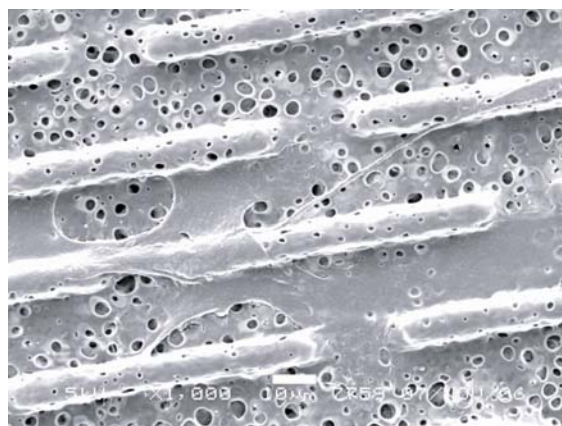


Figure 4

SEM image illustrating pore blockage by cell spreading on the scaffold sheet surface. Bar in image represents 10 μ m.

8.4.3 Static culture conditions: multi-layer WS scaffolds

C2C12: Since glucose transport might be affected differently under standard culturing conditions, initial static multi-layer culture experiments were performed. Nutrient gradients and accompanying inhibiting effect on cell proliferation were analysed for 4-layer WS scaffolds. It was ensured that no air was entrapped under or between the layers, as direct contact to air has an adverse effect on cell viability and no diffusion of nutrients can occur.

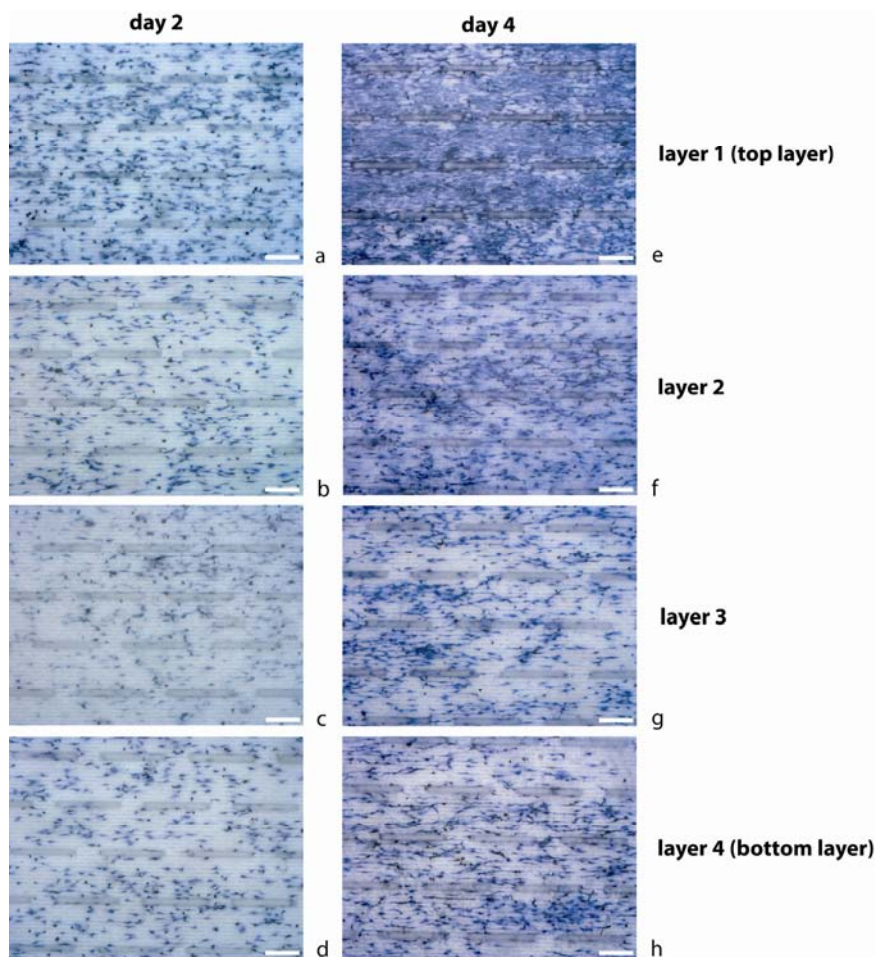


Figure 5 Light microscope images of C2C12 cells on separate layers of 4-layer WS scaffolds after (a-d) 2 and (e-h) 4 days of static culturing. Sheets feature the double brick pattern, seeding density 15.000 cells/cm², cells stained by methylene blue, magnification of all images 5x, bars represent 200 µm.

Figure 5 presents light microscopy images of methylene blue stained C2C12 cells per layer at day 2 (Figure 5a-d) and day 4 (Figure 5e-h). Figure 5a and e show the 1st (top) layer, where the cells were in direct contact to the medium. Figure 5b and f present the images for the 2nd (pre-top) layer, and Figure 5c and g for the 3rd (pre-bottom) layer. Figure 5d and h depict the 4th (bottom) layer, which is located furthest from the bulk medium. This data shows that at day 2, layer 1 has slightly more cells compared to layers 2-4. However, at day 4 the inhibited proliferation of cells on the lower layers is much more pronounced; at layer 2 already fewer cells are present compared to layer 1, but especially on layers 3 and 4 cell proliferation is inhibited and cell numbers resemble those of day 2. This data is in accordance with literature, where inhibited cell numbers were found at a distance of 200 μm or more from the periphery of the scaffold [1], corresponding to the 3rd layer of our WS scaffolds. In some WS scaffolds, layer 4 seems to have slightly higher number of cells compared to layer 3 which might be attributed to a small amount of medium entrapped under the stacked layers. In this case, nutrients can diffuse from this entrapped medium layer to the cells grown on layer 4 until depletion.

A4-4: To examine the observed effects in more detail, an additional experiment was performed with A4-4 cells. A4-4 is an established Chinese hamster ovary cell line transfected with an construct combining an hypoxia responsive promoter to a luciferase gene (HRE-Luc) to enable hypoxia-report. Upon activation, luciferase oxidizes its substrate, the protein luciferin, and emits light at a wavelength of ~ 560 nm. The HRE-luc construct is hypoxia inducible factor 1 (HIF-1) dependent and therefore luciferase activity is coupled to HIF-1 activation. HIF-1 consists of an α - and β -subunit, where the stability of the α -subunit is responsible for activation of HIF-1. Upon normal oxygen tensions (normoxia), HIF-1 α is degraded by hydroxylation. Under hypoxic conditions, oxygen-dependent hydroxylation can not take place and HIF-1 α will accumulate and activate HIF-1 dependent pathways [3, 18]. Therefore, these cells will only respond with luciferase activity measured by light emission under hypoxic conditions and not under normoxia, making these cells a good tool to report hypoxia (more details will be presented in a future publication).

In this set-up, no cells were cultured on the top layer to eliminate the nutrient limiting effect of this cell layer to the lower layers. Besides, nonpatterned sheets were used and instead o-rings created space between the layers so little amount of medium present per layer could be aspirated during unstacking and nutrient concentrations could also be determined locally. As control, a single cultured sheet with cells in direct contact to the medium was used. Figure 6a presents the acquired DNA concentrations and luciferase activity of the cells grown at each layer after 2 days. Figure 6b and c express the glucose and lactate levels, respectively, of the medium aspirated between the sheet layers at both day 1 and 2. From the DNA concentrations it seems that the cell number is not affected highly within two days, although on the 3rd sheet layer fewer cells were observed compared to the

control sheet. However, the luciferase activity indicates that hypoxia per cell increases although no significance could be determined versus the control sheet due to the rather large standard deviations. When compared to the 2nd sheet within the stack, the 4th sheet does show a significant increase in luciferase activity per cell at day 2 (see Figure 6a). The drop in glucose levels is significant as the diffusion distance to the top layer increases; for the two bottom medium layers already at day 1 and for all enclosed layers at day 2, where for the bottom two layers the glucose levels are even below detection limits. Again, this data supports the theory that with a diffusion distance of 200 μm or more from the peripheral of the scaffold (corresponding to the 3rd layer in our WS scaffolds) combines with local nutrient depletion, as reported in literature [1]. Interestingly, the medium on top of the sheets (medium layer A) has a higher glucose level compared to the control situation (Figure 6b). This effect can be explained by the fact that no cells grew on the first sheet layer so no cells are in direct contact to this medium layer where in the control situation cells are directly consuming from the bulk medium on top. The results obtained for lactate are consistent with the glucose results; high lactate levels for all enclosed medium layers (Figure 6c). This effect was already significant for all enclosed layers at day 1, and is even more pronounced at day 2. Clearly, diffusion of nutrient from the medium bulk towards, and waste products of the cells from, the lower layers is insufficient under static conditions. Nevertheless, the cells stay viable up to 4 days as is indicated by the glucose consumption and lactate production and is confirmed by a viability assay (data not shown).

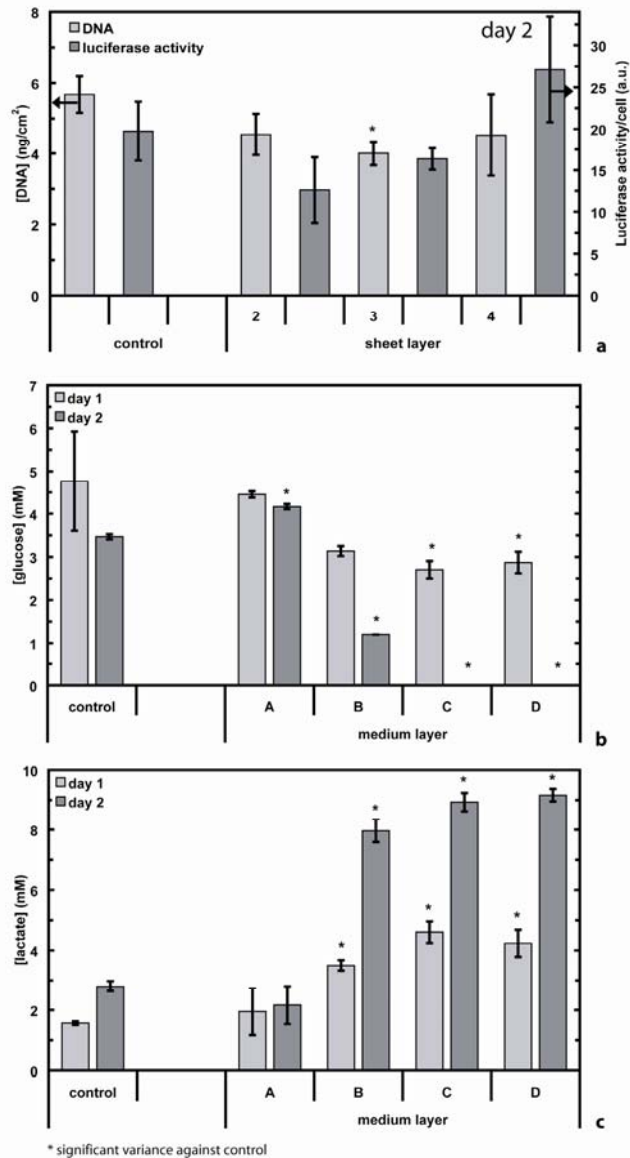


Figure 6

Analysis of A4-4-cultured WS scaffolds (a) DNA concentration and luciferase activity normalised over the DNA concentration at day 2 and, (b-c) nutrient levels in the medium at day 1 and 2 for (b) glucose and (c) lactate. Medium layer A refers to the medium on top of the sheets, medium layer B refers to the medium between sheet layers 1 and 2, medium layer C to the medium between sheet layers 2 and 3 and medium layer D to the medium between sheet layers 3 and 4. Control refers to one single cell-cultured layer with medium on top (standard culturing situation). Sheets have no micropattern, seeding density 15.000 cells/cm², significance was calculated by a two-tailed t-test with $P < 0.05$, error-bars indicate standard deviation.

8.4.4 Static culture conditions: multi-layer TS scaffolds

Due to the relatively high number of cells (4 layers cultured with cells) and comparatively low volume of medium for the WS scaffolds (restricted by well size), longer culturing periods would probably result in nutrient depletion even when medium is changed regularly. To rule out total nutrient depletion in the static experiments, also multi-layer TS scaffolds placed in larger wells were cultured under static conditions. Figure 7a displays a close-up image of a TS scaffold.

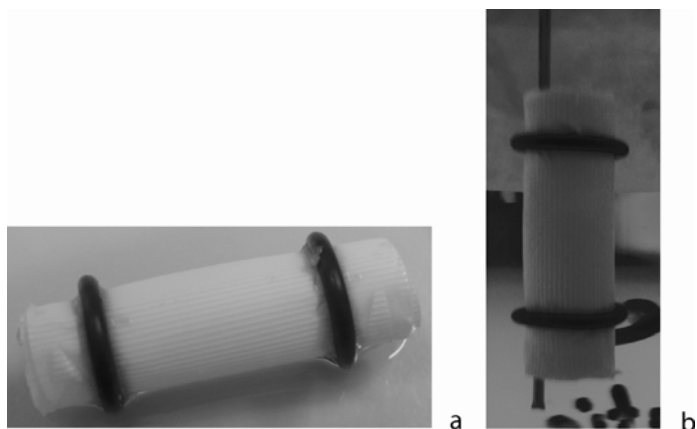


Figure 7 Multi-layer TS scaffolds featuring 250 μm channels, (a) close-up scaffold, (b) close-up of multi-layer TS scaffold attached to a needle to keep the vertical direction and immersed in medium in a spinner flasks.

Figure 8 presents the proliferation data per layer of C2C12 cells cultured on these multi-layer TS scaffolds placed in 6 well-plate wells (similar trends are observed for the A4-4 cells, data not shown here). There is clear nutrient deficiency towards the inner layers of the stack, which is more severe at higher cell density and when diffusion of nutrients from the inside of the TS scaffold is inhibited by an inner tube (porous or dense). At day 2, the variations are not that obvious yet, although the most inner layer in case of the porous tube and all three inner layers in case of the dense tube already have lower cell numbers compared to the outer layer. However, at day 4, in all cases the three inner layers have significantly lower number of cells compared to the outer layer, except for the sheet cultured without inner tube at lower seeding density of 7 500 cells/cm². For this scaffold, cell number on the most inner layer does not vary significantly compared to the outer layer and additionally cell number on all inner layers is significantly higher compared to the scaffolds with a (porous or dense) tube. This data indicates that nutrient diffusion from the inside of the scaffold indeed takes place through the inner-porosity of the sheets, despite the expected limitation imposed by the medium proteins and/or cell layer (see glucose diffusion experiment). When increasing seeding density from 7500 to 15.000 cells/cm², the drop in cell number between the 2nd and 4th layer seems to be larger,

although no significance could be determined. Furthermore, cell proliferation on the most inner sheets of the scaffolds with a (porous or dense) tube appears to be limited between day 2 to 4 (seeding density 15.000 cells/cm²), probably due to nutrient deficiency.

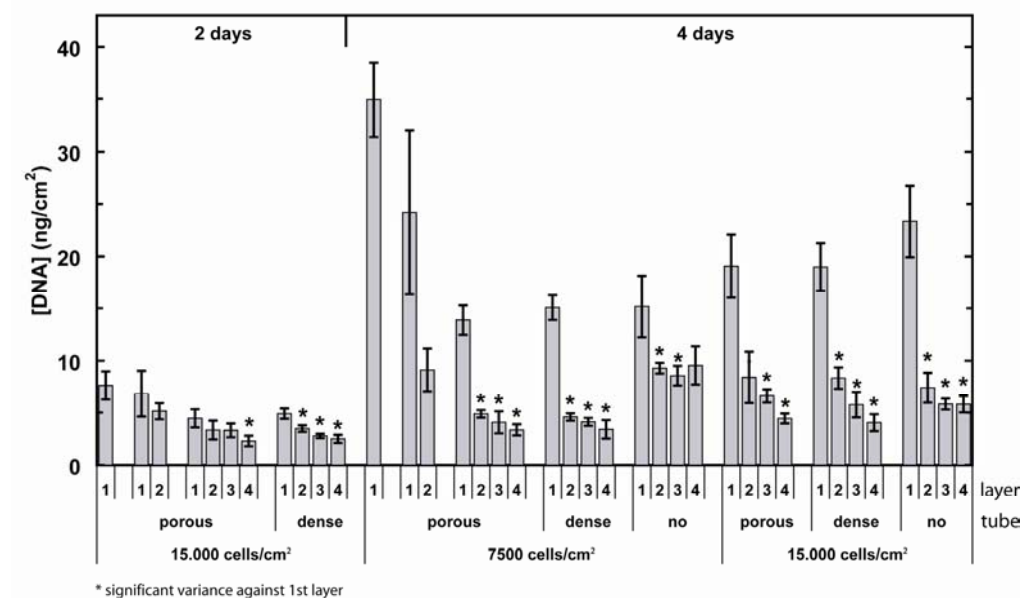


Figure 8 DNA assay for C2C12-cultured on 1-, 2- and 4-layer TS scaffolds in wells under static conditions at day 2 and 4. The sheets are stacked around a porous tube, dense tube or no tube during culturing. 1 refers to the 1st (outer) layer, with the cells in direct contact with the medium, 2, 3 and 4 refer to the next inner layers respectively. Sheets feature 250 μ m channels, seeding density 7500 or 15.000 cells/cm², significance was calculated by a two-tailed t-test with $P < 0.05$, error-bars indicate standard deviation.

Another important result is that with increasing number of sheets, the cell number on the first layer, i.e. the cells that are in direct contact to the medium, decreases. This phenomenon may be a result of nutrient deficiency in the medium due to the larger number of cells present in total and/or due to the cells on the inner layers affecting the cells on the outer layer. Medium analysis of the 4-stack scaffolds without tube (highest number of cells in total) reveals that during culturing, the nutrients are not yet depleted and lactate levels are high but not toxic [19]. For those samples glucose and lactate levels are 18.2 and 4.1 at day 2, 16.8 and 13.4 at day 4, respectively, with initial fresh medium values of 24.9 and 1.2, respectively (medium refreshed at day 2). These results suggest that the cells on the inner layers actually inhibit cell proliferation of the cells on the first layer although those cells are in direct contact to the medium. This phenomenon may be due to high local waste product concentrations produced by the (nutrient deprived) cells on the inner layers and/or signalling of these cells to the surrounding cells, including the cells on the outer layer that do not experience

nutrient limitations themselves. This result again indicates diffusion occurs between the layers through the inner-porosity of the sheets.

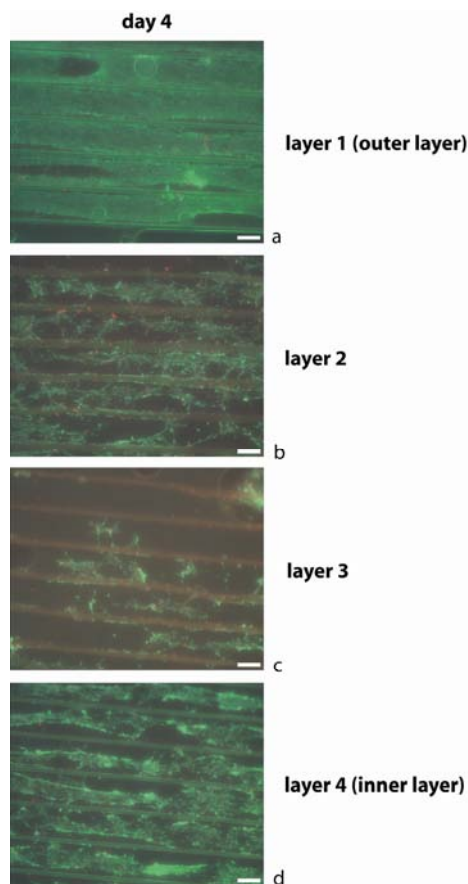


Figure 9 Typical fluorescence microscopy images of viability stained C2C12-cultured 4-layer TS scaffolds without inner tube under static conditions at day 4. Green indicates living cells and red indicates dead cells. Sheets feature 250 μm channels, seeding density 15.000 cells/ cm^2 , magnification of all images 4x, bars represent 200 μm .

Figure 9 presents the viability study of C2C12 cells at day 4 cultured on 4-layer TS scaffolds without inner tube. These microscopy images reveal that indeed cell number decreases for the inner layers, and especially for layers 2 and 3. Nonetheless, the cells on all layers are alive (green, >95%) and therefore, the DNA concentrations presented earlier in

Figure 8 correspond to the number of living cells. These results are in agreement with the data of the DNA assay and medium analysis presented in Figure 6 where despite constant DNA concentrations glucose consumption and lactate production occurs, indicating the cells are alive but not proliferating.

In conclusion, the culture experiments under static conditions clearly reveal the need of improved nutrient availability to the enclosed layers. A theoretical model (see appendix) enables prediction of the optimum way to improve nutrient delivery to the cells, of which the results are presented in the next section.

8.4.5 Model results and validation

Static conditions: The presented model was first validated by correlating the predictions for static conditions with the experimental data of Figure 6

Figure 8. The parameter values used in the model were determined experimentally or derived from literature; Table 1 presents the default values as well as the origin of these values (experiments and/or literature). Figure 10a and Figure 10b depict the model predictions for glucose and lactate concentrations, respectively, for multi-layer WS sheets for 48 hours under static conditions. For these predictions, diffusion can only originate from and to the medium on top. The y-axis displays nutrient concentrations normalised over the initial value, whereas the x-axis displays the height of the scaffold normalized over the total height of the scaffold. Therefore, value 1 on y-axis represents the initial nutrient value, whereas on x-axis value 1 represents the top of the scaffold and 0 the bottom. In case of the 5-layer scaffold, 1 on the x-axis indicates the top of layer 1, 0.8 the top of layer 2, ..., and 0.2 the top of layer 5. The 'black' symbols represent a cell number of 2×10^{12} cells/m³, equal to the seeding density. The 'grey' symbols represent a cell number 3×10^{13} cells/m³, corresponding to high confluency per layer in line with culturing for at least 4 days or more. The graphs show nutrient concentration gradients in case of 1 layer (control) and 5 stacked sheet layers.

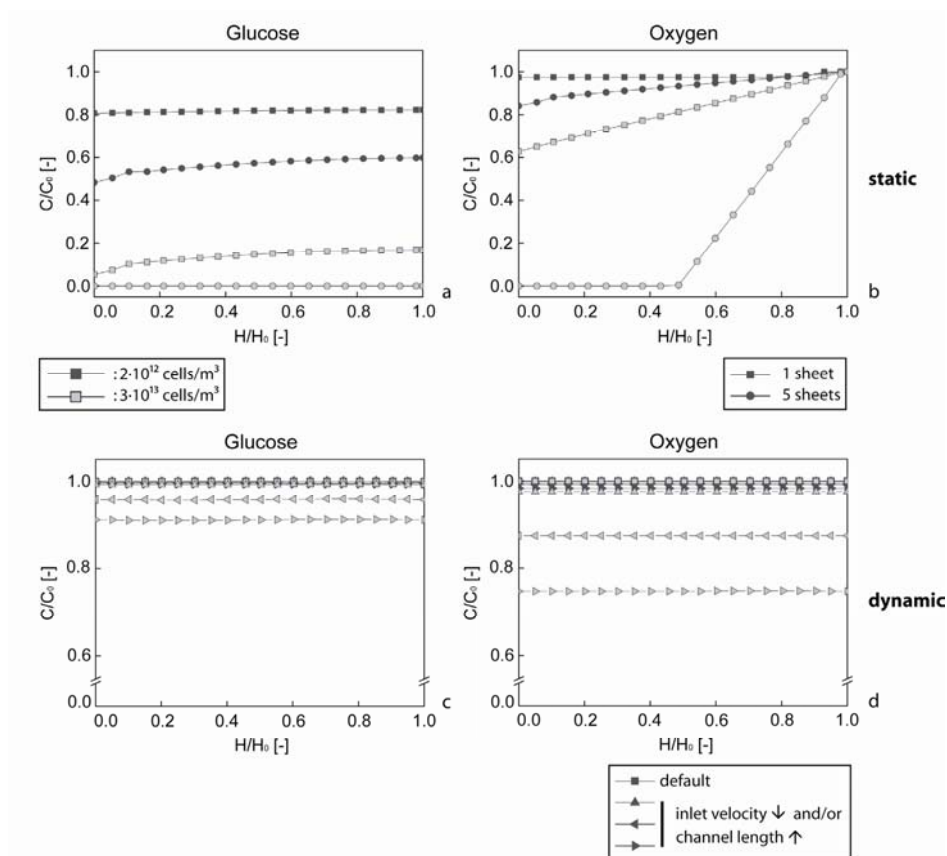


Figure 10 Graphs presenting modelled (a, c) glucose and (b, d) oxygen levels throughout a multi-layer scaffold for various cell densities at day 2 under (a, b) static and (c, d) dynamic conditions.

The predictions of the model correspond very well to the trends observed in the static culture experimental data. At lower cell density (black symbols), the model predicts no nutrient deficiency within 48 hours of culturing for both model nutrients, i.e. glucose and oxygen, as visualised in Figure 10a and Figure 10b, respectively. In both cases, the cells on 5-layer scaffolds consume significantly more compared to a single layer as expected due to the higher number of cells in total. These predictions indicate that refreshing the medium after 2 days would be sufficient at low cell densities. Since the nutrients are still at 50 % or more of their initial values, extrapolating this refreshing rate to the first days of culturing experiments seems valid even though the cell number will increase (not considered by the model). For cell density corresponding to high confluency levels (grey symbols), the model predicts significantly higher nutrient consumption and eventually nutrient depletion within 48 hours for the 5-layer scaffolds. In fact, the model predicts complete consumption of glucose (Figure 10a), whereas depletion of oxygen occurs only between the 2nd and 3rd layer due to

replenished oxygen levels into the bulk medium by diffusion from the air (Figure 10b). For 1 single sheet, the nutrients are predicted to be just sufficient, although the glucose levels are less than 20 % of the initial value almost zero close to the cell layer.

It is important to note that the results predicted by the model are consistent with the experimental results, where inhibited cell proliferation occurs mostly from the 3rd layer on (see Figure 5). In fact, during the experiments, glucose levels for layer 3 and 4 were already below detection limits at day 2 (Figure 6); that might be caused by increased cell number due to high proliferation rates of the A4-4 cells as these cells are fast-proliferating cells.

Refreshing the medium more often or increasing the medium volume will most likely improve these results; however, it may not be sufficient. Most likely, at some point in time, diffusion towards the lower layers will not be able to keep in pace with the consumption rate of the increased number of cells, independent of the nutrient concentration in the bulk medium and nutrient depletion will occur. This trend is also seen for oxygen in the 5-layer scaffolds. Dynamic culturing would improve the transport of nutrients towards the inner layers as the channels provide space throughout the complete scaffold for medium perfusion.

Dynamic conditions: The model predicts that culturing TS scaffolds under dynamic conditions, i.e., by introducing flow of medium through the channels, improves glucose and oxygen availability per layer (see Figure 10c and d, respectively). Nutrient concentrations for each layer are predicted to be sufficient in all calculated situations, indicating culturing under dynamic conditions should lead to improved nutrient availability already under mild flow conditions.

For these predictions, each layer was considered equal as convective transport through the channels was considered dominant neglecting diffusive transport. Besides, there was variation in nutrient concentration as function of residence time of the medium. The residence time is amongst others influenced by the length of the channel and inlet-flow of the medium; the variation with channel length is directly correlated to the inlet flow of the medium and both increased channel length as decreased inlet flow would prolong the residence time. The dynamic culturing experiments were performed in a spinner flask (see next section). Since the inlet flow could not exactly be controlled, and therefore not directly correlated to the residence times calculated by the model, no absolute values have been presented in the graphs. Instead, residence times representing experimental relevant conditions up to 10x default values are included; where the default is calculated from the selected parameter values presented in Table 1. An increase in residence time of 10x implies an increase in channel length of 10x (i.e. 30 cm), a decrease in the flow inlet velocity of 10x (i.e. 7.5×10^{-4} m/s) or a combined partial contribution of both. As can be appreciated from Figure 10c and Figure 10d, even for the longest residence time (10x the default value) the glucose and oxygen levels are predicted to be around 90 and 75 % of their initial values, respectively.

8.4.6 Dynamic culture conditions

The 4-layer TS scaffolds were placed in vertical direction in spinner flasks as visualised in Figure 7b. Two spinning rates of 15 and 30 rpm were compared to static culturing (no spinning); Figure 11a presents the DNA concentrations and Figure 11b the analysis of the bulk medium glucose and lactate levels in all cases. Clearly, dynamic culturing improves cell proliferation dramatically, especially on the long term.

When considering the DNA concentrations on the statically cultured TS scaffolds, two phenomena stand out (Figure 11a). Firstly, at 7 days all layers show lower proliferation in time compared to the single layer, including the outer layer; supporting the hypothesis discussed earlier that the cells on the inner layers induce inhibited cell proliferation on the outer layer. Especially, as during the experiments in the spinner flasks no nutrient depletion occurs in the bulk medium (see Figure 11b). Secondly, in contrast to the static experiments performed with the WS scaffolds, at both day 4 and 7 cell number on the outer layer does not deviate significantly from the inner layers. This result implies that the inhibited proliferation on the inner layers of the WS scaffolds is mostly caused by limited nutrient availability in the bulk medium.

Figure 12 shows microscopy images of the viability stained 4-layer scaffolds cultured under static and dynamic conditions at day 7. For the statically cultured scaffolds, cell distribution on the sheets varies largely, especially between the periphery and centre, and these images are typical for the middle part of the layers. In general, more cells grow near the periphery compared to the middle parts at the inner layers. This phenomenon is probably due to diffusion of medium from the sides of the channels improving nutrient availability locally; resulting in improved cell proliferation at and cell migration towards these areas, as illustrated in Figure 13a.

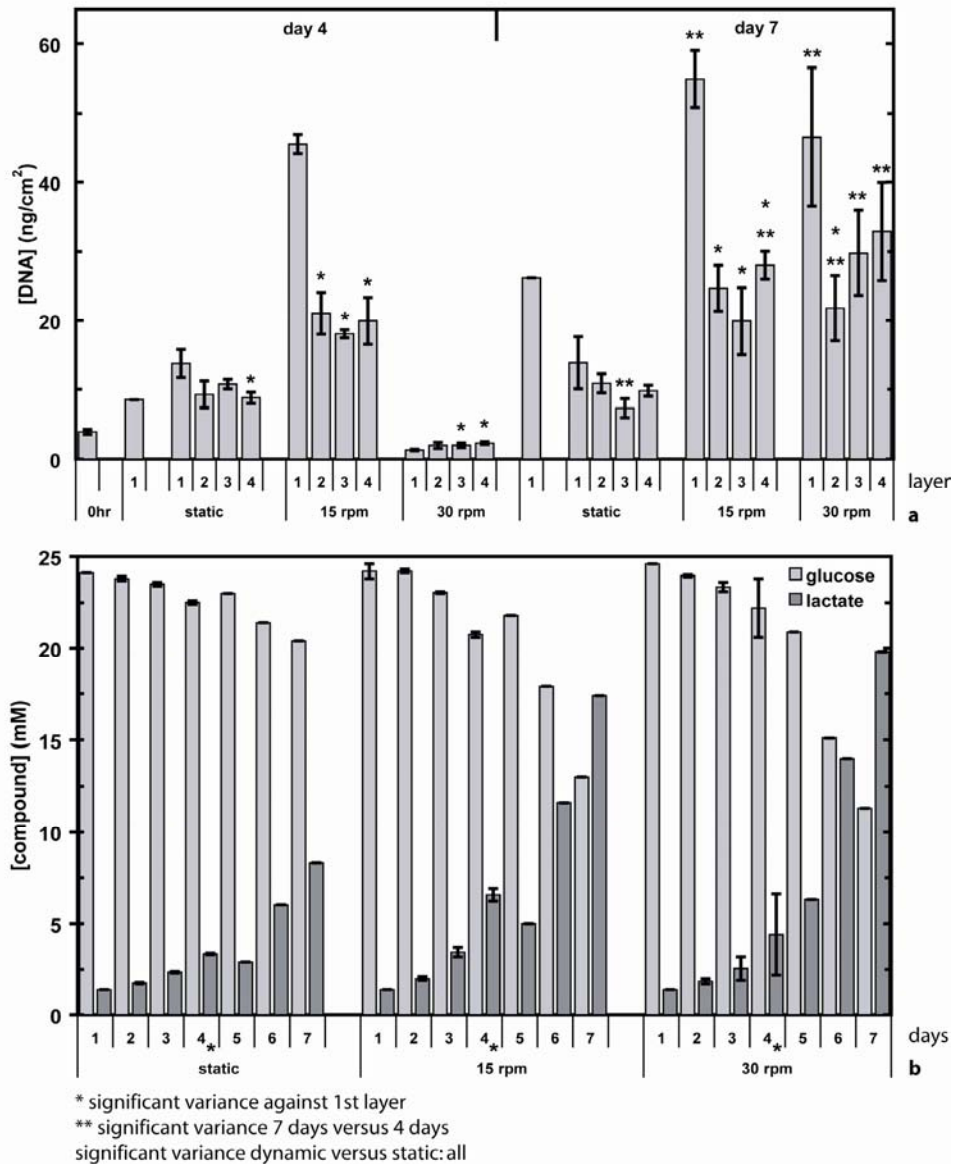


Figure 11

Analysis of C2C12-cultured 4-layer TS scaffolds under static and dynamic conditions, both in spinner flasks at day 4 and 7. (a) DNA concentrations per layer, (b-c) nutrient levels in the bulk medium at days 1-7 for (b) glucose and lactate. For dynamic conditions, spinning speeds of 15 and 30 rpm were applied. 1 refers to the 1st (outer) layer, with the cells in direct contact with the medium, 2, 3 and 4 refer to the next inner layers respectively. Sheets feature 250 μm channels, seeding density 15,000 cells/cm², significance was calculated by a two-tailed t-test with $P < 0.05$, error-bars indicate standard deviation.

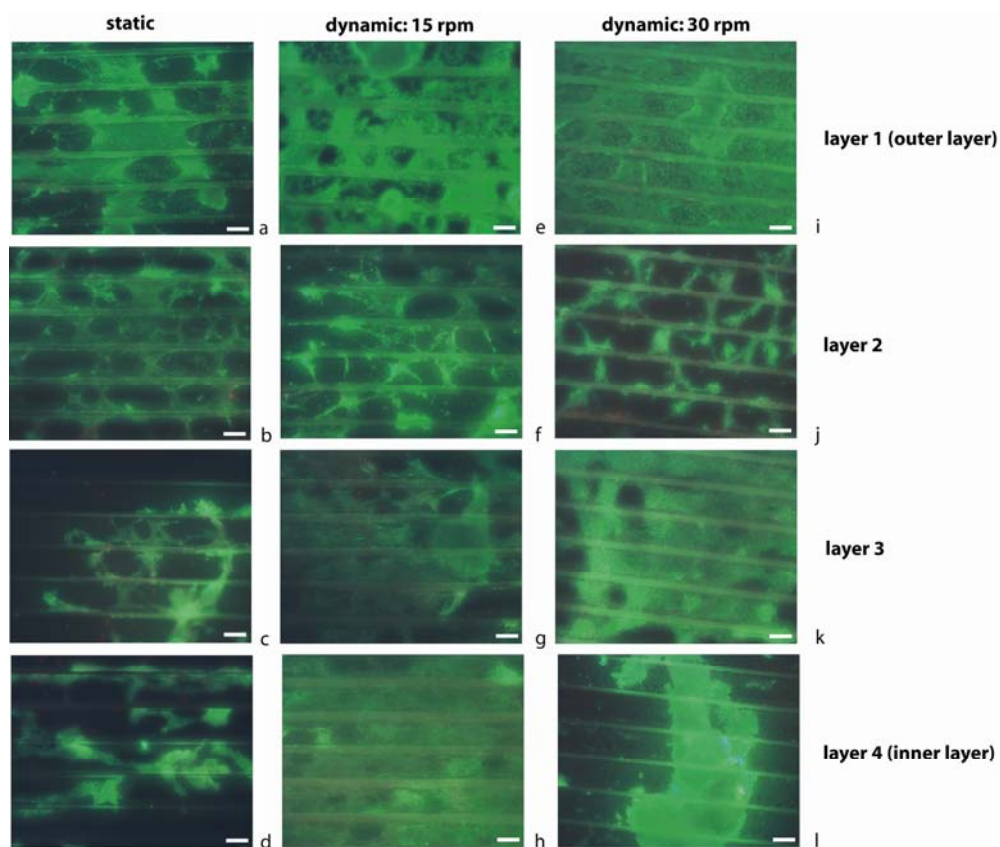


Figure 12 Typical fluorescence microscopy images of viability stained C2C12-cultured 4-layer TS scaffolds under static and dynamic conditions, both in spinner flasks at day 7 corresponding to the DNA concentration data presented in Figure 11. Sheets feature 250 μm channels, seeding density 15.000 cells/ cm^2 , magnification of all images 4x, bars represent 200 μm .

Clearly, the scaffolds cultured under dynamic conditions show higher cell number compared to the static cultured scaffolds. Only the scaffolds cultured with spinning rates of 30 rpm show a clear decline in DNA concentrations at day 4; which is completely recovered again at day 7. This drop in cell number might be due to the shear stresses the cells experience due to the medium flow. C2C12 cells can handle shear stresses to about 1-5 $\text{dyn}\cdot\text{cm}^2$, but above these values the cells might be affected [20]. Since the flow into the channels cannot exactly be determined for the spinner flask set-up, also exact shear stresses can not be calculated for these cultures. Nevertheless, cell aggregate formation was observed for culturing at both 15 and 30 rpm, more pronounced at the later, in contrast to the static cultures. Most of the aggregates attach to the outer layer of the scaffolds, and partially also on the glass of the spinner flask at the top level of the medium with the 30 rpm dynamic culture. A typical example of aggregate attachment to the outer layers of the dynamic cultured scaffolds is presented in Figure 13b, where the arrow indicates a large cell aggregate.

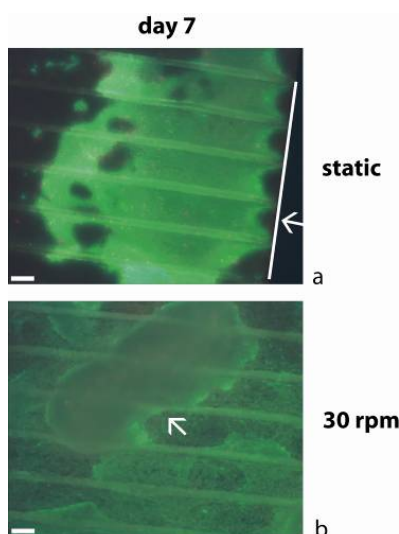


Figure 13 Typical fluorescence microscopy images of viability stained C2C12-cultured 4-layer TS scaffolds in spinner flasks at day 7 illustrating specific effects observed, (a) cell growth at the channel entrance observed at the inner layers (4th layer in this image) at scaffolds cultured under static conditions, line and arrow indicate side edge of the sheet, (b) aggregate formation on the outer layer of scaffolds cultured under dynamic conditions with 30 rpm, arrow indicates large cell aggregate. Sheets feature 250 μm channels, seeding density 15,000 cells/ cm^2 , magnification of all images 4x, bars represent 200 μm .

Most likely, the cells partially detach from the sheet layers due to the shear stresses and form aggregates. We hypothesize that cell aggregates can withstand higher shear stresses and therefore could reattach to the surface again. Due to the channel dimensions, shear stresses are higher within the channels compared to the outer layers. Besides, due to their sizes, larger aggregates can not enter the channels of the enclosed layers.

Combined, these phenomena might attribute for the majority of the aggregates attaching to the outer layer accounting for the very high DNA concentrations at these layers. Since the shear stresses experienced when culturing with 30 rpm are higher, reattaching and/or proliferation of the cells might have been delayed in comparison to culturing with 15 rpm; causing the difference in cell numbers on scaffolds cultured with 30 rpm at day 4 and 7 (Figure 11a).

Except for the scaffolds cultured with 30 rpm at day 4, the scaffolds cultured under dynamic conditions show about doubled DNA concentrations or more compared to the scaffolds under static conditions, and all inner layers show DNA concentrations comparable to one single layer (control) where all cells are in direct contact to the medium (Figure 11a). These results are also confirmed by the viability staining images presented in Figure 12.

When considering the medium analysis data of Figure 11b, clearly the cells consume significantly more glucose and produce more lactate in dynamic cultures compared to the static cell cultures, in

agreement with the DNA assay data (Figure 11a). This medium analysis data is also consistent with the variation in cell number between the 15 and 30 rpm cultures at day 4 and between day 4 and 7 of the 30 rpm culture. In the first 4 days, the scaffolds cultured at 30 rpm consume less glucose and produce less lactate compared to the scaffolds cultured at 15 rpm. Between day 5-7, the glucose consumption and lactate production per day are higher compared to that of the first 4 days as well as of day 5-7 for the scaffolds cultured at 15 rpm, indicating increased cell proliferation making up for the delay up to day 4.

The results of the DNA and medium analysis data (Figure 11) combined with the viability stained TS scaffold layers (Figure 12) clearly reveal the improved cell numbers for the dynamic cultured scaffolds compared to static conditions. In fact, the experimental results are consistent with the model predictions and prove that perfusion of the TS scaffolds improves nutrient supply throughout the scaffolds.

In conclusion, multi-layer stacking of micropatterned porous sheets into a 3D-scaffold is successful and culturing these scaffolds under dynamic conditions leads to appropriate nutrient supply to the cells combined with highly improved cell proliferation on all layers.

8.5 Conclusions

Applying PS μ M, porous micropatterned scaffold sheets were prepared and subsequently stacked into 3D-scaffolds. Nutrient diffusion through these multi-layer scaffolds was studied under both static and dynamic conditions.

The static culture experiments show critical nutrient limitations within 3 layers from the medium supply causing reduced cell proliferation but no cell death. Additionally, nutrient limitations experienced by the cells on the inner layers affect the cells on the outer layers that are in direct contact to the medium. Dynamic culturing using spinner flasks demonstrates that convective flow enables perfusion via the microchannels of the scaffolds improving nutrient supply to the cells and leading to a dramatic increase in cell proliferation compared to static culturing. Nonetheless, the spinning speed has an effect on cell attachment and aggregation of the cells and needs to be controlled to avoid cell detachment and possibly even harming of the cells. Experimental results under both static and dynamic culture conditions are consistent with the predictions by the designed model.

Future work will include study of the optimal flow conditions, preferably within a bioreactor set-up where the flow speed and direction can be controlled precisely. Besides, the development of multi-layer scaffolds having additional layers free of cells will be evaluated, so nutrients can be supplied by perfusion through these layers also when high confluency in the cell-cultured layers occurs. Finally, culturing different cell types on various layers will be evaluated. This approach is advantageous as it allows (I) co-culturing without running the risk of one cell type overgrowing the other, (II) suitable pattern design per cell type as the pattern can be tuned per layer and, (III) diffusion of signalling products between the layers due to the inner-porosity of the sheets.

Acknowledgements

B.J. Papenburg and D. Stamatialis acknowledge the Spearhead program: 'Advanced Polymeric Microstructures for Tissue Engineering' of the University of Twente (BMTi, Institute for Biomedical Technology) for financial support.

References

1. Dunn JCY, Chan W-Y, Cristini V, Kim JS, Lowengrub J, Singh S, et al. Analysis of Cell Growth in Three-Dimensional Scaffolds. *Tissue Engineering* 2006;12(4):705-716.
2. Ko HCH, Milthorpe BK, McFarland CD. Engineering thick tissues - The vascularisation problem. *Eur Cells Mater* 2007 Jul-Dec;14:1-18.
3. Malda J, Klein TJ, Upton Z. The roles of hypoxia in the In vitro engineering of tissues. *Tissue Engineering* 2007 Sep;13(9):2153-2162.
4. Sengers BG, Taylor M, Please CP, Oreffo ROC. Computational modelling of cell spreading and tissue regeneration in porous scaffolds. *Biomaterials* 2007;28(10):1926-1940.
5. Malda J, Rouwkema J, Martens DE, le Comte EP, Kooy FK, Tramper J, et al. Oxygen gradients in tissue-engineered PEGT/PBT cartilaginous constructs: Measurement and modeling. *Biotechnol Bioeng* 2004 Apr;86(1):9-18.
6. Martin Y, Vermette P. Bioreactors for tissue mass culture: Design, characterization, and recent advances. *Biomaterials* 2005;26(35):7481-7503.
7. Barron V, Lyons E, Stenson-Cox C, McHugh PE, Pandit A. Bioreactors for cardiovascular cell and tissue growth: A review. *Ann Biomed Eng* 2003 Oct;31(9):1017-1030.
8. Lemon G, King JR, Byrne HM, Jensen OE, Shakesheff KM. Mathematical modelling of engineered tissue growth using a multiphase porous flow mixture theory. *J Math Biol* 2006 May;52(5):571-594.
9. Vunjak-Novakovic G, Obradovic B, Martin I, Bursac PM, Langer R, Freed LE. Dynamic Cell Seeding of Polymer Scaffolds for Cartilage Tissue Engineering. *Biotechnology progress* 1998;14(2):193-202.
10. Shanbhag S, Wang SP, Kotov NA. Cell distribution profiles in three-dimensional scaffolds with inverted-colloidal-crystal geometry: Modeling and experimental investigations. *Small* 2005 Dec;1(12):1208-1214.
11. Karande TS, Ong JL, Agrawal CM. Diffusion in musculoskeletal tissue engineering scaffolds: Design issues related to porosity, permeability, architecture, and nutrient mixing. *Ann Biomed Eng* 2004 Dec;32(12):1728-1743.
12. Tsang VL, Bhatia SN. Three-dimensional tissue fabrication. *Advanced Drug Delivery Reviews* 2004;56(11):1635-1647.
13. Vidaurre A, Castilla Cortazar I, Gomez Ribelles JL. Polymeric scaffolds with a double pore structure. *Journal of Non-Crystalline Solids* 2007;353(11-12):1095-1100.
14. Lee J, Cuddihy MJ, Kotov NA. Three-Dimensional Cell Culture Matrices: State of the Art. *Tissue Engineering Part B: Reviews* 2008;14(1):61-86.
15. Lim JY, Donahue HJ. Cell Sensing and Response to Micro- and Nanostructured Surfaces Produced by Chemical and Topographic Patterning. *Tissue Engineering* 2007;13(8):1879-1891.
16. Papenburg BJ, Vogelaar L, Bolhuis-Versteeg LAM, Lammertink RGH, Stamatialis D, Wessling M. One-step fabrication of porous micropatterned scaffolds to control cell behavior. *Biomaterials* 2007;28(11):1998-2009.
17. Bartolo LD, Morelli S, Rende M, Campana C, Salerno S, Quintiero N, et al. Human Hepatocyte Morphology and Functions in a Multibore Fiber Bioreactor. *Macromolecular Bioscience* 2007;7(5):671-680.
18. Harris AL. Hypoxia - A key regulatory factor in tumour growth. *Nat Rev Cancer* 2002 Jan;2(1):38-47.

19. Gawlitta D, Oomens CWJ, Bader DL, Baaijens FPT, Bouten CVC. Temporal differences in the influence of ischemic factors and deformation on the metabolism of engineered skeletal muscle. *Journal of applied physiology* 2007 August 1, 2007;103(2):464-473.
20. Figallo E, Cannizzaro C, Gerecht S, Burdick JA, Langer R, Elvassore N, et al. Micro-bioreactor array for controlling cellular microenvironments. *Lab on a chip* 2007;7(6):710-719.
21. Abdullah NS, Das DB, Ye H, Cui ZF. 3D bone tissue growth in hollow fibre membrane bioreactor: implications of various process parameters on tissue nutrition. *International Journal of Artificial Organs* 2006 Sep;29(9):841-851.
22. Coletti F, Macchietto S, Elvassore N. Mathematical modeling of three-dimensional cell cultures in perfusion bioreactors. *Industrial & Engineering Chemistry Research* 2006 Nov 22;45(24):8158-8169.
23. Sengers BG, van Donkelaar CC, Oomens CWJ, Baaijens FPT. Computational study of culture conditions and nutrient supply in cartilage tissue engineering. *Biotechnology Progress* 2005 Jul-Aug;21(4):1252-1261.
24. Ye H, Das DB, Triffitt JT, Cui ZF. Modelling nutrient transport in hollow fibre membrane bioreactors for growing three-dimensional bone tissue. *Journal of Membrane Science* 2006 Mar 15;272(1-2):169-178.
25. Hessel V, Hardt S, Loewe H. *Chemical Micro Process Engineering: Fundamentals, Modelling and reactions*. Weinheim: Wiley-VCH, 2004.
26. Tabeling P, Cheng S. *Introduction to Microfluidics*. New York: Cambridge University Press, 2005.
27. COMSOL. *Manuals COMSOL 3.2 and 3.3*, 2005-2007.
28. Saltzman WM. *Tissue Engineering: principles for the design of replacement organs and tissues*. 1st ed. Oxford: Oxford University Press, 2004.
29. Lewis MC, MacArthur BD, Malda J, Pettet G, Please CP. Heterogeneous proliferation within engineered cartilaginous tissue: The role of oxygen tension. *Biotechnol Bioeng* 2005 Sep 5;91(5):607-615.
30. Stamatialis DF, Papenburg BJ, Gironés M, Saiful S, Bettahalli SNM, Schmitmeier S, et al. Medical applications of membranes: Drug delivery, artificial organs and tissue engineering. *Journal of Membrane Science* 2008;308(1-2):1-34.

Appendix to Chapter 8 Model description

Model Boundaries

The designed model is general and not specified to e.g. cell type, - age, - dimension or - shape but high mean constant metabolic rates are chosen for oxygen and glucose consumption, similar to models described before [21-24]. Furthermore, temperature and cell culture medium pH are considered constant, as the incubator where the experiments take place and the humid 5% CO₂ atmosphere in the incubator combined with the buffer capacity of the medium control these parameters, respectively.

Additional assumptions are:

- all processes are isothermal
- the cell culture medium is cell free
- location of the cells is homogeneously throughout the cell seeded microchannels

Change in cell number due to proliferation is taken into account by solving the system for two different cell densities; the lower value is comparable to the initial seeding density, the higher value represents higher confluency.

What has not been taken into account is:

- change in cell culture medium density
- cell differentiation and cell death
- influence of oxygen consumption on the glucose concentration and vice versa; the oxygen and glucose consumption are calculated independently
- scaffold material and –degradation; change in permeability is expressed by differences in diffusion coefficients obtained experimentally

Parameters

Table 1 lists the default parameter values which are taken from literature or are determined experimentally.

Table 1 Default parameter values used in the model

| | Parameter | Value | Unit | Ref ^(e) |
|----------------|-----------------------------------|------------------------|--|--------------------------------|
| General | Cell seeding density ^a | 2x10 ¹² | cells/m ³ | exp., [16, 24] |
| | Increased cell density | 3x10 ¹³ | cells/m ³ | exp., [24] |
| | Porosity inner-part sheets | 75 | % | exp., [16] |
| | Length microchannels | 0.03 | m | [24], exp. relevant |
| | Inlet velocity | 7.5x10 ⁻³ | m/s | [24] |
| Glucose | Inlet concentration ^b | 5.55 | mol/m ³ | exp. |
| | D ₁ ^c | 9x10 ⁻¹⁰ | m ² /s | [23, 28] |
| | D ₂ | 1.8x10 ⁻¹⁰ | m ² /s | [24] |
| | D ₃ | 1x10 ⁻¹⁰ | m ² /s | exp., [16, 24] |
| | Cell metabolic rate | 3.83x10 ⁻¹⁶ | Mol cell ⁻¹ s ⁻¹ | [24] |
| Oxygen | Inlet concentration ^b | 0.2 | mol/m ³ | [6, 24] |
| | D ₁ ^c | 3x10 ⁻⁹ | m ² /s | [20, 23, 24] |
| | D ₂ | 6x10 ⁻¹⁰ | m ² /s | [24] |
| | D ₃ | 3x10 ⁻¹⁰ | m ² /s | Calculated ^d , [24] |
| | Cell metabolic rate | 3.75x10 ⁻¹⁷ | mol cell ⁻¹ s ⁻¹ | [23, 24, 29] |

With Dx indicating the diffusion coefficient at domain x (1 = medium, 2 = cell-seeded microchannel, 3 = inner-porosity of the scaffold sheets)

^a Based on a cell seeding density of 15.000 cells/cm² as used in the culture experiments

^b Based on the glucose concentration in culture medium or blood and oxygen solubility of oxygen in water of 37°C in an environment of 5% CO₂ respectively

^c Based on the diffusion coefficient of glucose/oxygen in water at 37°C

^d Experimentally determined glucose diffusion coefficient through the scaffold sheet after which the oxygen diffusion coefficient has been calculated using the same ratio between D₁ and D₃ as for glucose

^e 'exp.' stands for 'experimentally determined'.

Equations static culturing

1 ml medium per cm² surface area is present on top of the multi-layer scaffolds and is refreshed every 2 days, similar to the experimental set-up. Based on the symmetry of the multi-layer scaffold in width and length, the model can be solved in 2D.

Nutrient transport is based on diffusion only; therefore the instationary diffusion equation based on Fick's law can be used to describe the static case:

$$\frac{\partial c}{\partial t} = \nabla \cdot (-D \nabla c) \quad (1)$$

Where c = nutrient concentration, t = time and D = nutrient diffusion coefficient; the term $(-D \nabla c)$ describes Fick's law for diffusive transport.

This model assumes no interaction between glucose and oxygen and therefore Fick's law can be applied.

The following general boundary conditions are applied:

$$\left(\frac{\partial c}{\partial x} + \frac{\partial c}{\partial y} \right) = 0 \quad (2)$$

representing zero flux over boundaries between domains with similar diffusion coefficients.

$$D_A \left(\frac{\partial c}{\partial x} + \frac{\partial c}{\partial y} \right) = D_B \left(\frac{\partial c}{\partial x} + \frac{\partial c}{\partial y} \right) \quad (3)$$

describing flux continuity over the boundaries between domains with different diffusion coefficients.

$$c(t_0) = c_0 \quad (4)$$

equating the initial conditions of the nutrient concentrations in the medium at the start of the experiment.

Three domains can be distinguished in the static case: cell culture medium (1), cell seeded microchannels (2) and the inner-porosity of the scaffold sheets (3). To solve the model; these three domains have to be considered separately with respect to the equations and the boundary and initial conditions to be used.

Cell culture medium

$$\frac{\partial c}{\partial t} = D_1 \left(\frac{\partial c}{\partial x} + \frac{\partial c}{\partial y} \right) \quad (5)$$

For the boundary and initial conditions the general boundary conditions are described as follows:

- Equation 2 is valid at the top boundary and at all exterior boundaries for glucose; representing no glucose flux between the medium-air boundary and at the sides of the stacked multi-layer scaffold sheets respectively
- At the top boundary $c = c_0$ can be applied for oxygen; describing solubility of oxygen from the air into the medium

- Equation 3 is valid at the boundary between the medium and the microchannels when $D_A = D_1$ and $D_B = D_2$ and for the boundary between the medium and inner porosity of the sheets when $D_A = D_1$ and $D_B = D_3$; describing flux continuity over the respective boundaries
- Equation 4 is valid as initial conditions; representing nutrient concentrations of fresh medium

Cell seeded microchannels

$$\frac{\partial c}{\partial t} - D_2 \left(\frac{\partial c}{\partial x} + \frac{\partial c}{\partial y} \right) = R = V \cdot d \quad (6)$$

with V = consumption rate per cell and d = cell seeding density, multiplied V and d express zero-order consumption rate of the nutrients.

For the boundary and initial conditions the general boundary conditions are described as follows:

- Equation 3 is valid at the boundary between the top of the microchannel of the first layer and the medium for $D_A = D_2$ and $D_B = D_1$ and for the boundary between the bottom of the microchannels and inner porosity of the sheets for $D_A = D_2$ and $D_B = D_3$; describing flux continuity over the respective boundaries
- Equation 4 is valid as initial condition; representing nutrient concentrations of fresh medium present in the scaffold at the start of the experiment

Inner-porosity scaffold sheets

$$\varepsilon \frac{\partial c}{\partial t} = D_3 \left(\frac{\partial c}{\partial x} + \frac{\partial c}{\partial y} \right) \quad (7)$$

where ε = porosity. Nutrients are only present in the pores of the inner-part of the scaffold sheets; the porosity term expresses a concentration gradient that will develop in time over the inner-porosity of the scaffold due to nutrient consumption by the cells.

For the boundary and initial conditions the general boundary conditions are described as follows:

- Equation 2 is valid at all exterior boundaries, except the top boundary, and all interior boundaries connecting the inner-parts of the stacked scaffold sheets; describing symmetry of the microchannels and inner-parts of the scaffolds for the stacked layers

- Equation 3 is valid at the boundary between the top of the ridges of the microchannels of the first layer and the medium for $D_A = D_3$ and $D_B = D_1$ and for the boundary between inner porosity of the sheets and the microchannel for $D_A = D_3$ and $D_B = D_2$; describing flux continuity over the respective boundaries
- Equation 4 is valid as initial condition; representing nutrient concentrations of fresh medium present in the scaffold at the start of the experiment

Equations dynamic culturing

With the introduction of flow of the cell culture medium, the system enters the fluidic regime combined with mass transfer of the nutrients. Although the scaffold sheets, including the micropattern, measures 90 μ m in thickness, well-known macro scale transport equations can be applied as for these scaffold sizes the same transport phenomena are still dominant [25, 26].

A pseudo3D mode has been used to model the nutrient concentrations over the perfused multi-layer scaffolds bringing about replacement of the space variable along the direction of the flow by time. Therefore, with a given velocity, an increment in time stands for a displacement in the direction of the flow.

This pseudo3D mode can be applied when the following requirements are satisfied:

- the model is defined steady-state;
cell proliferation is not modelled in time and therefore the system is considered steady-state
- Convection is constant and dominating solely in one direction;
full developed laminar flow is present in the microchannels and does not change over the length of the microchannel
- In the direction of the flow, diffusion is negligible
- The applied geometry can be described by extrusions and does not change in the direction of the flow

Since the designed model meets all the requirements, the use of the pseudo3D mode was valid. Based on these assumptions, the convection-diffusion equation can be written in the following form:

$$u_{dl} \frac{\partial c}{\partial t} + \nabla \cdot (-D \nabla c) = R \quad (8)$$

with u_{dl} a variable of interest as function of x and where R is as described in Equation 6.

The Navier-Stokes equation, for laminar flow of incompressible fluids, is used to describe the flow of nutrients in the microchannels of the scaffold sheets; where the channels are considered rectangular tubes [27]:

$$u_{dl} = \frac{u_{channel}}{\langle u_{channel} \rangle} = 2 \cdot \left(16 \cdot \frac{(x_1 - x) \cdot (x - x_0)}{(x_1 - x_0)^2} \cdot \frac{(y_1 - y) \cdot (y - y_0)}{(y_1 - y_0)^2} \right) \quad (9)$$

where x stands for the width of one symmetry element, i.e. the width of the microchannel calculated from one ridge of the microchannel to the next ridge; and y stands for the height of one symmetry element, i.e. the height of the microchannel calculated from the bottom of the microchannel to the top of the ridges (see also Figure 2c).

Two domains can be distinguished in the dynamic case: perfused and cell seeded microchannels (2) and the inner-porosity of the scaffold sheets (3). To solve the model; these two domains have to be considered separately with respect to the equations and the boundary and initial conditions to be used.

Cell seeded microchannels

$$u_{dl} \frac{\partial c}{\partial t} - D_2 \left(\frac{\partial^2 c}{\partial x^2} + \frac{\partial^2 c}{\partial y^2} \right) = R \quad (10)$$

For the boundary and initial conditions the general boundary conditions are described as follows:

- Equation 2 is valid at $(x, y) = (\frac{1}{2} (x_1 - x_0), \frac{1}{2} (y_1 - y_0))$; represents symmetry of the concentration gradient at the centre of the microchannels
- Equation 3 is valid at interior boundaries for $D_A = D_2$ and $D_B = D_3$ and at $y = 0$ and $y = y_1$; describing flux continuity over boundaries between the microchannels and the inner-porosity of the stacked sheets

- Equation 4 is valid as initial condition; representing nutrient concentrations of fresh medium at the inlet of the microchannels

Inner-porosity scaffold sheets

$$D_3 \left(\frac{\partial^2 c}{\partial x^2} + \frac{\partial^2 c}{\partial y^2} \right) = 0 \quad (11)$$

For the boundary and initial conditions the general boundary conditions are described as follows:

- Equation 2 is valid at all exterior boundaries, except $y = y_1$; represents symmetry of the microchannels
- Equation 3 is valid at interior boundaries for $D_A = D_3$ and $D_B = D_2$ and at $y = 0$ and $y = y_1$; describing flux continuity over boundaries connecting the inner-porosity of the stacked sheets with the microchannels
- Equation 4 is valid as initial condition with $c_0 = 0$; representing no flow of medium into the inner-porosity of the sheets at the inlet as well as absence of medium in the inner-porosity at the start of the experiment in this specific case

Nomenclature Model

| | |
|----------|--|
| X_0 | Initial value X |
| X_1 | Value X at domain 1: medium |
| X_2 | Value X at domain 2: cell-seeded microchannel |
| X_3 | Value X at domain 3: inner-porosity of the scaffold sheet |
| c | Nutrient concentration |
| d | Cell seeding density |
| D | Nutrient diffusion coefficient |
| R | Zero-order consumption rate of the nutrients ($V \cdot d$) |
| t | Time |
| u_{dl} | variable |
| V | Consumption rate per cell |



Chapter 9 Reflections and Outlook

9.1 Scaffold design at large

Tissue engineering, and scaffold design as part thereof, requires the fundamental understanding of a wide range of engineering and life science principles for the development of a functional tissue engineering construct [1]. Even when many aspects are understood, functional design still requires extensive optimization to determine the optimal characteristics for the specific application. The interdisciplinary character, combined with the extensiveness of the application field, yields the high level of complexity involved with tissue engineering. All pieces of the puzzle need to fall in place before the designed construct can be translated into clinical application. Regarding scaffold design, pieces of the puzzle include material properties, surface characteristics and 3D architecture. Within these parts, again many sub-categories need to be addressed implying vast multiplication of the number of possibilities.

Two approaches can be followed to optimize these distinct aspects for a specific application. Firstly and most commonly applied, systematically evaluate a gradient of one variable and extrapolate the findings to scaffold design at large. Secondly, screen a wide range of variables and determine the optimal result for a specific application, therewith refining the possibilities.

Both ways have their benefits and disadvantages, but most importantly, each can be applied to fulfil different needs. The first, bottom-up, approach allows gaining fundamental understanding how the specific variable affects the effectiveness of the scaffold in certain settings. The second, top-down, approach allows to pass over the limitations of our own imaginary and select the specific combination of variables yielding the most suitable response. This thesis generally follows the bottom-up design; however, we also propose a new top-down based design concept.

9.2 Scaffold design in this thesis

9.2.1 General discussion

This thesis aimed to give insight in various important issues concerning scaffold design and what parameters are involved addressing these topics to provide distinct strategies for functional scaffold design as part of the development of tissue engineering constructs.

Based on the work described in this thesis, we can now fill in important sub-categories into the data tree as presented already in Chapter 1, see Figure 1 below.

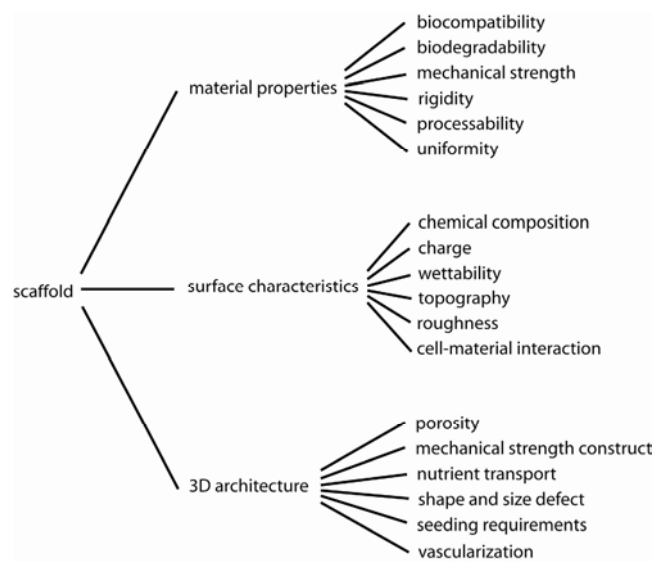


Figure 1 Data tree representing a number of categories involved in scaffold design.

The research described in this thesis relates to various aspects of scaffold design within the 3 main classes; from material properties to surface characteristics and 3D-architecture. The scaffold design framework at large is too extensive to address all topics in detail; hence, a selection of topics was evaluated regarding the main design concept of a multi-layer 3D scaffold incorporating porosity as well as topography. Figure 3 of Chapter 1 presented the various aspects addressed in this thesis. Certain topics within the concept at large were studied in more detail, where other sub-categories were only briefly addressed and therewith, providing distinct strategies for functional scaffold design.

9.2.2 General conclusions

PS μ M is a versatile and facile method for scaffold fabrication yielding sheets with both porosity as well as surface topography, and is applicable for a wide range of materials. The choice of scaffold material depends on the required material properties for the specific application, provided that these materials can be processed featuring an optimized scaffold design. Besides the material properties, also a wide range of surface characteristics determine the final functionality of a scaffold. Evaluation of how a number of these surface characteristics affect cell behaviour reveals the interactions on the scaffold-cell level are highly important and also highly complex. Hence, more in-depth knowledge is needed on how these parameters affect cell behaviour and optimization needs to occur per specific tissue engineering application. To overcome the limitations of the imposed complexity regarding suitability of certain surface characteristics for a specific application, a top-down approach can provide good cues to refine the large pool of variables.

Finally, the 3D multi-layer scaffold composed of micropatterned porous sheets is feasible and, when the various scaffold design aspects are taken into account, well supplied with nutrients and can provide sustained organized tissue growth.

9.3 Future directions

9.3.1 Materials properties: reinforcements

The work described in this thesis is based on polymer processing by PS μ M and relate mainly to soft tissue engineering applications. However, when considering hard tissue engineering applications, these polymer sheets might not provide sufficient mechanical strength. In this case, addition of reinforcements (e.g. ceramic) to the polymer solution enables fabrication of a composite material with improved mechanical properties [2, 3]. The composite can be applied as such or the polymer can be pyrolysed while sintering the ceramic particles. Herewith, PS μ M would allow the fabrication of micropatterned ceramic or polymer-ceramic composite sheets. Preliminary results applying a slurry of poly(ϵ -caprolactone) (PCL) and hydroxyapatite (HA) indicates a good distribution of the ceramic through the polymer matrix, as visualized in Figure 2. Further research and optimization is required to develop micropatterned sheets and study how well applicable these sheets are for certain tissue engineering applications.

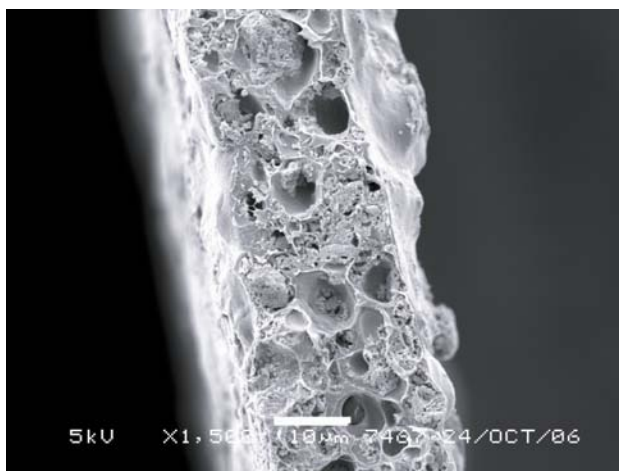


Figure 2 SEM image of a sheet fabricated by PS μ M of a PCL-HA slurry (10 wt% PCL + 5wt% HA in chloroform). Scale bar in image represents 10 μ m.

9.3.2 Surface characteristics: layer-by-layer architecture

Scaffold fabrication by multi-layer stacking of the micropatterned porous sheets, fabricated by PS μ M, allows for distinct micropattern architecture into a specifically selected material optimized for the cell type of interest. This approach even enables fabrication of layers of different materials and discriminating surface characteristics within one stack or graded porosity. In case optimization of one parameter results at the expenses of a second parameter, the multi-layer stack can be build-up combining layers expressing optimal composition regarding either of the parameters. This opportunity also should be assessed regarding special spacer layers without cells to ensure nutrient perfusion also with higher cell confluency layers within the cell cultured microchannels. Additionally, optimized layers can be included for distinct cell types of interest in case of co-culturing.

9.3.3 3D-architecture: nutrient supply *in-vivo* style

To take the multi-layer scaffold design a step further requires good nutrient supply throughout the construct under both *in vitro* as well as *in vivo* conditions, for which good connection to the host vascular system is required. The microchannel space throughout the scaffold provides *in vitro* good nutrient supply when cultured under dynamic conditions. These microchannels might actually also enable capillary growth and therewith, vessel ingrowth into the scaffold construct for connection to the host vasculature *in vivo*. Optimized layer-by-layer architectures could provide distinct layer design for the tissue of interest as well as for capillary formation; which might be an interesting approach to induce nutrient delivery and vascularization *in vivo* through angiogenesis.

In the human body, the capillary wall consists of a layer of endothelial cells. Literature studies suggest that the introduction of endothelial cells by co-culturing with the cell type of interest can induce capillary growth within the specific tissue of interest allowing connection to the host vasculature upon implantation *in vivo* [4].

Preliminary result of culturing human umbilical vein endothelial cells (HUVEC) on patterned as well as nonpatterned PLLA substrates indicates good suitability of these surfaces for HUVECs. The cells grow a monolayer and have tight cell-cell contact visualized by the stained cell-junctions of the cell membranes (anti-CD31 staining), distinguished by the enhanced fluorescent signal.

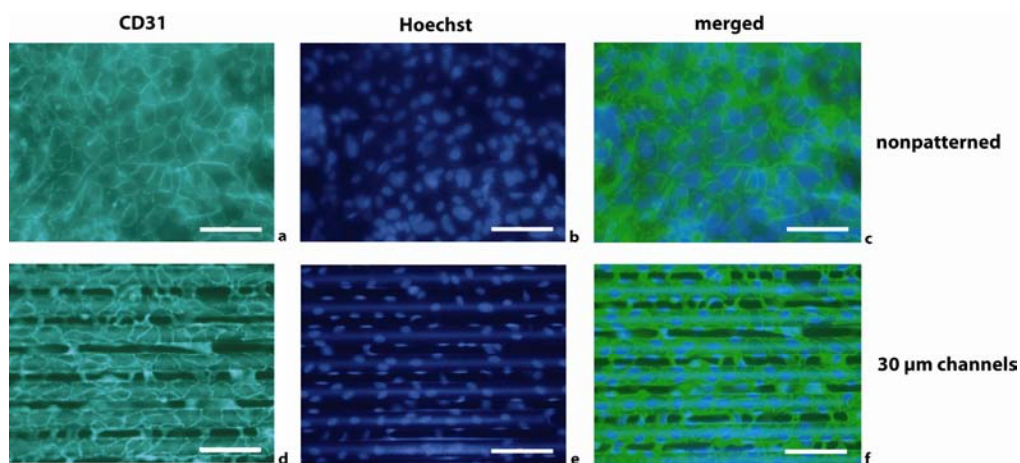


Figure 3 Typical fluorescent microscopy images of HUVEC's cultured at dense PLLA scaffold sheets at day 10, (a-c) nonpatterned surface, (d-f) surface featuring 30 μm wide channels. The cells are stained against (a, d) endothelial-cell specific antibody CD31 at the cell membrane and for (b, e) the nucleus by Hoechst, (c, f) merged image. Seeding density 35.000 cells/ cm^2 , all images at 20x magnification, scale bar represents 100 μm .

Preliminary results of culturing C2C12 cells with HUVEC on micropatterned PLLA sheets reveal the HUVEC cells might indeed grow capillaries, as can be appreciated in Figure 4. Here, the red colored regions are HUVEC cells; whereas the spread blue colored cells are the C2C12 cells. Furthermore, these preliminary results indicate a distinct influence of the micropattern towards the capillary organization. Capillary growth through co-culturing with HUVEC cells and possible organization of these grown capillaries on these micropatterned sheets requires further elaborate research. Possible research directions include direct co-culturing on the layers, but also co-culturing with the individual cell types on separate layers allowing signaling between the cell types but no direct cell-cell contact. Also, sheets seeded with discriminating cell types can be stacked facing each other to allow cell-cell contact during culturing but still enables distinct surface architecture adapted to the specific cell types.

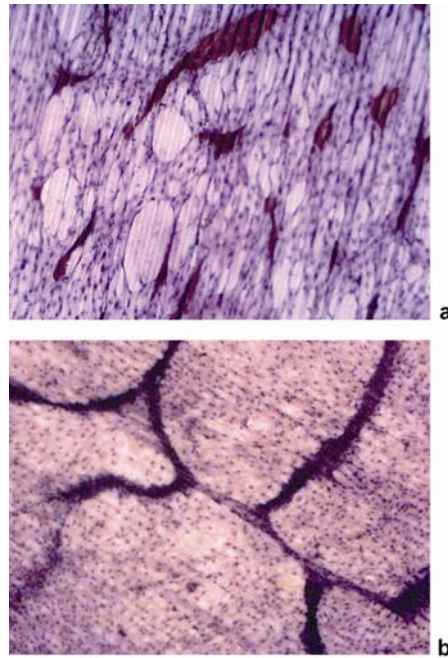


Figure 4

Light microscopy images of (a) dense and (b) porous PLLA sheets (preparation similar to Chapter 8) featuring 30 μm channels at day 4 of co-culturing C2C12 and HUVEC cells. C2C12 with haematoxylin and HUVEC stained for Anti-CD31, seeding density 140.000 cells/cm² C2C12 + 140.000 cells/cm² HUVEC (ratio 1:1). All images at 5x magnification.

References

1. Langer R, Vacanti JP. Tissue Engineering. *Science* 1993;260:920-926.
2. Causa F, Netti PA, Ambrosio L, Ciapetti G, Baldini N, Pagani S, et al. Poly- ϵ -caprolactone/hydroxyapatite composites for bone regeneration: In vitro characterization and human osteoblast response. *Journal of Biomedical Materials Research Part A* 2006;76A(1):151-162.
3. Rezwan K, Chen QZ, Blaker JJ, Boccaccini AR. Biodegradable and bioactive porous polymer/inorganic composite scaffolds for bone tissue engineering. *Biomaterials* 2006;27(18):3413-3431.
4. Levenberg S, Rouwkema J, Macdonald M, Garfein ES, Kohane DS, Darland DC, et al. Engineering vascularized skeletal muscle tissue. *Nature Biotechnology* 2005 Jul;23(7):879-884.



Summary

Material science

In the beginning years of tissue engineering research, only a limited range of materials were known for their biocompatible nature and the vast majority of studies involved one of these materials. However, after decades of biomaterials science, the range of materials to select from grew explosively and is still growing. Different classes of materials, of both natural as well as synthetic origin, allow for distinct gradual variations between materials and selection of optimal material properties for a specific application. **Chapter 2** presented an overview of commonly applied biomaterials of various classes, as well as fabrication techniques to process these materials into scaffolds. The large number of materials also requires distinct processing techniques to enable fabrication of these materials into the designed scaffold. However, many fabrication methods take into account only a single design parameter implying the need of multiple processing techniques to incorporate different parameters.

In contrast, phase separation micromolding (PS μ M), the scaffold fabrication technique generally applied in this thesis, allows tuning of the porosity as well as the surface topography within one step. The resulting porous micropatterned sheets can subsequently be multi-layer stacked to create the 3D scaffolds incorporating porosity as well as topography throughout the scaffold. PS μ M is based on phase separation of a polymer solution on a micropatterned mold yielding a polymer matrix containing surface topography. Tuning the process conditions results in adaptable porosity and morphology of the obtained sheets, whereas variation in the mold's micropattern enables adaptable surface topography. Besides inducing phase separation, evaporation of the solvent enables dense sheets featuring surface topography. One of the main advantages of PS μ M is the wide range of materials allowed for processing by this technique and the lack of harsh conditions, therewith preventing possible degradation of the materials during processing.

Chapter 3, 4 and 5 were devoted to the understanding and optimization of the PS μ M processing conditions to obtain micropatterned porous scaffold sheets. We presented the application of distinct polymers varying largely in material properties as mechanical strength, rigidity, processability and time to degrade. The most commonly applied polymer in the work described in this thesis is poly(L-lactic acid) (PLLA). Adapting the PS μ M process parameters for high molecular weight PLLA yields

micropatterned sheets expressing a wide variety of porosities from dense up to 86 % featuring a solid-wall pore morphology. When increasing the molecular weight of the PLLA, micropatterned sheets comprising a nano-fibrous morphology is achievable as well. These sheets feature nano-fibers of 50-500 nm, similar to the fibers making up the vast majority of the natural extra cellular matrix surrounding cells *in vivo*. Besides the semi-crystalline and rather rigid PLLA, processing of amorphous and flexible poly(tri-methylene carbonate) (PTMC) by PS μ M also yields porous micropatterned sheets when using poly(ethylene oxide) (PEO) as additive into the polymer solution. These chapters also evaluate the obtained sheets regarding scaffold-cell interaction and nutrient transport, two aspects also studied in further detail in the succeeding chapters.

Scaffold-cell interaction and up-scaling

Scaffold-cell interaction discussed in **Chapter 3, 4 and 5** mainly relates to the effect of surface topography design on cell and tissue organization. *In vivo*, tissue making up e.g. the cardiovascular system has a clear organization. However, when isolating the cells from a donor and culturing these cells *in vitro*, the cells lose their organization. Introduction of a specifically designed surface architecture can help the cells to restore their organization. Results reveal clear organization of the cells for distinct surface topographies, independently of the scaffold material. Depending on the topography dimensions, alignment over 80 % was achieved for C2C12 pre-myoblast cells on sheets featuring microchannels obtained by PS μ M. Interestingly, when the cells grow multi-layers and the cells overgrow the microchannels, they still maintain their organization. Besides the effect on cell organization, surface topography also affects other cell behavioural aspects as cell attachment, morphology and proliferation. In addition, our results suggest the choice of material and surface topography might also influence C2C12 differentiation through the myogenesis pathway. **Chapter 6** relates the level of cell attachment, morphology and proliferation and gives a more fundamental understanding of the scaffold-cell interaction. Cells do not directly attach to a surface, but through an adsorbed protein layer on the biomaterial surface. Proteins present in the blood, or supplemented to the culture medium via serum, adhere to the surface and specific proteins thereof provide ligands for the cells to bind to through their integrin receptors. Several parameters influence this process, besides the obvious availability of proteins and type of cells; for example the composition of the adsorbed protein layer and the extent of unfolding of the proteins regulating their activity. This chapter did not deal with in-dept analysis of the protein layer, but rather correlates surface characteristics as topography and wettability to total protein adsorption and cell attachment, proliferation and morphology. Incorporating surface topography alters the surface wettability to a certain extent without changing other surface properties as composition and charge; tuning of the micropattern dimensions allows adaptation of the surface wettability without the need to change the

surface composition. The results show that both the wettability as well as the surface topography influence attachment and proliferation. Cell morphology evaluation suggests that the surface topography is a dominant factor, even though wettability can be important under specific conditions. To broaden the range of the surface characteristics that can be evaluated for a specific application, **Chapter 7** presents a new top-down design concept regarding surface-cell interactions. This concept is based on high-throughput screening of a 2x2 cm² chip featuring a library comprising almost 8500 unique surface topography combinations, the TopoChip. By variation in the TopoChip surface material, the number of variations can expand rapidly. High-content imaging, data acquisition and analysis should reveal which of those unique surface characteristics elicit the appropriate bio-active response required for a specific application.

Going 3D and Nutrient supply

Transport of nutrients throughout the scaffold is of vital importance for cell viability. Under static conditions, nutrient transport solely relies on diffusion and nutrient diffusion is limited to a region at short distance to a direct nutrient source, i.e., generally the periphery of the scaffold. Tissue engineering constructs, however, require size dimensions of at least 1 mm to be considered clinically relevant. This gap between the nutrient diffused region and the actual construct size requires additional measures to overcome these nutrient limitations. *In vitro*, a commonly applied method is culturing under dynamic conditions, which induces convective flow of the medium which can lead to perfusion of the scaffold. Enabling this perfusion throughout the complete scaffold requires high porosity and good pore interconnectivity.

Chapter 3, 4 and 5 were concerned with the transport through single micropatterned porous sheets for the respective biomaterials and related to the yielded sheet porosity and morphology. Determination of glucose diffusion, used as model nutrient, revealed good diffusion through the majority of sheets with high porosity of the distinct materials; this data indicated good pore interconnectivity. In **Chapter 8**, we discuss multi-layer stacking of these sheets into 3D, resulting in tubular scaffolds where microchannels provide space for the cells to grow. Correlation of nutrient availability per layer with cell viability and proliferation clearly indicated that transport of nutrients and cell signalling between the layers occurs, however, is not sufficient for sustained culture. To enhance the supply of nutrients towards the cells in a larger region than the limited distance from the periphery, nutrient perfusion through the microchannels was performed. The results clearly revealed improved cell viability and proliferation at levels even equal to one single layer, where the cells are in direct contact to the medium. Hence, the results support successfulness of the multi-layer 3D scaffolds comprised of micropatterned porous sheets as proposed in this thesis.



Nederlandse Samenvatting

Er wordt al lang gesproken over het vervangen van organen, maar het vakgebied om weefsel (tissue) *in vitro* (buiten het lichaam) te ontwikkelen om beschadigd weefsel *in vivo* (in het lichaam) te herstellen, is slechts zo'n twee decennia geleden ontstaan uit de reconstructieve chirurgie waar transplantatie van donorweefsel wordt uitgevoerd. Echter, er rijzen verscheidene complicaties bij het gebruik van donorweefsel, zoals een tekort aan donoren, afstotingsverschijnselen en transmissie van ziektekiemen. Een *in vitro* ontwikkeld vervangend orgaan, dat gebruik maakt van de patiënt z'n eigen cellen, zou daarom ook een zeer welkom alternatief zijn. Om de ontwikkeling van zo'n vervangend weefsel via 'tissue engineering' mogelijk te maken, kunnen verschillende strategieën gevolgd worden. Dit proefschrift richt zich voornamelijk op het ontwerp van een dragermateriaal (scaffold) voor de cellen, welke de extra cellulaire 3D-matrixomgeving van de cellen nabootst, en op de fabricage en analyse van deze ontwikkelde scaffolds.

Materiaalkunde

In de beginjaren van 'tissue engineering' onderzoek was er slechts een gelimiteerde verscheidenheid aan materialen bekend met biocompatibele eigenschappen en de meeste studies maakten dan ook gebruik van een van deze materialen. Maar na decennia van biomateriaalonderzoek is de verscheidenheid aan materialen waaruit gekozen kan worden, explosief gestegen en deze stijgt nog steeds. Verschillende klassen van materialen, van zowel natuurlijke als synthetische aard, maken graduele variatie tussen de materialen mogelijk en daarmee een selectie van optimale materiaaleigenschappen gericht op een specifieke toepassing. **Hoofdstuk 2** presenteert zowel een overzicht van veel gebruikte biomaterialen uit verschillende klassen alsook fabricagetechnieken om deze materialen te verwerken tot scaffold. Het grote aantal beschikbare materialen vereist een grote verscheidenheid aan verwerkingstechnieken om deze materialen in de ontworpen scaffold te fabriceren. Echter, vele fabricagemethoden houden slechts rekening met één enkele ontwerpparameter, wat inhoudt dat verschillende verwerkingstechnieken nodig zijn om meerdere parameters op te nemen in een ontwerp.

In tegenstelling daarmee maakt 'phase separation micromolding' (PS μ M), de scaffoldfabricagetechniek, die hoofdzakelijk wordt toegepast in dit proefschrift, het mogelijk in één stap zowel de porositeit alsook de topografie van het scaffoldoppervlak te variëren. De porositeit maakt goed transport van voedingsstoffen van en naar de cellen door de hele scaffold mogelijk. Met oppervlaktetopografie kan de organisatie van de cellen gestuurd worden en daarmee de opbouw van het weefsel, zodat deze een gelijksoortige structuur kan aannemen als *in vivo*-weefsel. De verkregen microgestructureerde scaffoldfilms kunnen in multi-lagen gestapeld worden om een 3D-scaffold te creëren die porositeit en oppervlaktetopografie bezit door de hele scaffold heen. PS μ M is gebaseerd op fasescheiding van een polymeeroplossing op een microgestructureerde mal waarbij een polymeermatrix ontstaat die de specifieke oppervlaktetopografie bevat. Variatie in de verwerkingscondities resulteert in verscheidenheid in porositeit en morfologie van de verkregen polymerenfilms, en variatie in het micropatroon aanwezig op de mal leidt tot aanpassing van de verkregen oppervlaktetopografie. In plaats van het induceren van fasescheiding, kan verdampen van het oplosmiddel fabricage van niet-poreuze (dichte) films met oppervlaktetopografie mogelijk maken. Een van de voornaamste voordelen van PS μ M is de grote verscheidenheid aan materialen die verwerkt kunnen worden in combinatie met het ontbreken van veeleisende verwerkingscondities, waardoor eventuele degradatie van de materialen tijdens de verwerking voorkomen wordt.

Hoofdstuk 3, 4 en 5 zijn gewijd aan het begrijpen en optimaliseren van de PS μ M verwerkingscondities voor het verkrijgen van microgestructureerde poreuze scaffolds. Wij presenteren de toepassing van verschillende polymeren die sterk afwijken in hun materiaaleigenschappen zoals mechanische sterkte, rigiditeit, verwerkbaarheid en de tijd die nodig is voor degradatie. Het polymeer dat voornamelijk is toegepast in dit proefschrift, is polymelkzuur (PLLA). Aanpassing van de PS μ M verwerkingsparameters voor hoogmoleculair PLLA brengt microgestructureerde films voort met een grote verscheidenheid aan porositeiten van dicht (0 %) tot 86 % met een cellulaire poriemorfologie. Verhoging van het moleculaire gewicht resulteert in microgestructureerde PLLA-films met een nano-vezelmorfologie. Deze nano-vezels zijn 50-500nm in diameter, net als de vezels die de meerderheid vormen van de natuurlijke extracellulaire matrix in de directe omgeving van cellen *in vivo*. Naast het semi-kristallijne en redelijk rigide PLLA is ook verwerking van amorf en flexibel poly(trimethyleen carbonaat) (PTMC) mogelijk met PS μ M. Door middel van toevoeging van poly(etheleen oxide) (PEO) als additief aan de polymeeroplossing kunnen poreuze microgestructureerde PTMC-films gefabriceerd worden. Deze hoofdstukken evalueren de verkregen films ook met betrekking tot de scaffold-celinteractie en het voedingstransport, twee aspecten die ook in verder detail worden behandeld in de opvolgende hoofdstukken.

Scaffold-celinteractie en opschaling

Scaffold-celinteractie besproken in **Hoofdstuk 3, 4 en 5** is voornamelijk gerelateerd aan de mate waarin het oppervlaktetopografie ontwerp de organisatie van cellen beïnvloedt. *In vivo* heeft weefsel dat bijvoorbeeld het cardiovasculaire systeem vormt een duidelijke organisatie, maar cellen geïsoleerd van een donor en *in vitro* gekweekt verliezen veelal hun organisatie. Introductie van specifiek ontworpen oppervlaktetopografie kan helpen de cellen hun organisatie terug te geven. De verkregen resultaten laten duidelijk zien dat cellen gekweekt op films met een specifiek ontworpen oppervlaktetopografie zich organiseren, ongeacht het scaffoldmateriaal. Afhankelijk van de topografiedimensies is tot 80 % 'alignment' (het richten van de cellen naar de structuur) bereikt voor C2C12 pre-myoblastcellen op films met 30 µm breede microkanalen. Wetenswaardig is dat wanneer de cellen in multi-lagen groeien en daarbij de microkanalen overgroeien, die cellen hun organisatie ook behouden. Naast het effect op de celorganisatie, beïnvloedt de oppervlaktetopografie ook ander celgedrag, zoals de hechting van cellen aan het oppervlak, celmorfologie en -proliferatie. Verder suggereren onze resultaten dat de keuze van het scaffoldmateriaal en de oppervlaktetopografie ook de differentiatie van de C2C12 cellen beïnvloedt door activatie van de myogene route.

Hoofdstuk 6 gaat in op de relatie tussen het niveau van celhechting, -morfologie en -proliferatie onderling en geeft een meer fundamenteel begrip van de scaffold-celinteractie. Cellen hechten niet direct aan een oppervlakte maar aan een eiwitlaag die op het oppervlak geadsorbeerd is. Eiwitten aanwezig in het bloed, of via serum toegevoegd aan het kweekmedium, adheren aan het oppervlak en specifieke eiwitten daarbinnen verschaffen liganden waaraan de cellen zich aan kunnen binden door middel van integrine receptoren. Verschillende parameters beïnvloeden dit proces, naast de voor de hand liggende toereikendheid van eiwitten en celtype, zoals de compositie van de geabsorbeerde eiwitlaag en de mate waarin de eiwitten zich ontvouwen, wat hun activiteit weer reguleert. Dit hoofdstuk gaat niet in detail in op de analyse van de eiwitlaag, maar behandelt de correlatie tussen oppervlaktekenmerken zoals topografie en hydrofobiciteit met de totale eiwitadsorptie en celhechting, celproliferatie en celmorfologie. Het introduceren van een oppervlaktetopografie verandert de oppervlaktehydrofobiciteit tot op zekere hoogte, zonder overige oppervlakte eigenschappen te beïnvloeden zoals de compositie en lading. Variatie van de micropatroondimensies maakt het mogelijk om de oppervlaktehydrofobiciteit aan te passen zonder daarbij de oppervlaktecompositie te hoeven veranderen. De resultaten laten zien dat zowel de hydrofobiciteit als de oppervlaktetopografie celhechting en -proliferatie beïnvloeden. Evaluatie van de morfologie van de cellen suggereert dat de oppervlaktetopografie een dominerende factor is, ondanks dat de hydrofobiciteit van groot belang kan zijn onder specifieke omstandigheden.


Om de verscheidenheid van oppervlaktekenmerken die geëvalueerd kunnen worden te kunnen verbreden, presenteert **Hoofdstuk 7** een nieuw 'top-downontwerp' voor oppervlakte-celinteracties.

Dit concept maakt gebruik van 'high-throughput screening' van een 2x2 cm² chip die een bibliotheek van bijna 8500 unieke oppervlaktetopografie-combinaties bevat, genaamd de 'TopoChip'. Door middel van variatie in het oppervlaktemateriaal kan de hoeveelheid variaties snel expanderen. 'High-content imaging', dataverwerking en -analyse zullen duidelijk moeten maken welke van de unieke oppervlaktekennmerken de gewenste reactie uitlokken nodig voor een specifieke toepassing.

Naar 3D en voedingstransport

Transport van voedingsstoffen door een scaffold is van essentieel belang voor de levensvatbaarheid van de cellen. Onder statische kweekcondities is voedingstransport geheel afhankelijk van diffusie, welke gelimiteerd is tot een gebied aangrenzend aan een directe voedingsbron, meestal de buitenste rand (periferie) van de scaffold. Constructen vervaardigd door middel van tissue engineering vereisen veelal een minimale grootte van 1 mm of meer om klinisch relevant te worden bevonden. De kloof tussen het gebied dat bereikt wordt door middel van diffusie en de daadwerkelijke grootte van het construct dat nodig is, vraagt om extra maatregelen om het voedingstekort te overwinnen. *In vitro* is kweken onder dynamische condities een algemeen gebruikte methode, waarbij een convectieve stroom van kweekmedium kan leiden tot perfusie van de scaffold. Om perfusie door de hele scaffold mogelijk te maken, dient de scaffold een hoge porositeit en connectiviteit van de poriën te bezitten.

Hoofdstuk 3, 4 en 5 behandelen voedingstransport door een enkele microgestructureerde poreuze film van de respectievelijke biomaterialen, gerelateerd aan de verkregen porositeit en poriënmorfologie van deze films. Meting van de diffusie van glucose, gebruikt als modelvoedingsstof, toont aan dat er goede diffusie is door de meerderheid van de films met hoge porositeit. **Hoofdstuk 8** bespreekt het stapelen van de films in 3D-multilagen, resulterend in buisvormige scaffolds waarbij de microkanalen ruimte verschaffen voor de cellen. Het correleren van de beschikbaarheid van voedingsstoffen per laag met de levensvatbaarheid van de cellen en hun proliferatie toont duidelijk aan dat voedingstransport en signaaloverdracht tussen de cellen optreedt, hoewel niet voldoende voor langdurige kweekperiodes. Om de aanvoer van voedingsstoffen naar de cellen te verbeteren in een groter gebied dan de gelimiteerde perifere laag van de scaffold, is perfusie van voedingsstoffen door de microkanalen toegepast. De verkregen resultaten tonen duidelijk aan dat de levensvatbaarheid en proliferatie van de cellen hierdoor duidelijk verbeteren, zelfs tot eenzelfde niveau als voor een enkele laag waarbij alle cellen in direct contact zijn met het bulkmedium. Hiermee ondersteunen de resultaten het idee dat de ontworpen 3D multilaagscaffold, bestaande uit microgestructureerde poreuze films, zoals voorgesteld in dit proefschrift, een kansrijk concept is.



Acknowledgments - Dankwoord

And then ‘at once’ it is finished, ‘het zit er op’! To phrase in short what these past four years brought me, I like to borrow Martha Graham’s (who founded contemporary dance) quote *Dancing is just discovery, discovery, discovery* to twist it into:

Doing a PhD is just discovery, discovery, discovery

These four years make up a period where I saw, heard and learned a lot and I am very pleased that I could share these experiences on both scientific as social field with many persons. This is the right place to thank everybody who contributed to higher or lesser extent to this wonderful time. Some I would like to mention by name.

First of all, Dimitris, you have been a great supervisor. You have always shown confidence in me and in the obtained results, even if I didn’t see it. Although my project involved a whole new discipline for our group and you personally, you made sure you were well informed on the related topics and never hold back to ask. I’m grateful for your personal interest, enthusiasm (doe maar) and humor during our meetings and conferences, and the space you left to not agree on everything. To tell you something nice for on a bad day: it’s finished and it worked! You well deserve the bright-colored ‘thank God it’s over’ t-shirt ☺.

Ook wil ik Matthias Wessling van harte bedanken voor de mogelijkheid te promoveren binnen de membraantechnologie groep, ondanks de minimale ‘klassieke’ toepassing van membranen in mijn werk, en voor de ruimte die je me gegeven hebt om mijn eigen weg hierbij in te slaan.

Grote dank ben ik verschuldigd aan Clemens van Blitterswijk en Jan de Boer die mij de kans hebben geboden al het cel-gerelateerde werk uit te voeren binnen hun groep, Department of Tissue Regeneration. In eerste instantie nog in Bilthoven, maar gelukkig (voor mij) na anderhalf jaar in Enschede. Clemens, je persoonlijke interesse in mijn werk heb ik altijd zeer gewaardeerd. Heel erg bedankt daarvoor, alsook voor het plaatsnemen in mijn promotiecommissie. Jan, ik ben nog steeds geen bioloog maar ik heb zeker veel bijgeleerd over de cel- en moleculaire biologie, heel erg bedankt voor jouw aandeel daarin (en mijn ‘adoptie’ ☺).

Daarnaast wil ik ook graag Dirk Grijpma en Jan Feijen bedanken voor de samenwerking op het materiaal-gerelateerde werk. Dirk, bedankt voor je input in mijn werk, en ook voor de organisatie van het overkoepelende ‘Advanced Microstructures’ project welke de verschillende samenwerkingsverbanden mede mogelijk maakten. Verder wil ik je bedanken voor het plaatsnemen in mijn promotiecommissie. Jan Feijen, hartelijk dank voor uw input en uw gevoel voor detail in de manuscriptcorrecties.

I would also like to thank Aldo Boccaccini, David Kaplan and Ruud Bank for taking place in the defense committee.

My project enabled to work in collaboration with many different people, within the UT as well as outside. Personally, I considered these collaborations as enrichment, regardless of the outcome. Thanks to Aldo Boccaccini, Hedeer Jawad and Mirka El Fray on the work of flexible cardiac patches, and Stephanie Schmitmeier on the hepatocyte culturing.

Hemant, thanks for all the work we did on 'our' TopoChip. I think we created a nice platform that can serve as starting point for many potential applications.

Gustavo and Jun, thanks for the collaboration on the bioreactor culturing; Gustavo, thanks for the digging the sand ☺.

Laura, bedankt voor je aandacht en je aanmoedigen tijdens mijn masteropdracht. Je hebt me laten zien dat promoveren 'best leuk' kan zijn.

Also within the project at large much common work was performed, as was the main goal of the project. Siggi and Tomasz as fellow PhD students as well as Miriam, Roman and Sandra as PostDocs, thanks for the talks, collaborations and for cheering up the meetings.

In addition, I would like to thank the bachelor and master students who have worked within my project on different topics: Bart, Emilie, Ida-Jacoba, Liesbeth, and Wolf. You can find back parts of your work to higher or lower extent within various chapters. Besides the research-related input, I would like to thank each of you as well for your personal input and dedication. Lodewijk, bedankt voor je literatuur-overzicht.

Lydia, dankjewel voor je tips en voor het vele praktische werk dat je hebt uitgevoerd.

Besides, I would like to thank many persons for their assistance and tips on experimental and theoretical basis. I hardly can mention everybody, but I will give it a try.

Antoine, bedankt voor je veiligheidsanalyse en vooral voor je toestemmingen/toespelingen; Greet, alle bureaucratische rompslomp werd een stuk overzichtelijker door jou; Rob, bedankt voor al je black-in-white en white-in-black omrekeningen; en verder Erik Rol, Harmen, Herman (SEM), Jon, Jorrit, Marcel (computer-ruzie's sussend), Matias, Wilbert en een ieder van MTO die hier niet genoemd is maar hier misschien wel had horen te staan.

Anouk, bedankt voor je organisatie en schoonmaaktalent ;) Hugo Andre, for all your assistance at cell and assays related work; Hugo, for assisting with the transfections and all kinds of tips and tricks; Jeroen L., PCRen zal nooit meer hetzelfde zijn zonder jou; Jeroen R., bedankt voor je hulp met alle celwerk en de immuno-lesjes; Sanne en Jojanneke, voor jullie hulp in Bilthoven wanneer de afstand-tijd verhoudingen af en toe wel erg ver te zoeken waren; and of course Aart, Ana, Audrey, Ineke, Joyce, Karolina, Liliana, Lorenzo, Nicolas, Ram, and anyone else who I might have forgotten to mention here.

En verder Tom Groothuis en Henk-Jan van Manen voor jullie hulp met de microscopen, and Stefan Schlautmann for your assistance regarding mold fabrication.

The discoveries were certainly not all achieved on scientific basis, but also many go along with the many activities organized by MTO'ers as well as TR-members. I consider it a privilege that I was part of two great research groups and the parties, bicycle-tours, BBQ's, movies, bowling, diners, sailing trips, sport activities, weekend-trips, dancing, ..., and borrels (picture-of-the-month and Friday-afternoon, even with the 'wrong' crisps) were an very important part for making the past four years such great ones. Also the lab-work, meetings and conferences would have been a whole lot more boring without you guys there, thank you all!

Also all roommates with whom I shared the offices the past years I would like to thank for their joy, talks, tea and 'dropjes' sharing, and just for being there to vent whatever what was there to vent. Thanks 1330 (ja, dat was echt prettig): Alisia, Jens, Laura en Sander and 321: Anne-Corine, Jigar, Maik, Matías.

Daarnaast wil ik speciaal Jorrit en Wilbert noemen voor hun gezelschap, en voor hun humor en advies gedurende deze jaren. Ik heb veel van jullie geleerd waar het gaat om aio te zijn. Daarnaast hebben we (al lunch-wandelend) veel meegemaakt met z'n drieën, van kleine hoogte- of dieptepunten tot waar het om gaat in het leven. De lach en de traan die we met elkaar hebben kunnen delen zal ik nooit vergeten.

Natuurlijk bestaat het leven niet alleen uit werk of semi-werk gerelateerde zaken, maar ook vooral uit totaal niet-werkgerelateerde bezigheden. Dansen is een van mijn grote passies en Arabesque heeft hier een belangrijke rol in gespeeld. Ik ben blij 10 jaar (!) lid te zijn geweest van deze vereniging. Bedankt iedereen, en Soosan in het bijzonder; laten we de komende voorstelling wederom een hele mooie maken (Arabesque DANST ...). Ook salsa is een belangrijke noemer geweest in het los kunnen laten van alles, Astrid bedankt dat je me in aanraking hebt gebracht met het salsa-virus.

Verder wil ik bij deze ook mijn vrienden en (schoon)familie bedanken voor hun continue steun en vertrouwen. Maar vooral voor alle gezellige momenten gedurende terras-hangen, kletsen, shoppen, sauna-dagjes, etentjes, weekendjes-weg, feestjes, oud-en-nieuwnachten, vakanties (ook als zo'n vakantie volledig in de regen valt), sporten, filmpje pakken, En ik ben er van overtuigd dat er nog vele zullen volgen, in Nederland of waar dan ook ter wereld.

Patricia, aka MB, dankjewel voor alle b... acties en momenten ☺. Ik vind het een eer en een geruststellende gedachte dat jij naast me op het podium zal staan. Let's go girl!

Gart en Wiep, broertjes, jullie betekenen enorm veel voor me. Ik ben trots en gelukkig jullie zus(je) te zijn, en dat we wat er ook gebeurde altijd voor elkaar opgekomen zijn. Wiep, als representant van jullie beide, weet ik dat je dat nu ook zal doen als mijn paranimf. Gart, grote broer, ik hoef jou alleen maar aan te kijken en weet dat het goed is. Dank-jullie-wel.

Jocé en Margreet, jullie ook heel erg bedankt voor jullie interesse en gezelligheid.

Pap en mam, Goos en Gré, jullie hebben altijd in me geloofd en me gesteund in wat ik wilde doen, of jullie het er nu mee eens waren of niet. Hierdoor kon ik me vol vertrouwen in het onbekende storten, want ik wist dat jullie me toch wel opgevangen zouden hebben. Die vrijheid is het mooiste wat jullie me hebben kunnen geven.

Lieve Roy, we hebben het gedaan! Van lineaire structuren tot het afronden van dit boekje, je was er altijd om me te motiveren, vertrouwen te geven en voor afleiding te zorgen. Maar vooral je enthousiasme, je humor en je liefde maakt dat we zo goed zijn samen. Bijna 10 jaar, en hopelijk nog heel wat veelvouden daarvan te gaan, waar dan ook ter wereld. Samen lukt het ons. Je maakt me gelukkig, ik hou van je.



Curriculum Vitae

Bernke Papenburg was born at the 22nd of July, 1981 in Dedemsvaart, The Netherlands. In July 1999, she received her diploma for pre-university education (VWO) from the CSG Liudger in Drachten, The Netherlands. In August 1999 she started her study Chemical Engineering at the University of Twente in Enschede, The Netherlands, which she graduated for in December 2004 providing her the MSc diploma (Ir.). Within her studies, she focussed at biomedical materials engineering at large with emphasis on tissue engineering. During her internship at Gambro GmbH in Hechingen, Germany, she worked at characterization of protein separation membranes. She performed her master assignment at the Membrane Science and Technology research group of the University of Twente and focussed at design and fabrication of tissue engineering scaffolds by means of phase separation and analysis thereof. After briefly working within the same group as researcher, she started her PhD under supervision of Prof. M. Wessling on the topic of Design Strategies for Tissue Engineering Scaffolds described in this thesis. This multi-disciplinary PhD project allowed for close collaborations with various research groups within and outside the University of Twente, amongst which Polymer Chemistry and Biomaterials of Prof. J. Feijen and the Department of Tissue Regeneration of Prof. C.A. van Blitterswijk. From April till medio of August 2009, she works as a PostDoc researcher within the same project. Per September 2009, she will start a new line of PostDoc research at department of Biomedical Engineering at the Tufts University, Medford, MA, USA under the supervision of Prof. D. Kaplan.

List of Publications

Peer-reviewed papers

B.J. Papenburg, L. Vogelaar, L.A.M. Bolhuis-Versteeg, R.G.H., Lammertink, D., Stamatialis, M. Wessling, One-step fabrication of porous micropatterned scaffolds to control cell behavior, *Biomaterials*, 28 (2007) 1998-2009

D. Stamatialis, **B.J. Papenburg**, B.J., M. Girones, S. Saiful, S.N.M. Bettahalli, S. Schmitmeier, M. Wessling, Review: Medical applications of membranes: Drug delivery, artificial organs and tissue engineering, *Journal of Membrane Science* 308 (2008) 1–34

B.J. Papenburg, S. Schüller-Ravoo, L.A.M. Bolhuis-Versteeg, L. Hartsuiker, D.W. Grijpma, J. Feijen, M. Wessling, D. Stamatialis, Designing Porosity and Topography of Poly(1,3-trimethylene carbonate) Scaffolds, *accepted for publication in Acta Biomaterialia*

B.J. Papenburg, J. Liu, G.A. Higuera, I.J. de Vries, A.M.C. Barradas, J. de Boer, C.A. van Blitterswijk, M. Wessling, D. Stamatialis, Understanding Nutrient Supply through Multi-layer Scaffolds, *submitted*

B.J. Papenburg, L.A.M. Bolhuis-Versteeg, D.W. Grijpma, J. Feijen, M. Wessling, D. Stamatialis, A Facile Method to Fabricate Poly(L-lactide) Nano-fibrous Morphologies by Phase Inversion, *submitted*

In vitro and in vivo bioluminescence imaging of hypoxia in tissue engineered grafts, J. Liu, A. Barradas, F. Janssen, H. Fernandes, **B.J. Papenburg**, D. Stamatialis, A. Martens, C. van Blitterswijk, J. de Boer, *submitted*

B.J. Papenburg, E. Doods-Rodrigues, M. Wessling, D. Stamatialis, Cell behavior as Function of Contact Angle and Surface Topography, *in preparation*

B.J. Papenburg, H. Unadkat, R. Truckenmueller, M. Wessling, D. Stamatialis, C.A. van Blitterswijk, J. de Boer, An Arrayed Approach to Screening Cell-Surface Topographic Interactions, *in preparation*

Selection of abstracts selected for oral presentation at international conferences

B.J. Papenburg, J. Liu, I.-J. De Vries, D. Stamatialis, J. de Boer, C.A. van Blitterswijk, M. Wessling, Effective Nutrient Supply through Multi-layer Scaffolds, *TERMIS-EU chapter meeting, Porto, Portugal, June 2008 (the abstract of this oral presentation was selected within the 50 best abstract)*

B.J. Papenburg, D. Stamatialis, J. de Boer, C.A. van Blitterswijk, M. Wessling, Multi-layer Scaffolds to Combine Porosity and Micropatterning, *World Biomaterials Congress, Amsterdam, The Netherlands, May 2008*

B.J. Papenburg, J. Rouwkema, D. Stamatialis, J. de Boer, C.A. van Blitterswijk, M. Wessling, Porous Micropatterned Scaffolds to Control Tissue Organization, *TERMIS-EU chapter meeting, London, UK, September 2007*

B.J. Papenburg, J. Rouwkema, J. de Boer, D. Stamatialis, C.A. van Blitterswijk, M. Wessling, Porous Micropatterned Scaffolds to Control Cell Behavior, *1st TERMIS-EU summerschool, Funchal, Madeira, Portugal, May 2007 (granted a travel award)*

B.J. Papenburg, L. Vogelaar, L.A.M. Bolhuis-Versteeg, R.G.H. Lammertink, D. Stamatialis, and M. Wessling, Advanced Micropatterned Polymeric Scaffolds, *TERMIS-EU chapter meeting, Rotterdam, The Netherlands, October 2006*

B.J. Papenburg, L. Vogelaar, L.A.M. Bolhuis-Versteeg, R.G.H. Lammertink, D. Stamatialis, M. Wessling, Micropatterned Membrane Sheets for Tissue Engineering Scaffolds, *Euromembrane, Taormina, Italy, September 2006 (rewarded with the Wiley student prize for oral presentations)*

Patent

University of Twente, **B.J. Papenburg**, H. Unadkat, M. Wessling, D. Stamatialis, C.A. van Blitterswijk, J. de Boer, *P8262, High throughput screening method, 2007*

